Chapter 6

Asymmetric SST Profile (CONTROL_5N, CONTROL)

The multi-model mean comparing the CONTROL and CONTROL_5N experiments excludes FRCGC, ECM-CY29, UKMO(48) and UKMO(96). In addition the multi-model mean for the eddy statistics (based on MF files) excludes CGAM and MRI. These same sets will be used later in Chapter 7 which considers the response to tropical SST anomalies.

6.1 Mean State

6.1.1 Zonal-Time Averages, 2-D Fields

The zonal-time averages for the multi-model mean for single level fields tppn, cppn, dppn, evap, emp, cld_frac, albedo, ps and tauu are shown in Figure 6.1. The fields sw_toa, lw_toa, rflux_toa, ssw, slw, rfluv_sfce, slh, ssh and rflux are shown in Figure 6.2. The same fields for the individual models, along with tauv, are shown in Figures 6.3 through 6.21.

6.1.2 Zonal-Time Averages, 3-D Fields

Figure 6.22 shows the multi-model mean u, t, v and om while Figure 6.23 shows q and rh. The individual model om fields are shown in Figure 6.24.

6.2 Parameterization Forcing

The parameterization convection and cloud tendencies for temperature and specific humidity (t_conv, t_cld, q_conv and q_cld) are shown in Figures 6.25 through 6.28.

6.3 Tropical Variability

6.3.1 Wavenumber-Frequency Spectra

Since the tropical precipitation in the CONTROL_5N experiment moves poleward of 10°N latitude (Figure 6.1 and 6.3) the log of the power is averaged from 20°S to 20°N as was done in Section 5.3.1 which showed the response to the SST profile. To help detect any shift from symmetric modes to anti-symmetric modes in comparing CONTROL_5N to CONTROL, the symmetric and anti-symmetric modes are plotted side-by-side in the same figures. The wavenumber-frequency diagrams for the precipitation (tppn) are shown in Figure 6.29 and for diagrams for OLR (lw_toa) in Figure 6.30.

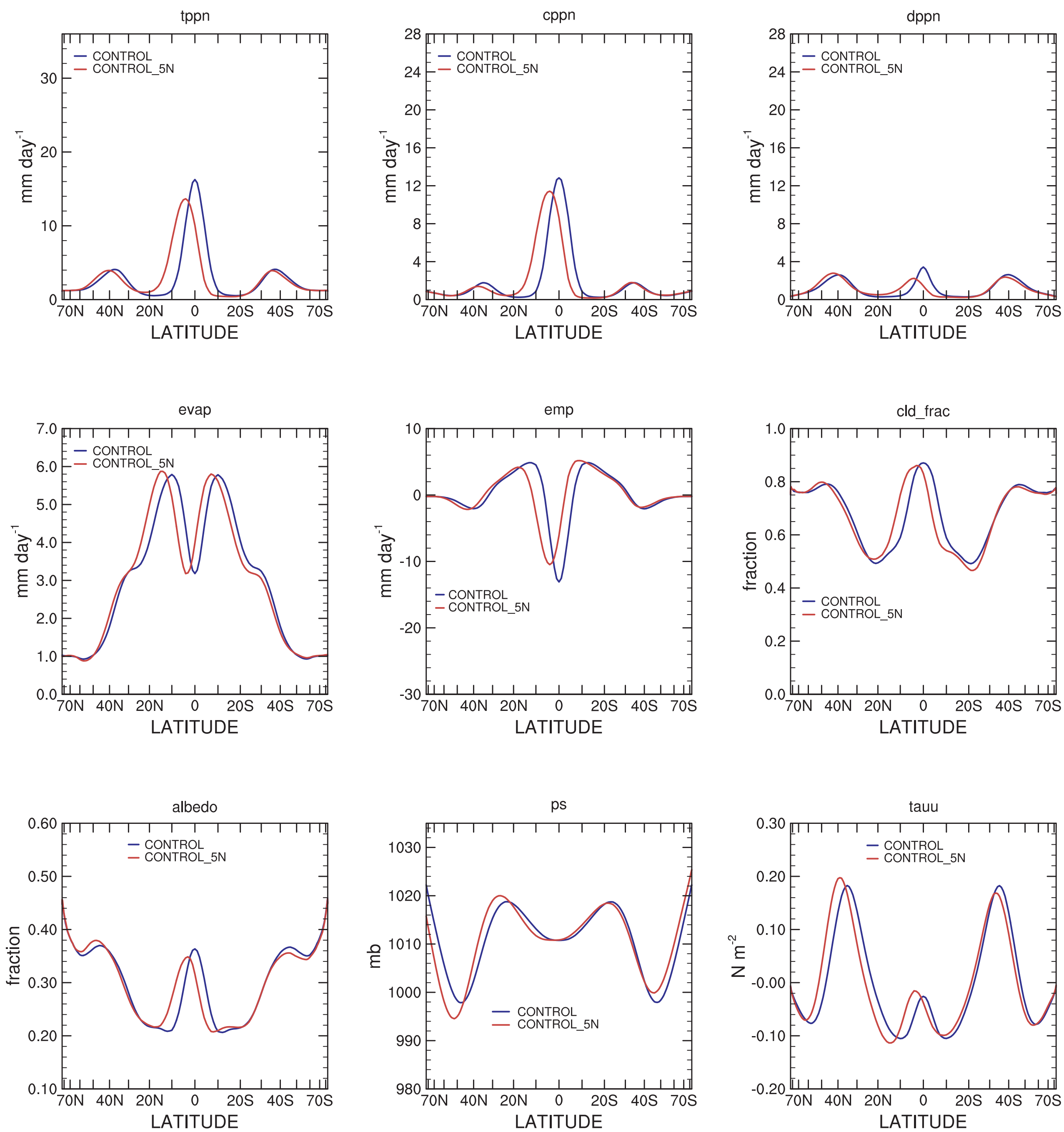

Figure 6.1: Multi-model mean zonal-time average total precipitation (tppn), convective precipitation (cppn), large-scale precipitation (dppn), evaporation (evap), evaporation minus precipitation (emp), cloud fraction (cld_frac), albedo (albedo), surface pressure (ps) and zonal surface stress (tauu) from CONTROL and CONTROL_5N SST distributions.

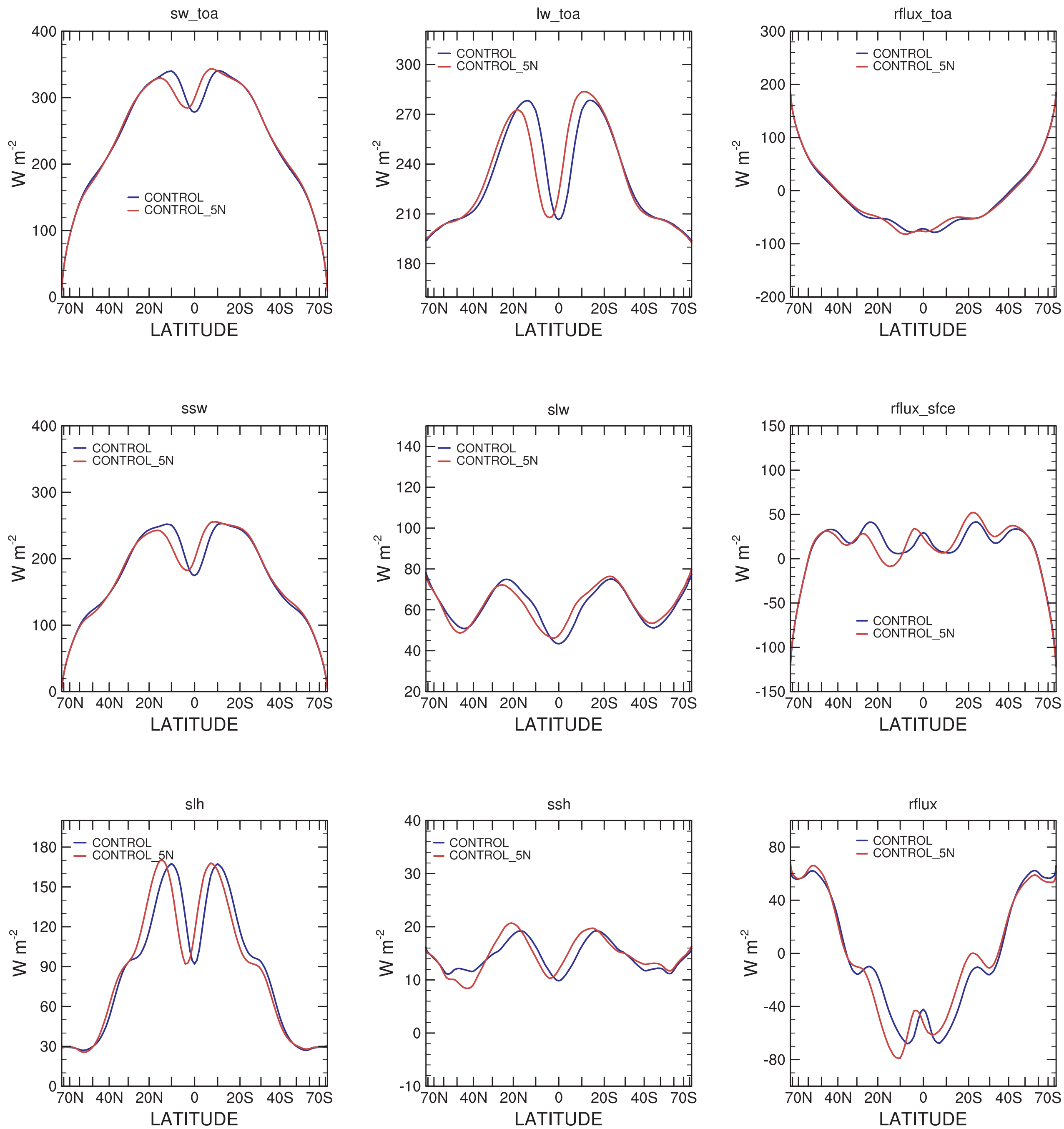

Figure 6.2: Multi-model mean zonal-time average TOA net shortwave (sw_toa, +ve downward), TOA net longwave (lw_toa, +ve upward), TOA residual (rflux_toa, +ve upward), surface net shortwave (ssw, +ve downward), surface net longwave (slw, +ve upward), surface residual (rflux_sfce, +ve downward), surface latent heat (slh), surface sensible heat (ssh) and net total (rflux, +ve out of atmosphere) fluxes from CONTROL and CONTROL_5N SST distributions.

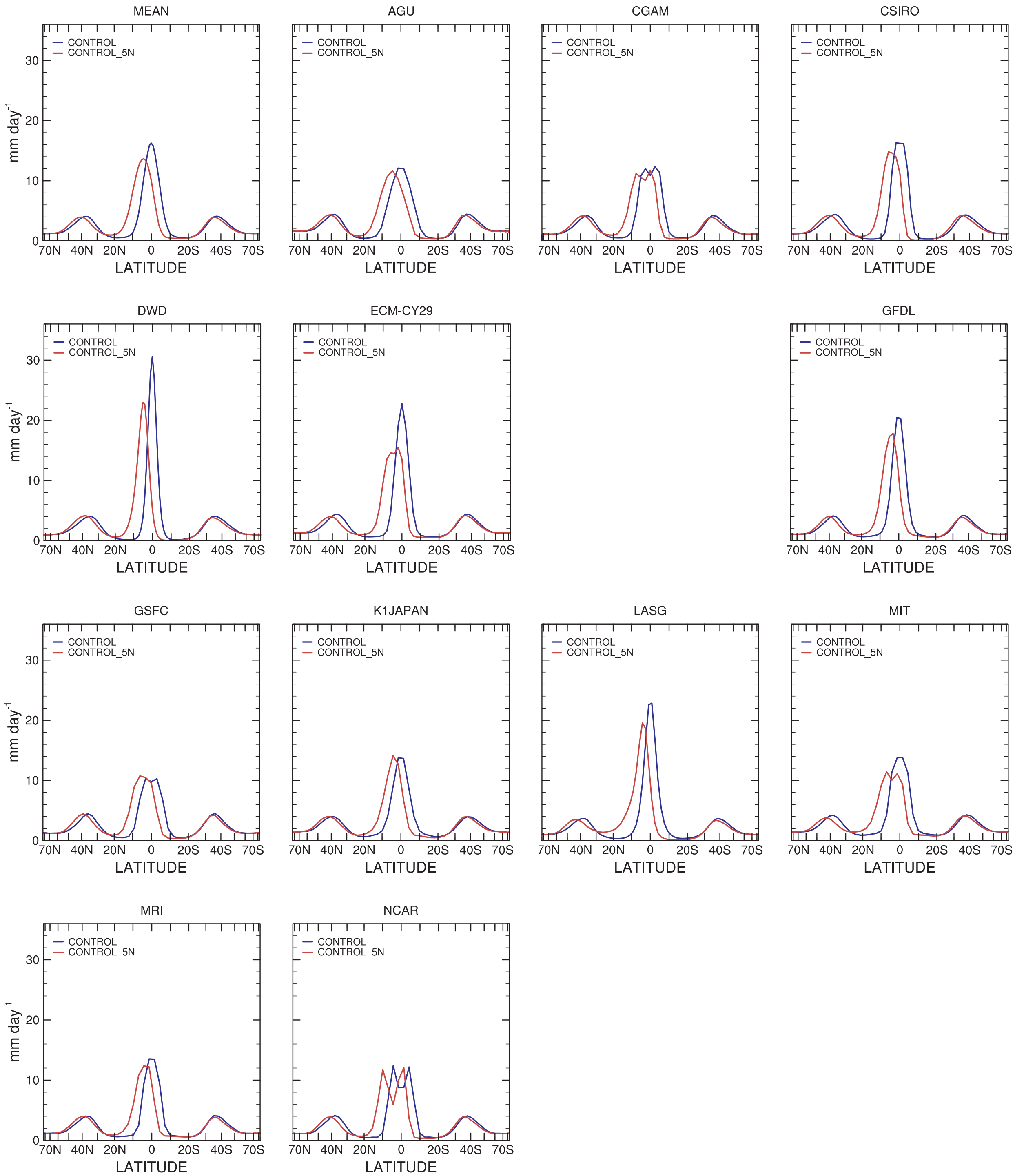

Figure 6.3: Zonal-time average precipitation (tppn) for individual models from CONTROL and CONTROL_5N SST distributions, mm day^{-1}.

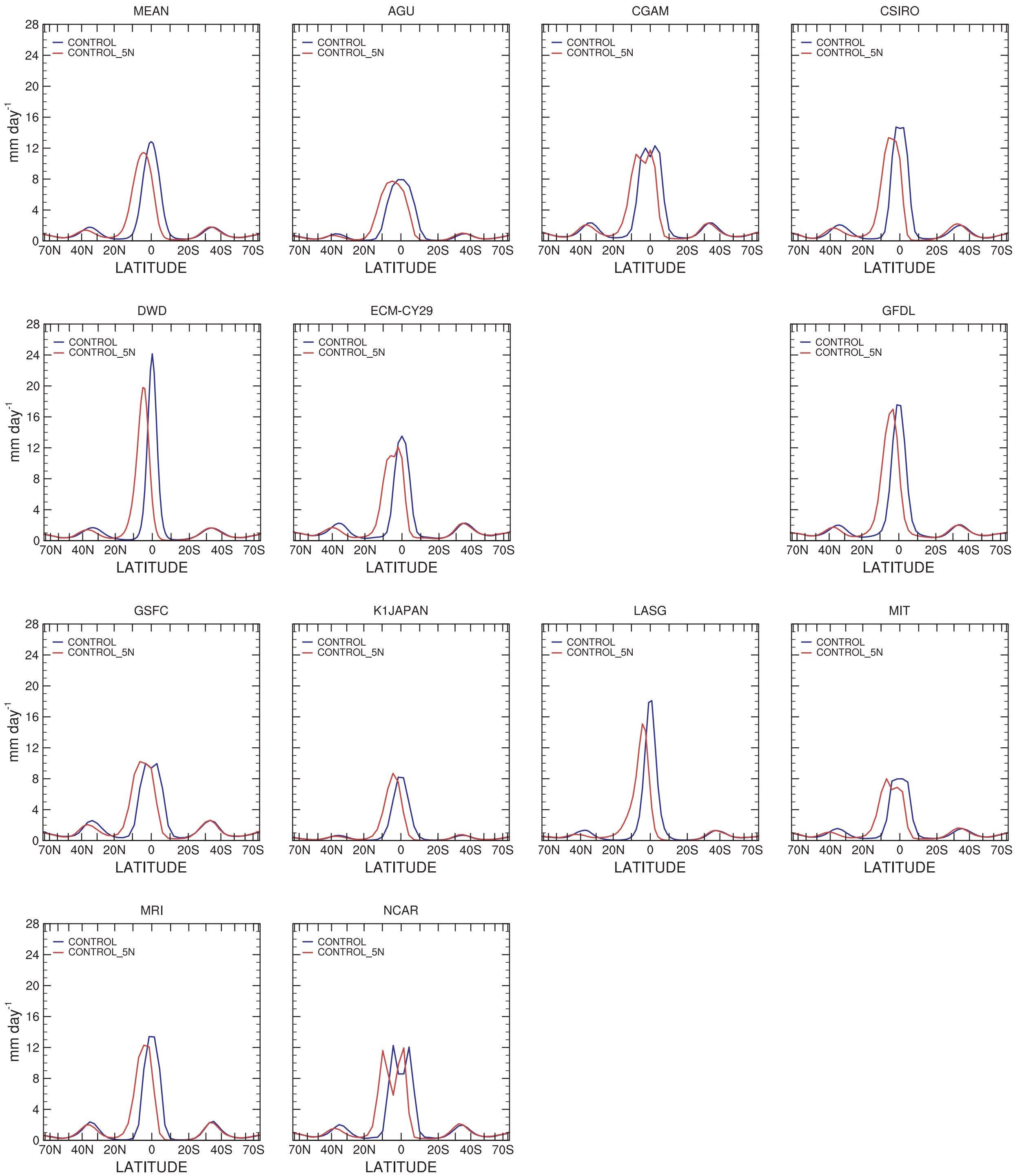

Figure 6.4: Zonal-time average convective precipitation (cppn) for individual models from CONTROL and CONTROL_5N SST distributions, mm day^{-1}.

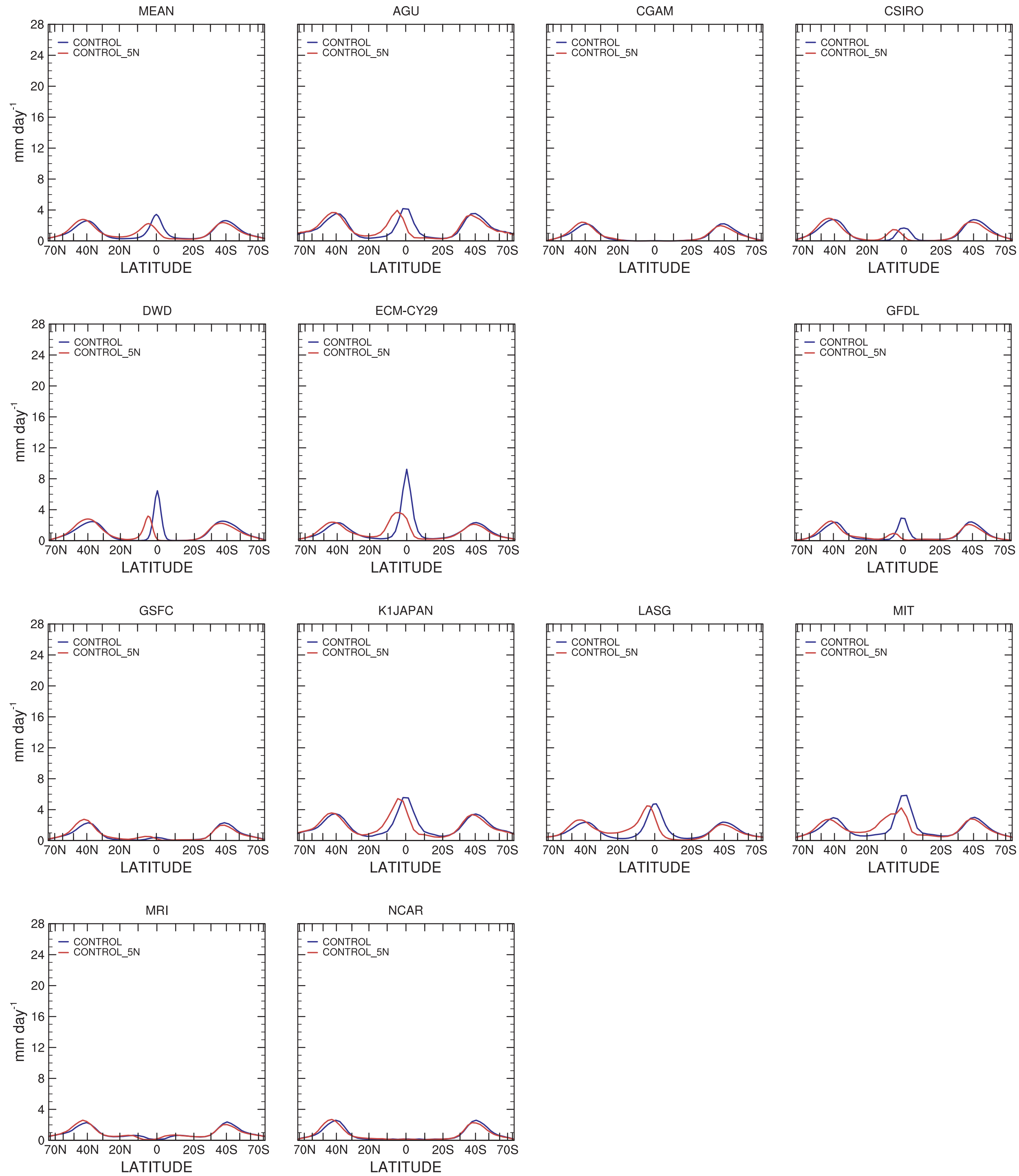

Figure 6.5: Zonal-time average large-scale precipitation (dppn) for individual models from CONTROL and CONTROL_5N SST distributions, mm day^{-1}.

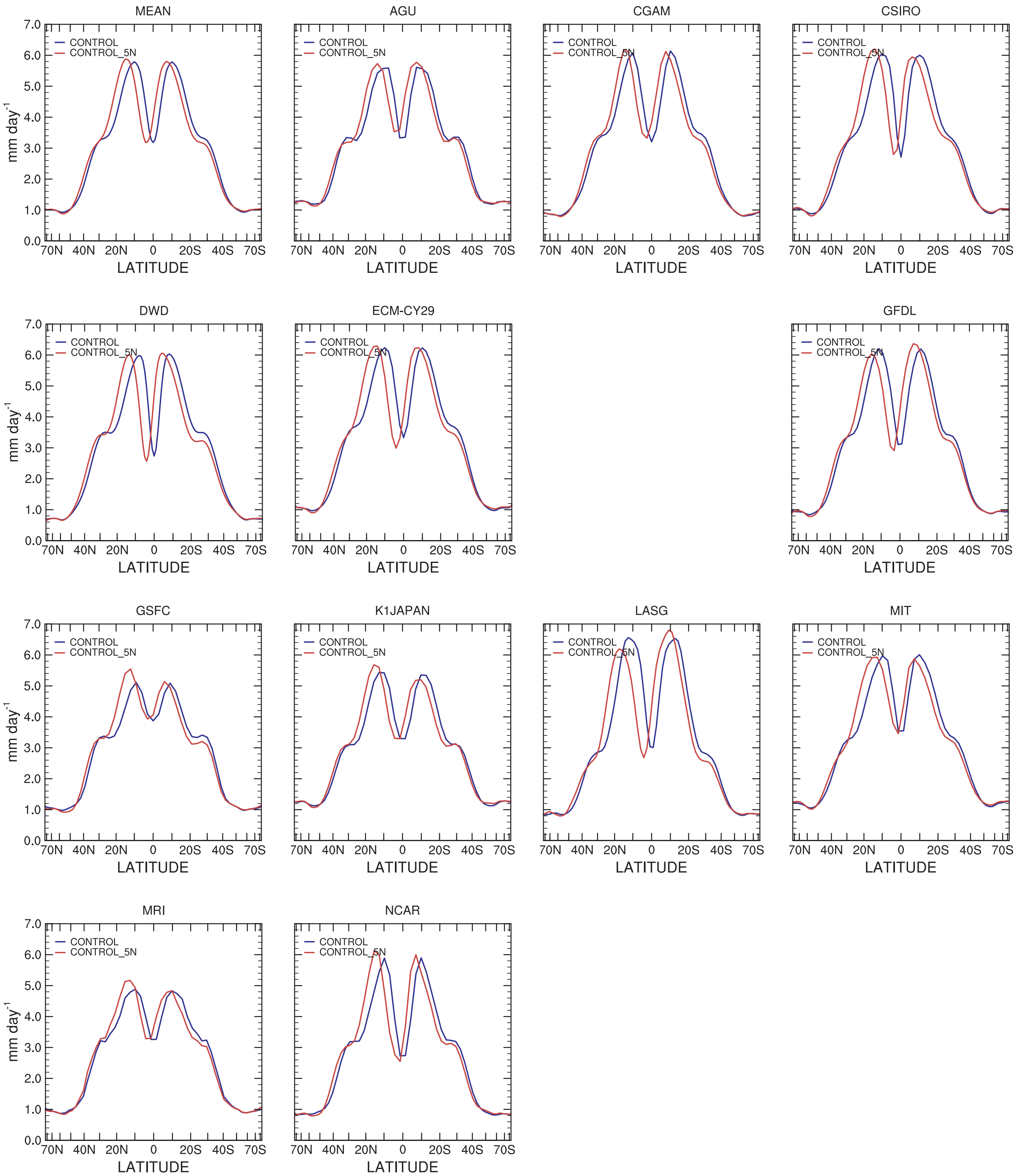

Figure 6.6: Zonal-time average evaporation (evap) for individual models from CONTROL and CONTROL_5N SST distributions, mm day^{-1}.

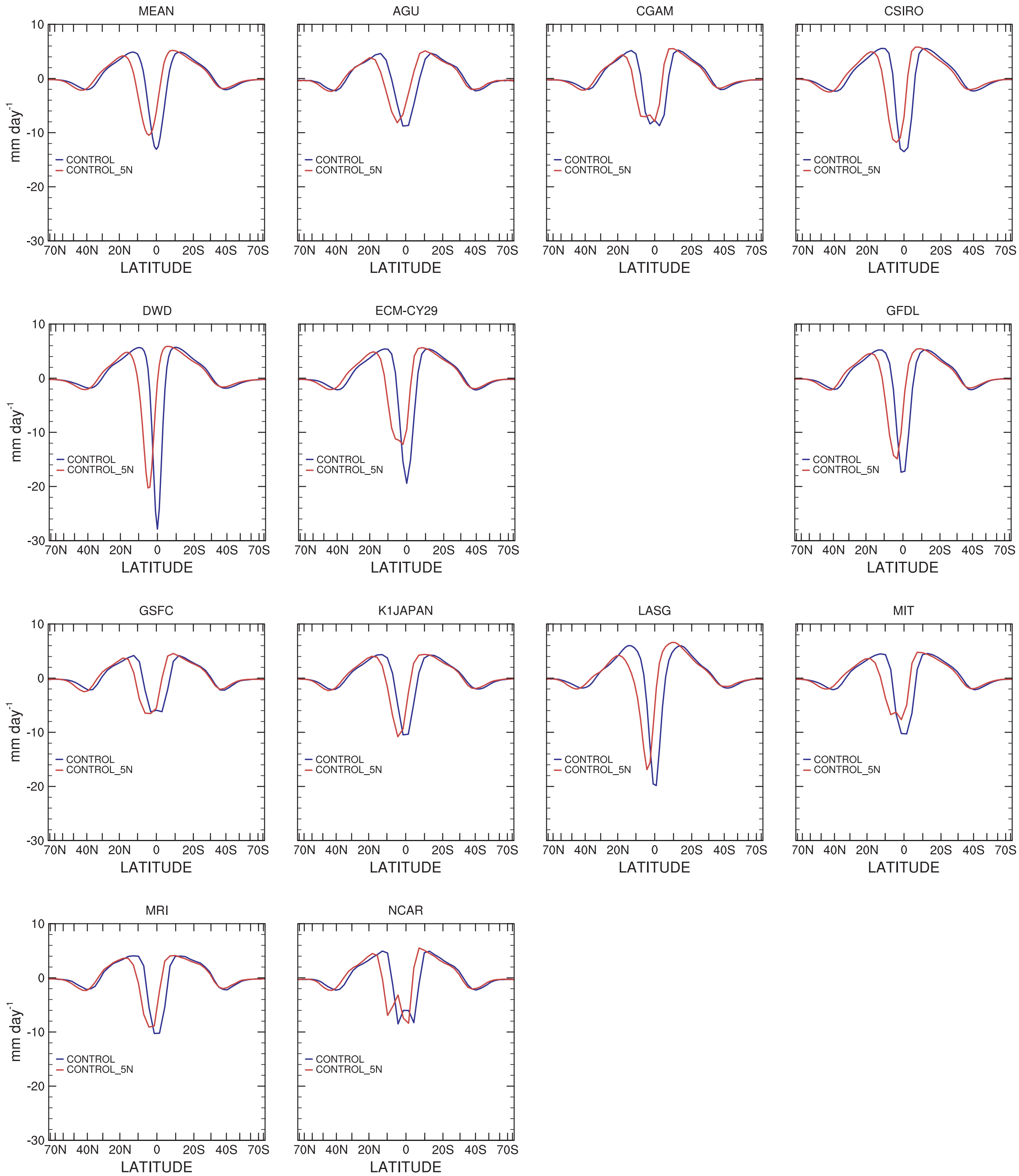

Figure 6.7: Zonal-time average evaporation minus precipitation (emp) for individual models from CONTROL and CONTROL_5N SST distributions, mm day^{-1}.

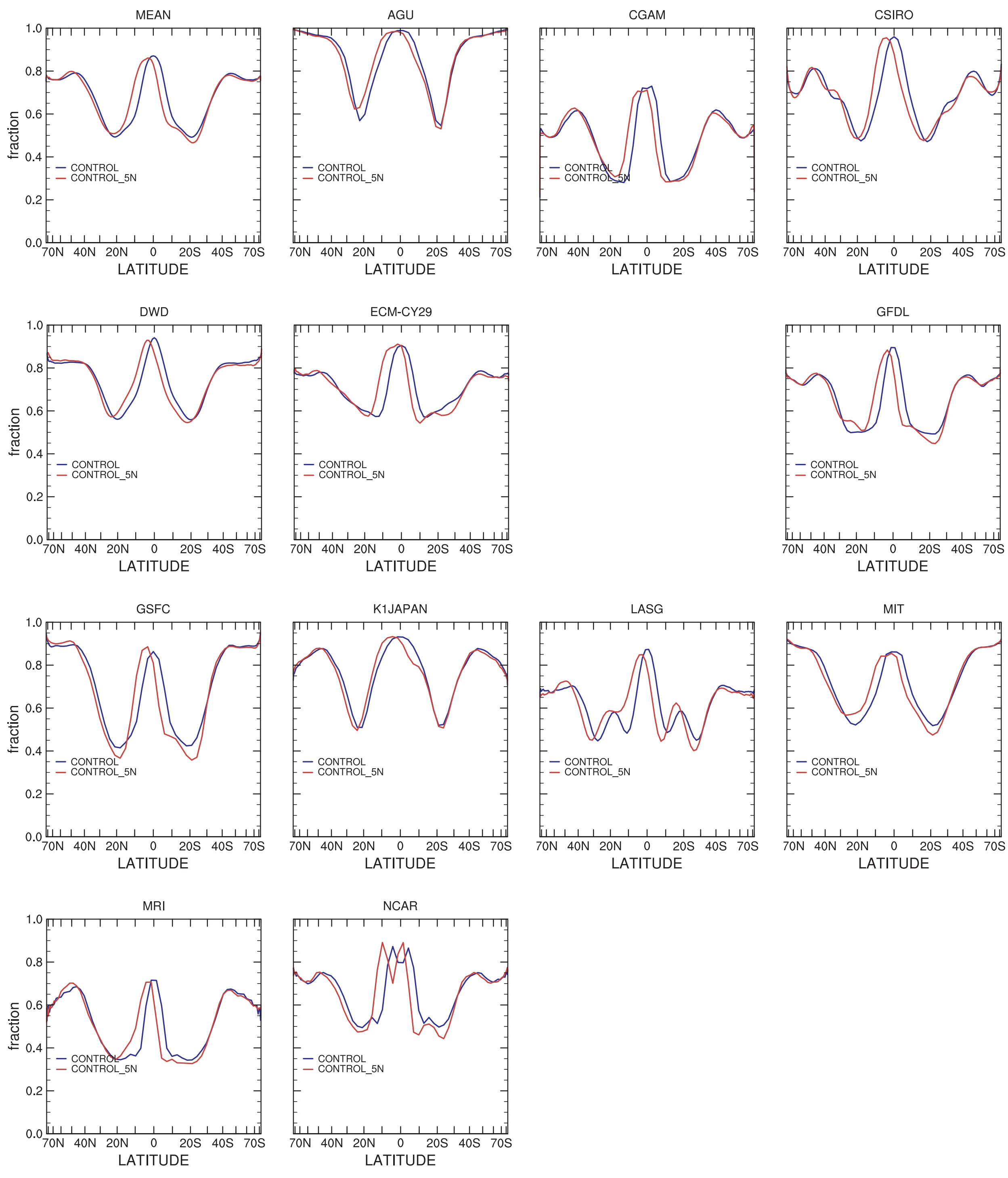

Figure 6.8: Zonal-time average cloud fraction (cld_frac) for individual models from CONTROL and CONTROL_5N SST distributions, fraction.

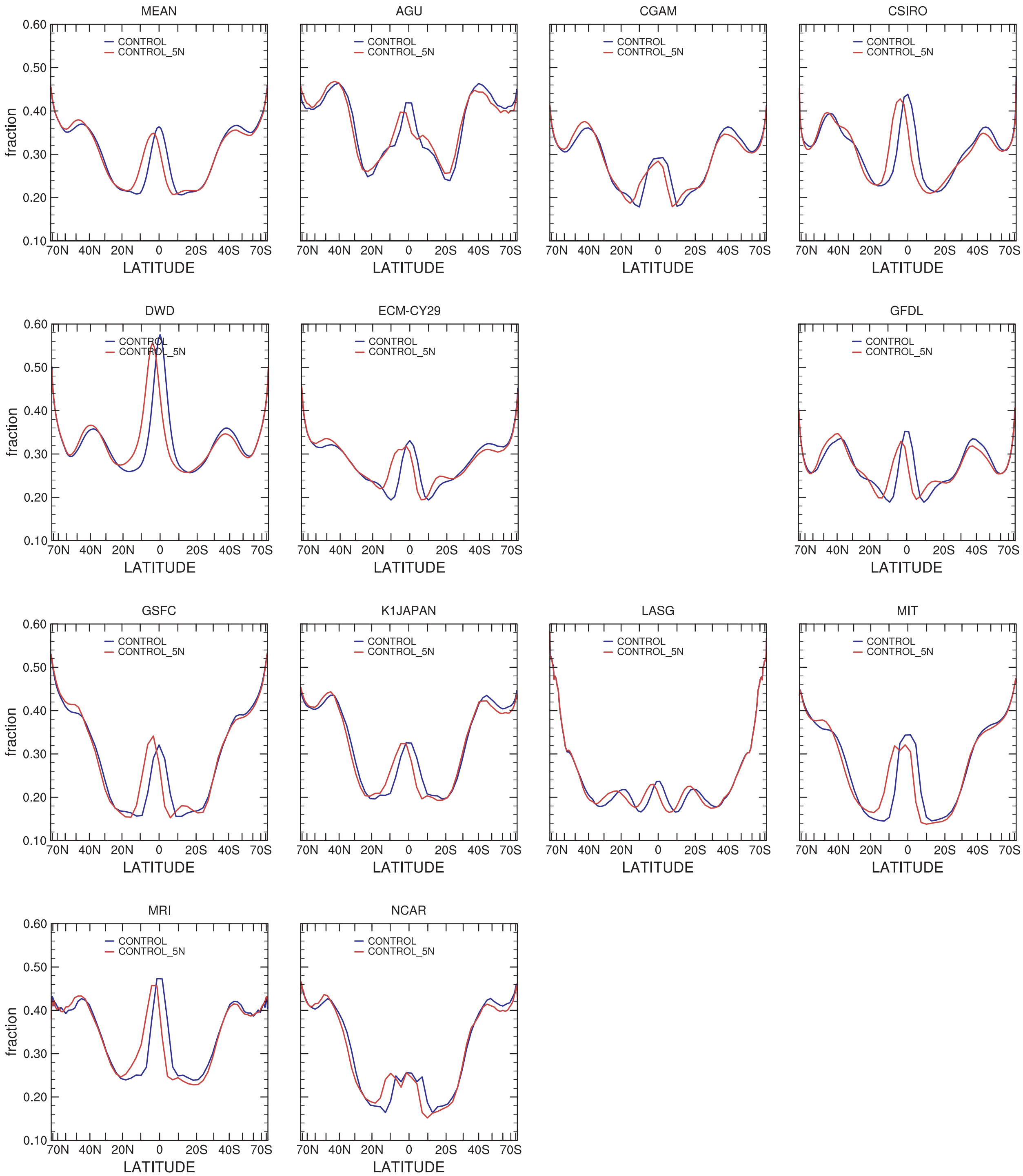

Figure 6.9: Zonal-time average albedo (albedo) for individual models from CONTROL and CONTROL_5N SST distributions, fraction.

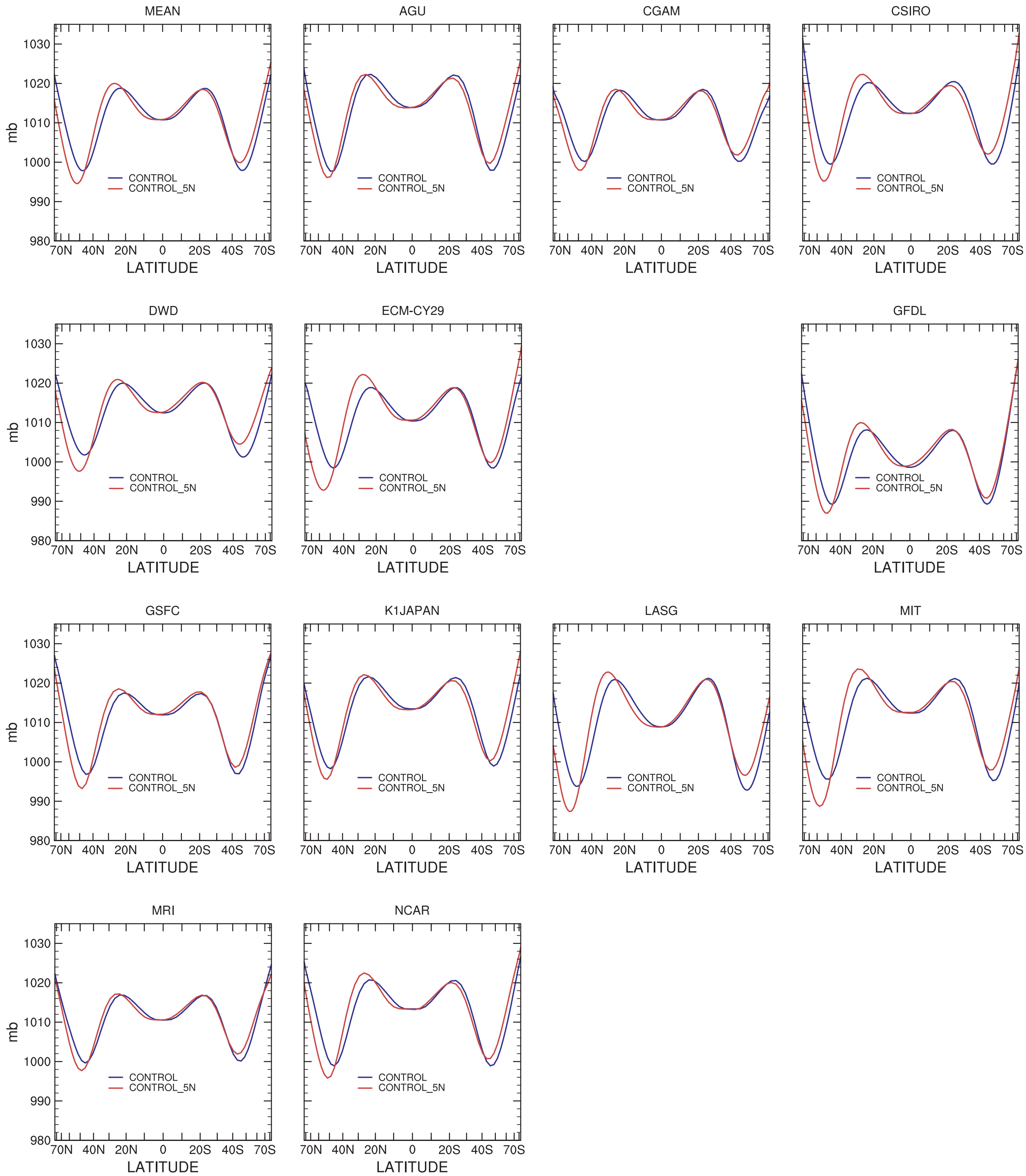

Figure 6.10: Zonal-time average surface pressure (ps) for individual models from CONTROL and CONTROL_5N SST distributions, mb.

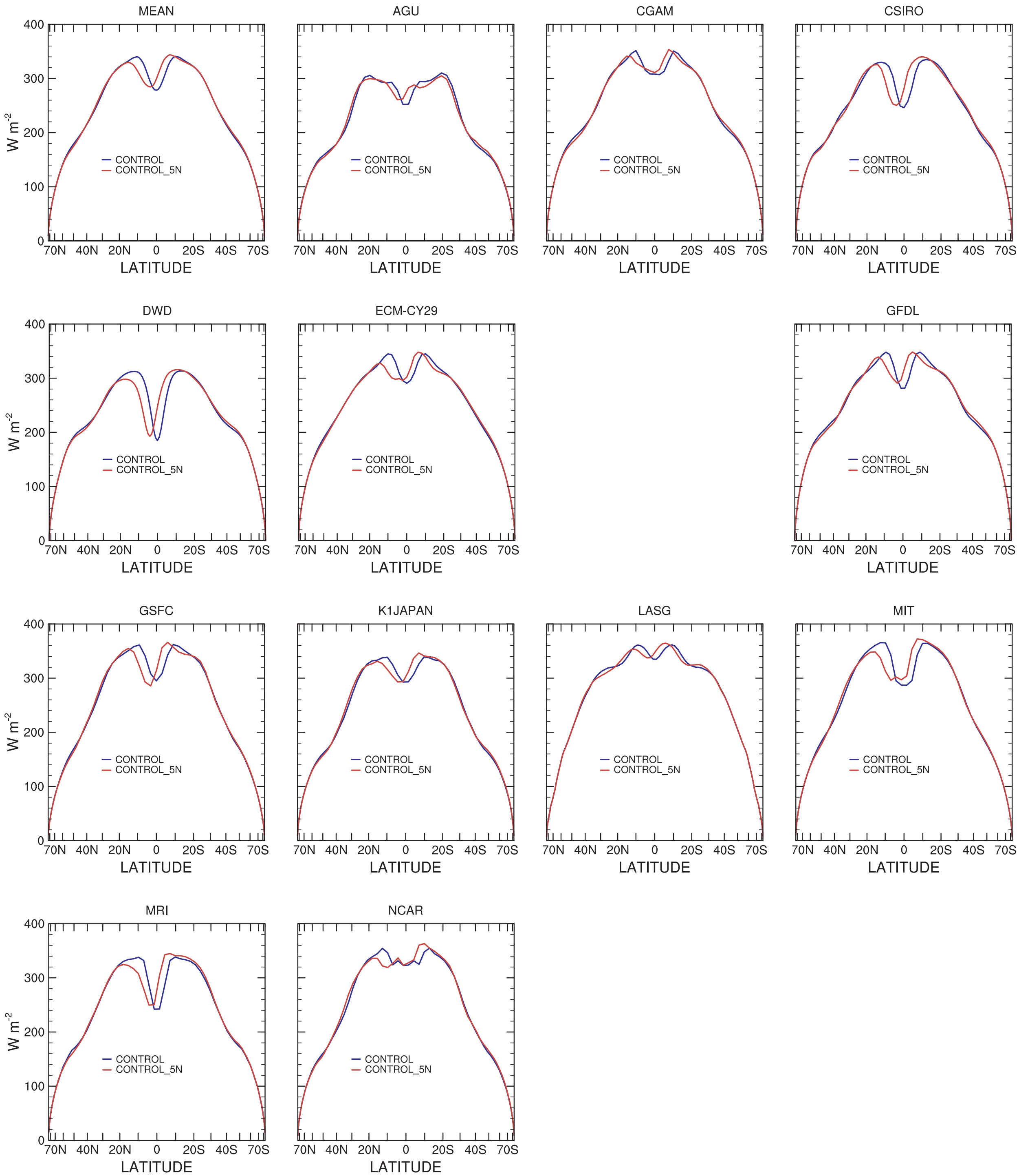

Figure 6.11: Zonal-time average TOA net shortwave radiation (sw_toa) for individual models from CONTROL and CONTROL_5N SST distributions, W m^{-2}, +ve downward.

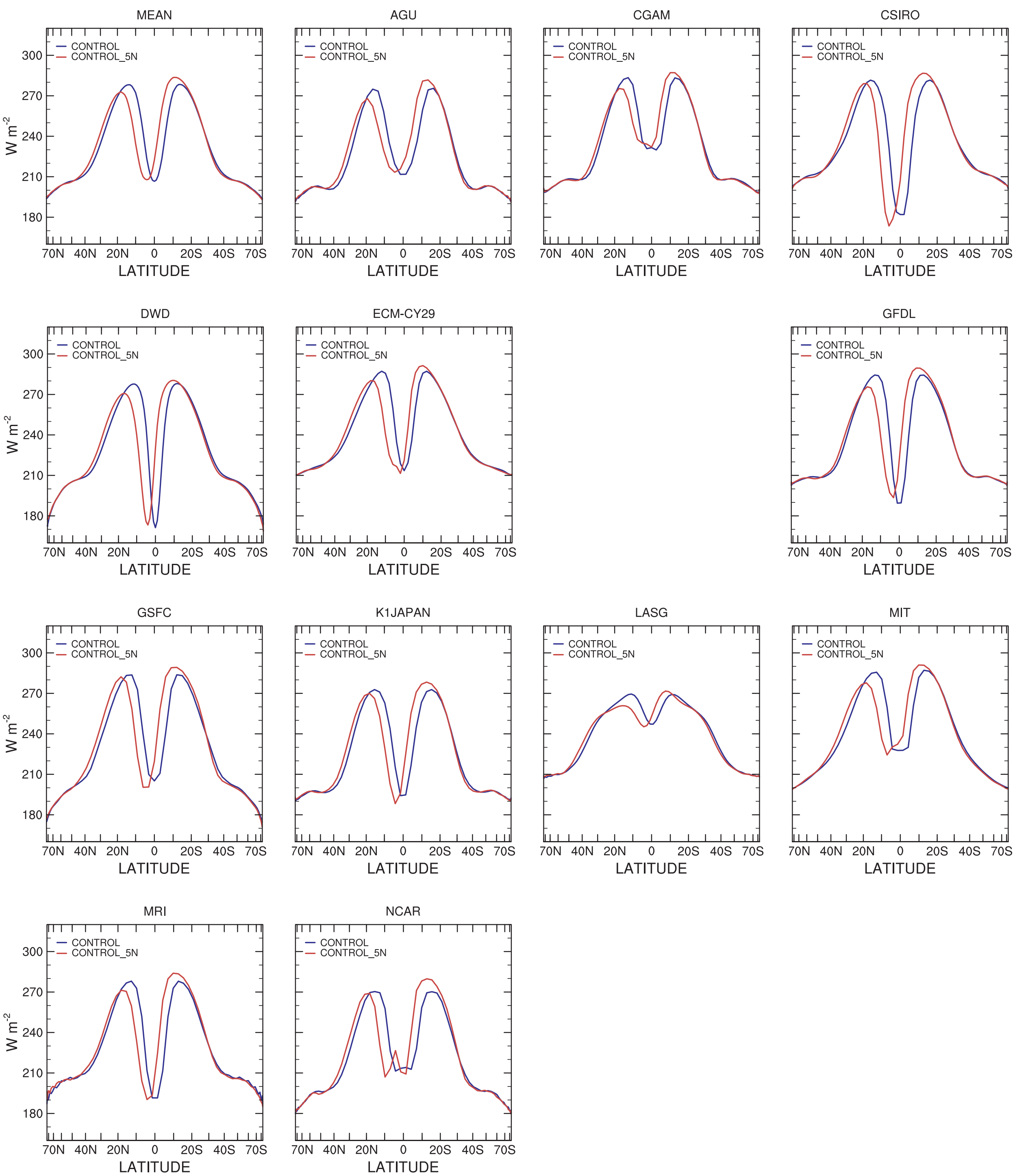

Figure 6.12: Zonal-time average TOA net longwave radiation (lw_toa) for individual models from CONTROL and CONTROL_5N SST distributions, W m^{-2}, +ve upward.

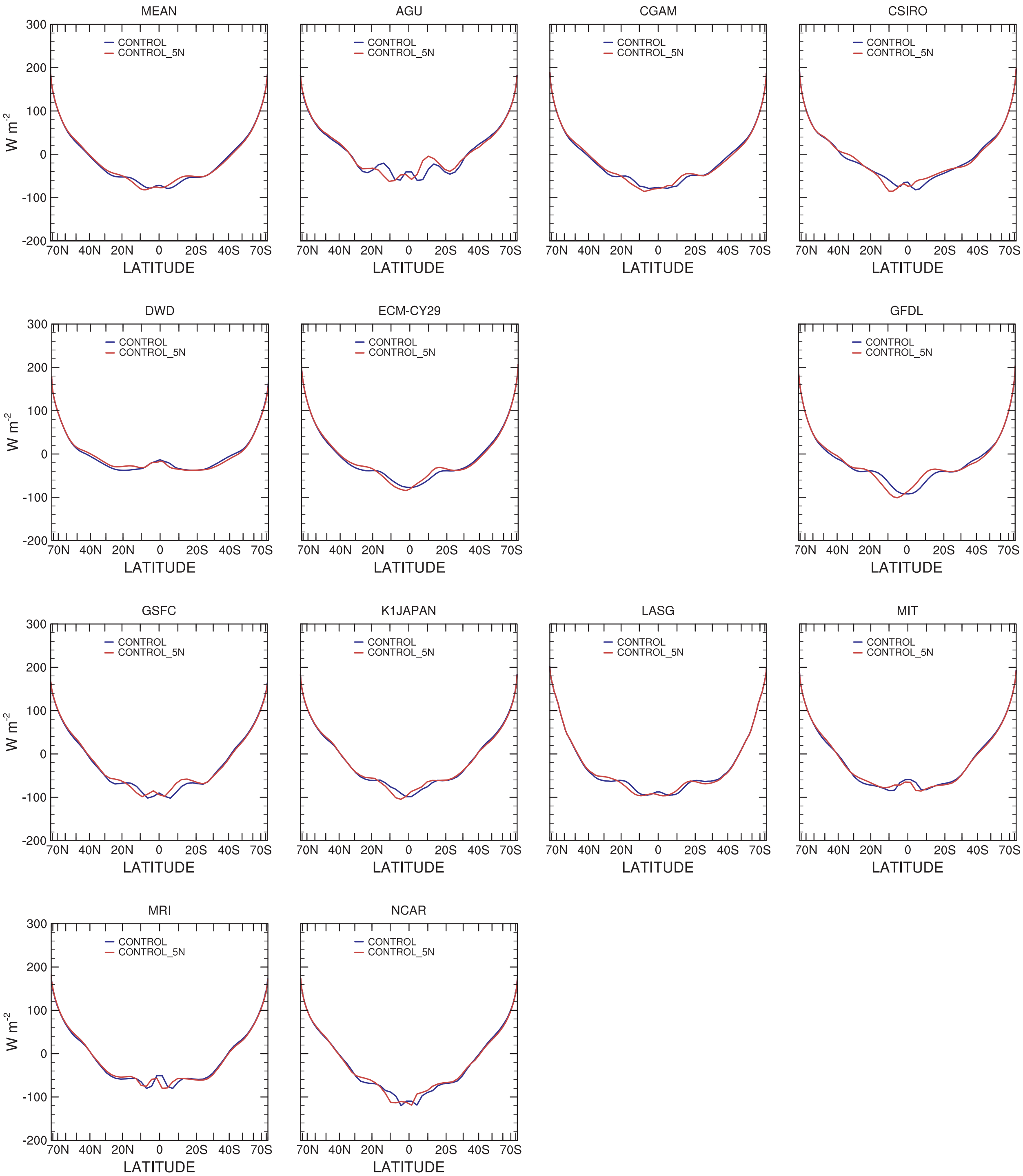

Figure 6.13: Zonal-time average TOA net radiation flux (rflux_toa) for individual models from CONTROL and CONTROL_5N SST distributions, W m^{-2}, +ve upward.

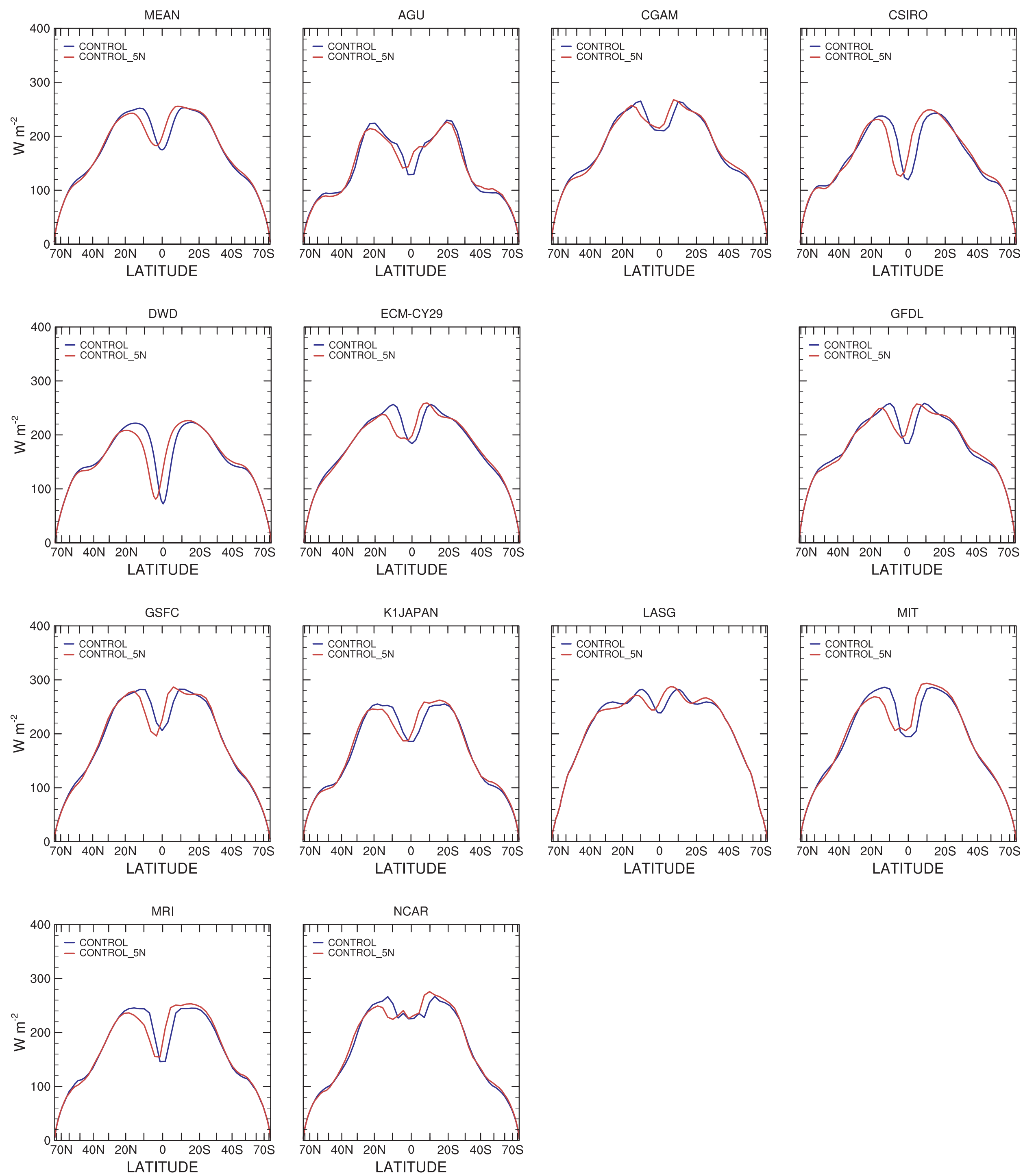

Figure 6.14: Zonal-time average surface net shortwave radiation (ssw) for individual models from CONTROL and CONTROL_5N SST distributions, W m^{-2}, +ve downward.

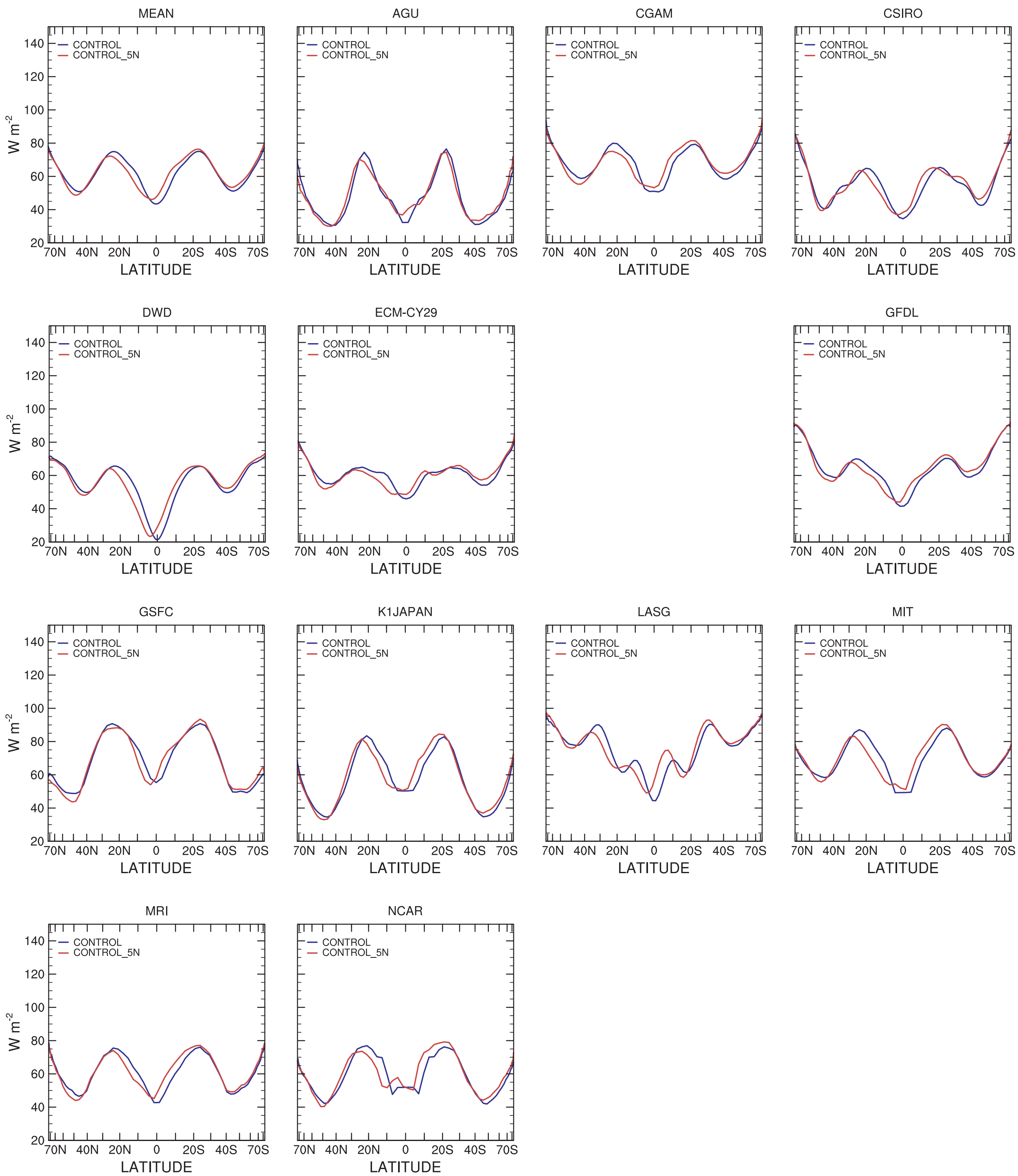

Figure 6.15: Zonal-time average surface net longwave radiation (slw) for individual models from CONTROL and CONTROL_5N SST distributions, W m^{-2}, +ve upward.

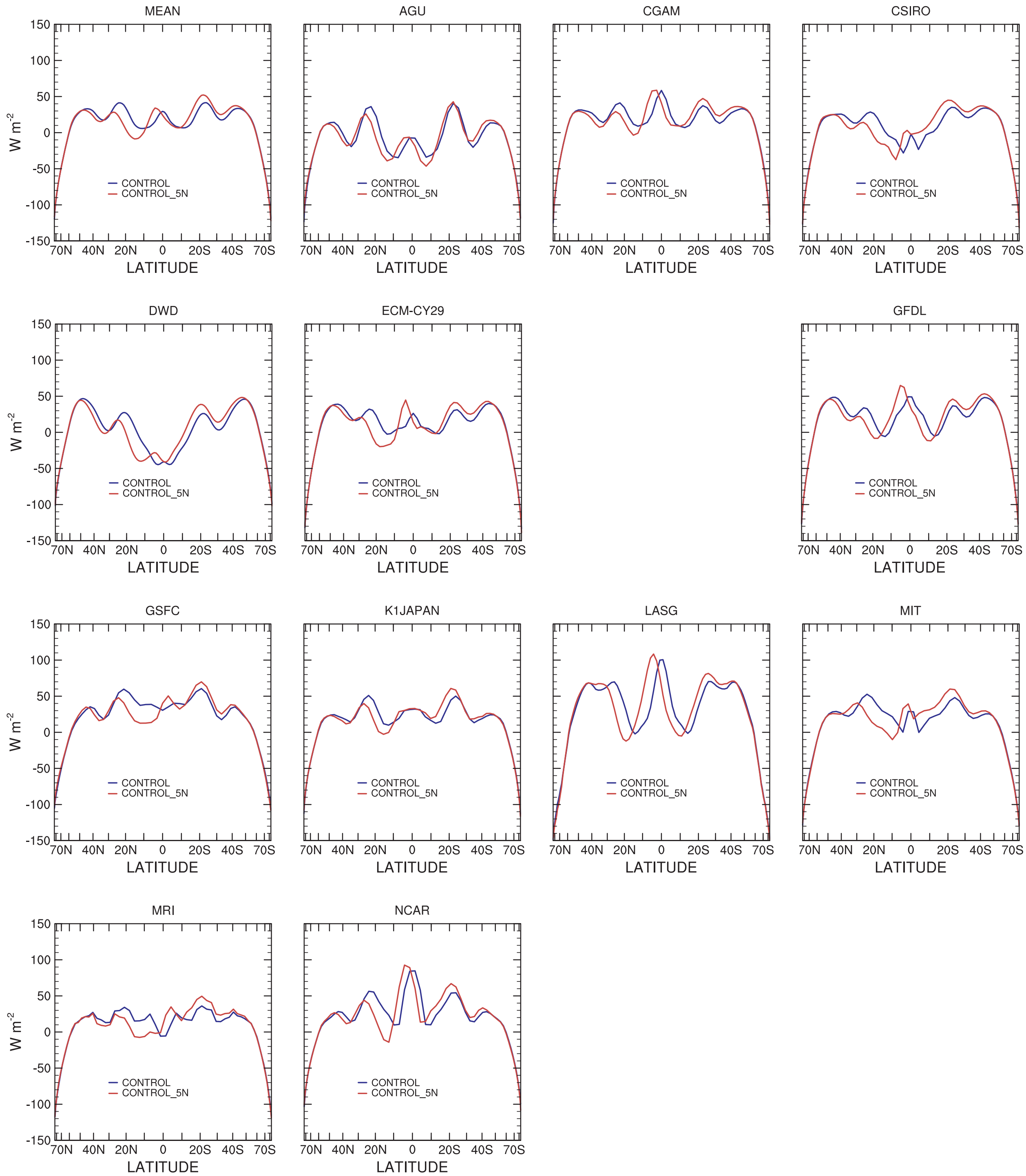

Figure 6.16: Zonal-time average surface net flux (rflux_sfce) for individual models from CONTROL and CONTROL_5N SST distributions, W m^{-2}, +ve downward.

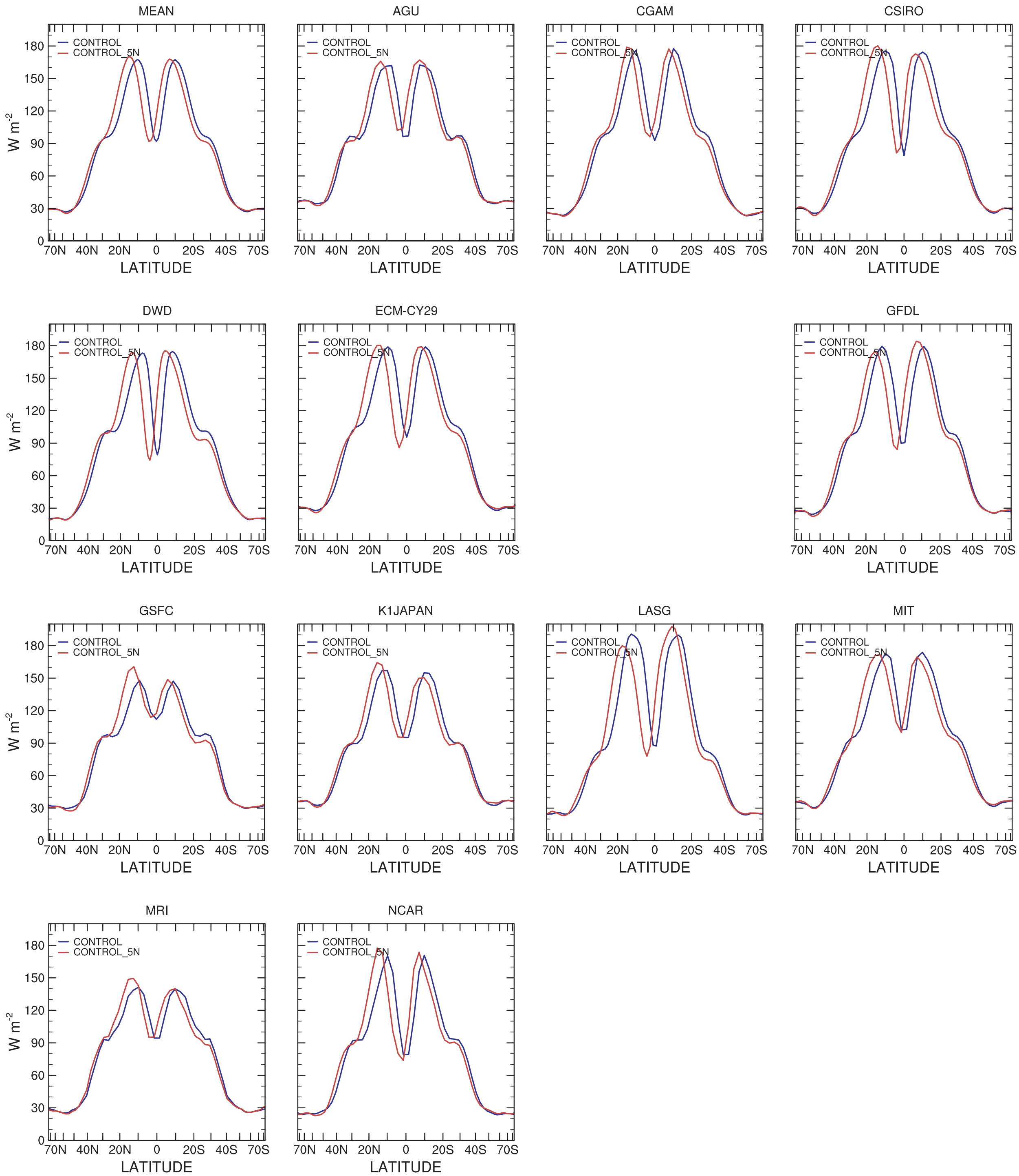

Figure 6.17: Zonal-time average surface latent heat flux (slh) for individual models from CONTROL and CONTROL_5N SST distributions, W m^{-2}.

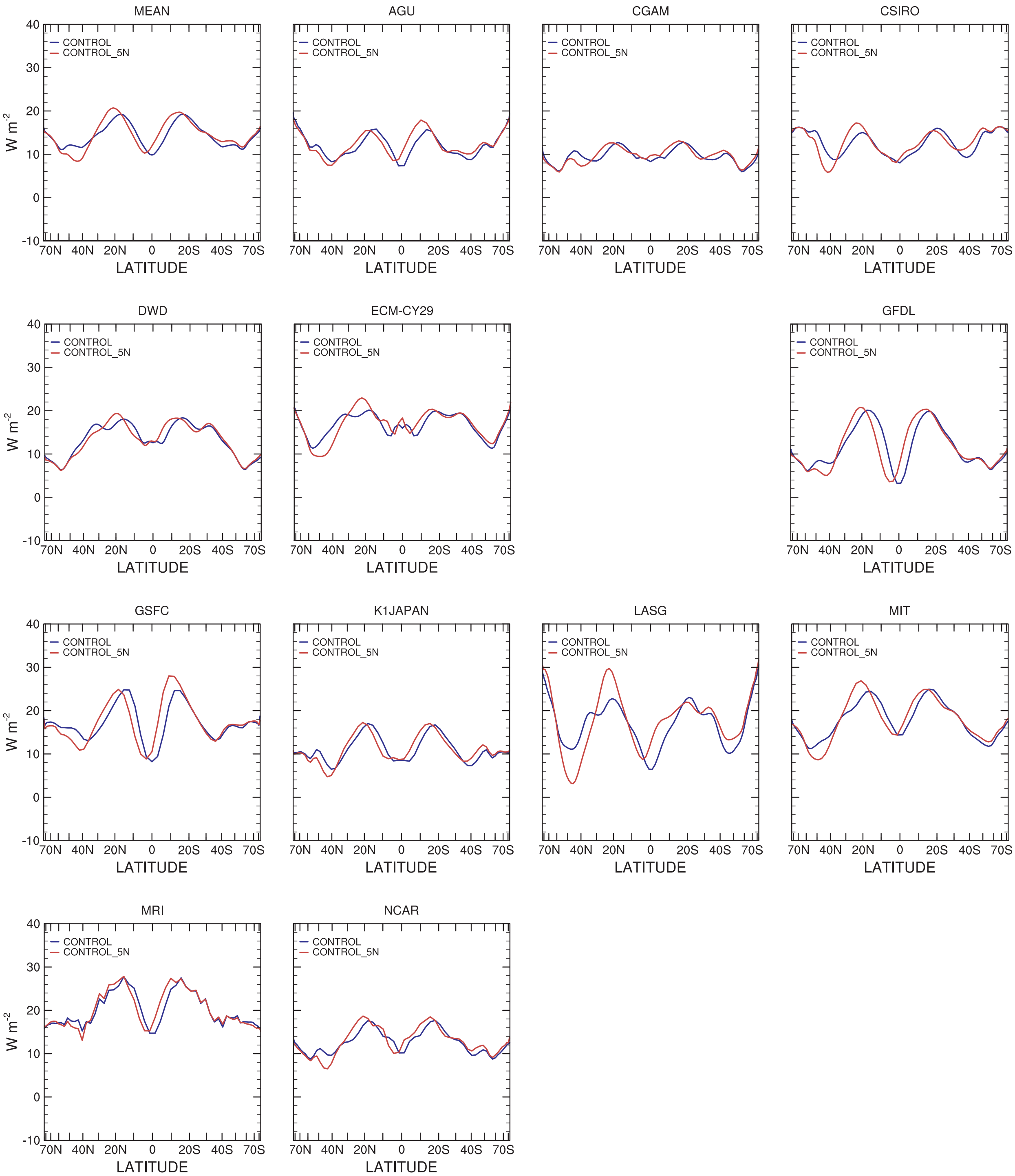

Figure 6.18: Zonal-time average surface sensible heat flux (ssh) for individual models from CONTROL and CONTROL_5N SST distributions, W m^{-2}.

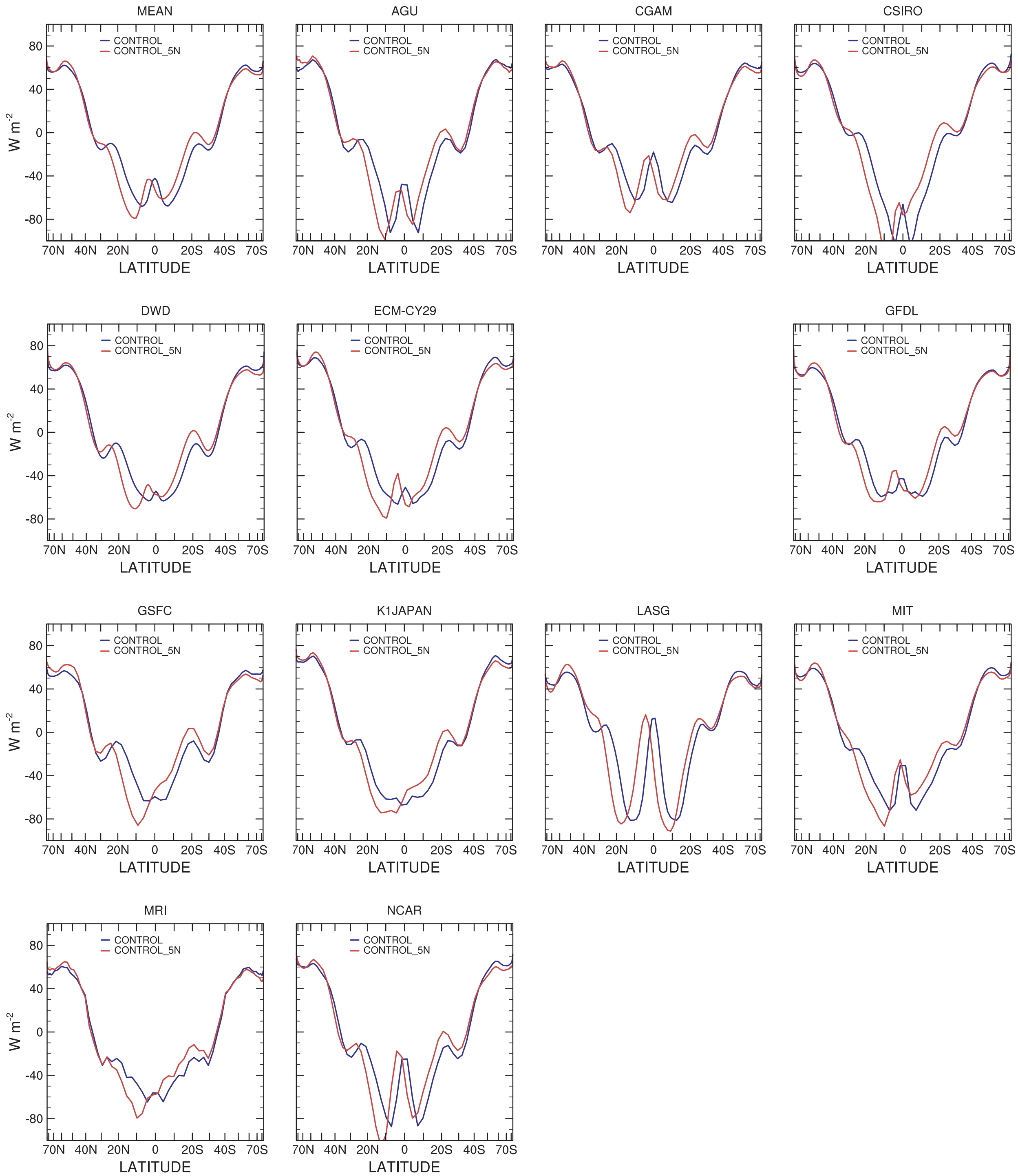

Figure 6.19: Zonal-time average net flux (rflux) for individual models from CONTROL and CONTROL_5N SST distributions, W m^{-2}, +ve out of atmosphere.

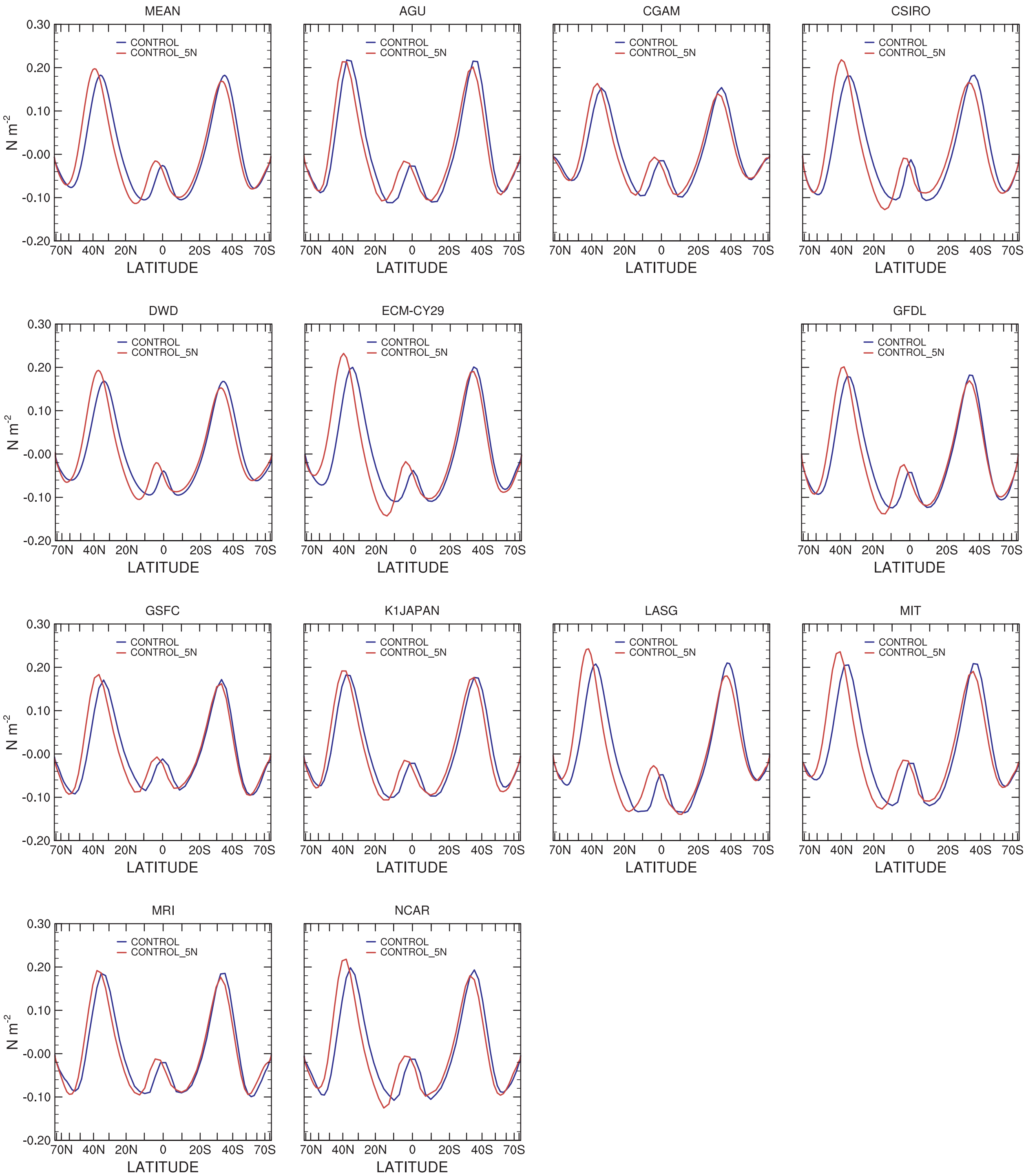

Figure 6.20: Zonal-time average zonal surface stress (tauu) for individual models from CONTROL and CONTROL_5N SST distributions, N m^{-2}.

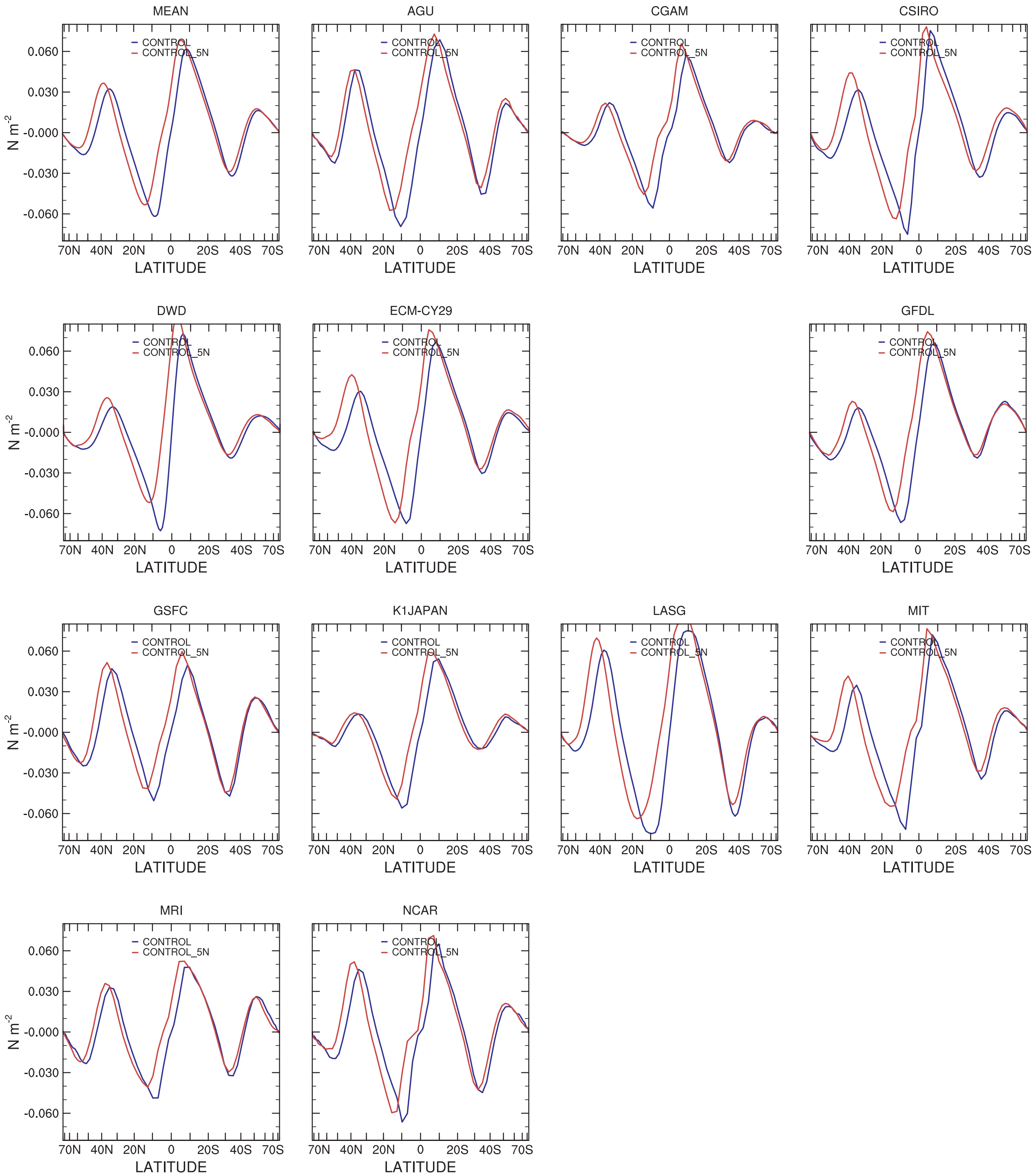

Figure 6.21: Zonal-time average meridional surface stress (tauv) for individual models from CONTROL and CONTROL_5N SST distributions, N m^{-2}.

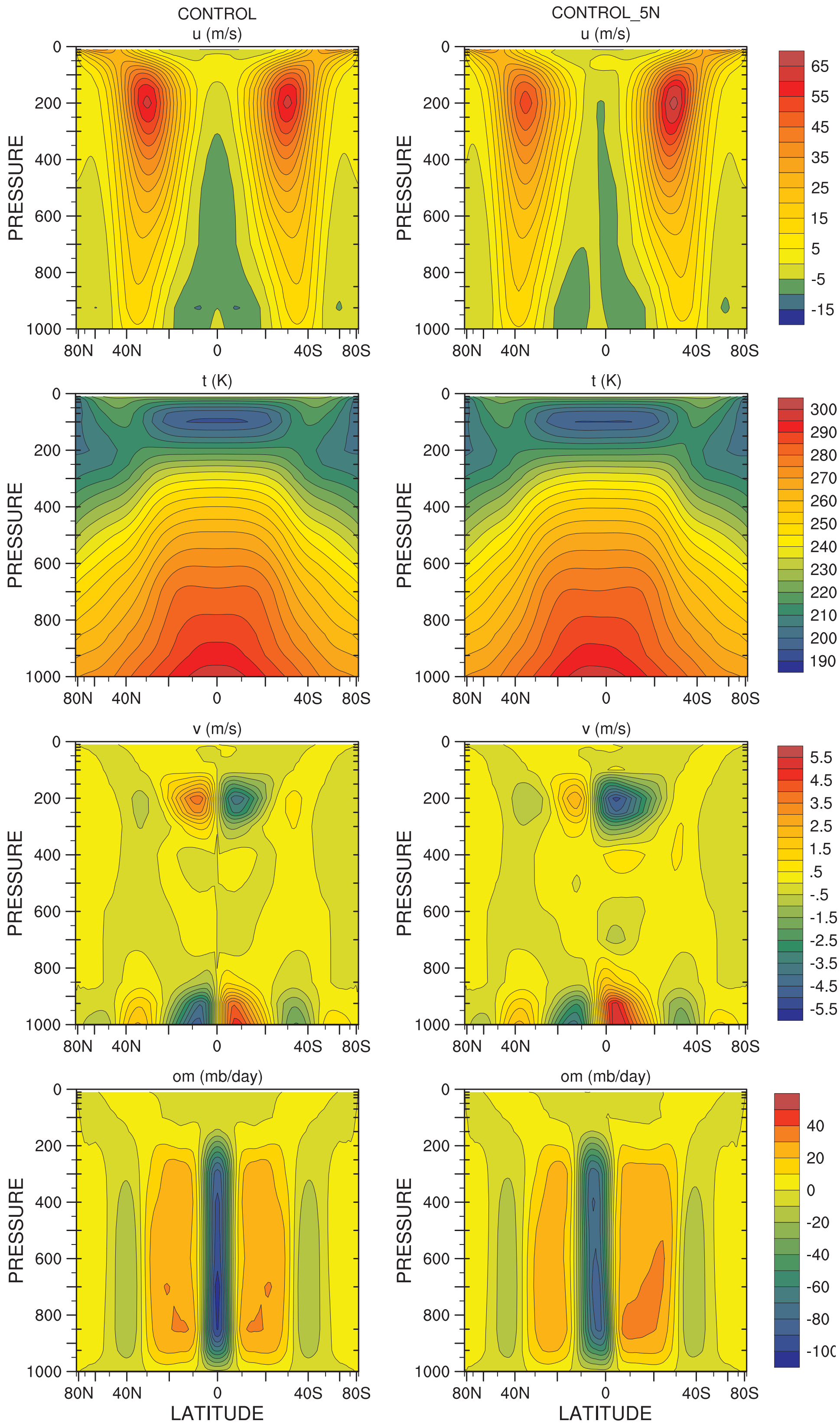

Figure 6.22: Zonal-time average multi-model mean zonal wind (u), temperature (t), meridional wind (v) and vertical wind (om) for CONTROL and CONTROL_5N SST.

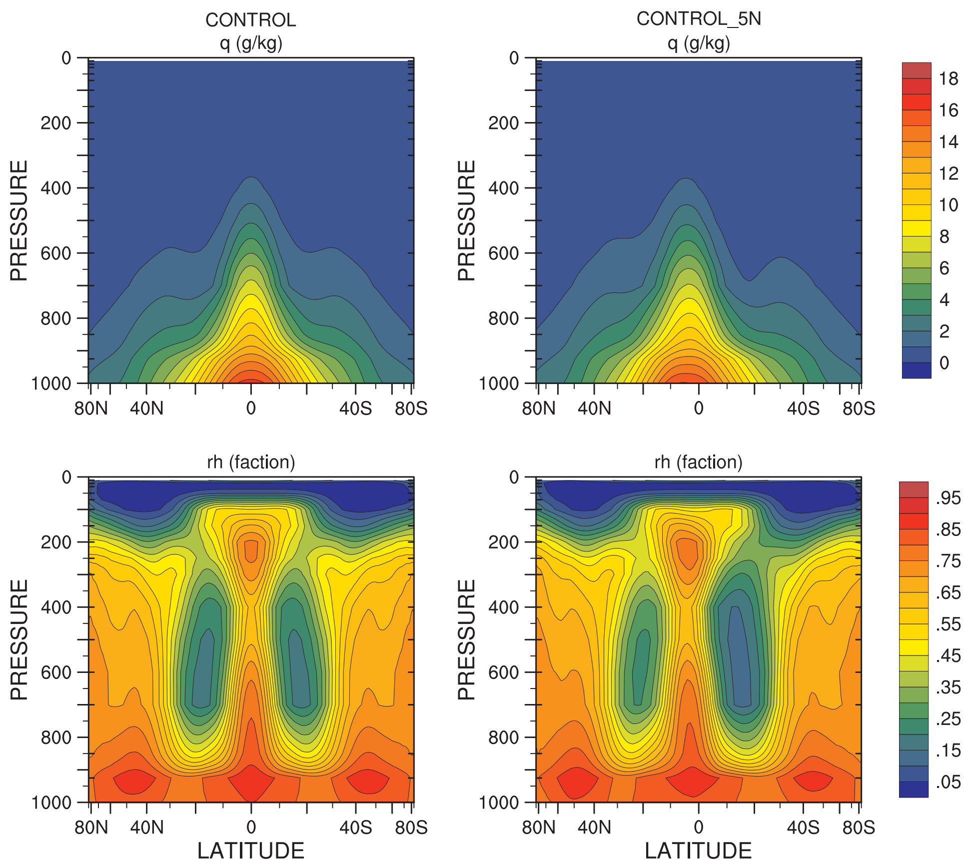

Figure 6.23: Zonal-time average multi-model mean specific humidity (q) and relative humidity (rh) for CONTROL and CONTROL_5N SST.

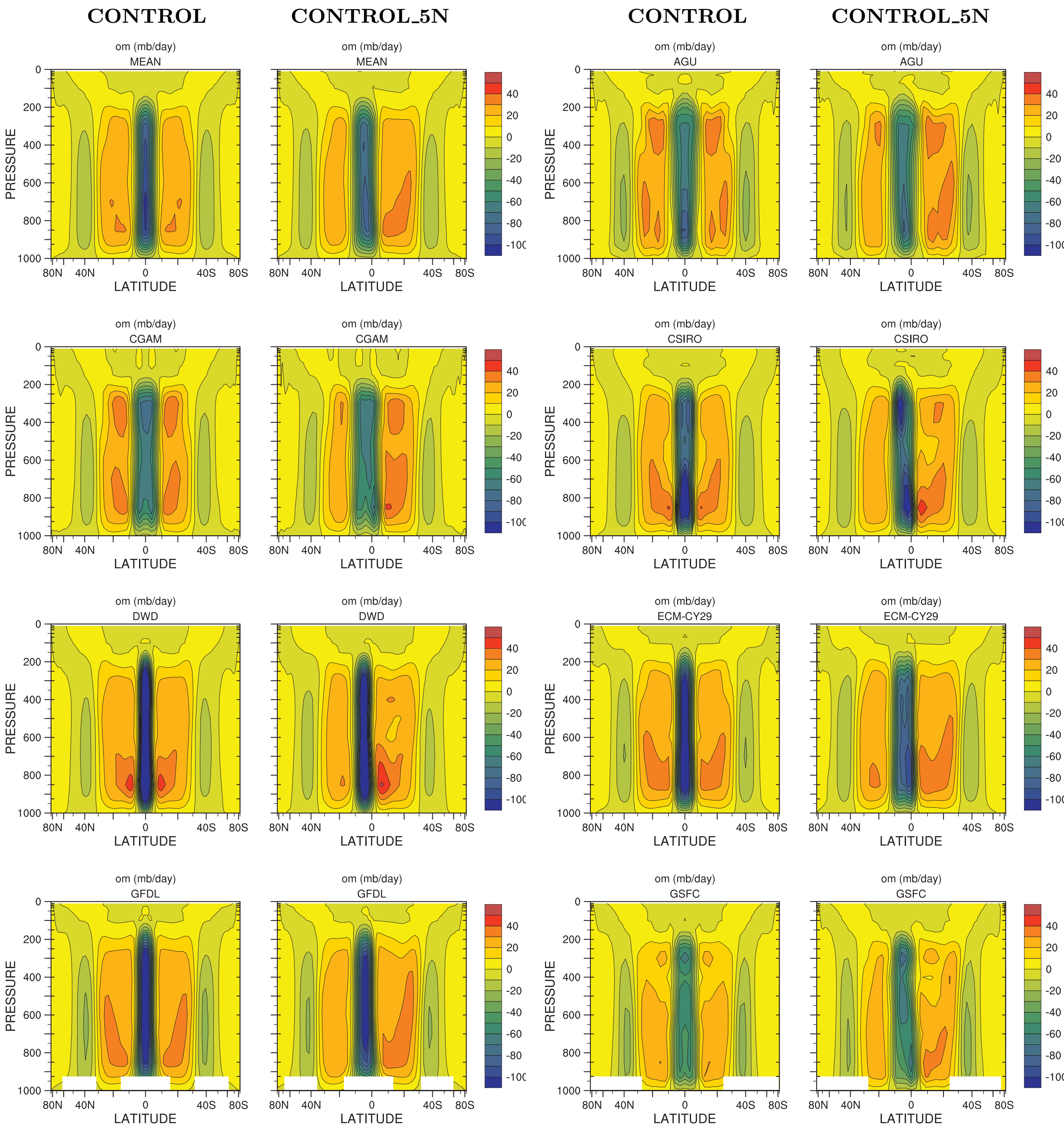

Figure 6.24: Zonal-time average vertical velocity (om), CONTROL and CONTROL_5N, individual models, mb day^{-1}.

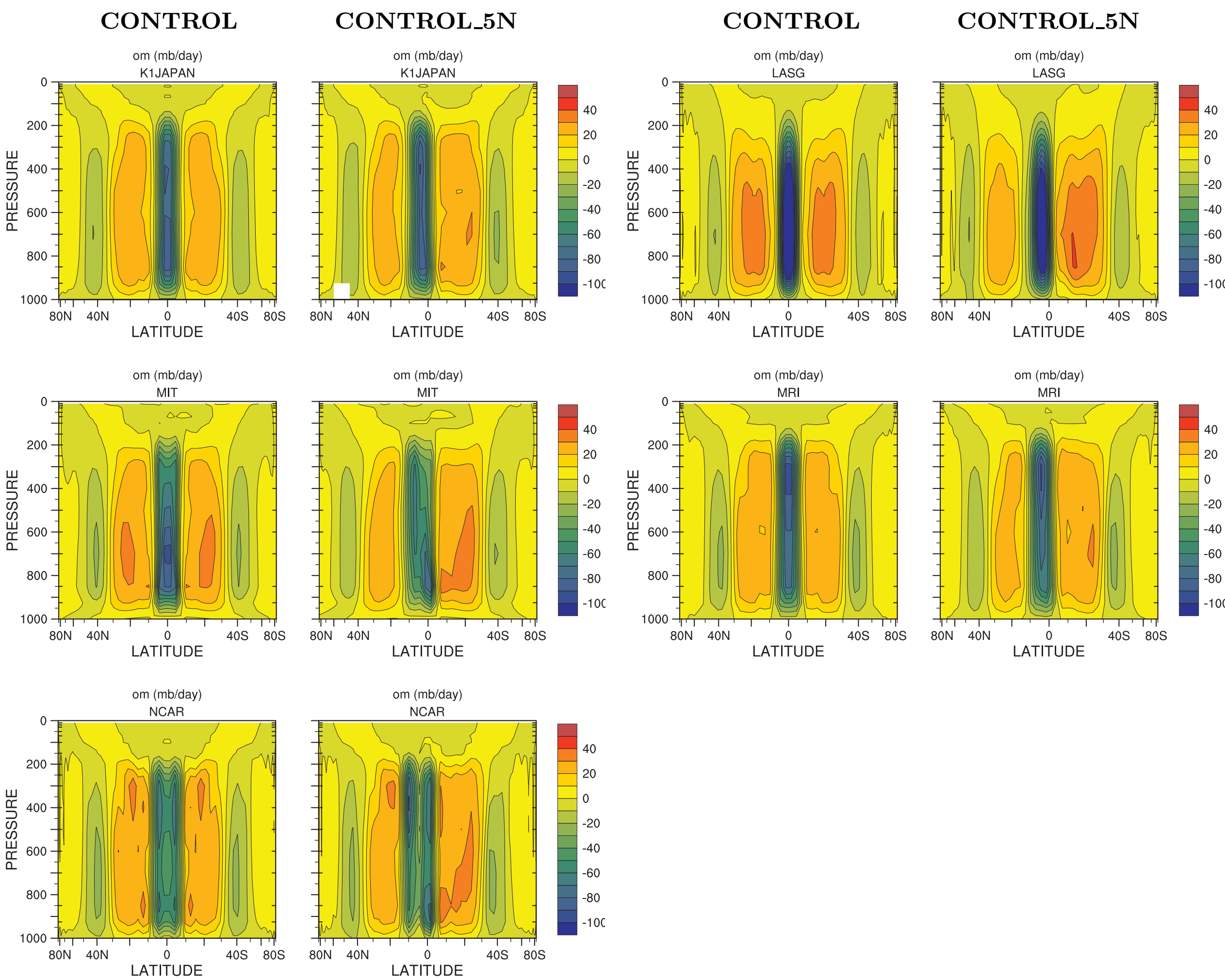

Figure 6.24 (continued): Zonal-time average vertical velocity (om), CONTROL and CONTROL_5N, individual models, mb day^{-1}.

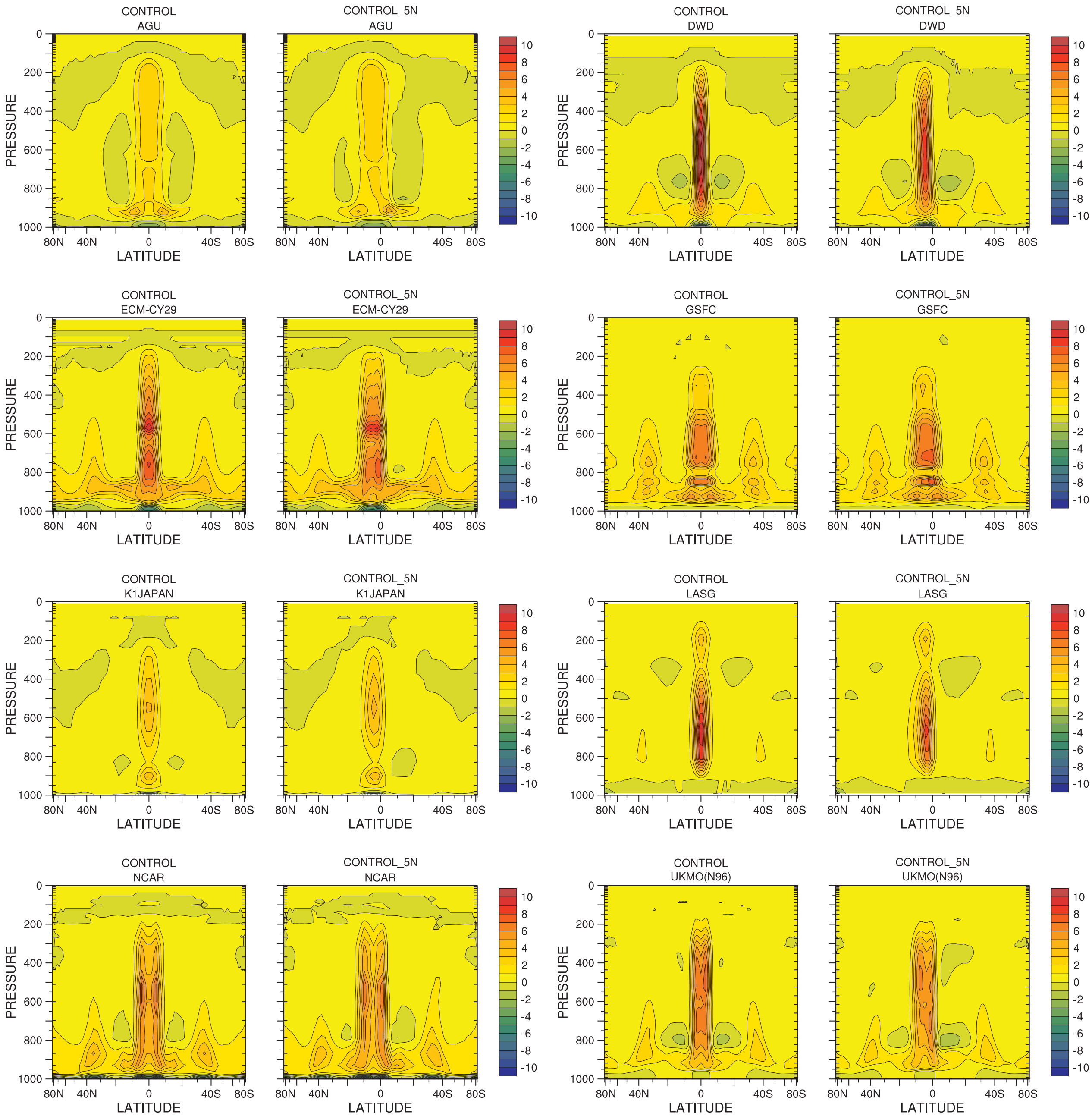

Figure 6.25: Zonal-time average parameterized convection temperature tendency (t_conv) for individual models for CONTROL and CONTROL_5N, K day^{-1}.

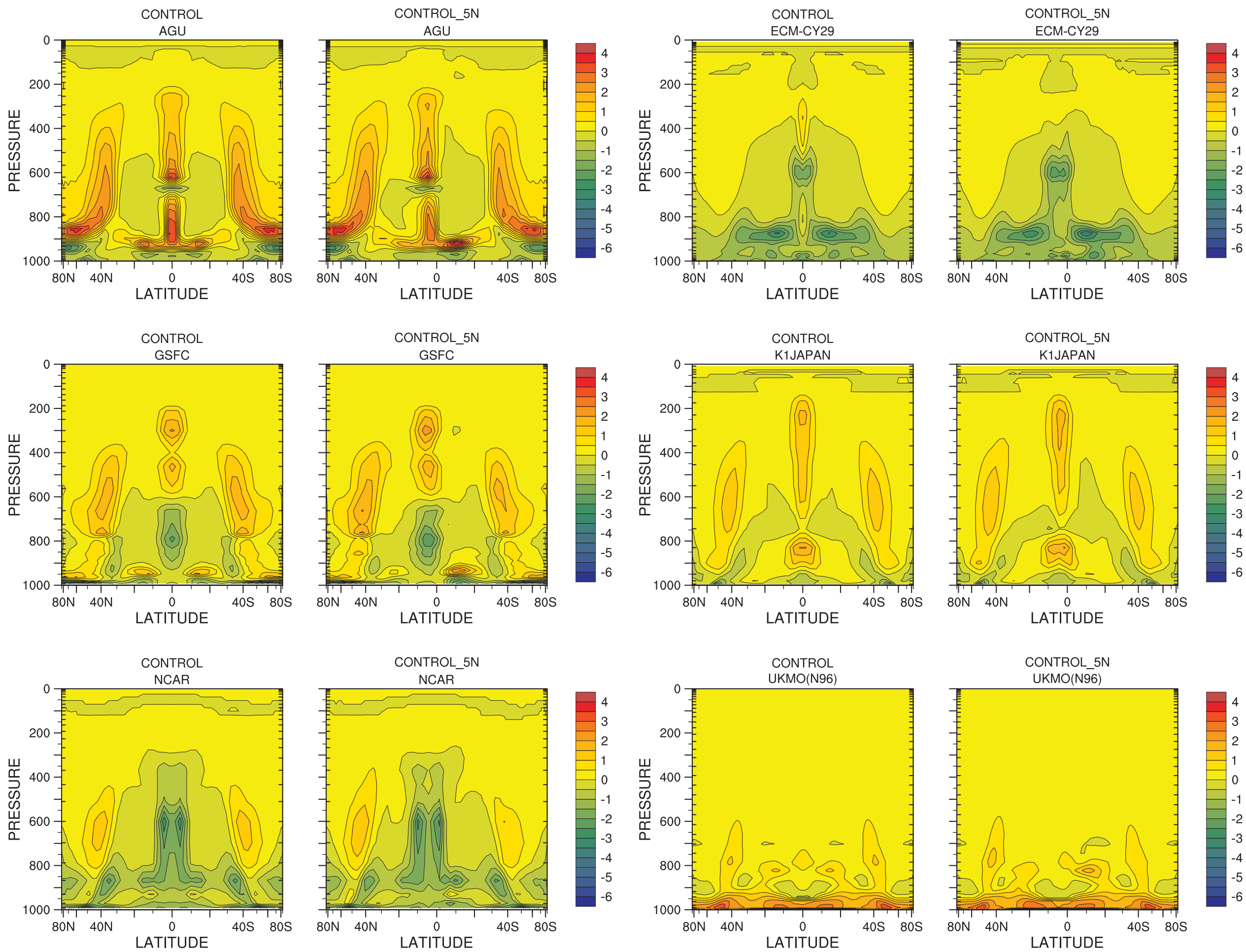

Figure 6.26: Zonal-time average parameterized cloud temperature tendency (t_cld) for individual models for CONTROL and CONTROL_5N, K day^{-1}.

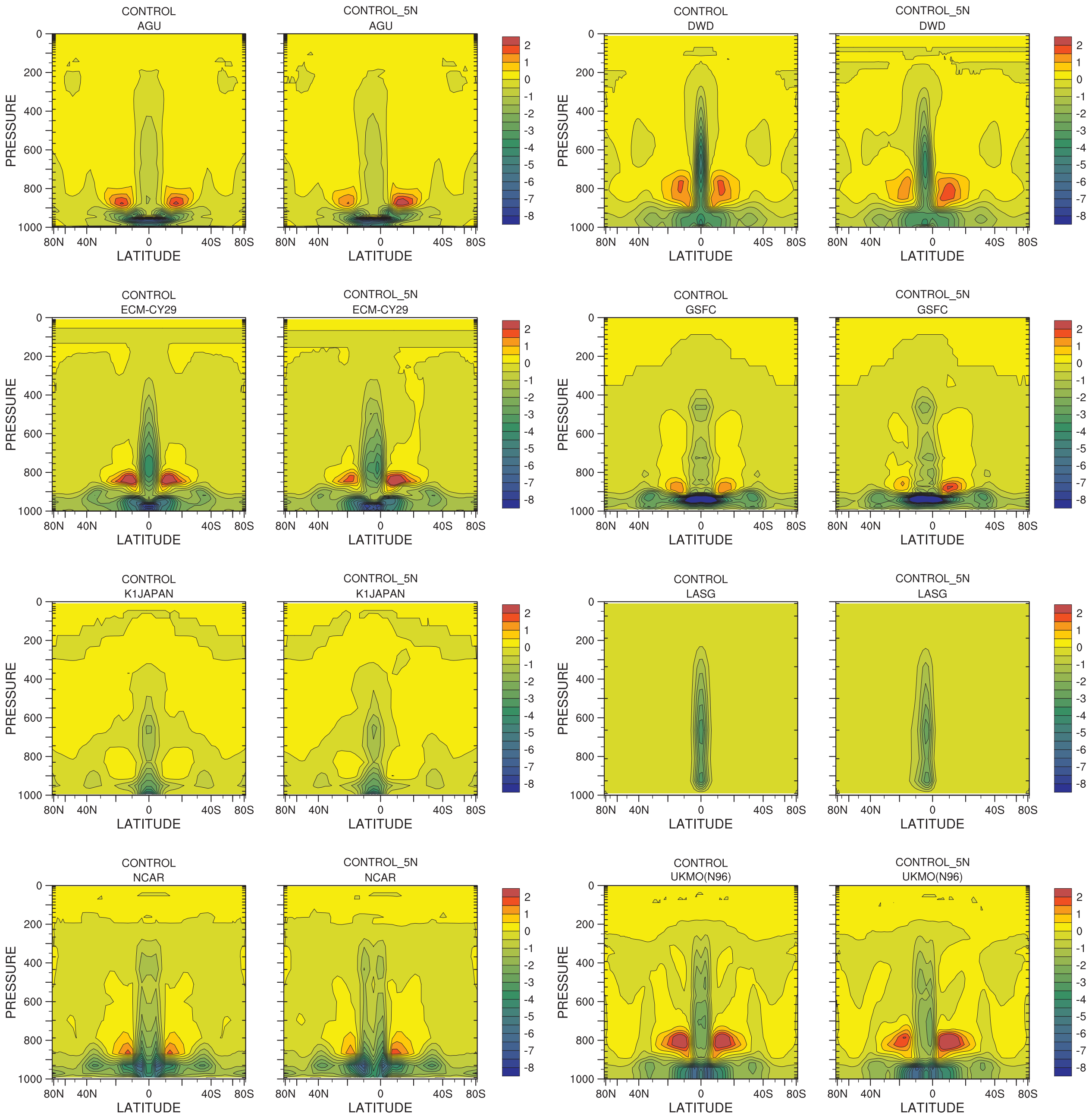

Figure 6.27: Zonal-time average parameterized convection specific humidity tendency (q_conv) for individual models for CONTROL and CONTROL_5N, g kg^{-1} day^{-1}.

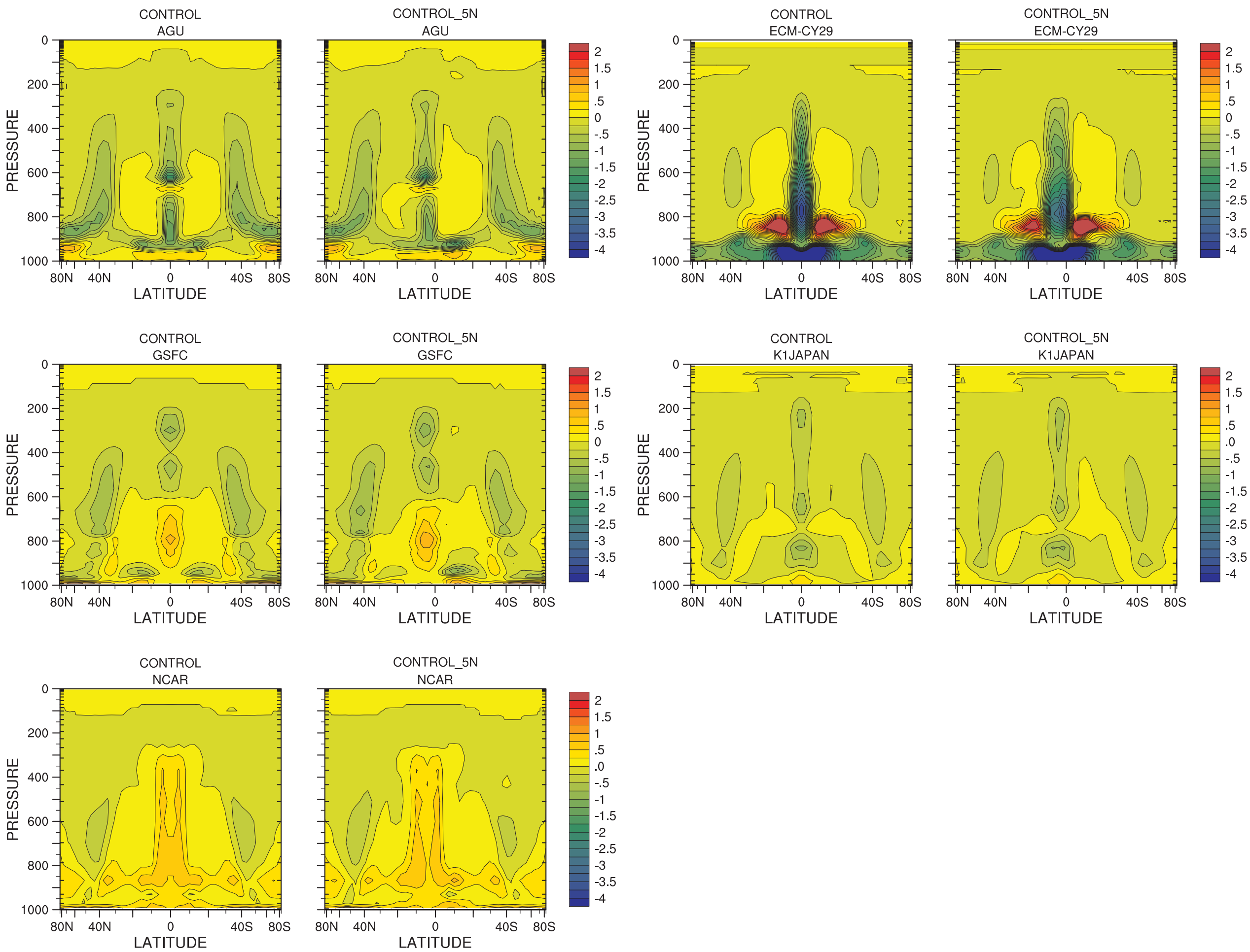

Figure 6.28: Zonal-time average parameterized cloud specific humidity tendency (q_cld) for individual models for CONTROL and CONTROL_5N, g kg^{-1} day^{-1}.

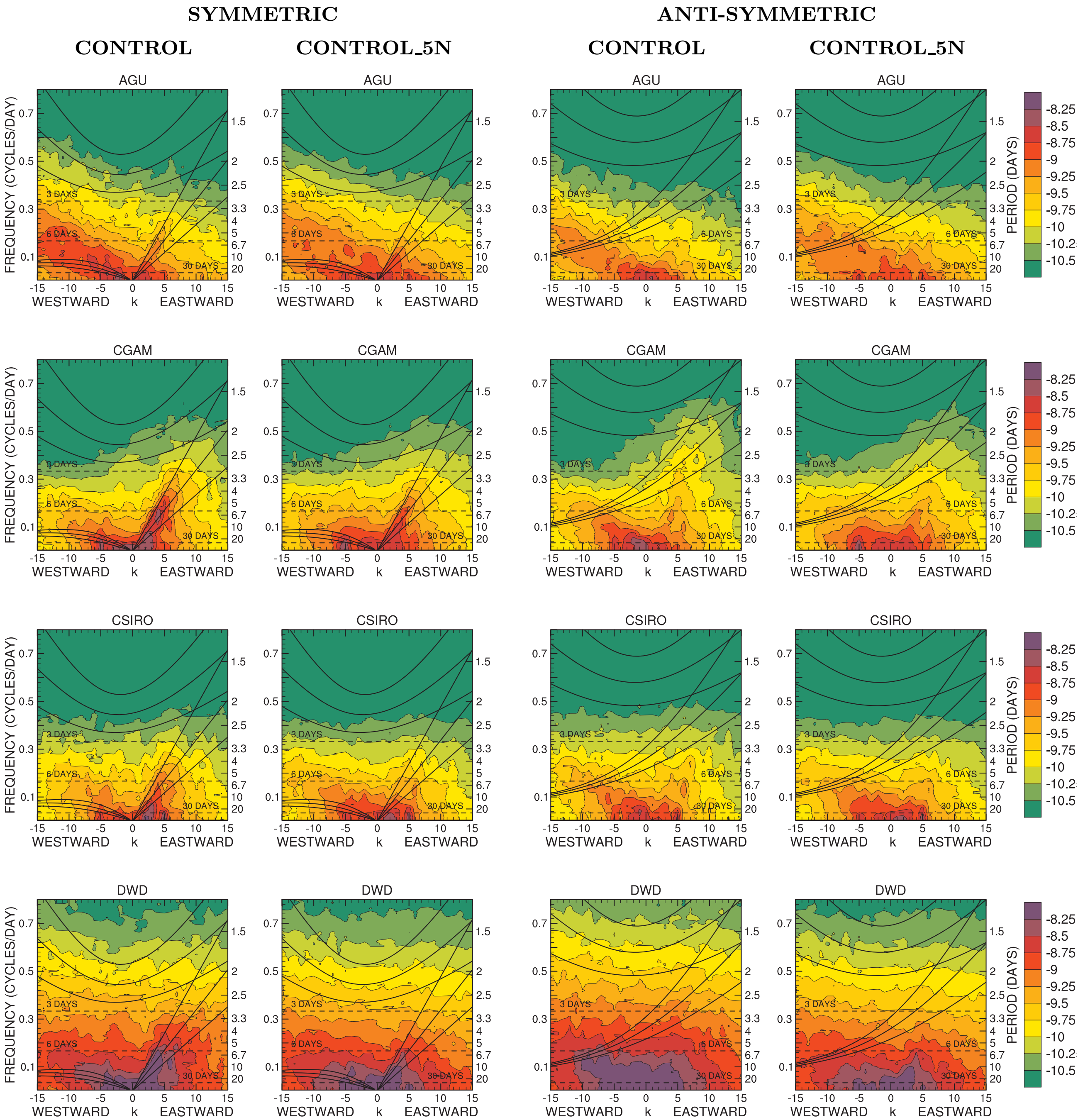

Figure 6.29: Wavenumber-frequency diagrams of log of power of symmetric and anti-symmetric modes of equatorial precipitation (tppn) for CONTROL and CONTROL_5N, 20°S to 20°N.

SYMMETRIC **ANTI-SYMMETRIC**

CONTROL **CONTROL_5N** **CONTROL** **CONTROL_5N**

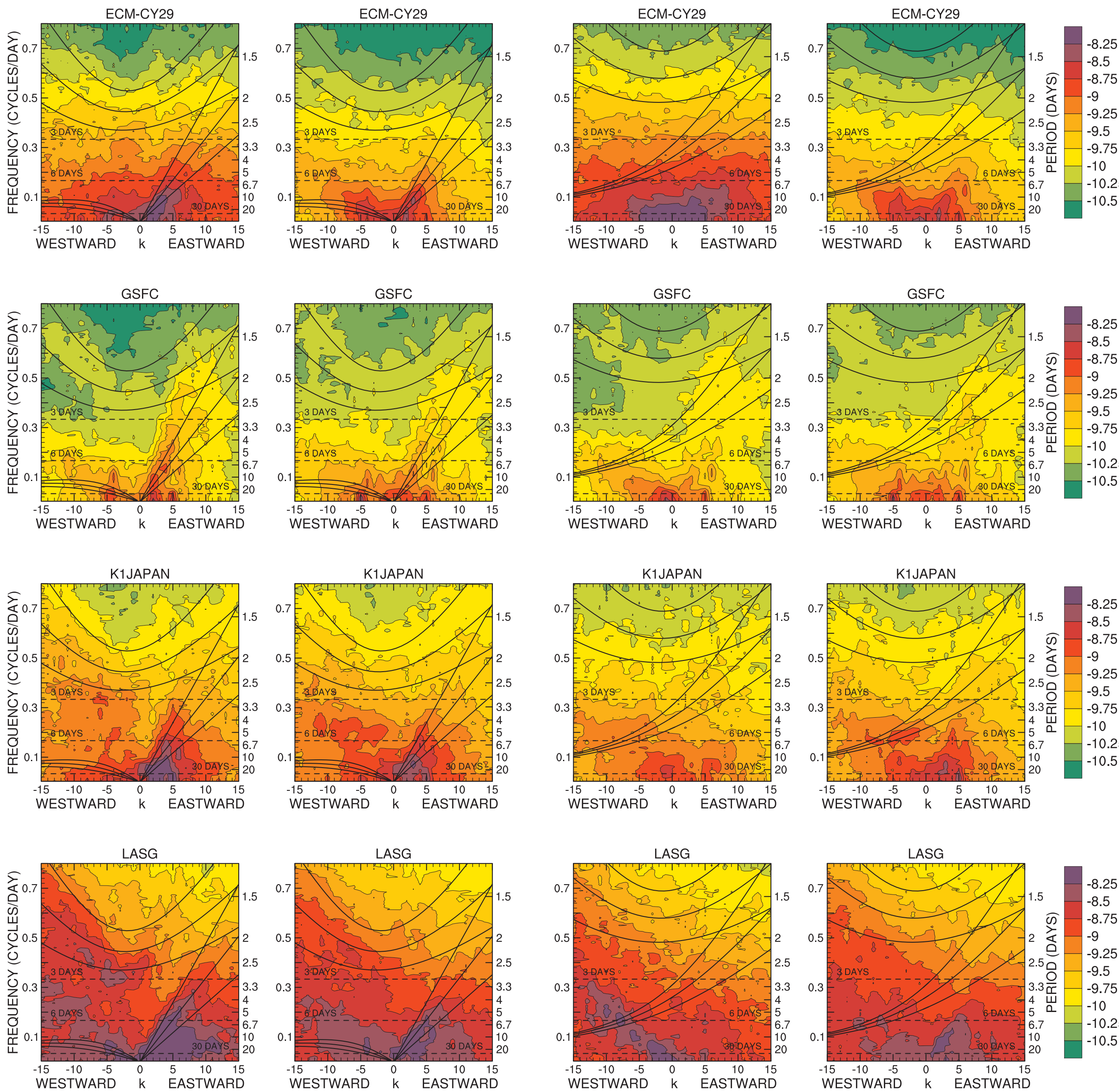

Figure 6.29 (continued): Wavenumber-frequency diagrams of log of power of symmetric and anti-symmetric modes of equatorial precipitation (tppn) for CONTROL and CONTROL_5N, 20°S to 20°N.

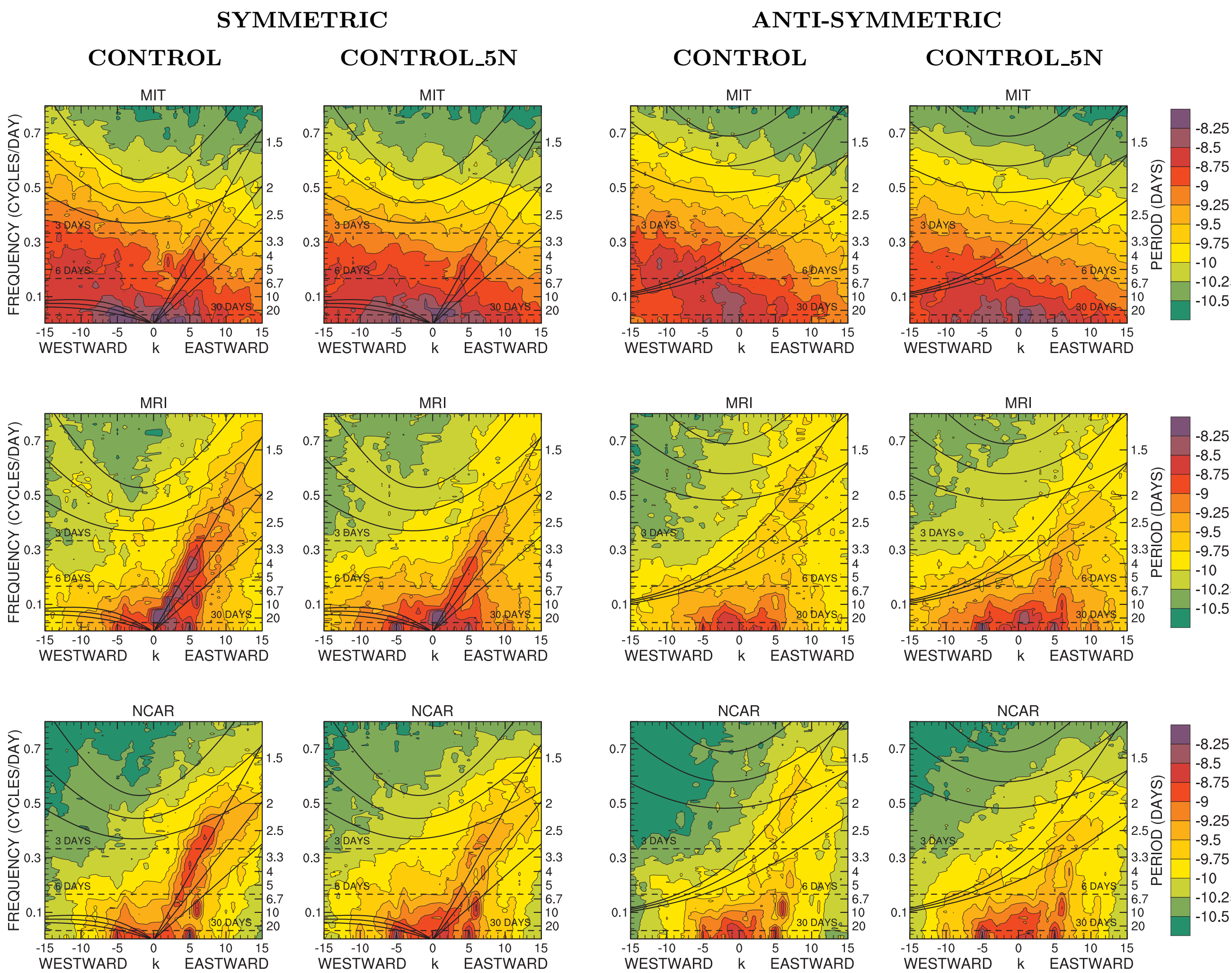

Figure 6.29 (continued): Wavenumber-frequency diagrams of log of power of symmetric and anti-symmetric modes of equatorial precipitation (tppn) for CONTROL and CONTROL_5N, 20°S to 20°N.

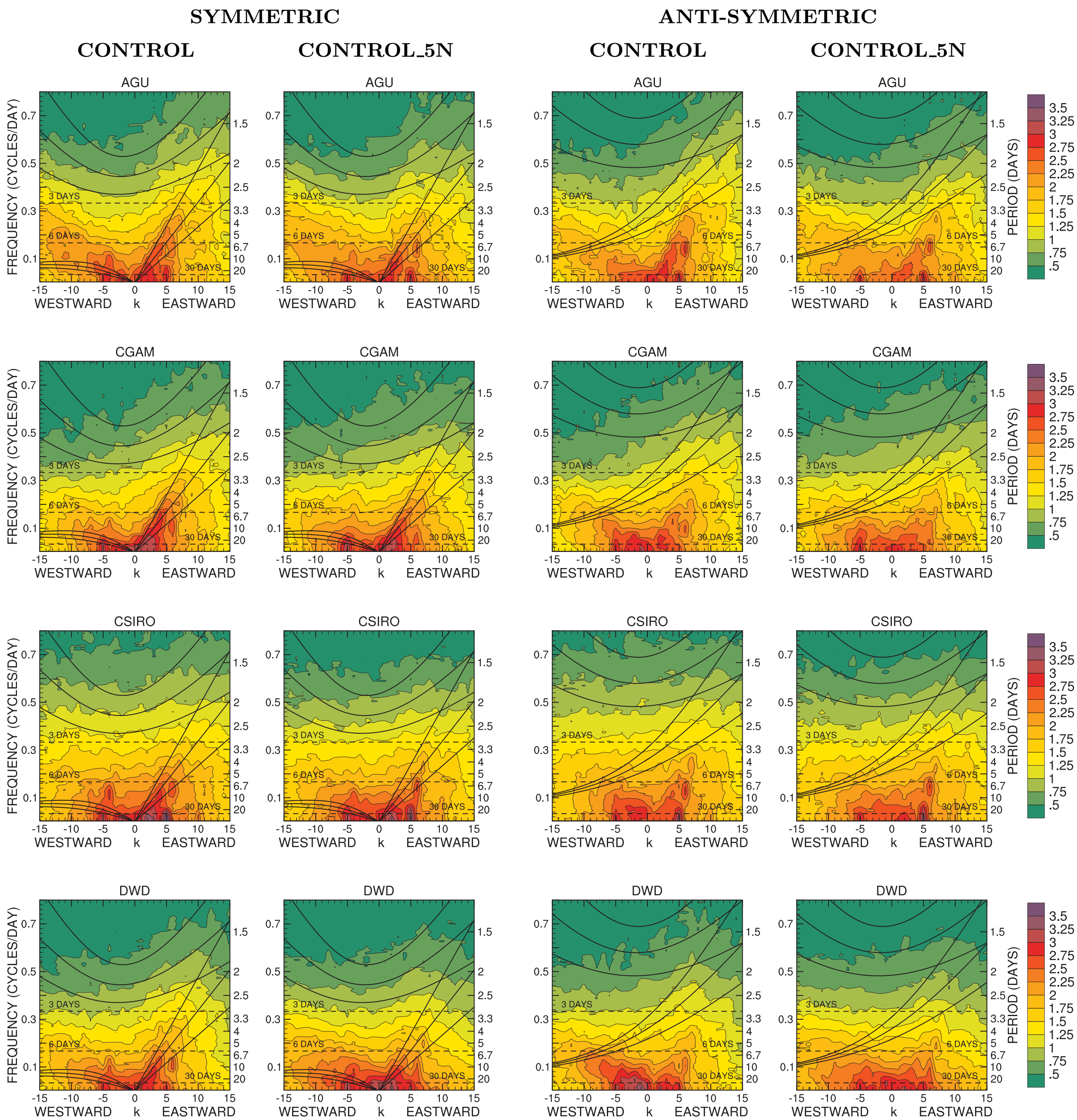

Figure 6.30: Wavenumber-frequency diagrams of log of power of symmetric and anti-symmetric modes of equatorial OLR (lw_toa) for CONTROL and CONTROL_5N, 20°S to 20°N.

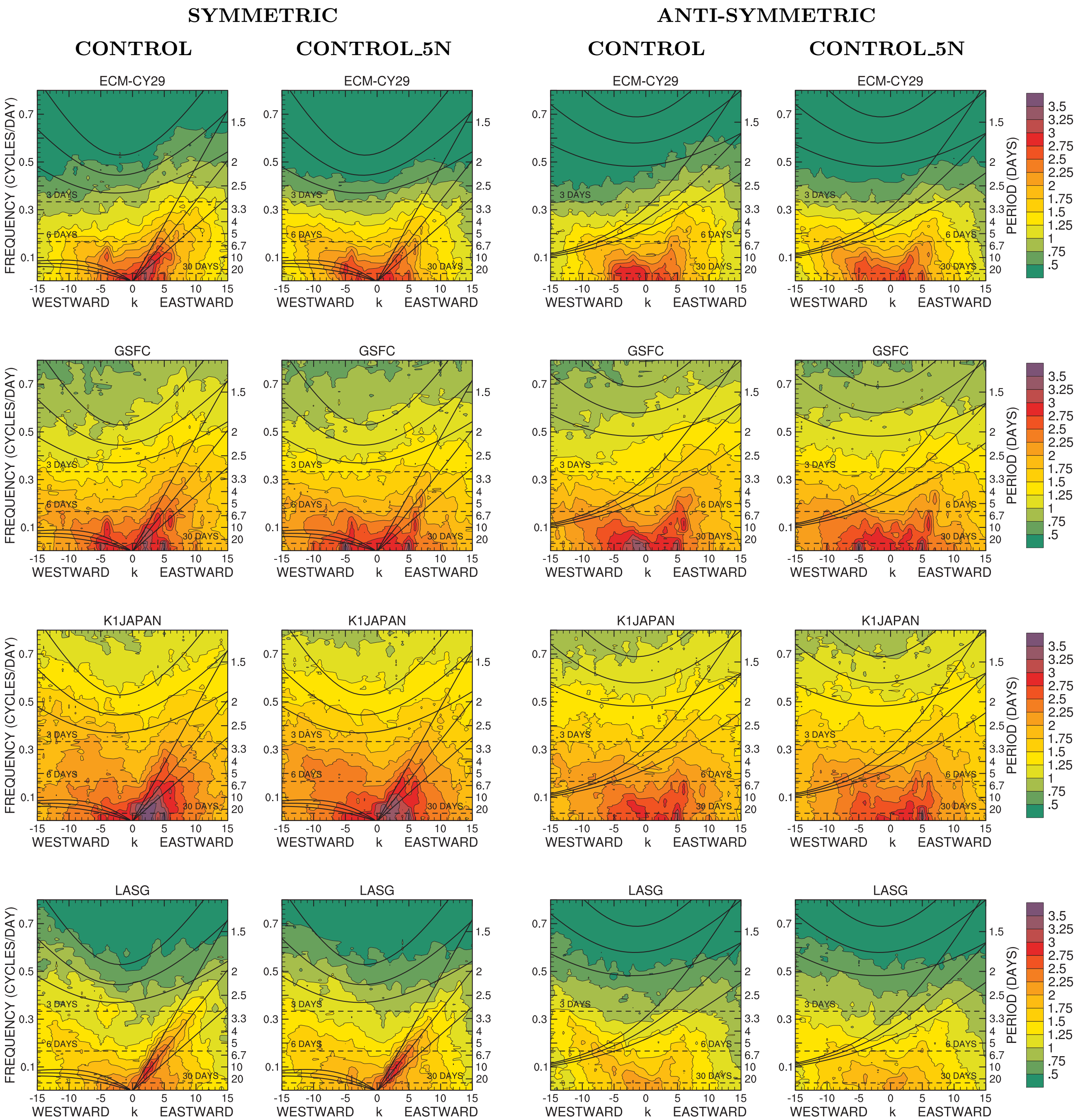

Figure 6.30 (continued): Wavenumber-frequency diagrams of log of power of symmetric and anti-symmetric modes of equatorial OLR (lw_toa) for CONTROL and CONTROL_5N, 20°S to 20°N.

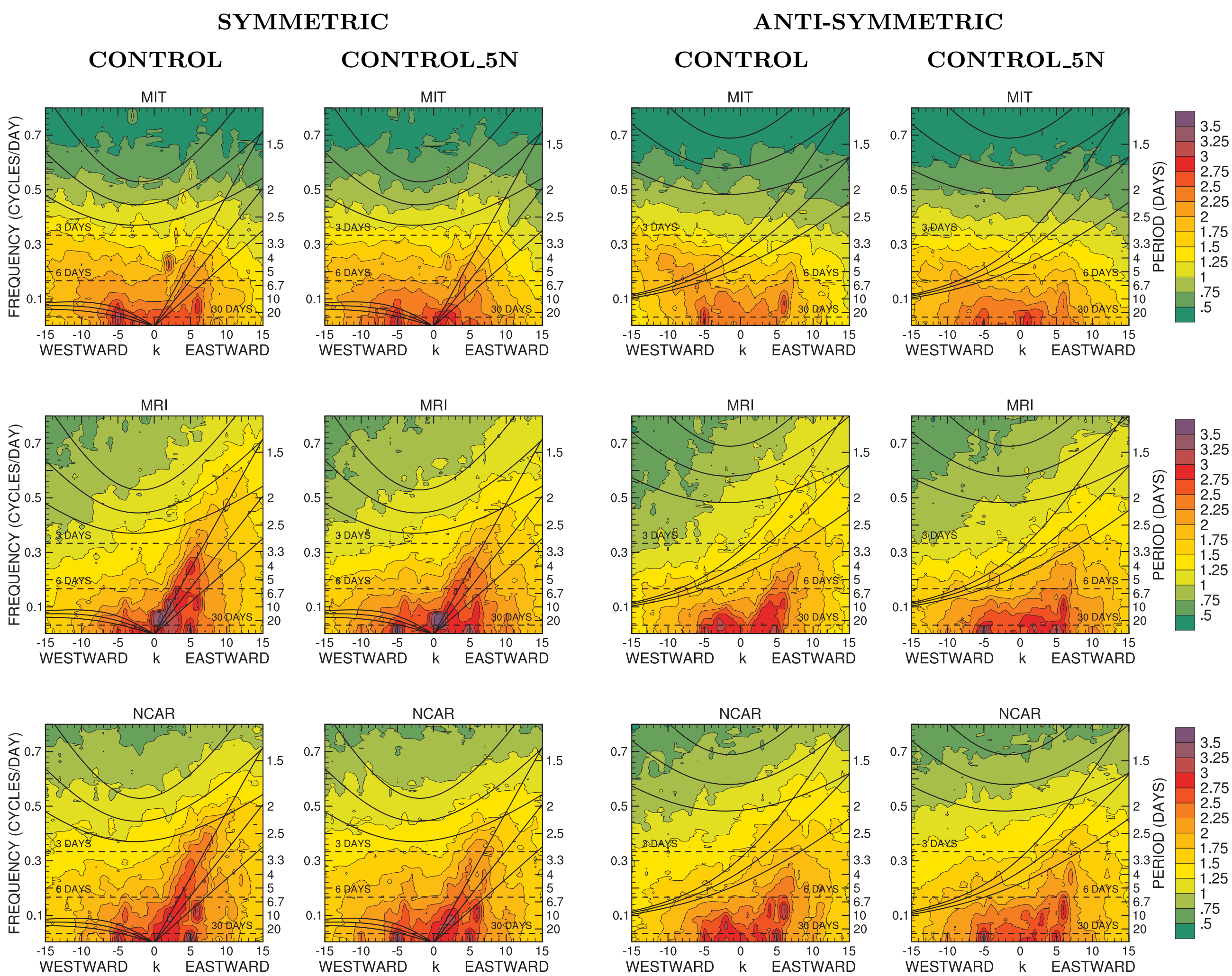

Figure 6.30 (continued): Wavenumber-frequency diagrams of log of power of symmetric and anti-symmetric modes of equatorial OLR (lw_toa) for CONTROL and CONTROL_5N, 20°S to 20°N.

Chapter 7

Response to Tropical SST Anomalies (1KEQ, 3KEQ, 3KW1, CONTROL)

The multi-model mean comparing the CONTROL, 1KEQ, 3KEQ and 3KW1 experiments excludes FRCGC, ECM-CY29, UKMO(48) and UKMO(96). In addition the multi-model mean for the eddy statistics (based on MF files) excludes CGAM and MRI. These are the same sets of models that were used in the preceding Chapter 6 which considered the asymmetric SST profile.

After the analyses presented in this section were completed it was discovered that the latitudinal extent of the 3KW1 SST anomaly in ECM-CY32 was accidentally set to 30° latitude instead of the specified 60° (Eqn. 2.8). As a test of the effect of this error on the multi-model mean, the mean for single level fields was re-calculated omitting ECM-CY32. For most fields it had no observable effect on the graphs of the latitudinal structure, for a few the lines shifted about the thickness of the lines. The impact on the multi-model mean of omitting ECM-CY32 is at most small and almost certainly dominated by the "bias" of ECM-CY32 seen in all the experiments (including CONTROL), rather than demonstrably due to the SST error. With 11 models for most of the variables and 9 for the MF fluxes, ECM-CY32 shifts the multi-model mean by only $\sim$10% of its difference from the mean. There is also good reason to think that the impact of the latitudinal width of the 3KW1 SST anomaly is modest. Most variables in this chapter do not show the width clearly. Precipitation anomalies take the width of the ITCZ in CONTROL and the circulation response appears to be rather insensitive to the width, presumably because the Rossby wave source is determined by the latitudinal scale of the divergence which is similar to that of the precipitation. Since the effect on the multi-model mean is small the Figures in this Chapter were left as originally produced and the multi-model mean includes ECM-CY32.

7.1 Mean State

7.1.1 Zonal-Time Averages, 2-D Fields

The zonal-time averages for the multi-model mean for single level fields tppn, cppn, dppn, evap, emp, cld_frac, albedo, ps and tauu are shown in Figure 7.1. The fields sw_toa, lw_toa, rflux_toa, ssw, slw, rfluv_sfce, slh, ssh and rflux are shown in Figure 7.2. The same fields for the individual models, with the addition of tauv, are shown in Figures 7.3 through 7.21.

Table 7.1: Ratio of the maximum precipitation of 3KEQ-[CONTROL] to the maximum precipitation of 1KEQ-[CONTROL].

MODEL	RATIO	MODEL	RATIO	MODEL	RATIO
AGU	4.2	ECM-CY32	2.1	LASG	2.4
CGAM	4.0	GFDL	2.1	MIT	2.2
CSIRO	2.4	GSFC	3.5	MRI	3.4
DWD	2.1	K1JAPAN	2.3	NCAR	2.9

7.1.2 Zonal-Time Averages, 3-D Fields

The zonal-time averages for the multi-model mean u, t, v and om are shown in Figure 7.22 and q and rh in Figure 7.23. The zonal wind for the individual models is shown in Figure 7.24 for 3KW1 and in Figure 7.25 for 3KW1 minus the CONTROL.

7.1.3 Time Averages, Latitude-Longitude

Horizontal plots of precipitation (tppn) from the individual models are shown in Figures 7.26, 7.27 and 7.28 for 1KEQ minus zonal average of CONTROL, 3KEQ minus zonal average of CONTROL and 3KW1 minus zonal average of CONTROL, respectively. Horizontal plots of the zonal wind at 200mb (u200) are shown in Figure 7.29 for 3KW1 minus zonal average of CONTROL.

The response of the models to the tropical SST anomalies is shown in Table 7.1 calculated from the precipitation (tppn) as the ratio of the maximum value of the difference of 3KEQ minus the zonal average of the CONTROL to the maximum value of the difference of 1KEQ minus the zonal average of the CONTROL. We note that Neale and Hoskins (2000b) report a value of five for HadAM3 which is larger than any value reported here. For APE, CGAM used the same model at the same horizontal resolution but different vertical resolution than Neal and Hoskins. It gives the smaller value seen here.

7.1.4 Time Averages, Equatorial Slice (Longitude-Height)

The multi-model means and standard deviations of meridional-time averages taken from 10°S to 10°N latitude are shown in Figures 7.30 through 7.35. The averages of the zonal wind (u), temperature (t) and deviation of temperature from the zonal mean (t-[t]) for 1KEQ, 3KEQ and 3KW1 are shown in Figures 7.30, 7.32 and 7.34, respectively. Those of vertical wind (om), specific humidity (q) and relative humidity (rh) for 1KEQ, 3KEQ and 3KW1 are shown in Figures 7.31, 7.33 and 7.35, respectively. The square brackets [ ] denote the zonal average.

The meridional-time averages of the zonal wind (u) and vertical wind (om) for the individual models are shown in figures 7.36 and 7.37.

7.2 Maintenance of Mean State (1KEQ, 3KEQ, 3KW1, CONTROL)

7.2.1 Dynamical Budgets (variances and co-variances)

Figure 7.38 shows the multi-model mean transient eddy (co-)variances te_uu $\overline{\left[(u'^*)^2\right]}$, te_vv $\overline{\left[(v'^*)^2\right]}$, te_uv $\overline{[u'^*v'^*]}$ and te_vt $\overline{[v'^*T^*]}$. Figure 7.39 shows the multi-model mean stationary eddy (co-)variances se_uu $[\overline{u}^*\overline{u}^*]$, se_vv $[\overline{v}^*\overline{v}^*]$, se_uv $[\overline{u}^*\overline{v}^*]$ and se_vt $\left[\overline{v}^*\overline{T}^*\right]$. Plots of the above (co-)variances for the individual models are shown in Figures 7.40 through 7.47.

7.2.2 Parameterization Forcing (1KEQ, 3KEQ, 3KW1, CONTROL)

The zonal-time average of the parameterization convection (t_conv) and cloud (t_cld) temperature tendencies are shown in Figures 7.48 and 7.49, respectively. The equatorial-time average from 7°S to 7°N of the parameterization convection (t_conv) and cloud (t_cld) temperature tendencies are shown in Figures 7.50 and 7.51. The zonal-time averages in Figures 7.48 and 7.49 indicate that this latitudinal averaging range captures the major signal for these terms.

7.3 Tropical Variability

7.3.1 Wavenumber-Frequency Spectra

Even though in these experiments the zonal average tropical precipitation is confined within latitudes 10°S to 10°N as seen in Figures 7.1 and 7.3, we continue to average the power from 20°S to 20°N. As was discussed in Section 5.3.1, for experiments where the tropical precipitation is within 10°S to 10°N, the different domains have little effect on the structure of the wavenumber-frequency plots. They primarily affect the magnitudes.

Figure 7.52 shows the wavenumber-frequency diagrams of symmetric modes of tropical precipitation (tppn) for CONTROL, 1KEQ, 3KEQ and 3KW1 for each model. Figure 7.53 shows the anti-symmetric modes of tropical precipitation. Figures 7.54 and 7.55 show the symmetric and anti-symmetric modes of OLR (lw_toa), respectively.

7.3.2 Precipitation Frequency Distributions

We also continue to use the domain 20°S to 20°N to calculate the frequency distributions of precipitation even though in this set of experiments the zonal average tropical precipitation is confined within latitudes 10°S to 10°N. Such a change simply reduces the fraction of large values of precipitation and increases the fraction of small values. But the relative differences between the experiments is not affected. We continue to base the calculation on the 6-hour averages (TR data.)

Figure 7.56 shows the fraction of time precipitation (tppn) is in 1 mm day^{-1} bins ranging from 0 to 120 mm day^{-1} for all models for CONTROL, 1KEQ, 3KEQ and 3KW1 experiments. Figure 7.57 shows the fractions for 10 mm day^{-1} bins ranging from 0 to 1200 mm day^{-1}.

Several models, most notably AGU, CGAM and NCAR, show an increase in fraction of larger rainfall rates from CONTROL to 1KEQ to 3KEQ to 3KW1. The zonal average precipitation (Figure 7.3) does not mirror this behavior, unlike the PEAKED to CONTROL to QOBS to FLAT variation discussed earlier. In fact, the 3KW1 experiment has lower zonal average precipitation at the equator than the other experiments. The different behavior in the series of experiments arises from the longitudinal variation in precipitation in the equatorial region (Figure 7.26.)

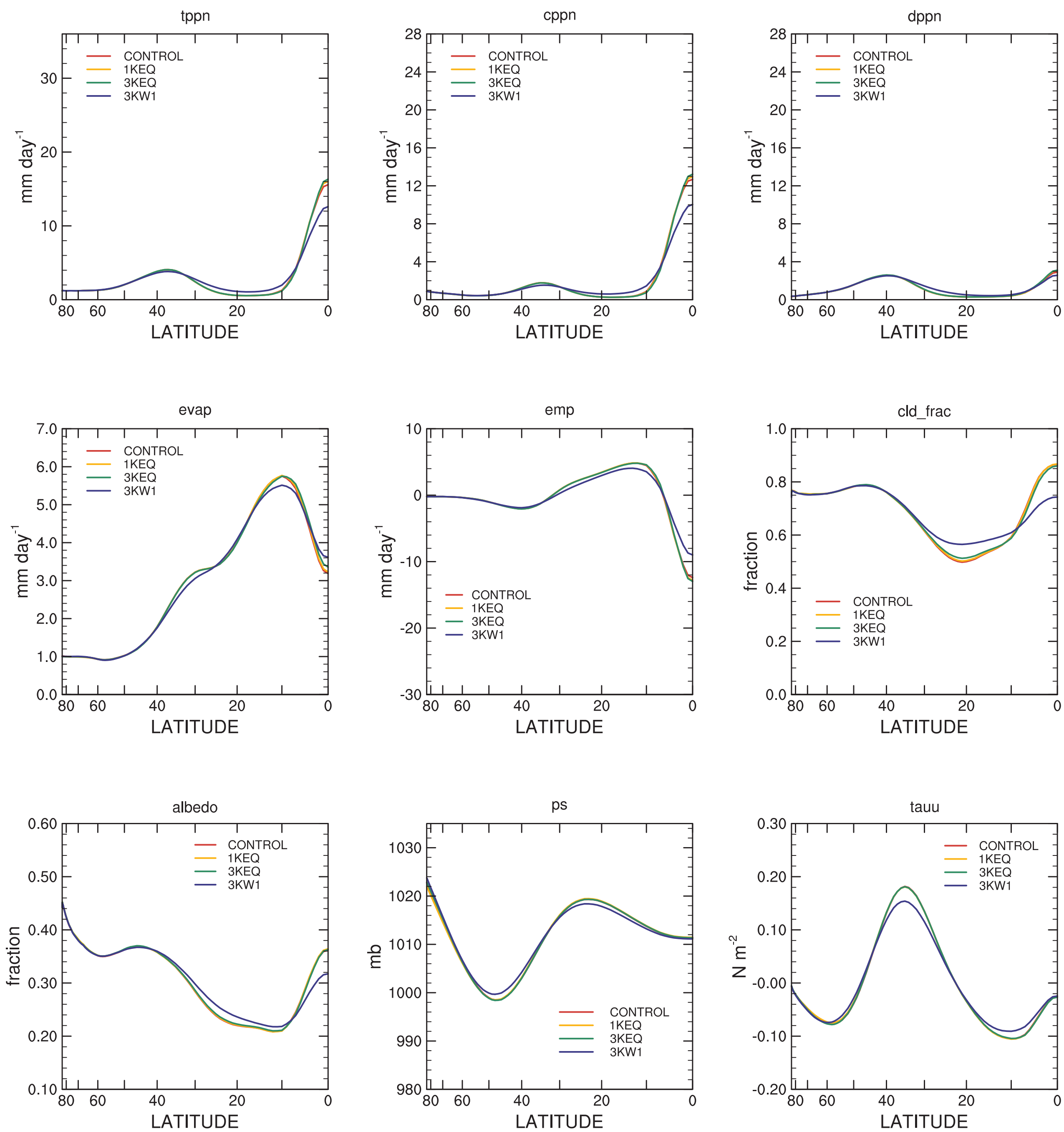

Figure 7.1: Multi-model mean zonal-time average total precipitation (tppn), convective precipitation (cppn), large-scale precipitation (dppn), evaporation (evap), evaporation minus precipitation (emp), cloud fraction (cld_frac), albedo (albedo), surface pressure (ps) and zonal surface stress (tauu) from CONTROL, 1KEQ, 3KEQ and 3KW1 SST distributions.

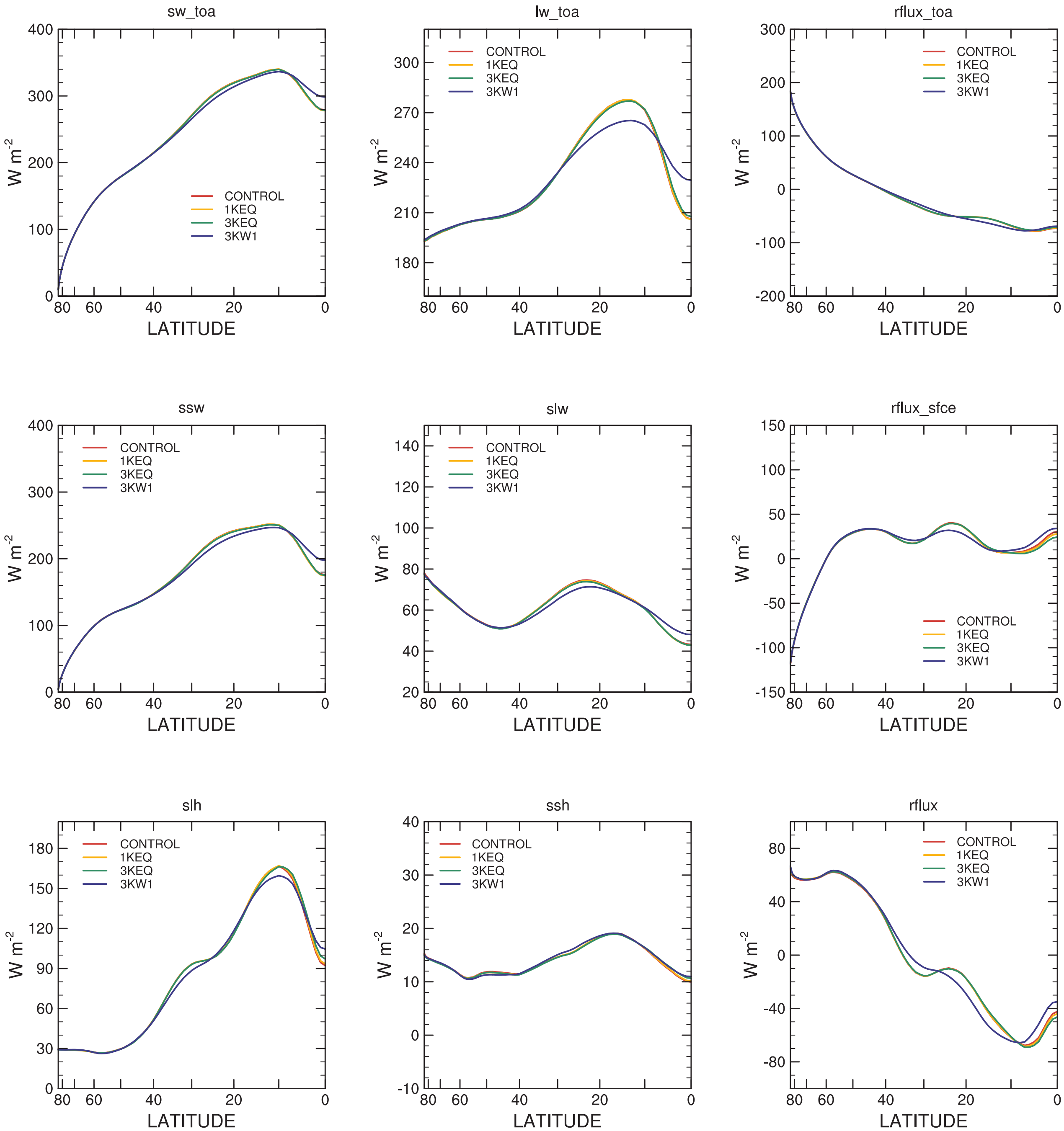

Figure 7.2: Multi-model mean zonal-time average TOA net shortwave (sw_toa, +ve downward), TOA net longwave (lw_toa, +ve upward), TOA residual (rflux_toa, +ve upward), surface net shortwave (ssw, +ve downward), surface net longwave (slw, +ve upward), surface residual (rflux_sfce, +ve downward), surface latent heat (slh), surface sensible heat (ssh) and net total (rflux, +ve out of atmosphere) fluxes from CONTROL, 1KEQ, 3KEQ and 3KW1 SST distributions.

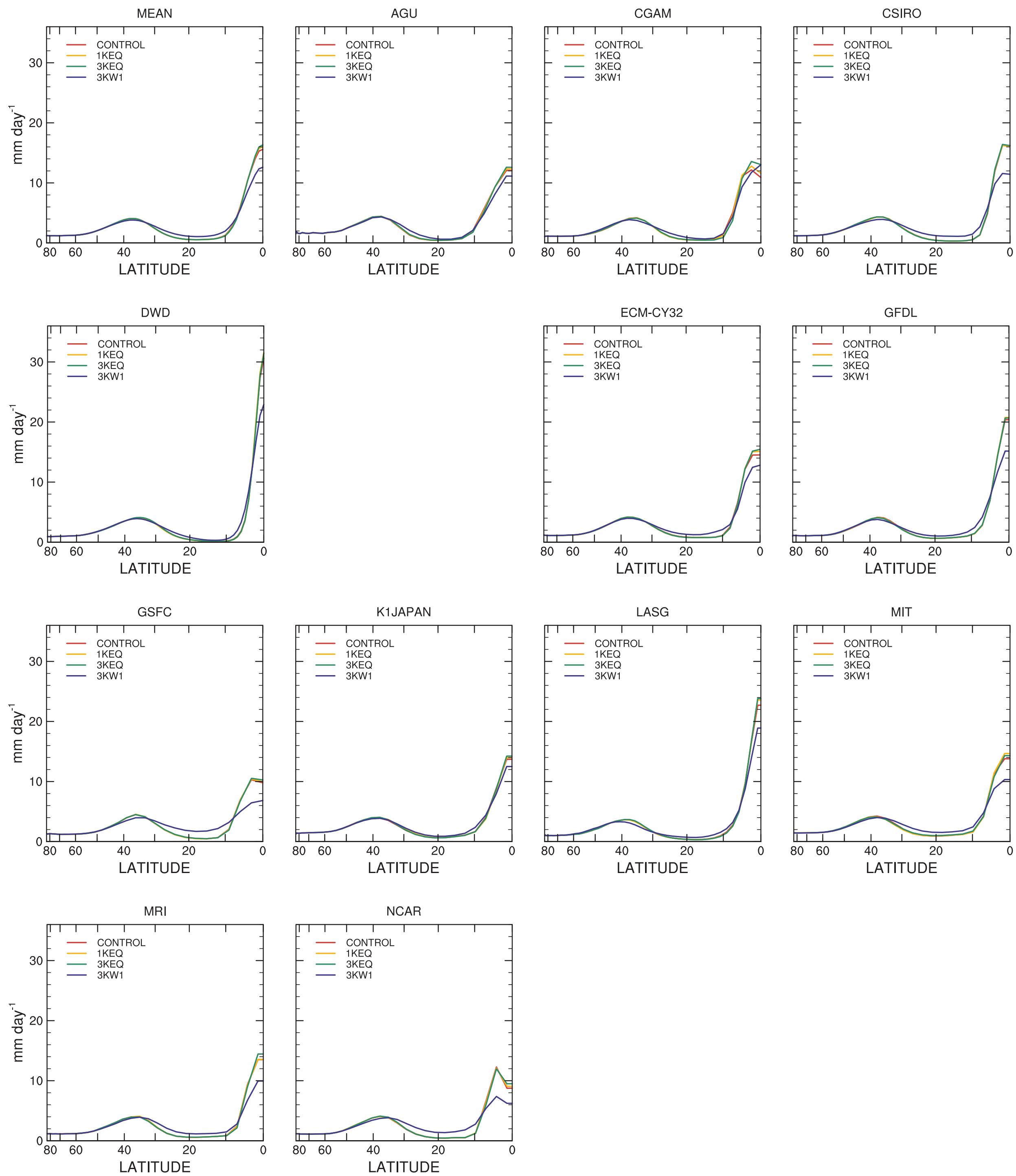

Figure 7.3: Zonal-time average precipitation (tppn) for individual models from CONTROL, 1KEQ, 3KEQ and 3KW1 SST distributions, mm day^{-1}.

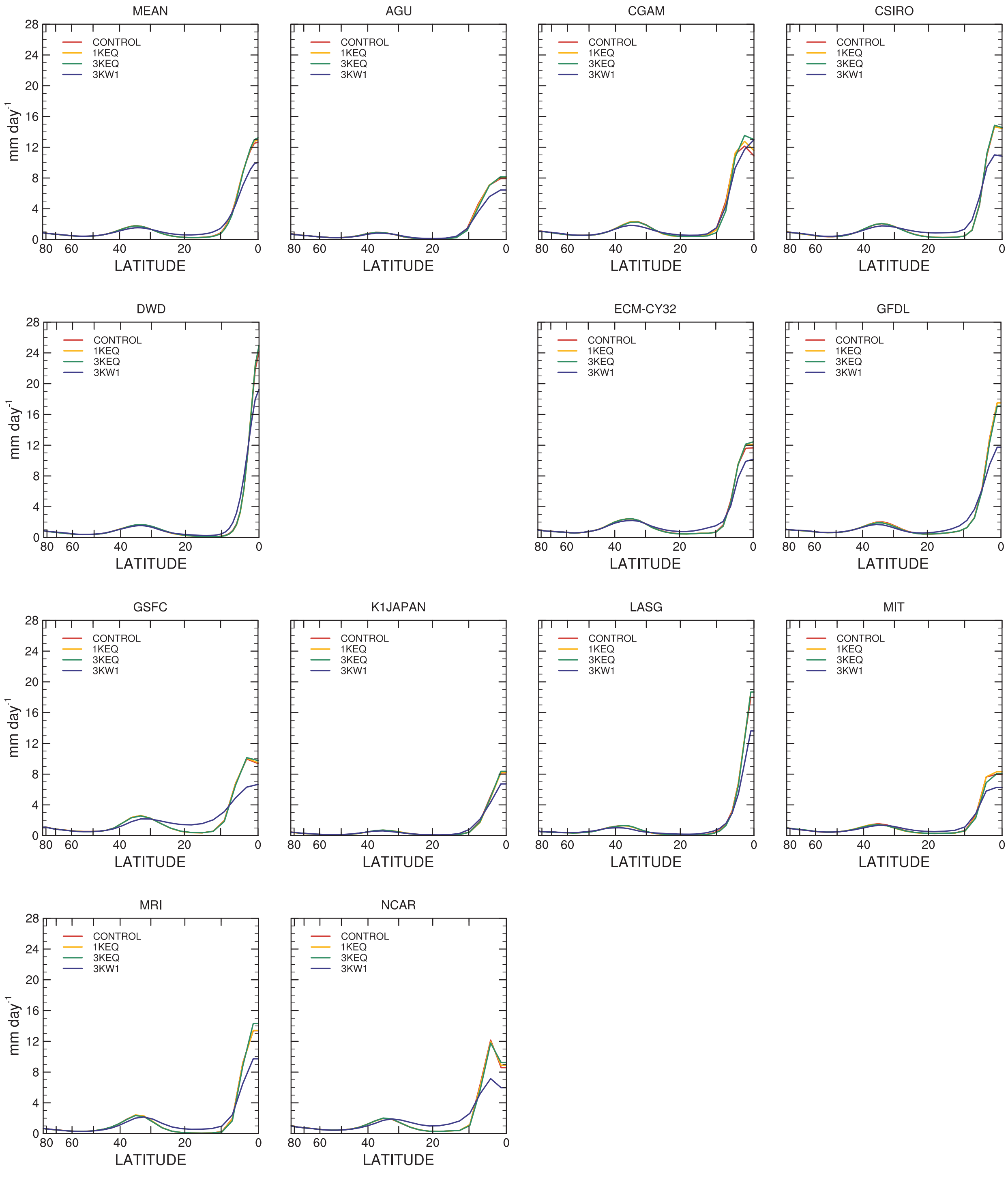

Figure 7.4: Zonal-time average convective precipitation (cppn) for individual models from CONTROL, 1KEQ, 3KEQ and 3KW1 SST distributions, mm day^{-1}.

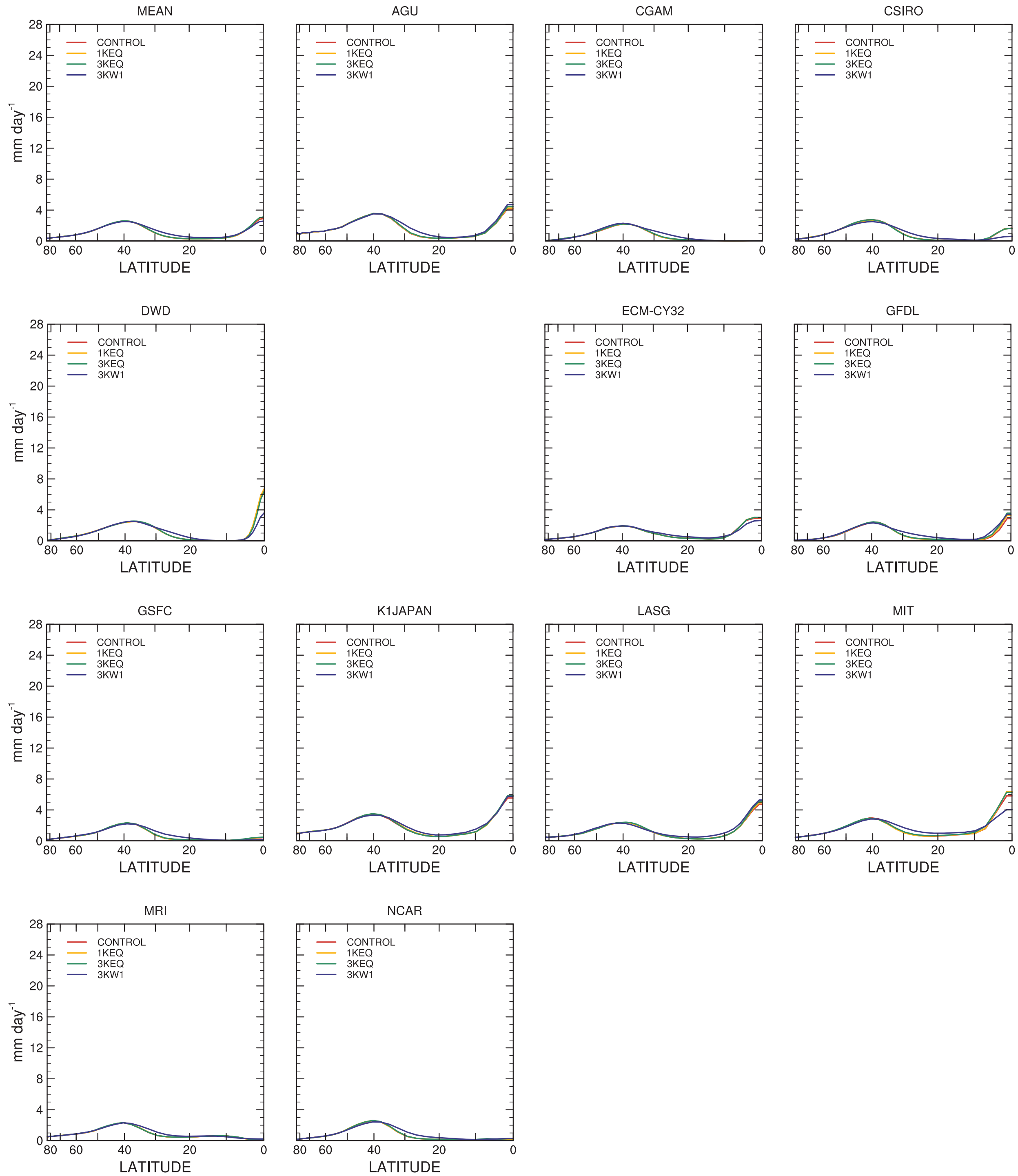

Figure 7.5: Zonal-time average large-scale precipitation (dppn) for individual models from CONTROL, 1KEQ, 3KEQ and 3KW1 SST distributions, mm day^{-1}.

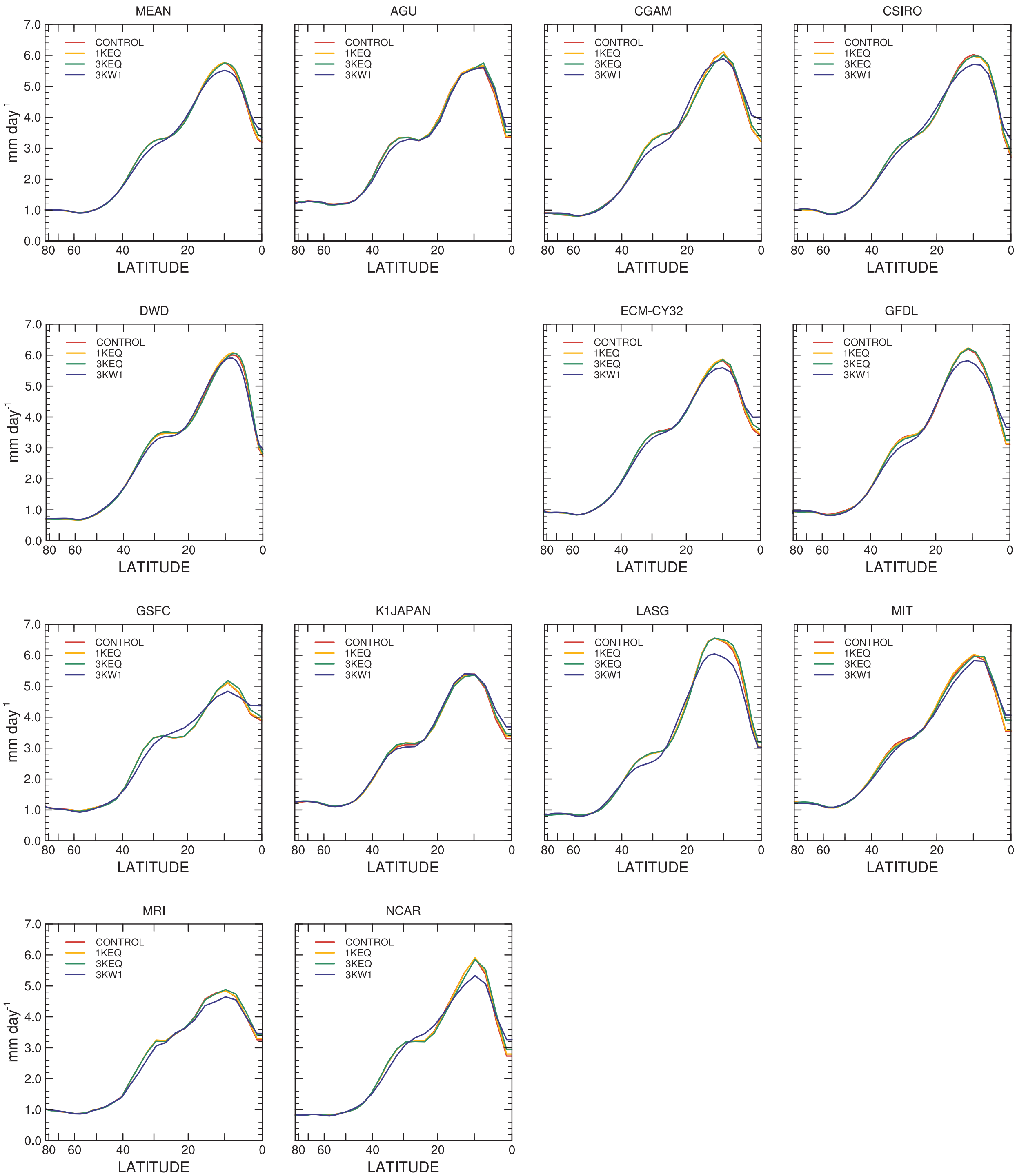

Figure 7.6: Zonal-time average evaporation (evap) for individual models from CONTROL, 1KEQ, 3KEQ and 3KW1 SST distributions, mm day^{-1}.

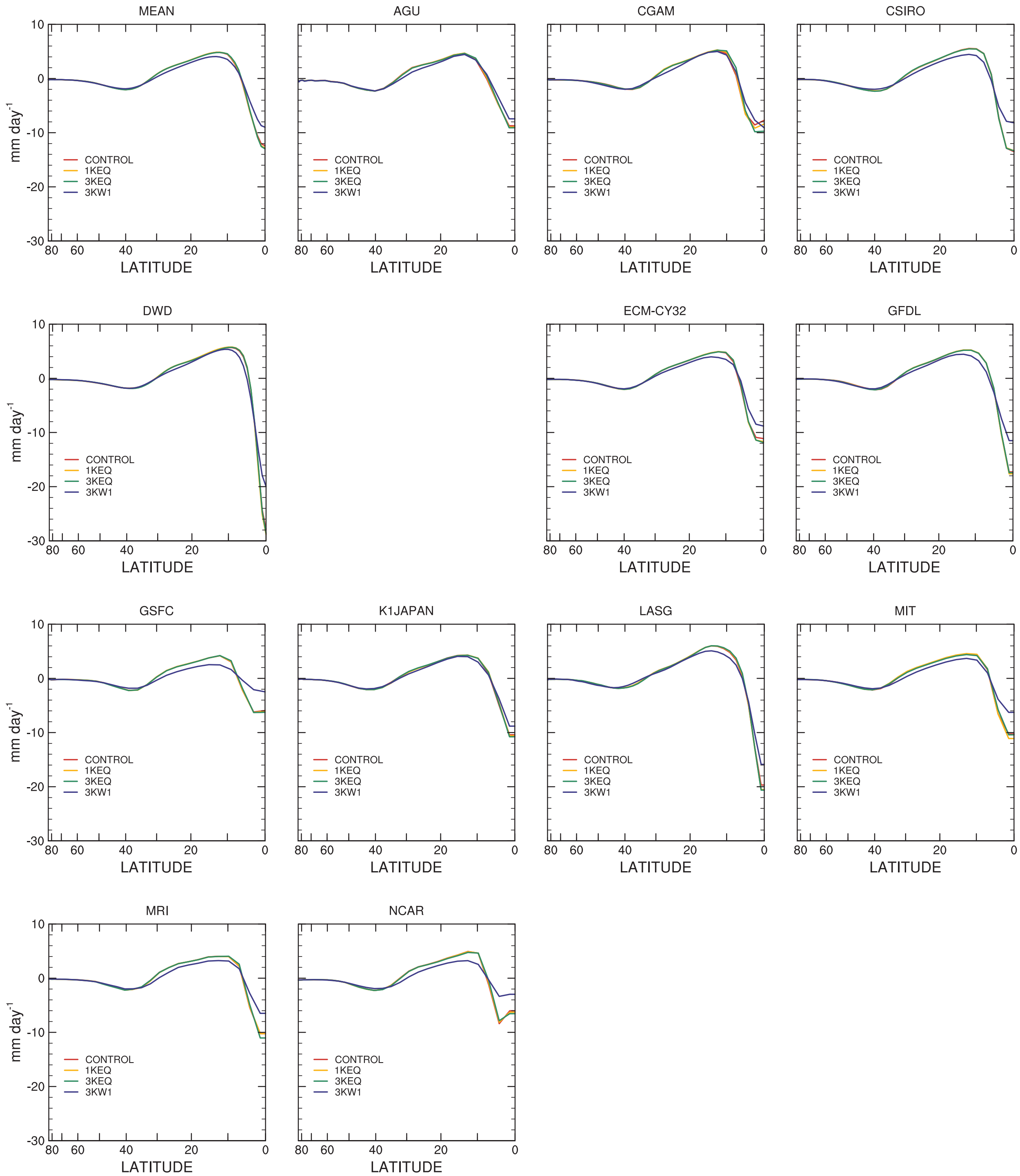

Figure 7.7: Zonal-time average evaporation minus precipitation (emp) for individual models from CONTROL, 1KEQ, 3KEQ and 3KW1 SST distributions, mm day^{-1}.

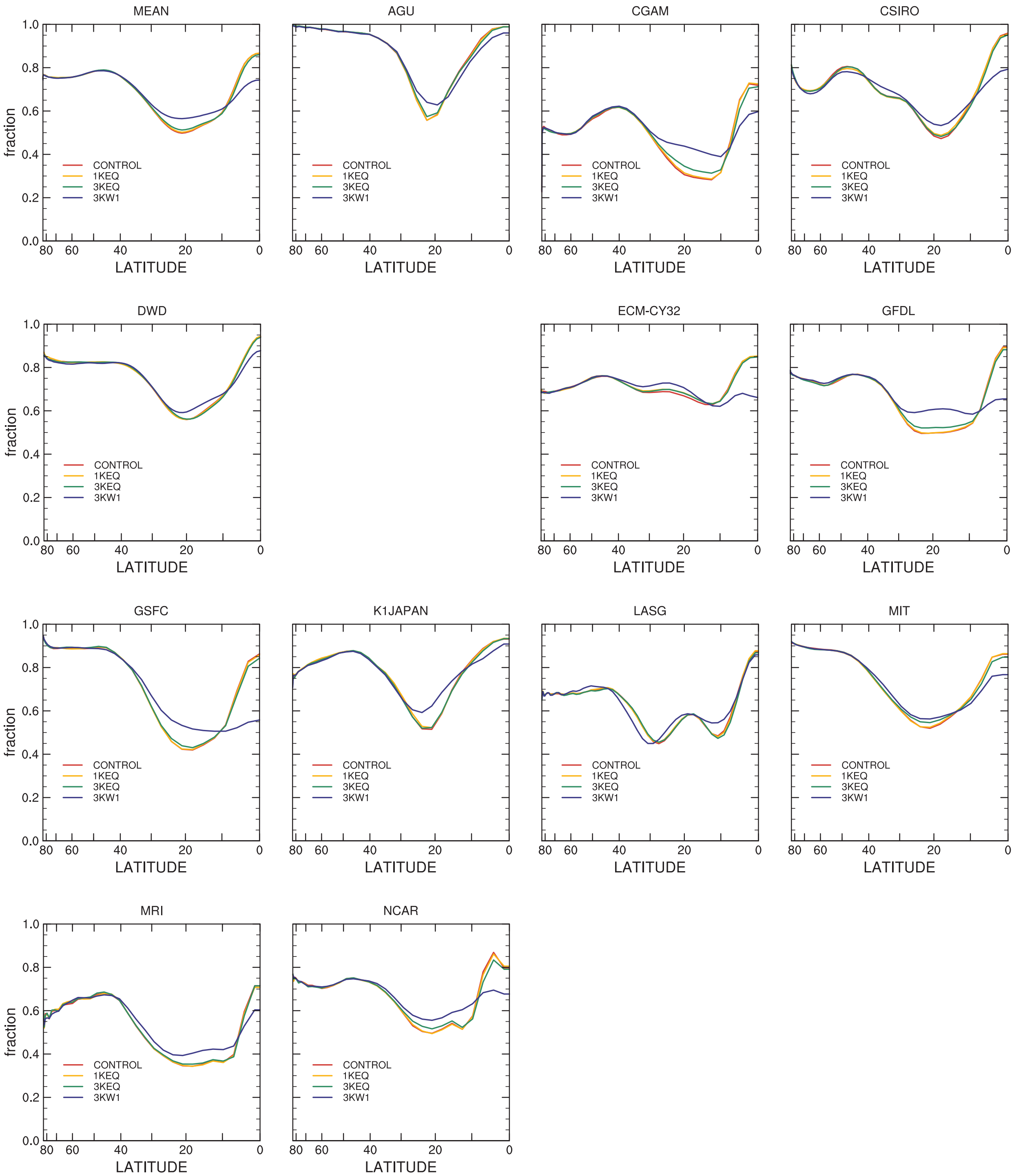

Figure 7.8: Zonal-time average cloud fraction (cld_frac) for individual models from CONTROL, 1KEQ, 3KEQ and 3KW1 SST distributions, fraction.

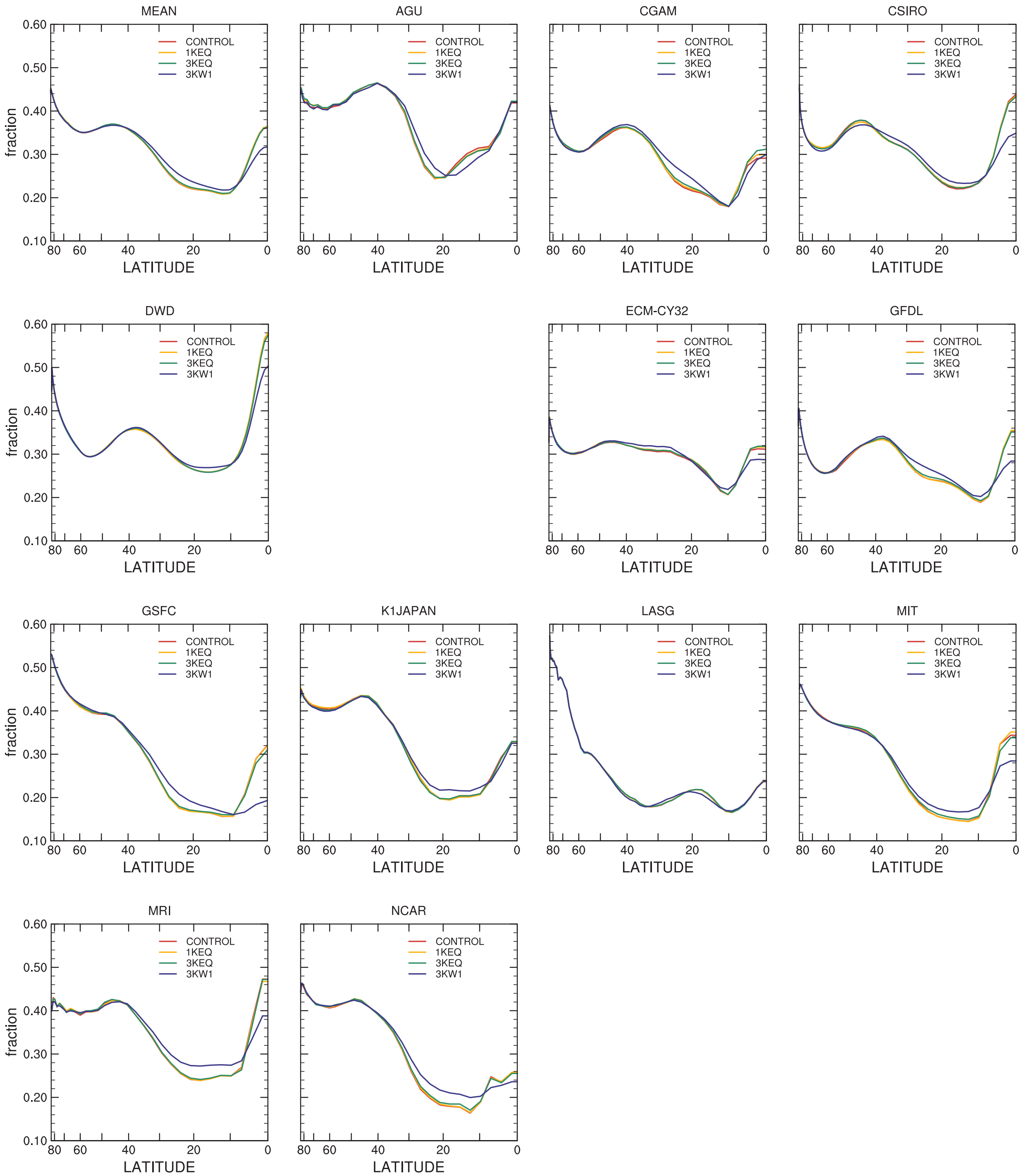

Figure 7.9: Zonal-time average albedo (albedo) for individual models from CONTROL, 1KEQ, 3KEQ and 3KW1 SST distributions, fraction.

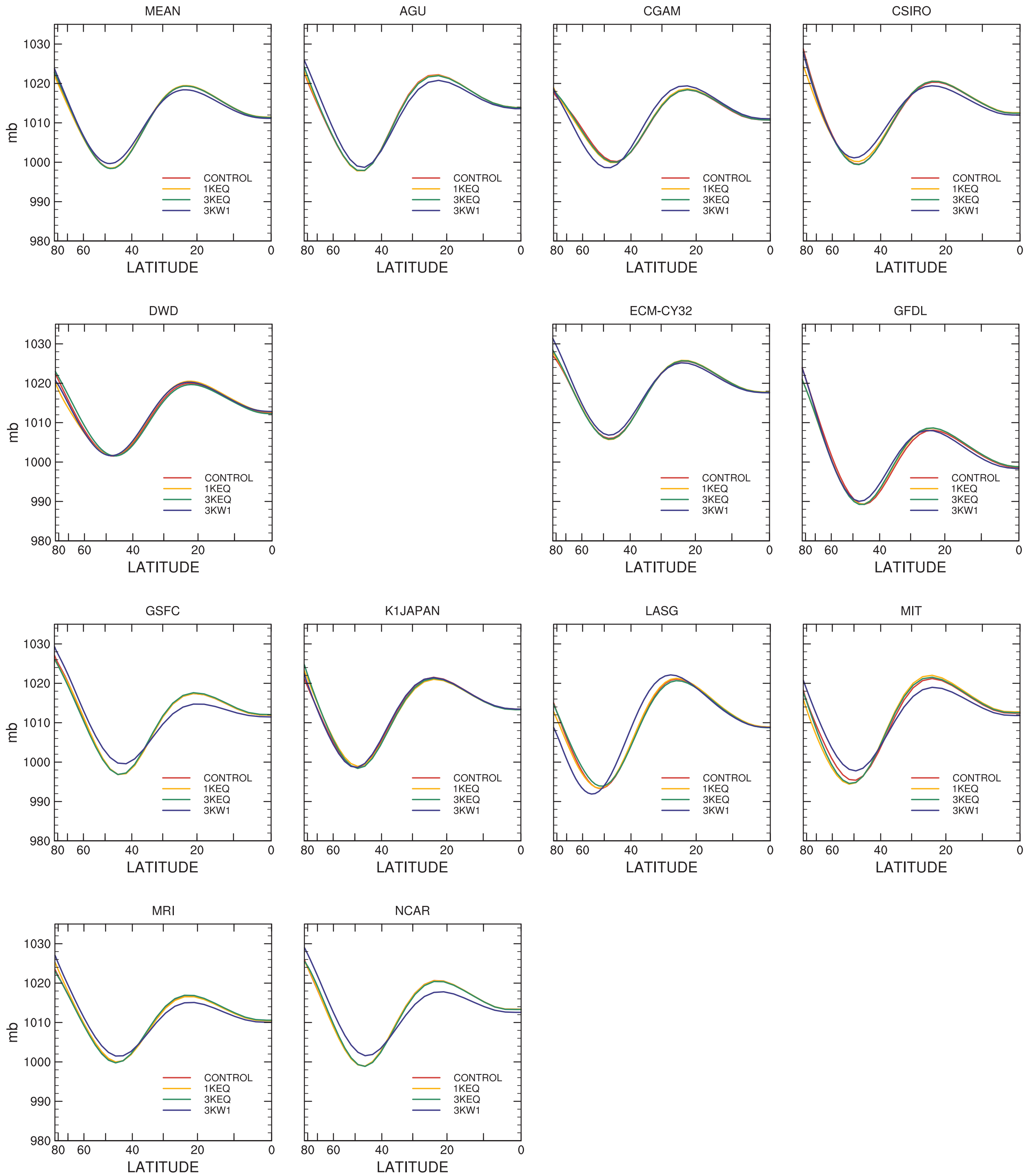

Figure 7.10: Zonal-time average surface pressure (ps) for individual models from CONTROL, 1KEQ, 3KEQ and 3KW1 SST distributions, mb.

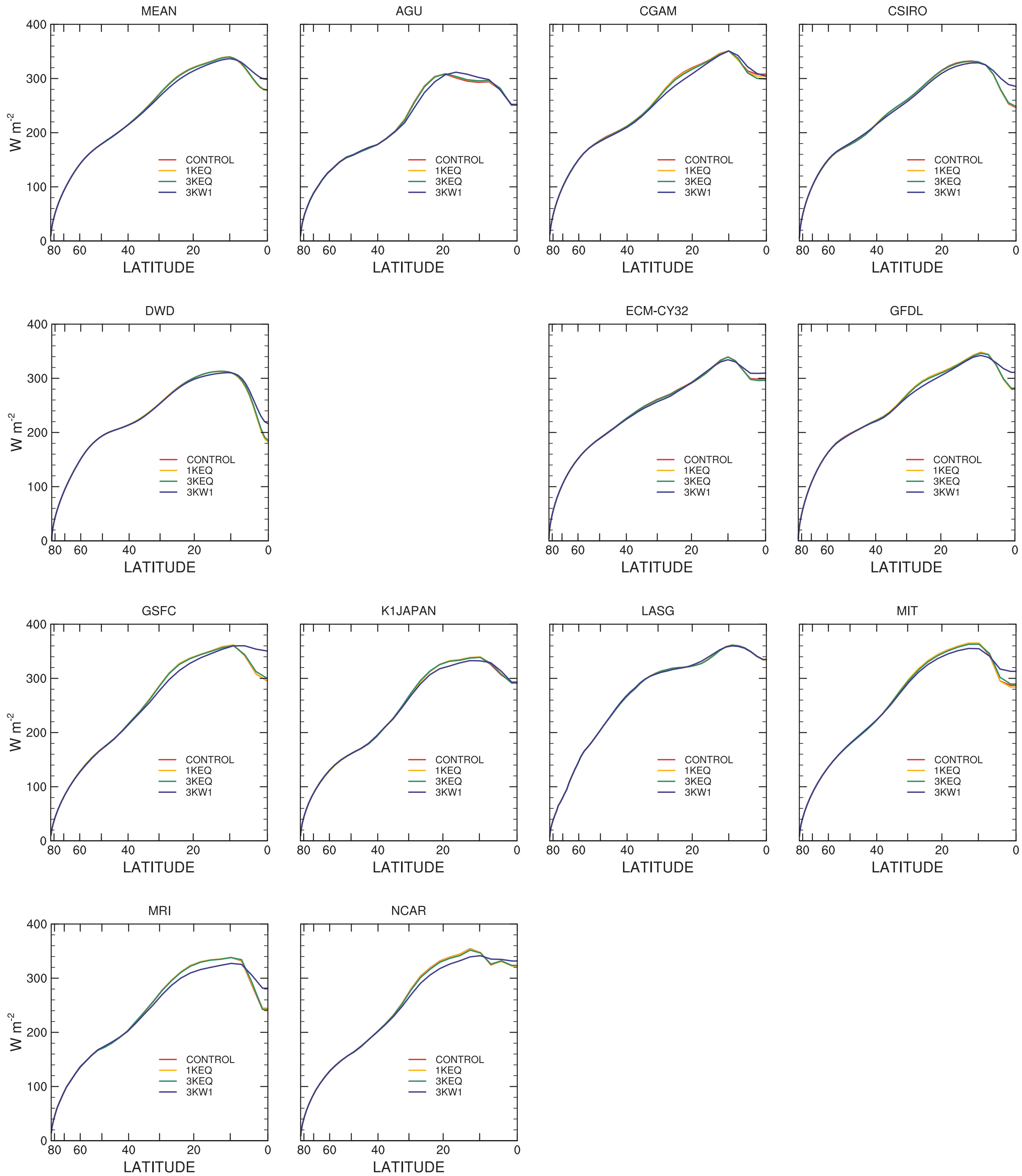

Figure 7.11: Zonal-time average TOA net shortwave radiation (sw_toa) for individual models from CONTROL, 1KEQ, 3KEQ and 3KW1 SST distributions, W m^{-2}, +ve downward.

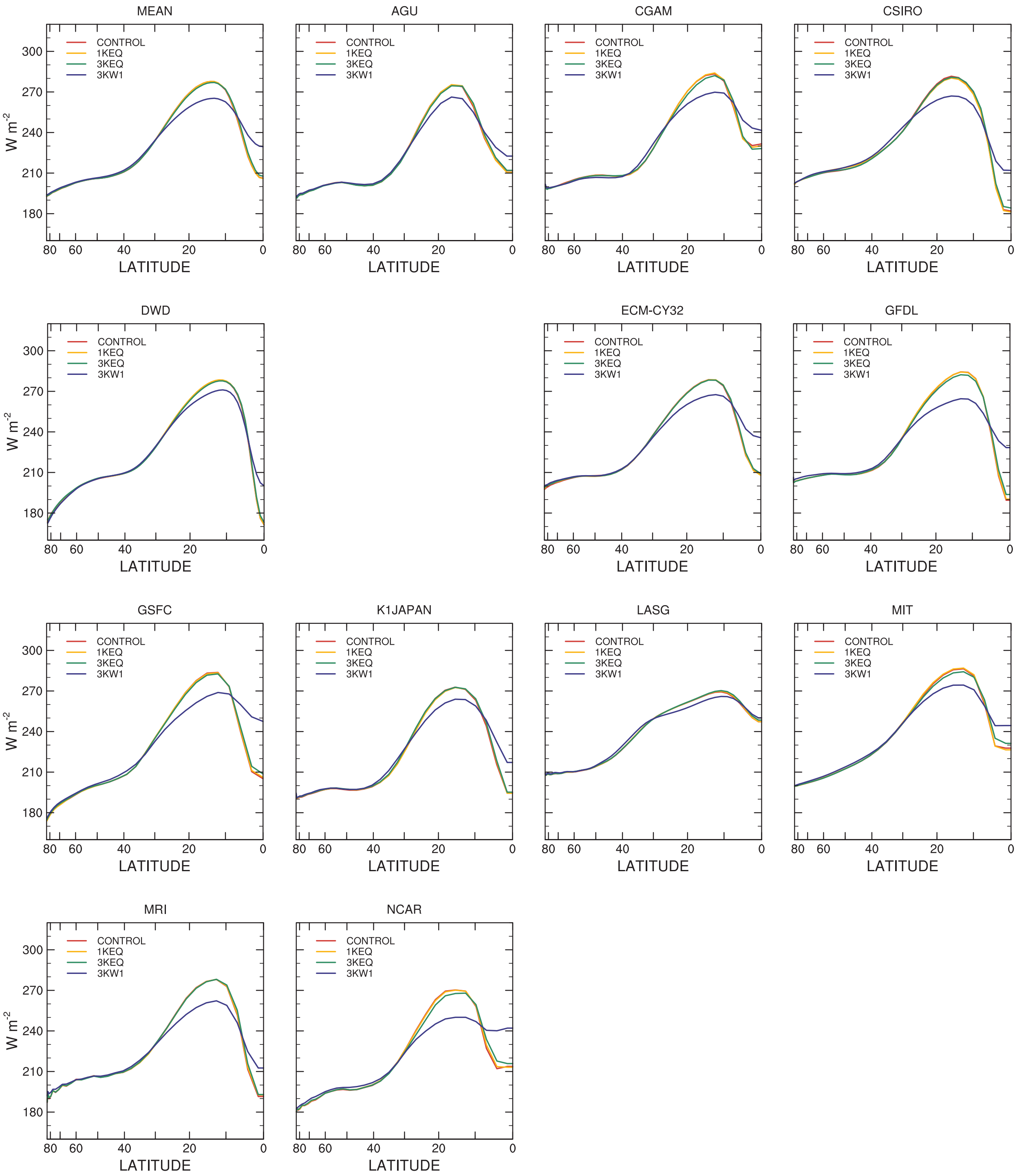

Figure 7.12: Zonal-time average TOA net longwave radiation (lw_toa) for individual models from CONTROL, 1KEQ, 3KEQ and 3KW1 SST distributions, W m^{-2}, +ve upward.

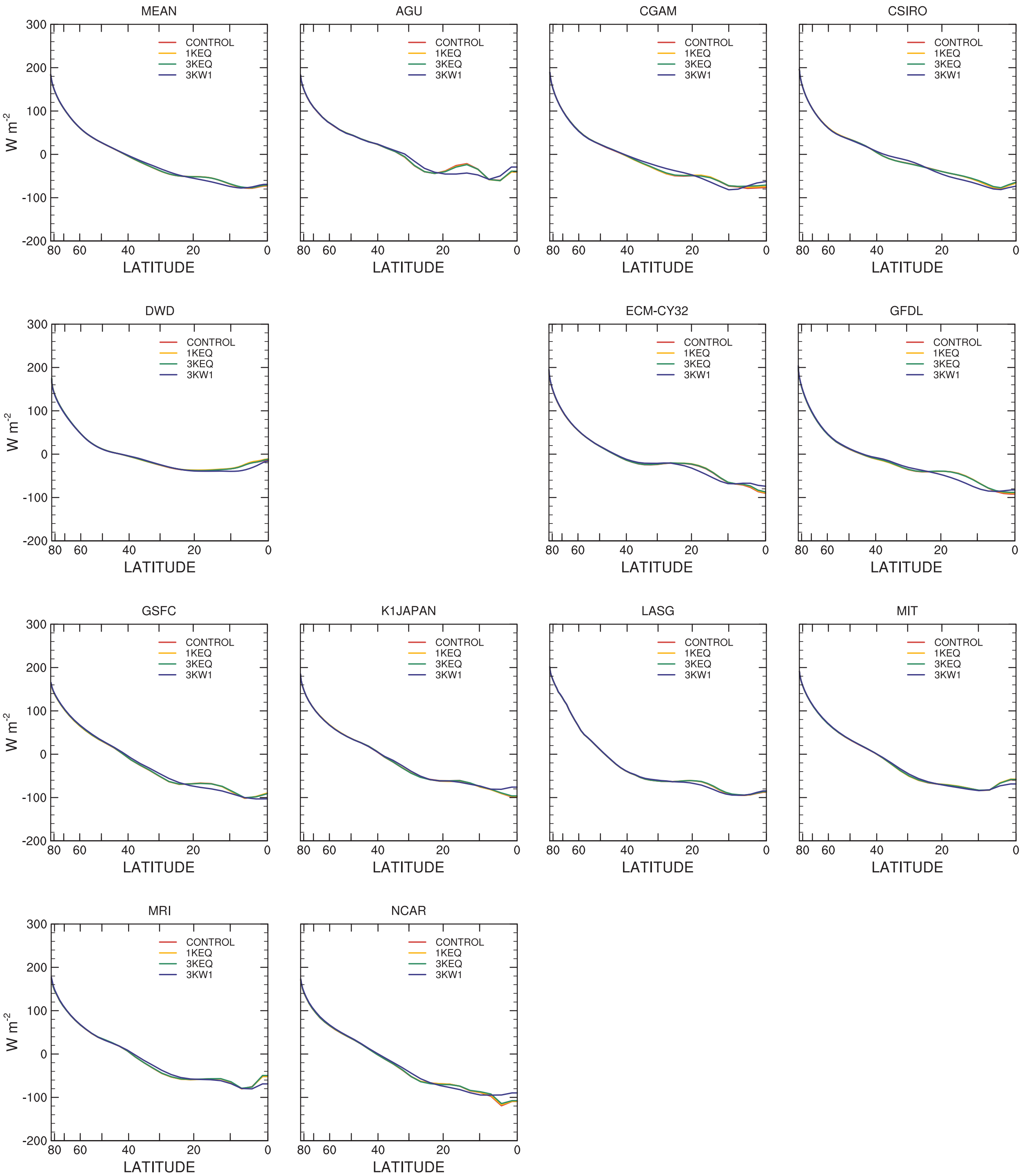

Figure 7.13: Zonal-time average TOA net radiation flux (rflux_toa) for individual models from CONTROL, 1KEQ, 3KEQ and 3KW1 SST distributions, W m^{-2}, +ve upward.

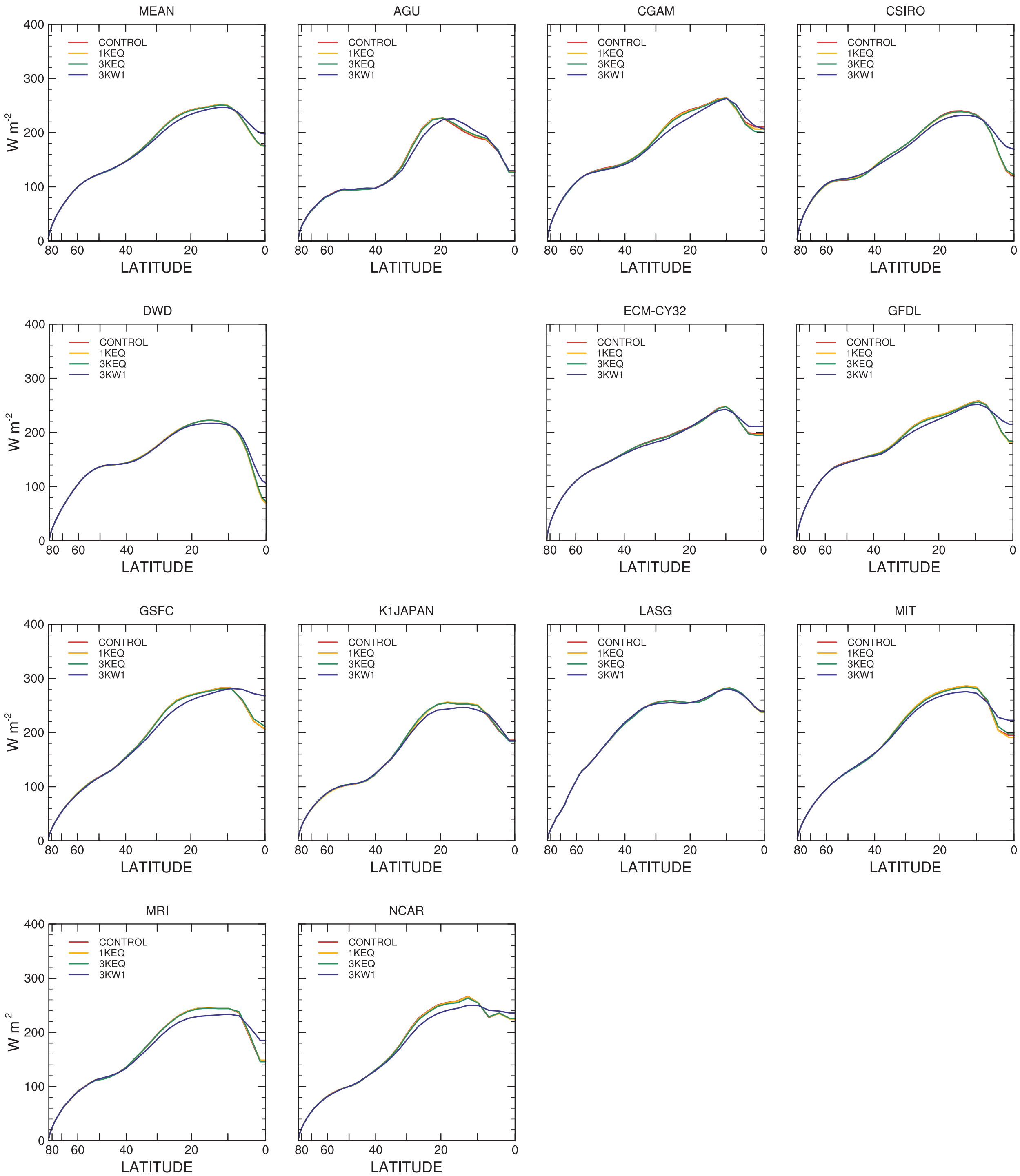

Figure 7.14: Zonal-time average surface net shortwave radiation (ssw) for individual models from CONTROL, 1KEQ, 3KEQ and 3KW1 SST distributions, W m^{-2}, +ve downward.

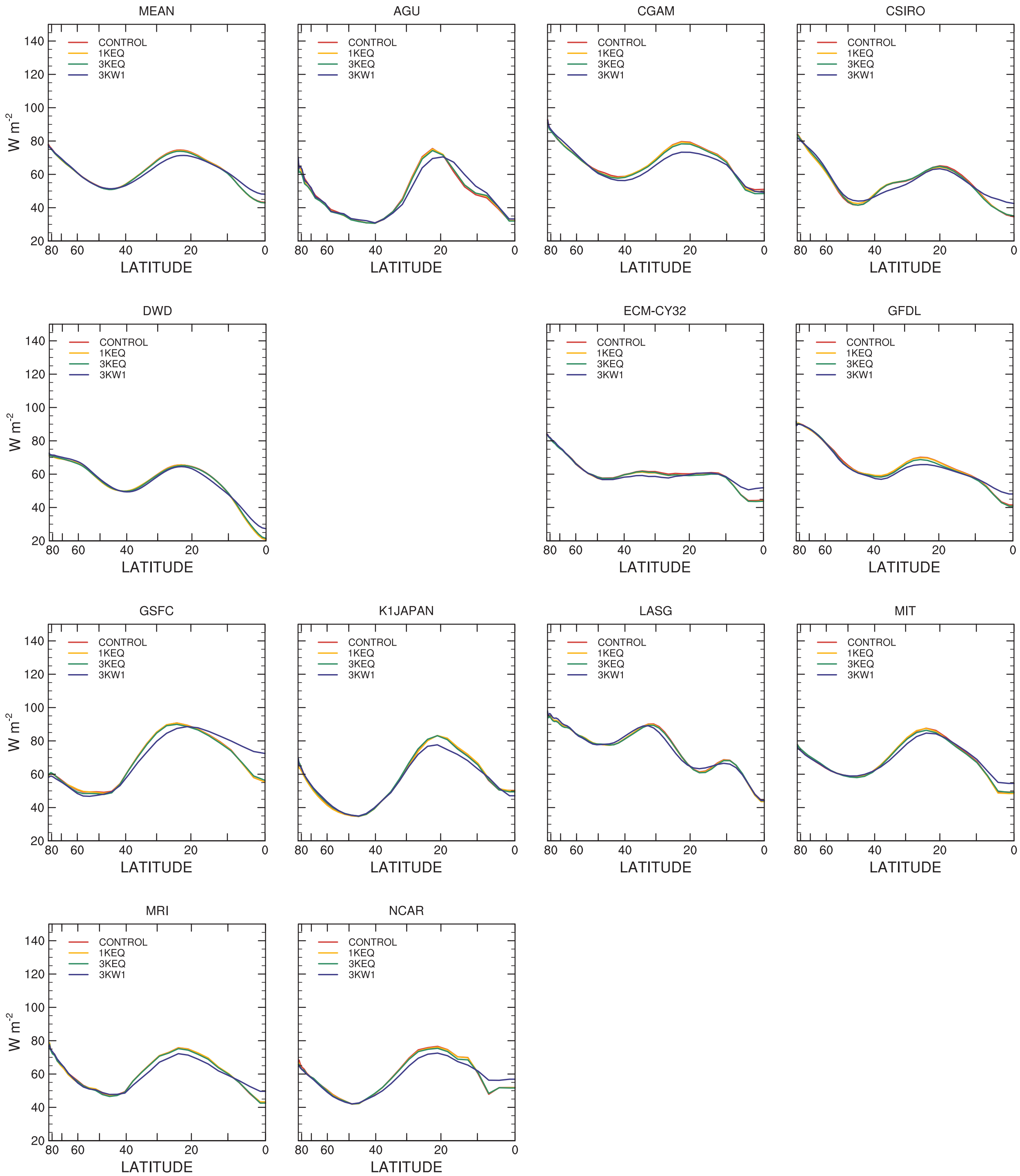

Figure 7.15: Zonal-time average surface net longwave radiation (slw) for individual models from CONTROL, 1KEQ, 3KEQ and 3KW1 SST distributions, W m^{-2}, +ve upward.

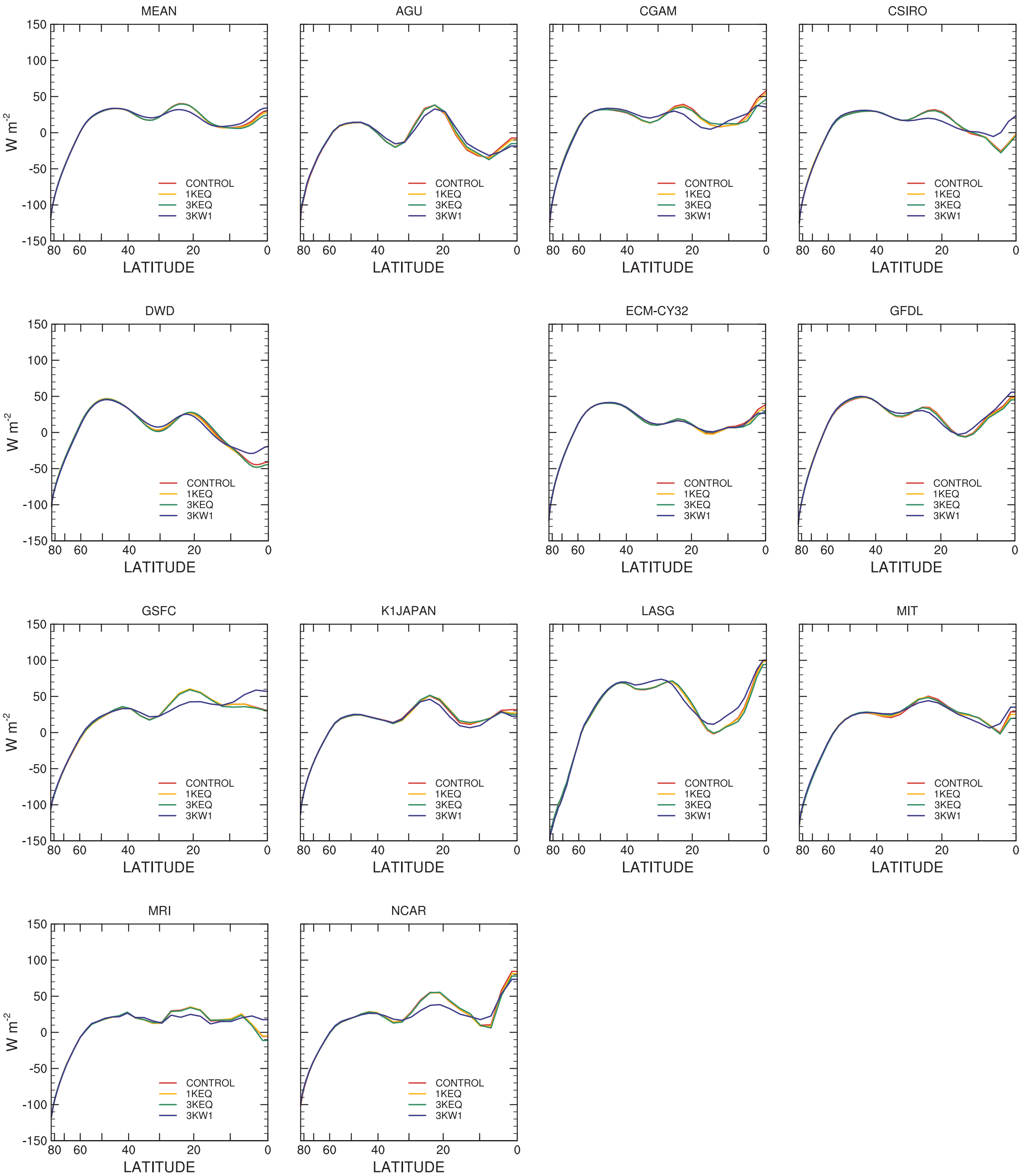

Figure 7.16: Zonal-time average surface net flux (rflux_sfce) for individual models from CONTROL, 1KEQ, 3KEQ and 3KW1 SST distributions, W m^{-2}, +ve downward.

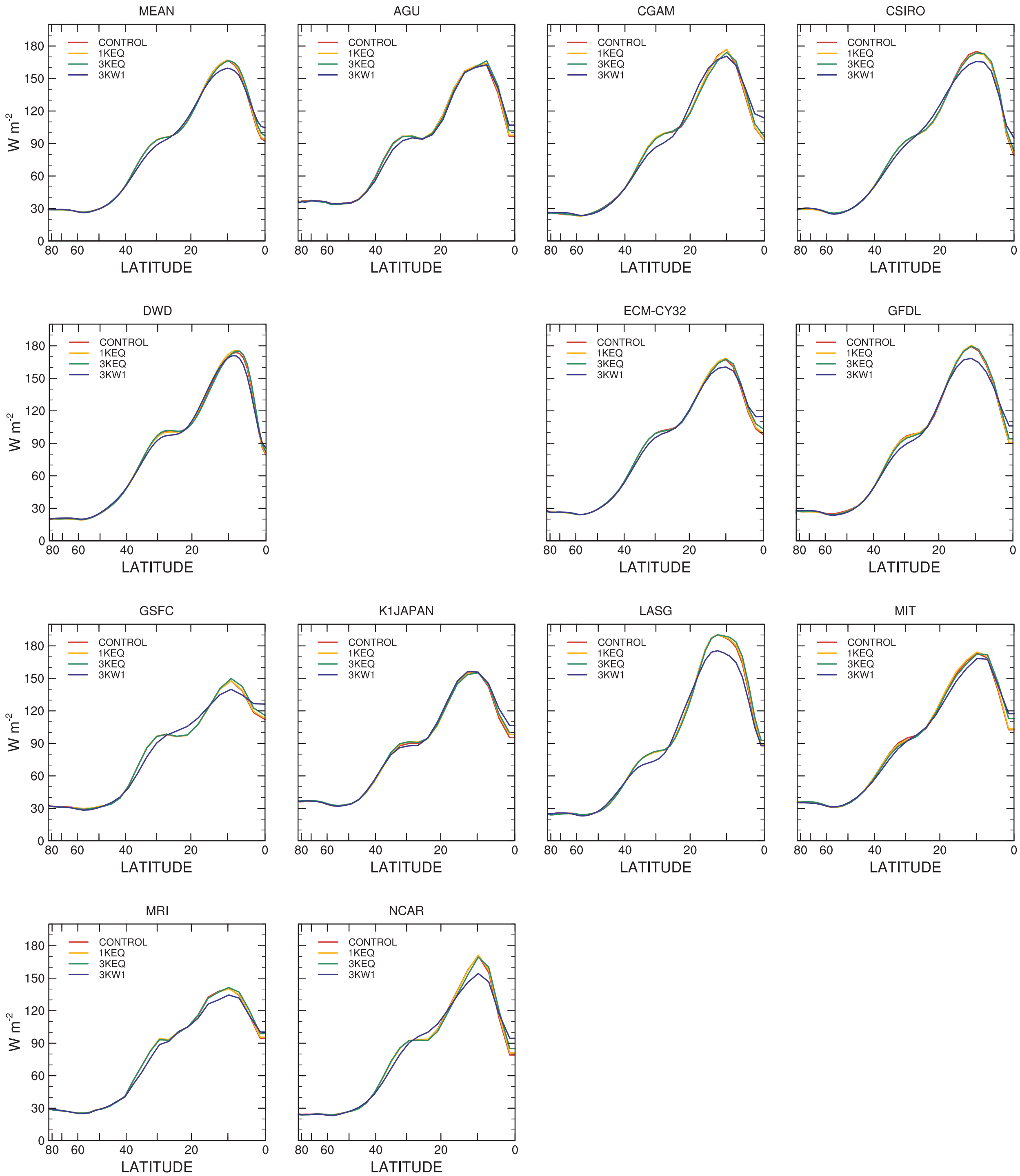

Figure 7.17: Zonal-time average surface latent heat flux (slh) for individual models from CONTROL, 1KEQ, 3KEQ and 3KW1 SST distributions, W m^{-2}.

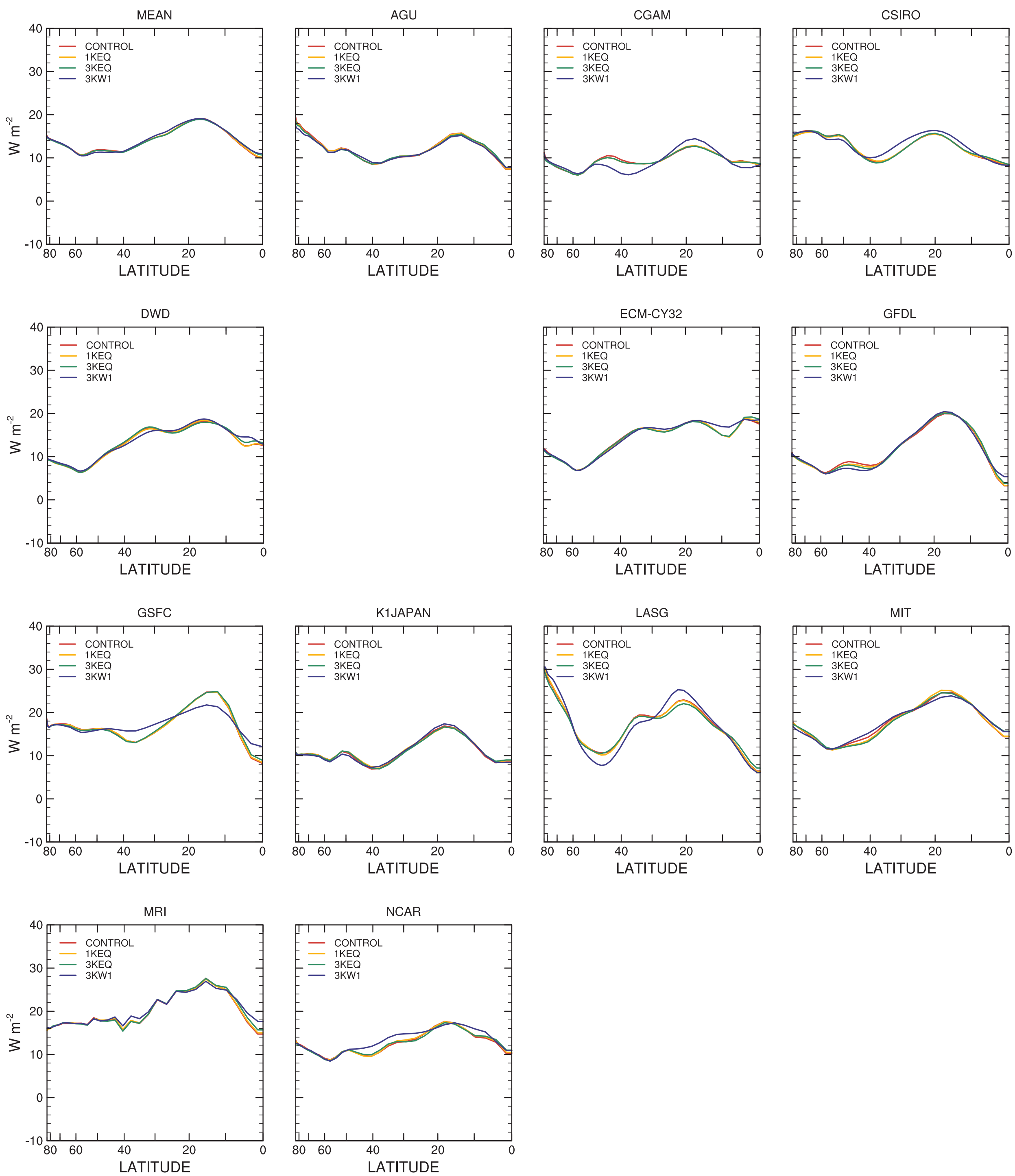

Figure 7.18: Zonal-time average surface sensible heat flux (ssh) for individual models from CONTROL, 1KEQ, 3KEQ and 3KW1 SST distributions, W m^{-2}.

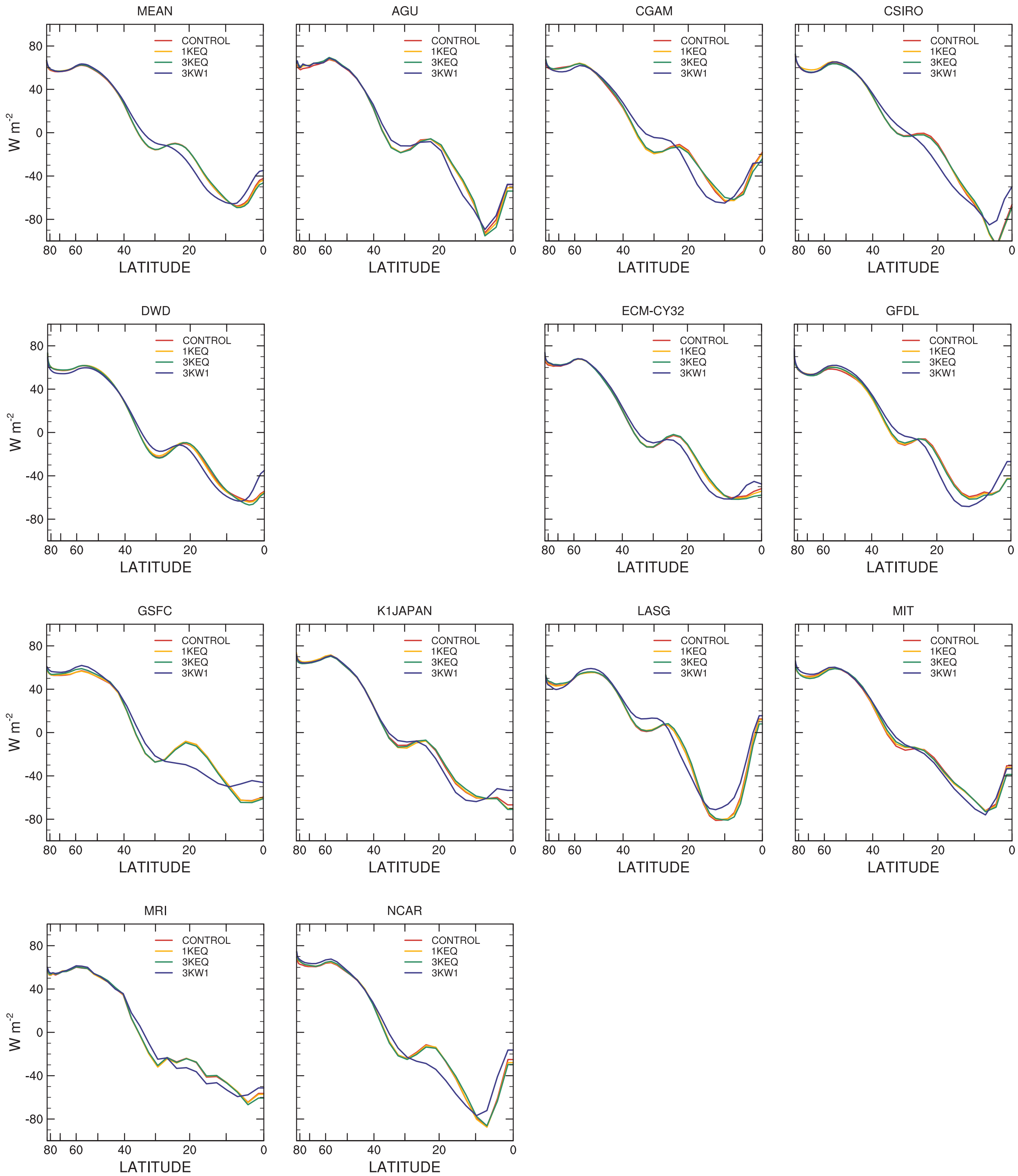

Figure 7.19: Zonal-time average net flux (rflux) for individual models from CONTROL, 1KEQ, 3KEQ and 3KW1 SST distributions, W m^{-2}, +ve out of atmosphere.

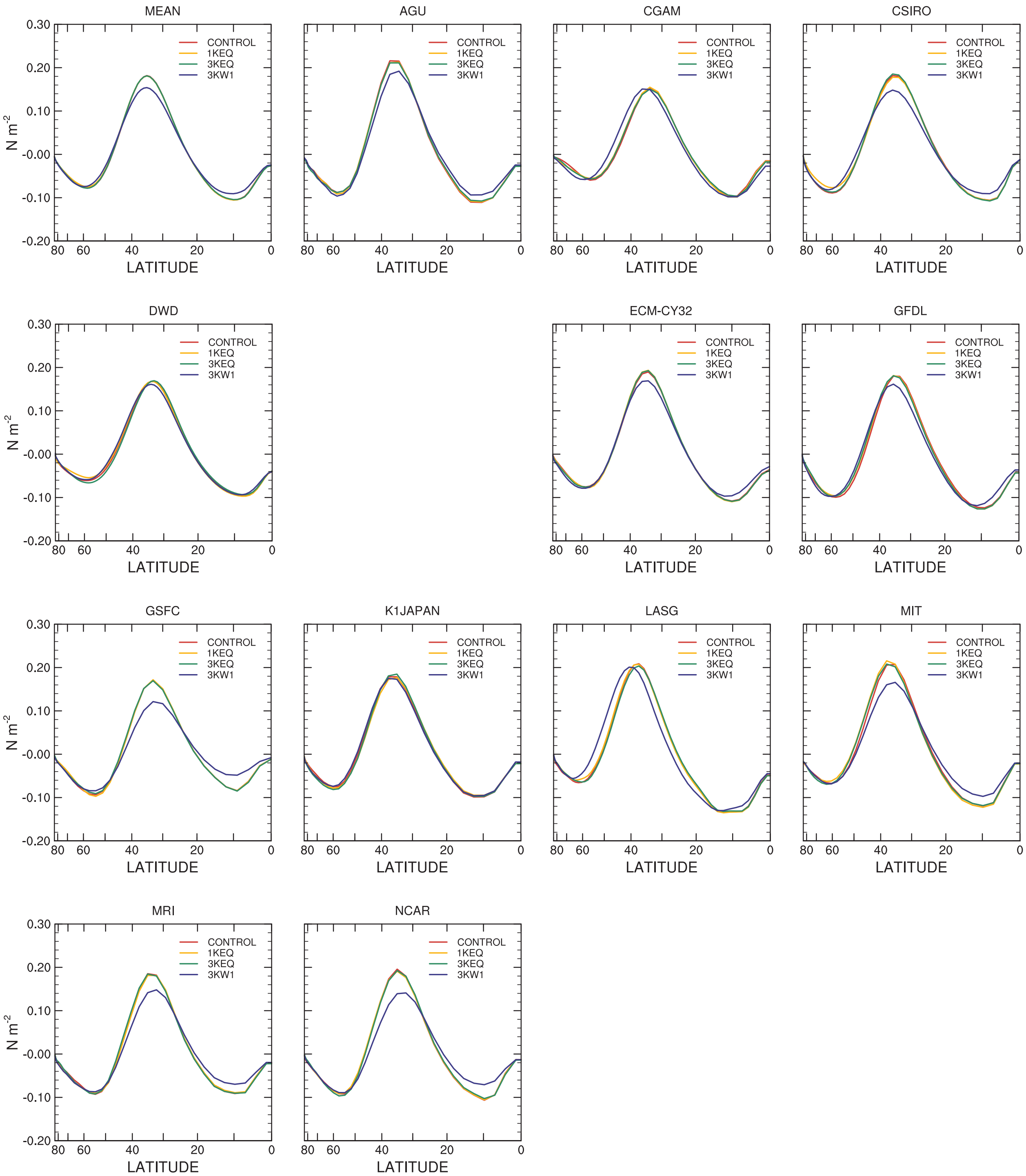

Figure 7.20: Zonal-time average zonal surface stress (tauu) for individual models from CONTROL, 1KEQ, 3KEQ and 3KW1 SST distributions, N m^{-2}.

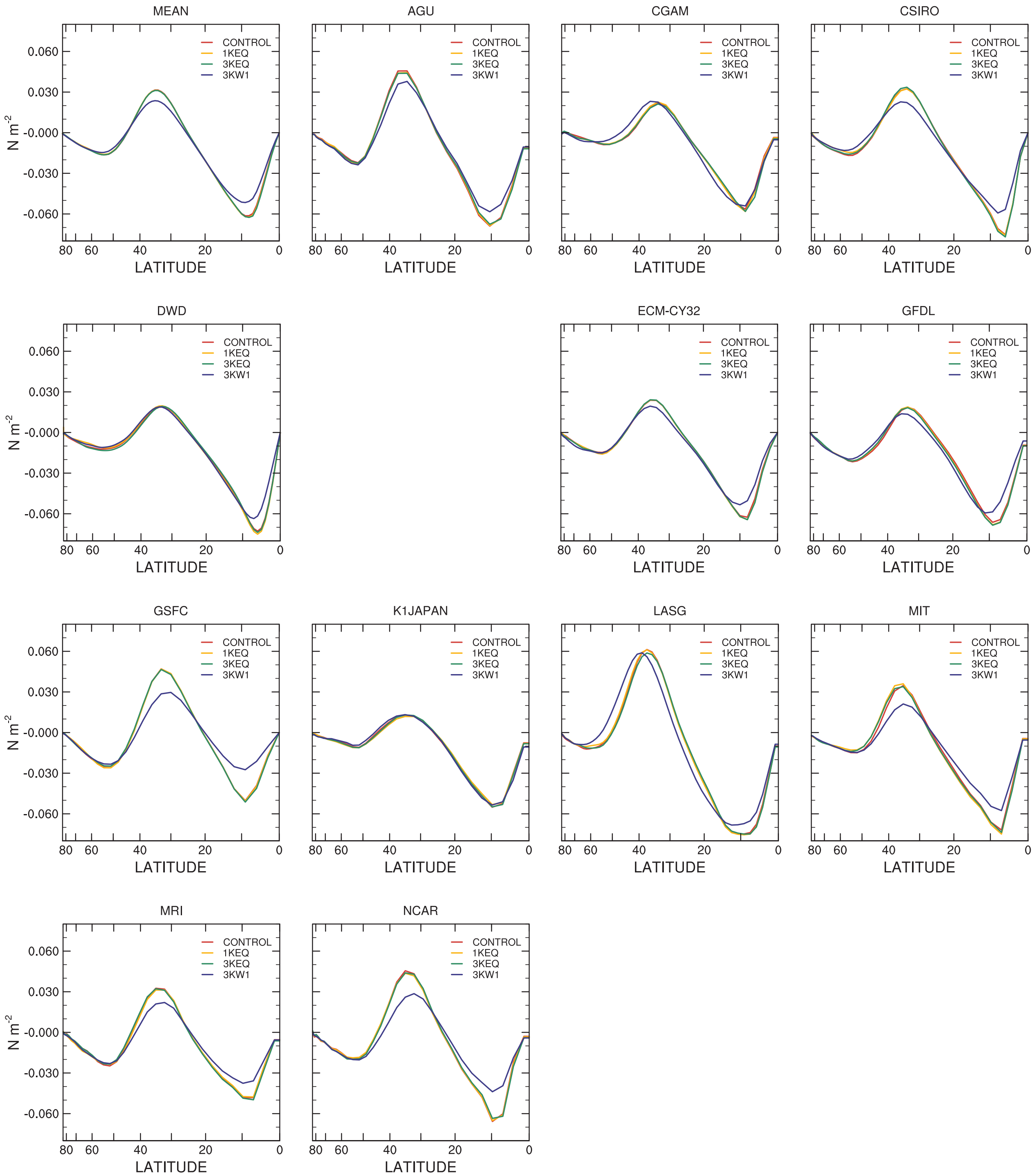

Figure 7.21: Zonal-time average meridional surface stress (tauv) for individual models from CONTROL, 1KEQ, 3KEQ and 3KW1 SST distributions, N m^{-2}.

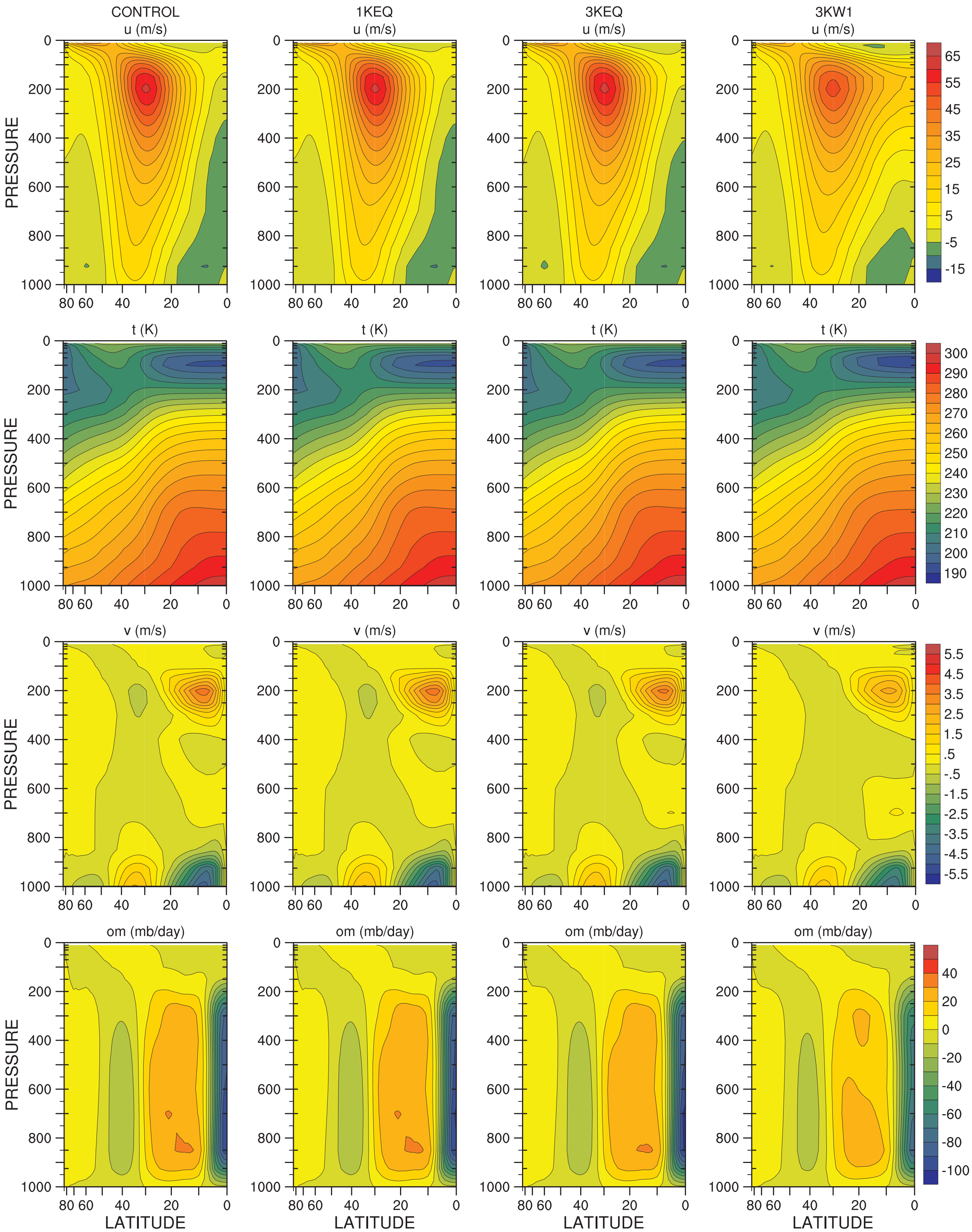

Figure 7.22: Zonal-time average multi-model mean zonal wind (u), temperature (t), meridional wind (v) and vertical wind (om) for CONTROL, 1KEQ, 3KEQ and 3KW1.

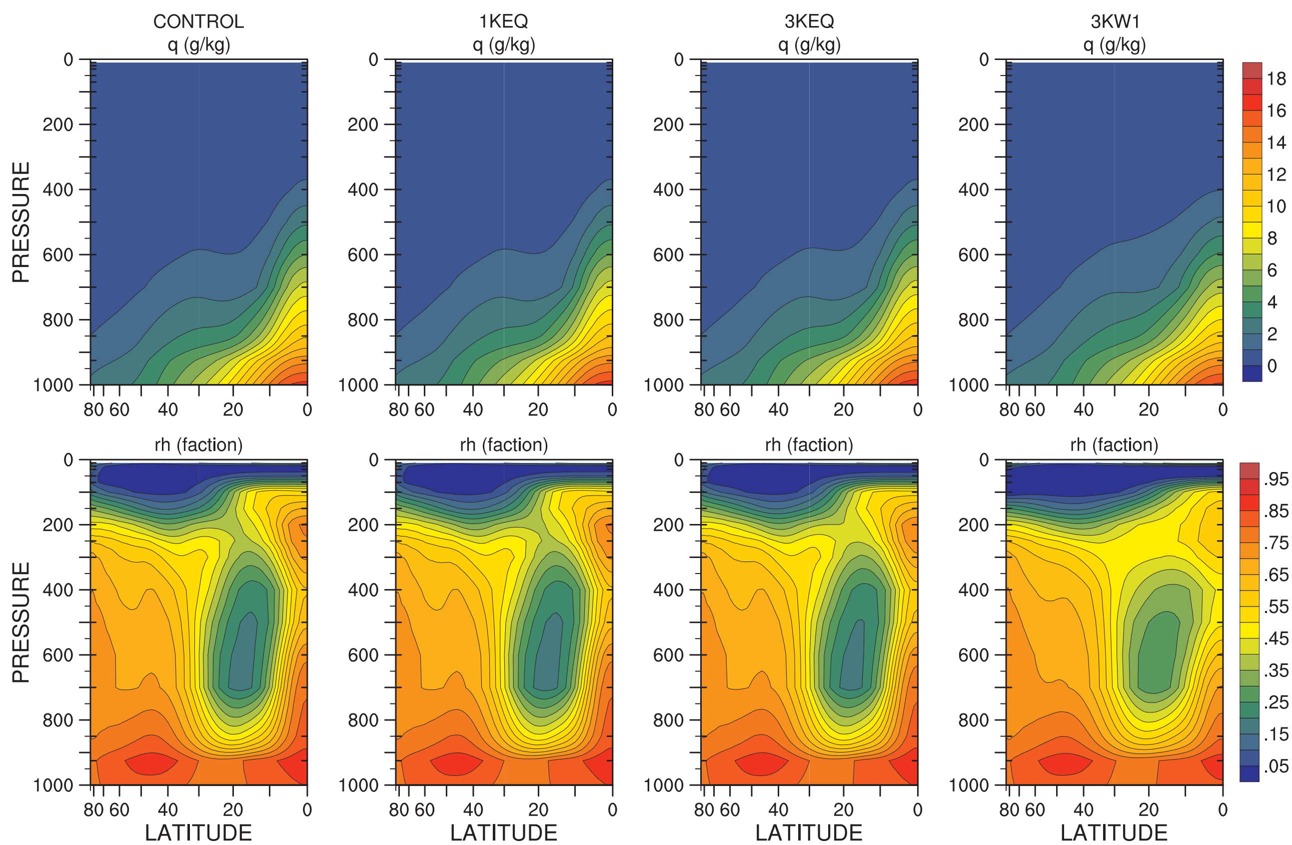

Figure 7.23: Zonal-time average multi-model mean specific humidity (q) and relative humidity (rh) for CONTROL, 1KEQ, 3KEQ and 3KW1.

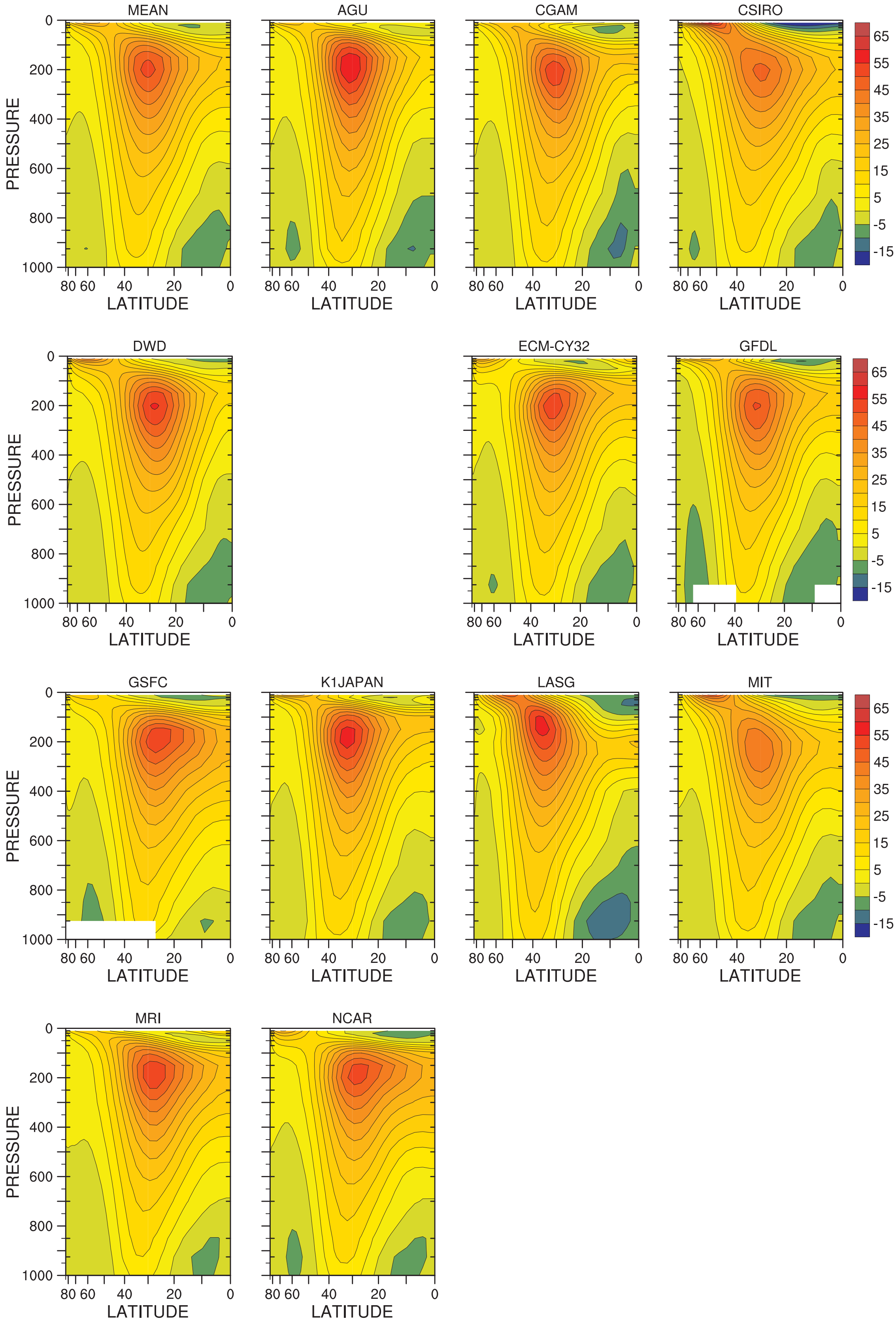

Figure 7.24: Zonal-time average zonal wind (u) from 3KW1, individual models, m s^{-1}.

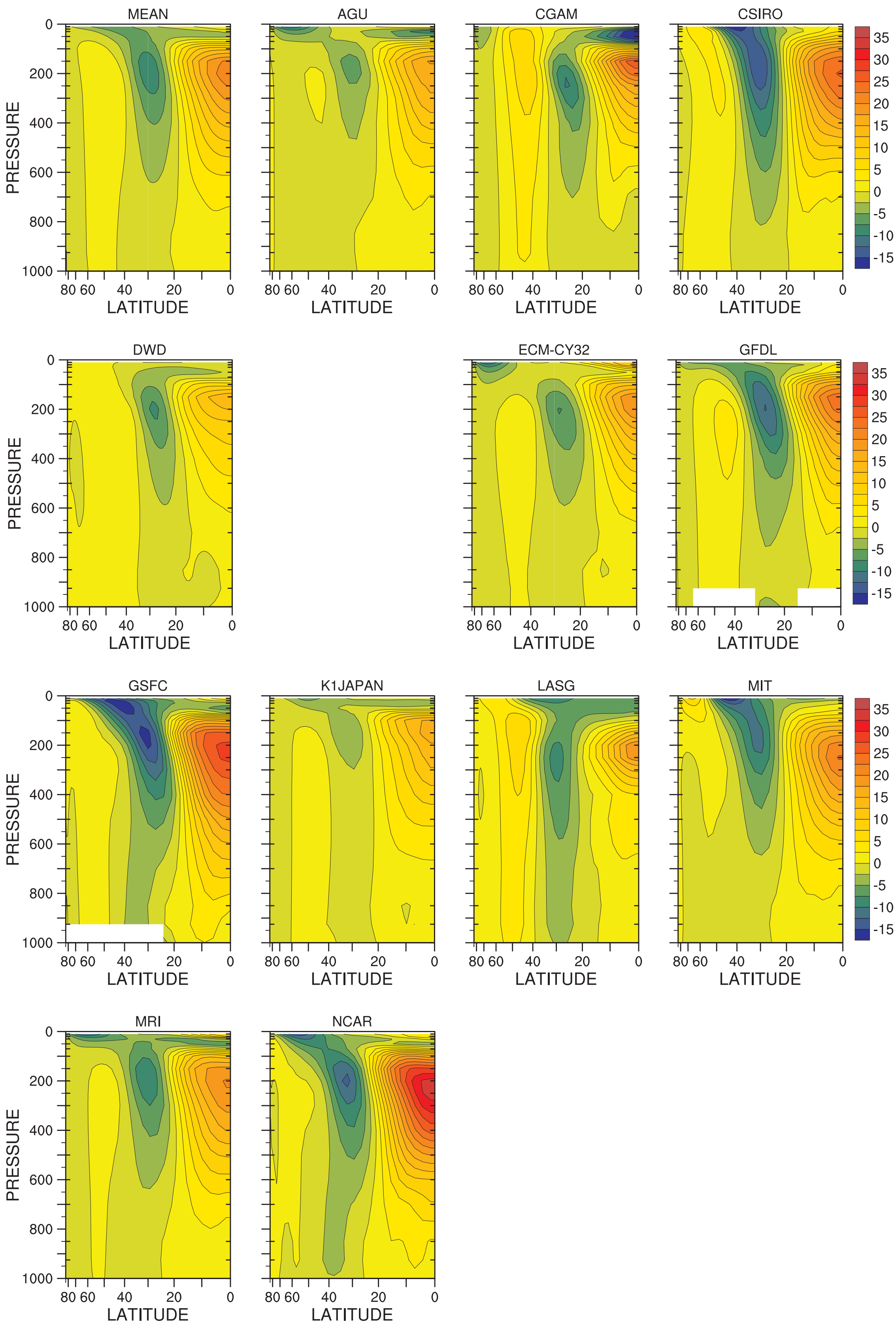

Figure 7.25: Zonal-time average zonal wind (u) from 3KW1 minus CONTROL, individual models, m s^{-1}.

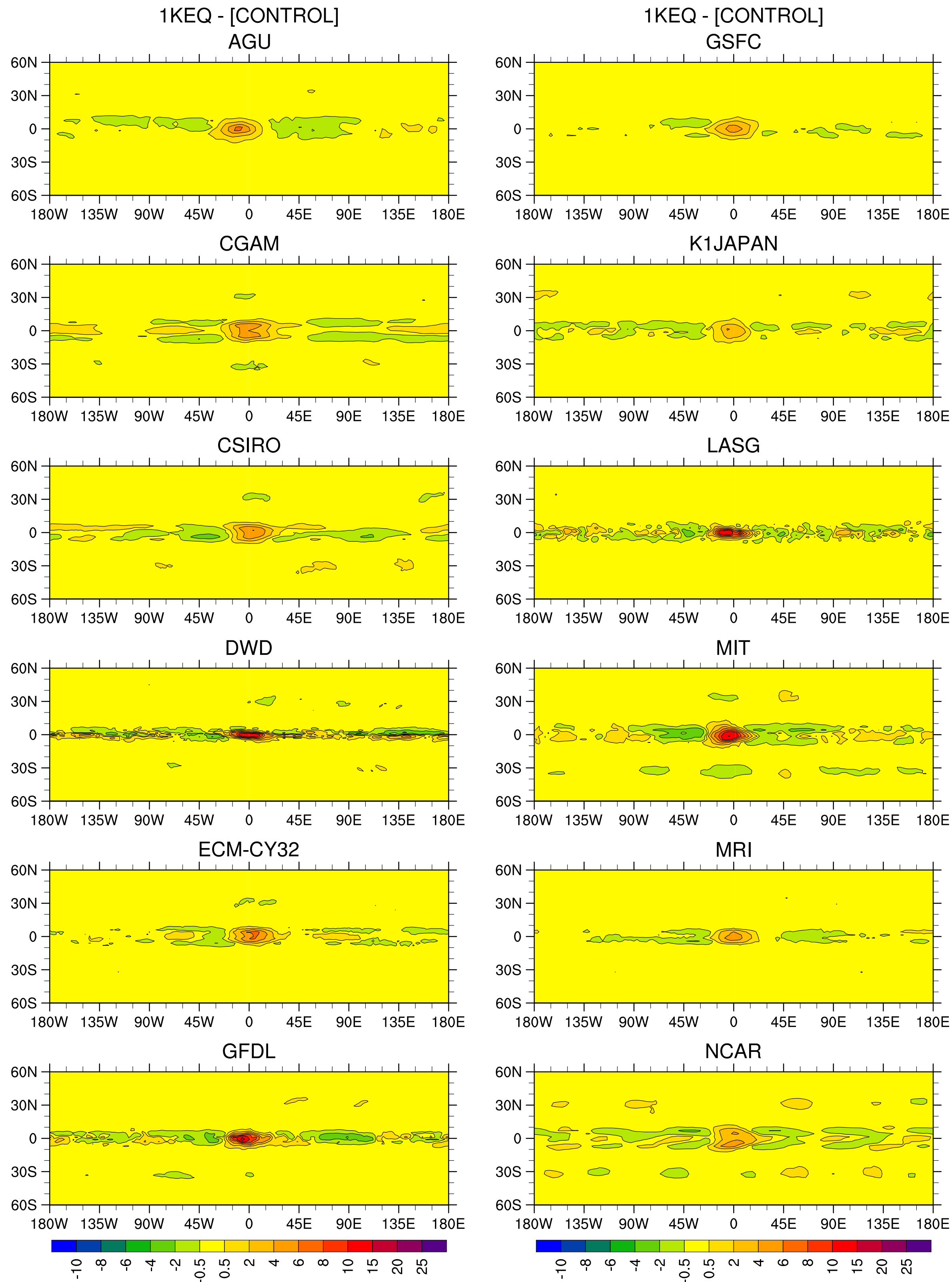

Figure 7.26: Time average precipitation (tppn), 1KEQ minus the zonal average of the CONTROL for individual models, mm day^{-1}.

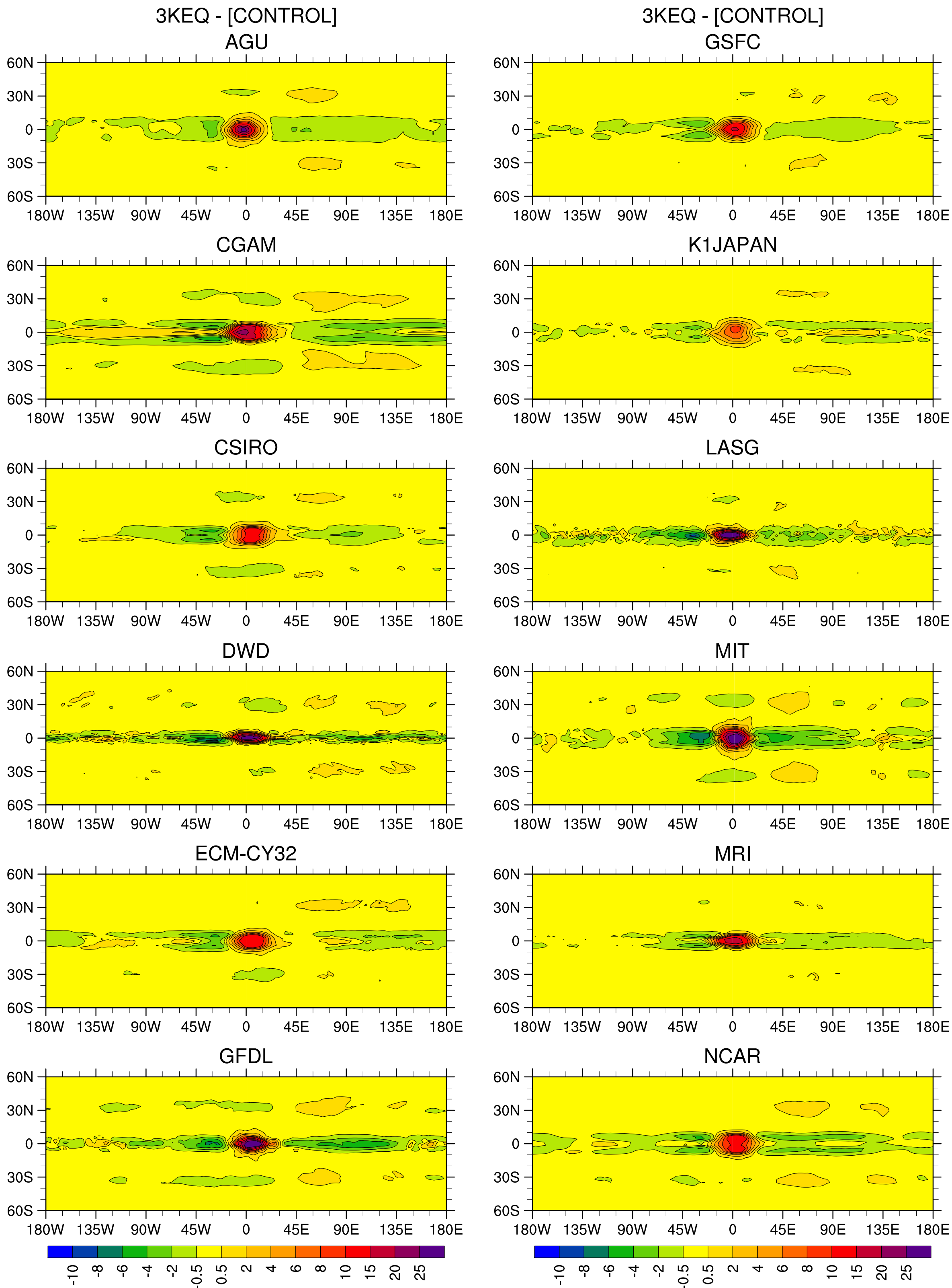

Figure 7.27: Time average precipitation (tppn), 3KEQ minus the zonal average of the CONTROL for individual models, mm day^{-1}

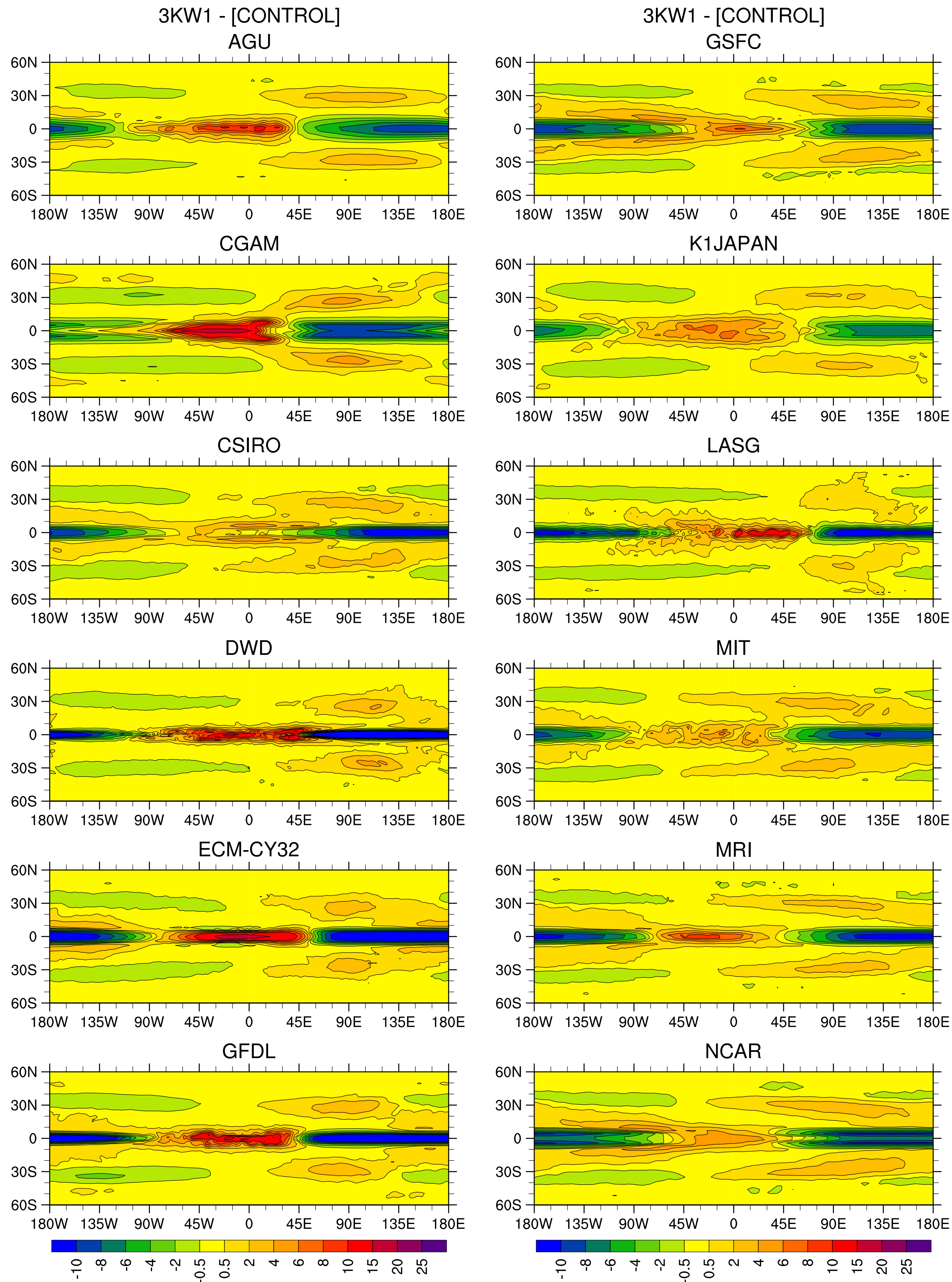

Figure 7.28: Time average precipitation (tppn), 3KW1 minus the zonal average of the CONTROL for individual models, mm day^{-1}

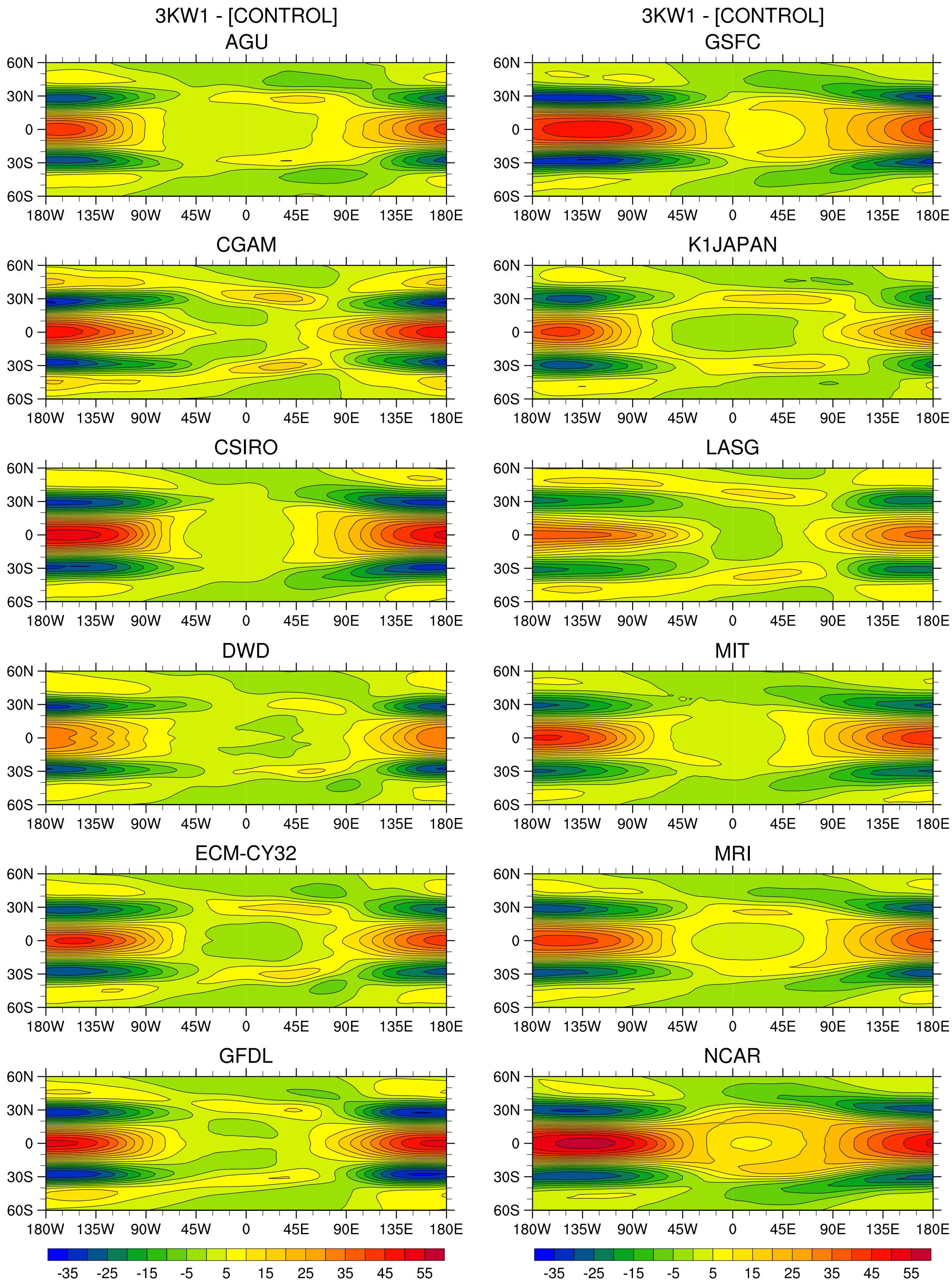

Figure 7.29: Time average zonal wind at 200mb (u200), 3KW1 minus the zonal average of the CONTROL for individual models, m sec^{-1}.

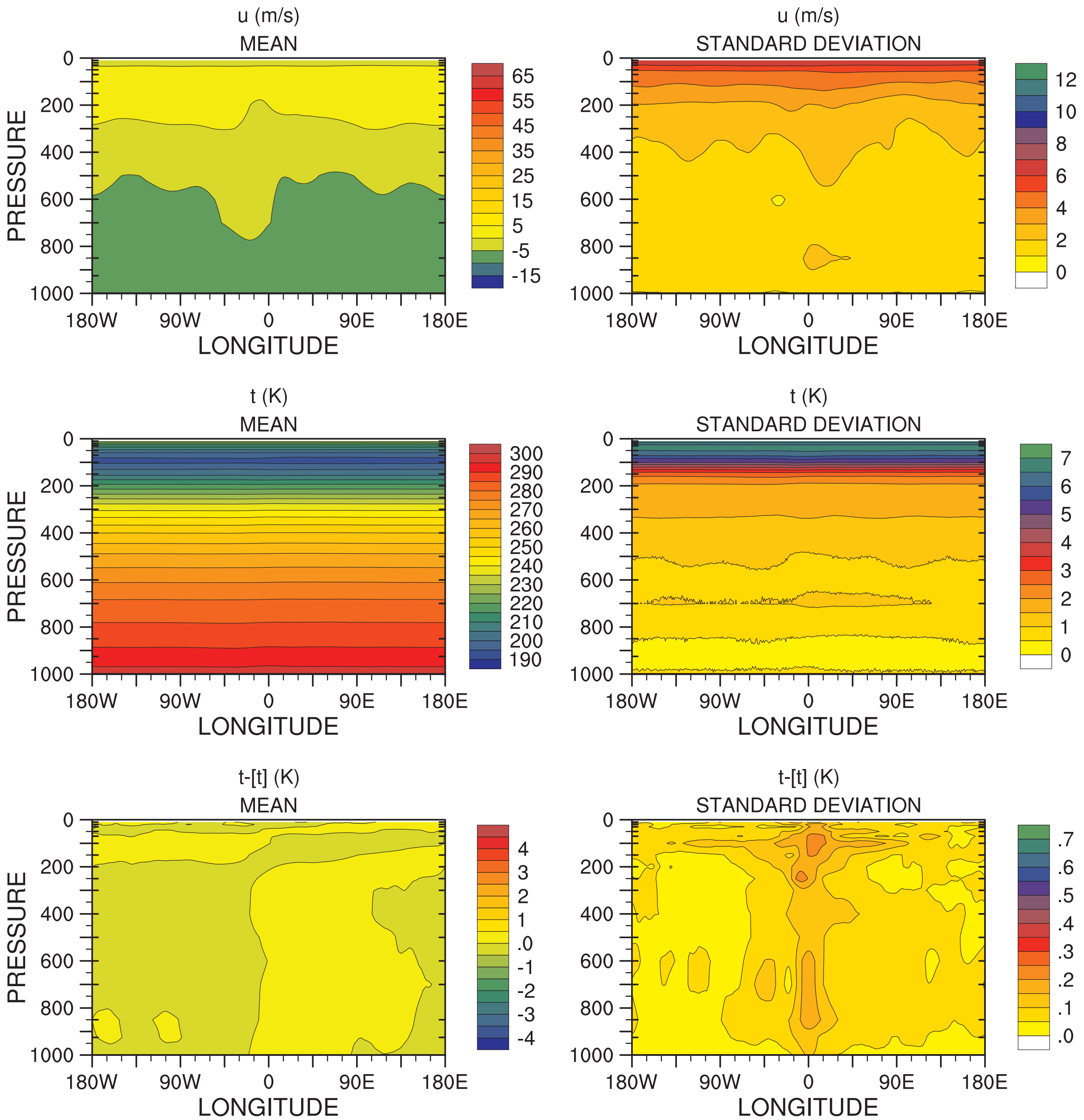

Figure 7.30: Meridional-time average, $-10 < \varphi < +10$, multi-model mean and standard deviation zonal wind (u), temperature (t) and temperature minus zonal average temperature (t-[t]) for 1KEQ.

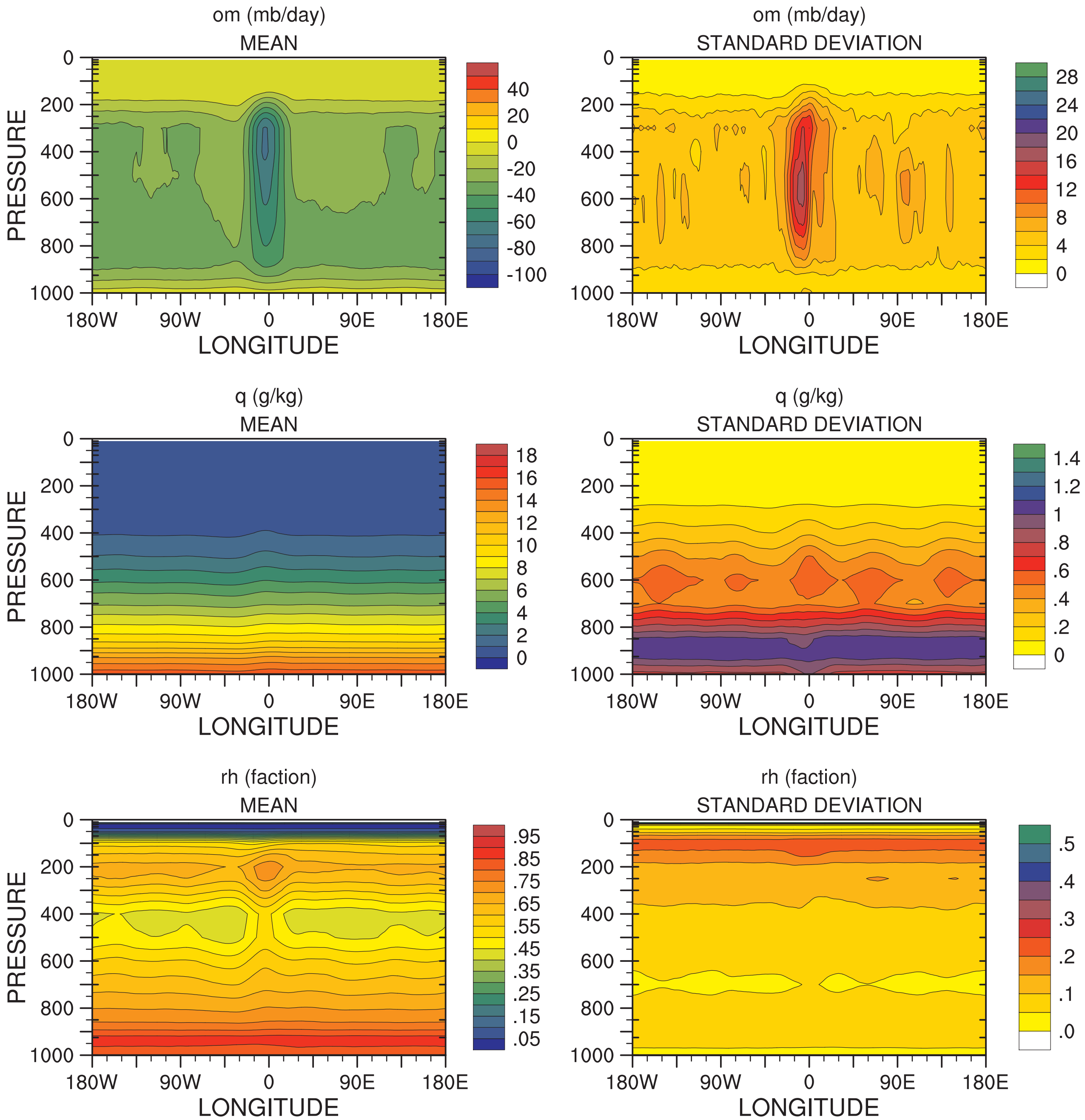

Figure 7.31: Meridional-time average, $-10 < \varphi < +10$, multi-model mean and standard deviation vertical wind (om), specific humidity (q) and relative humidity (rh) for 1KEQ.

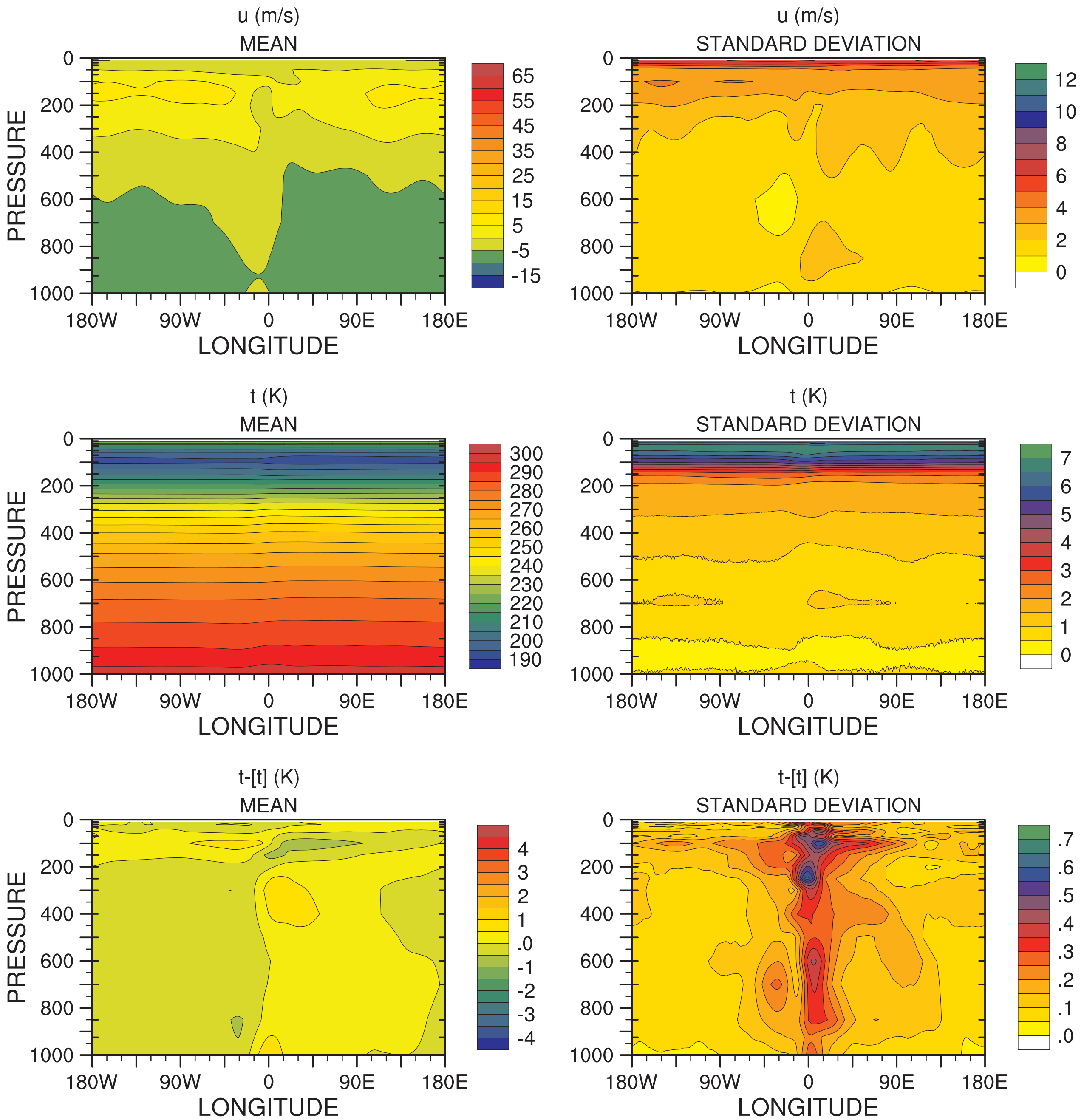

Figure 7.32: Meridional-time average, $-10 < \varphi < +10$, multi-model mean and standard deviation zonal wind (u), temperature (t) and temperature minus zonal average temperature (t-[t]) for 3KEQ.

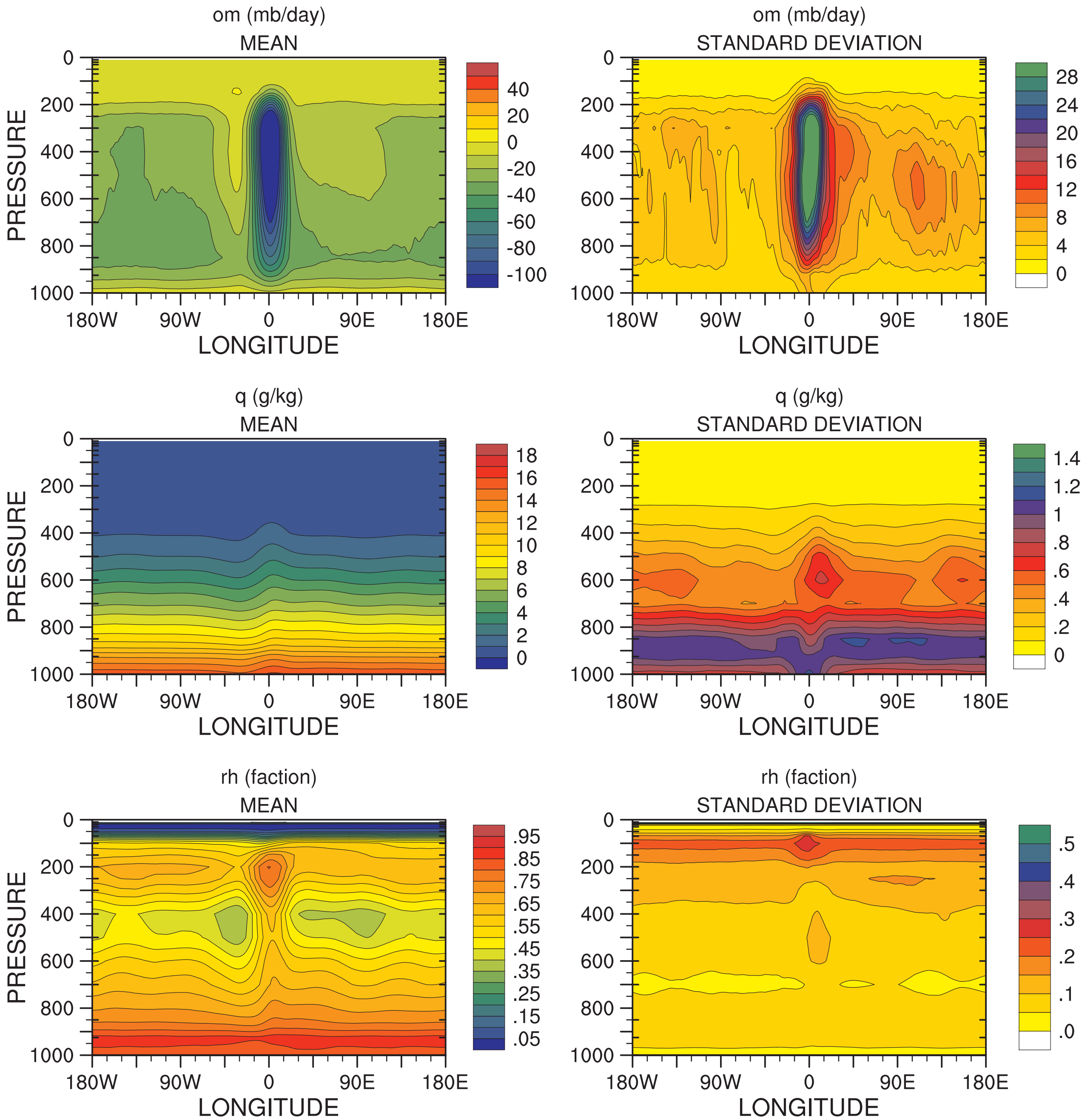

Figure 7.33: Meridional-time average, $-10 < \varphi < +10$, multi-model mean and standard deviation vertical wind (om), specific humidity (q) and relative humidity (rh) for 3KEQ.

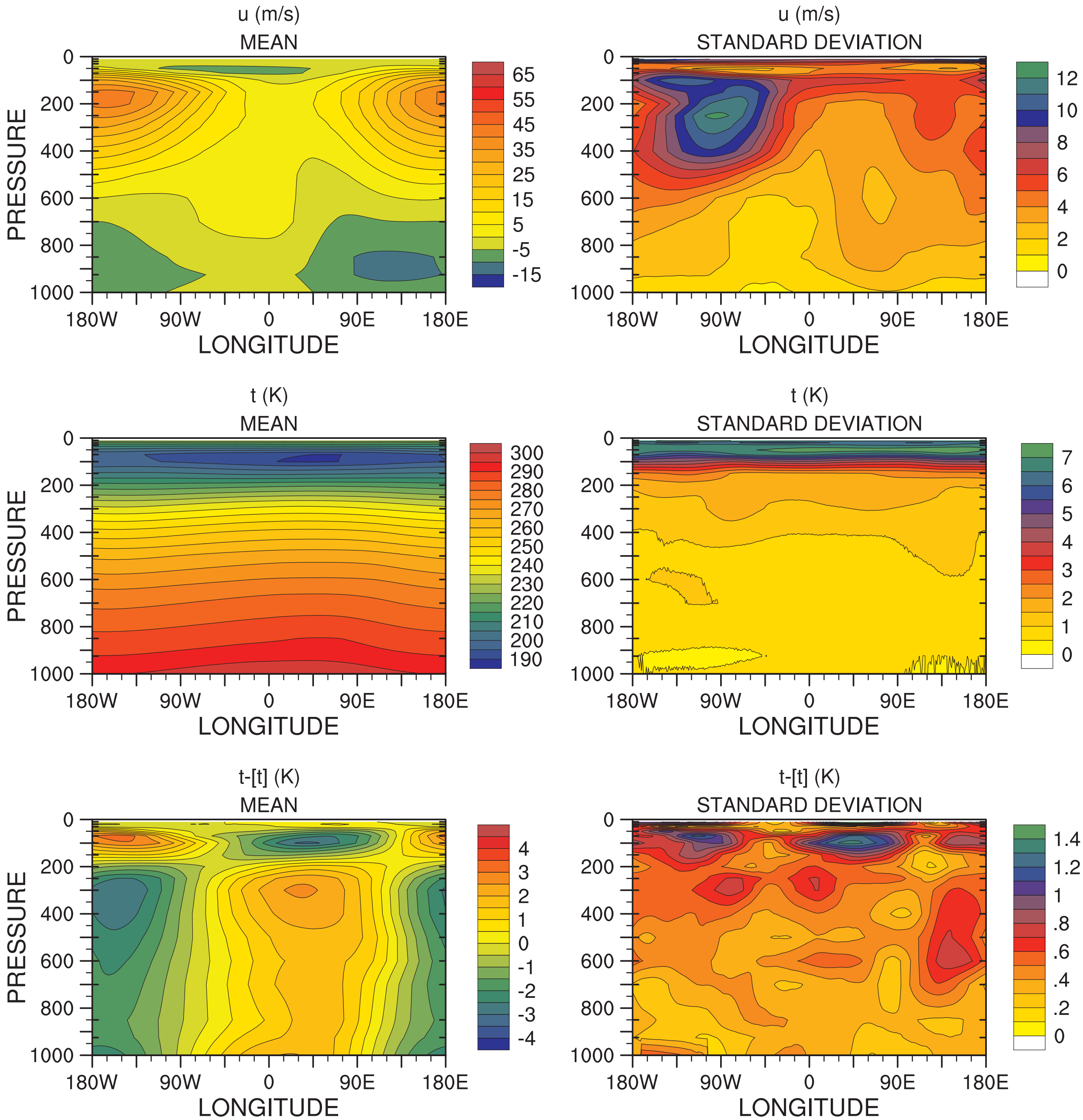

Figure 7.34: Meridional-time average, $-10 < \varphi < +10$, multi-model mean and standard deviation zonal wind (u), temperature (t) and temperature minus zonal average temperature (t-[t]) for 3KW1.

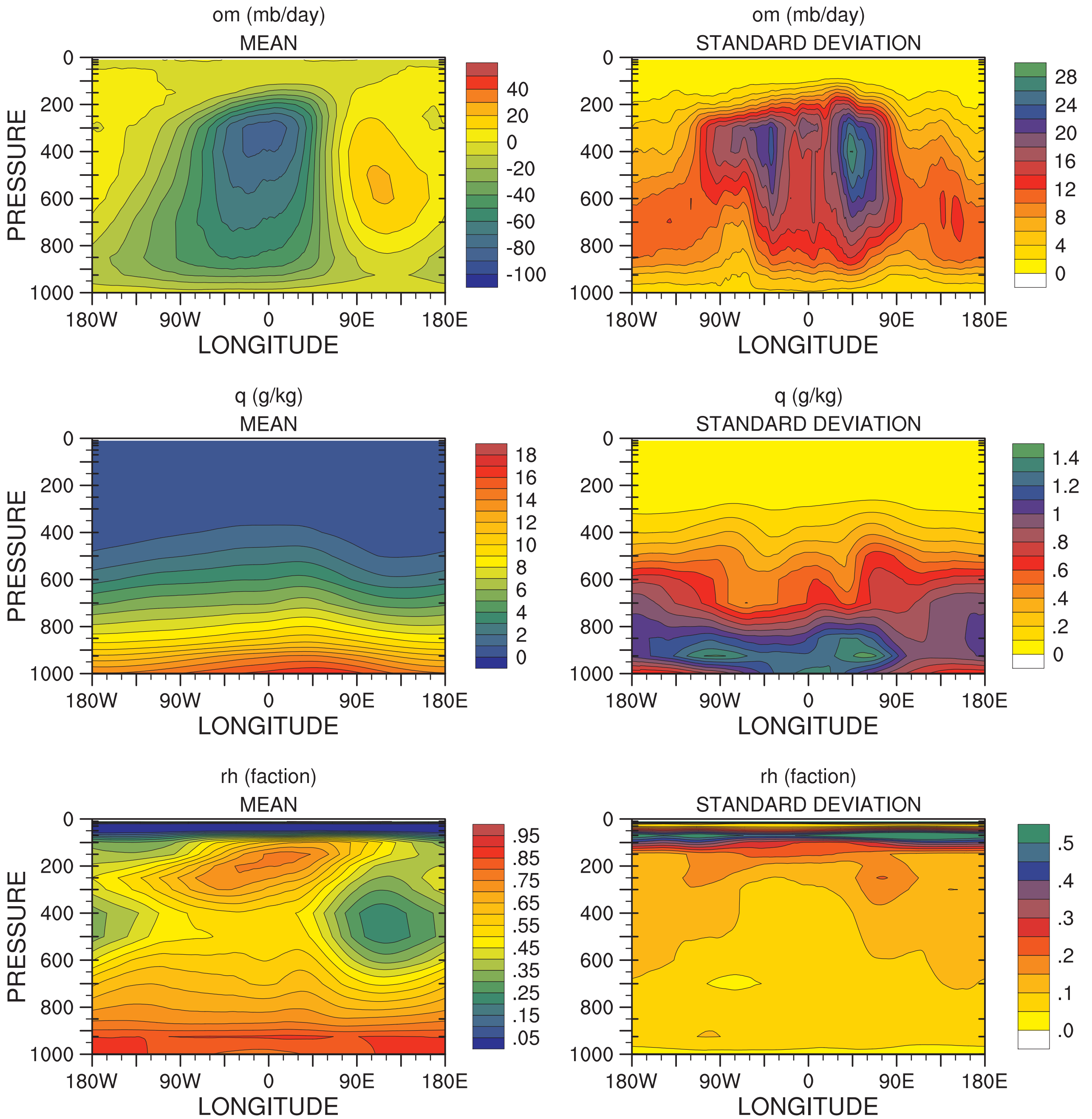

Figure 7.35: Meridional-time average, $-10 < \varphi < +10$, multi-model mean and standard deviation vertical wind (om), specific humidity (q) and relative humidity (rh) for 3KW1.

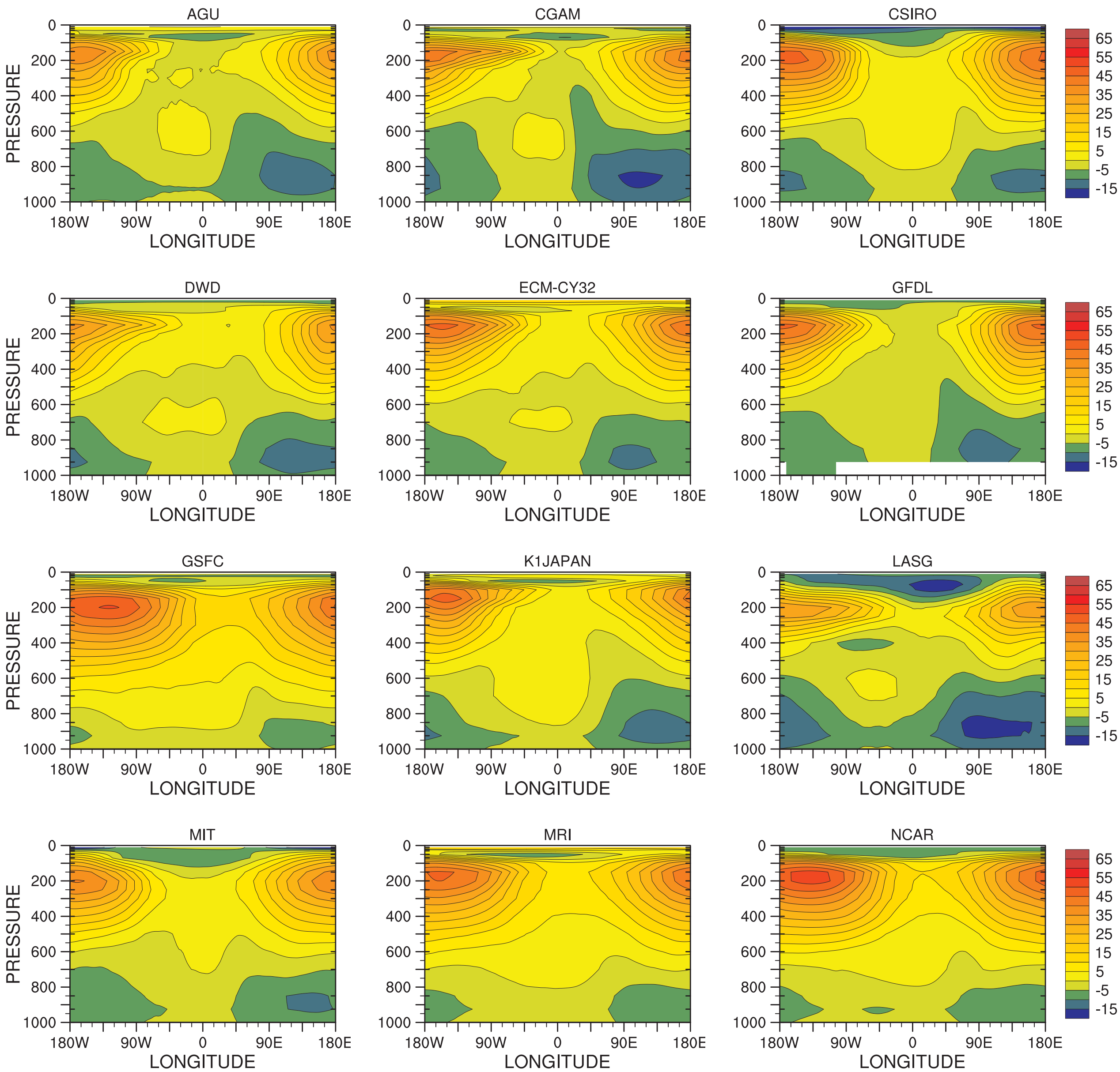

Figure 7.36: Meridional-time average, $-10 < \varphi < +10$, zonal wind (u) for 3KW1 for individual models, m s^{-1}.

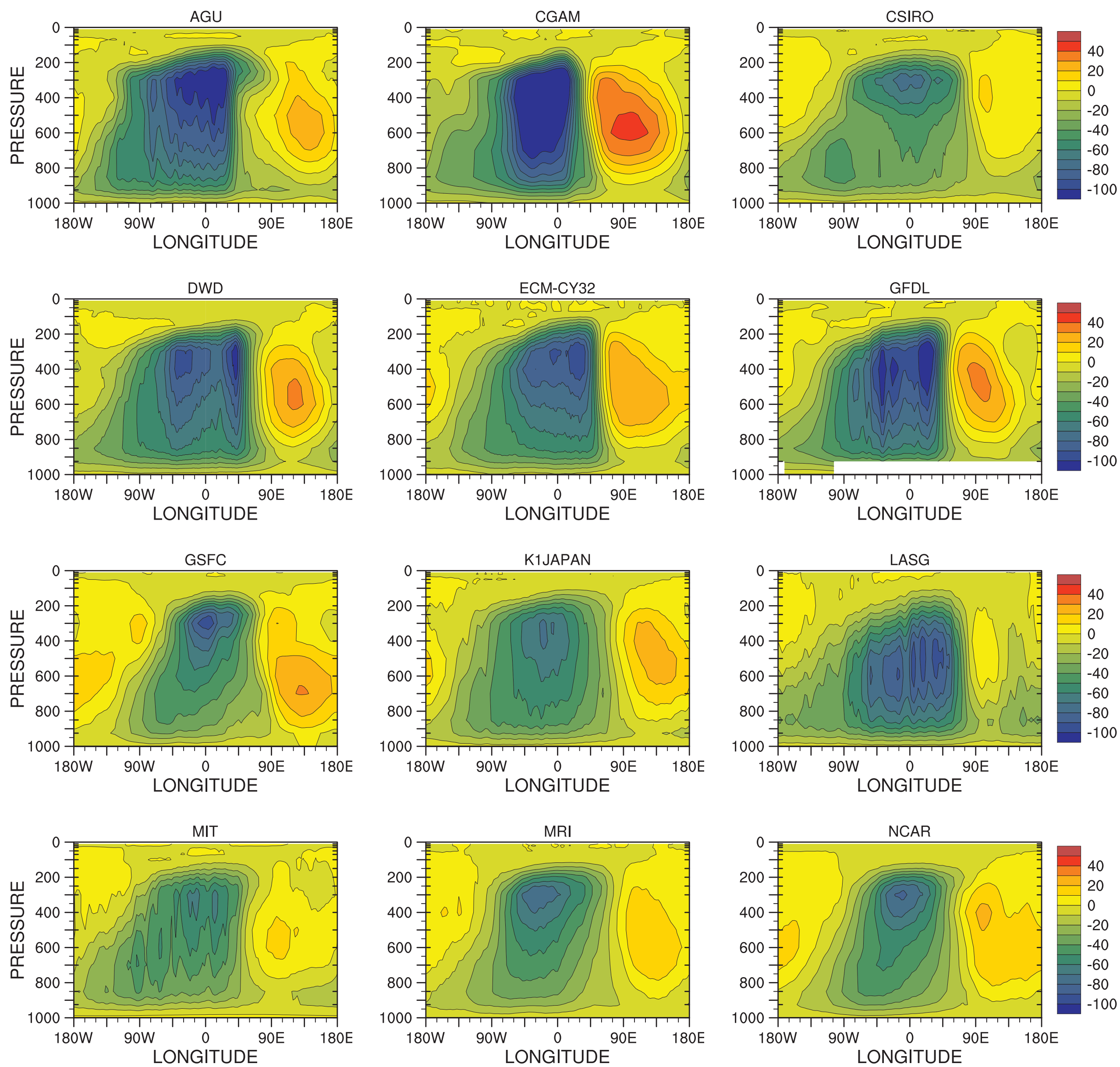

Figure 7.37: Meridional-time average, $-10 < \varphi < +10$, vertical velocity (om) for 3KW1 for individual models, mb day^{-1}.

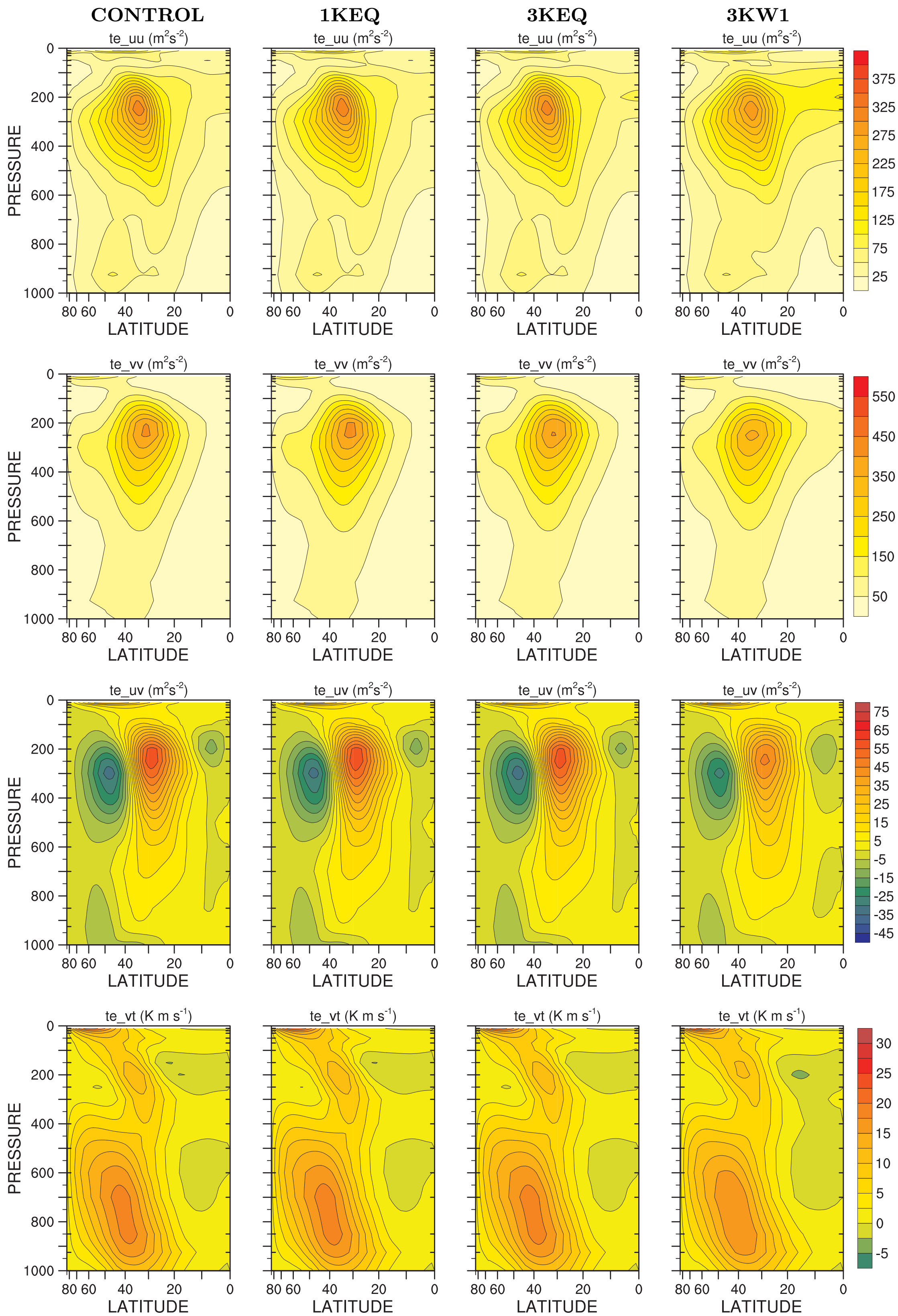

Figure 7.38: Multi-model mean transient eddy te_uu, $\overline{\left[(u'^*)^2\right]}$, te_vv, $\overline{\left[(v'^*)^2\right]}$, te_uv, $\overline{[u'^* v'^*]}$ and te_vt, $\overline{[v'^* T^*]}$ for CONTROL, 1KEQ, 3KEQ and 3KW1.

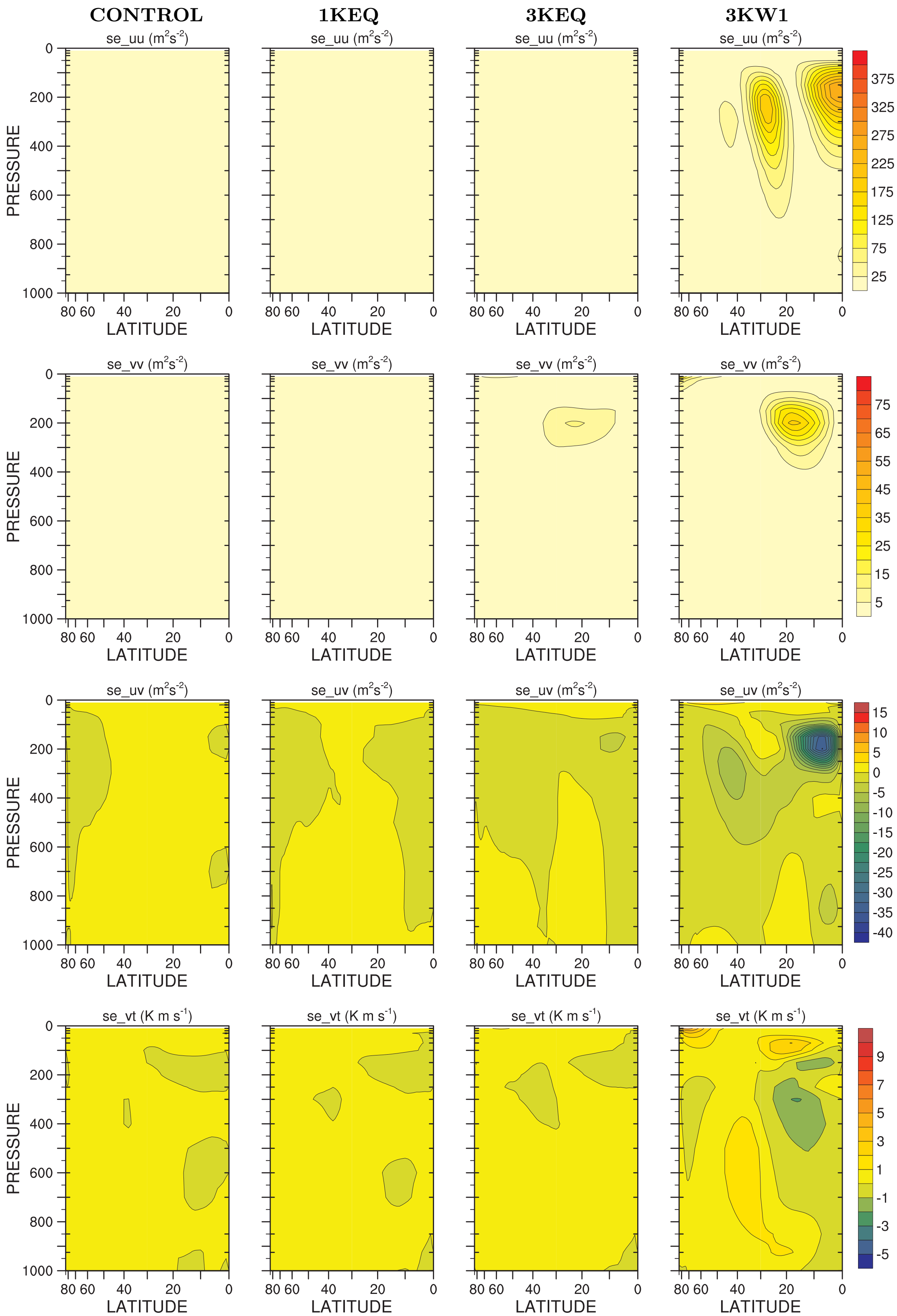

Figure 7.39: Multi-model mean stationary eddy se_uu, $[\overline{u}^*\overline{u}^*]$, se_vv, $[\overline{v}^*\overline{v}^*]$, se_uv, $[\overline{u}^*\overline{v}^*]$ and se_vt, $\left[\overline{v}^*\overline{T}^*\right]$ for CONTROL, 1KEQ, 3KEQ and 3KW1.

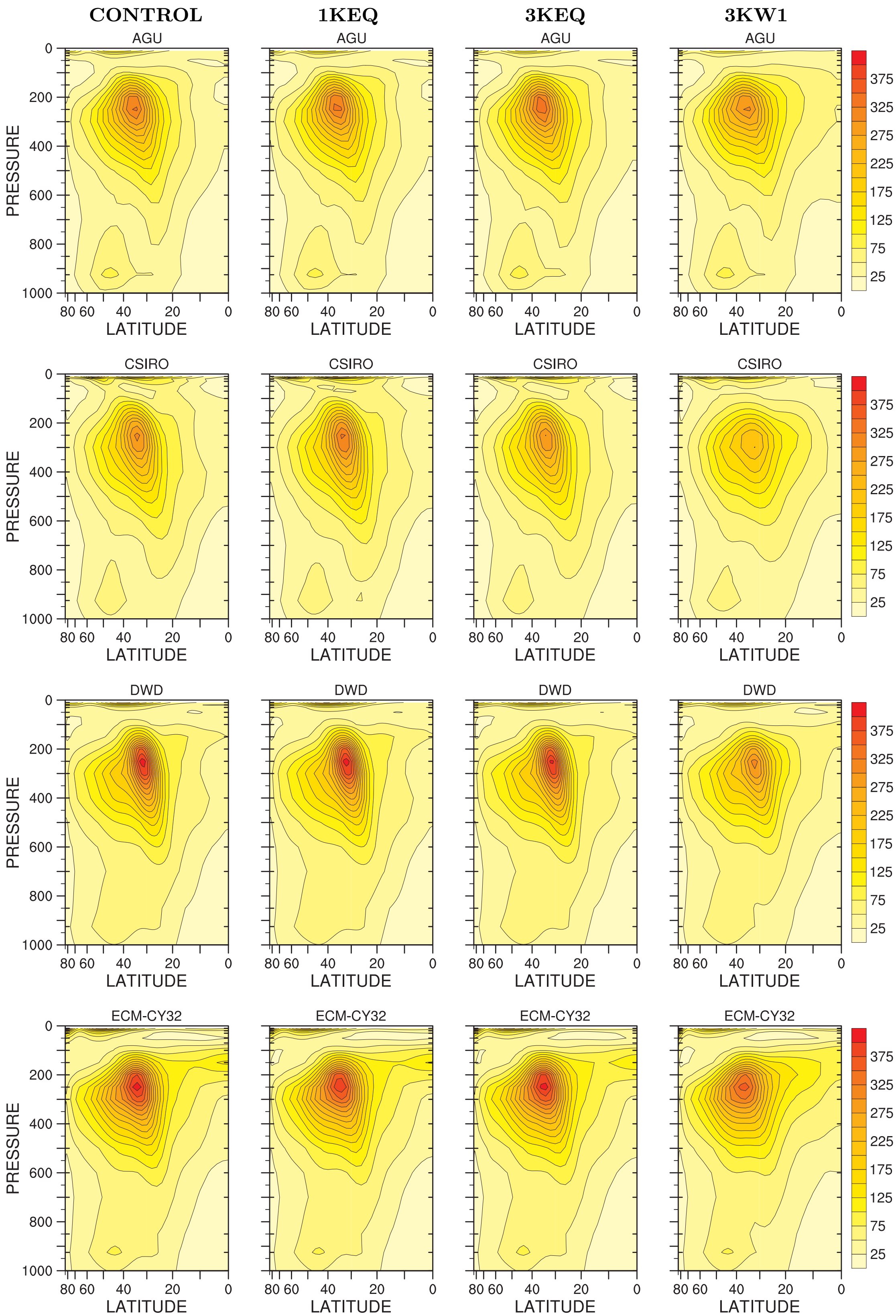

Figure 7.40: Individual model u variance, transient eddy, te_uu, $\overline{\left[(u'^{*})^{2}\right]}$, $m^2\ s^{-2}$.

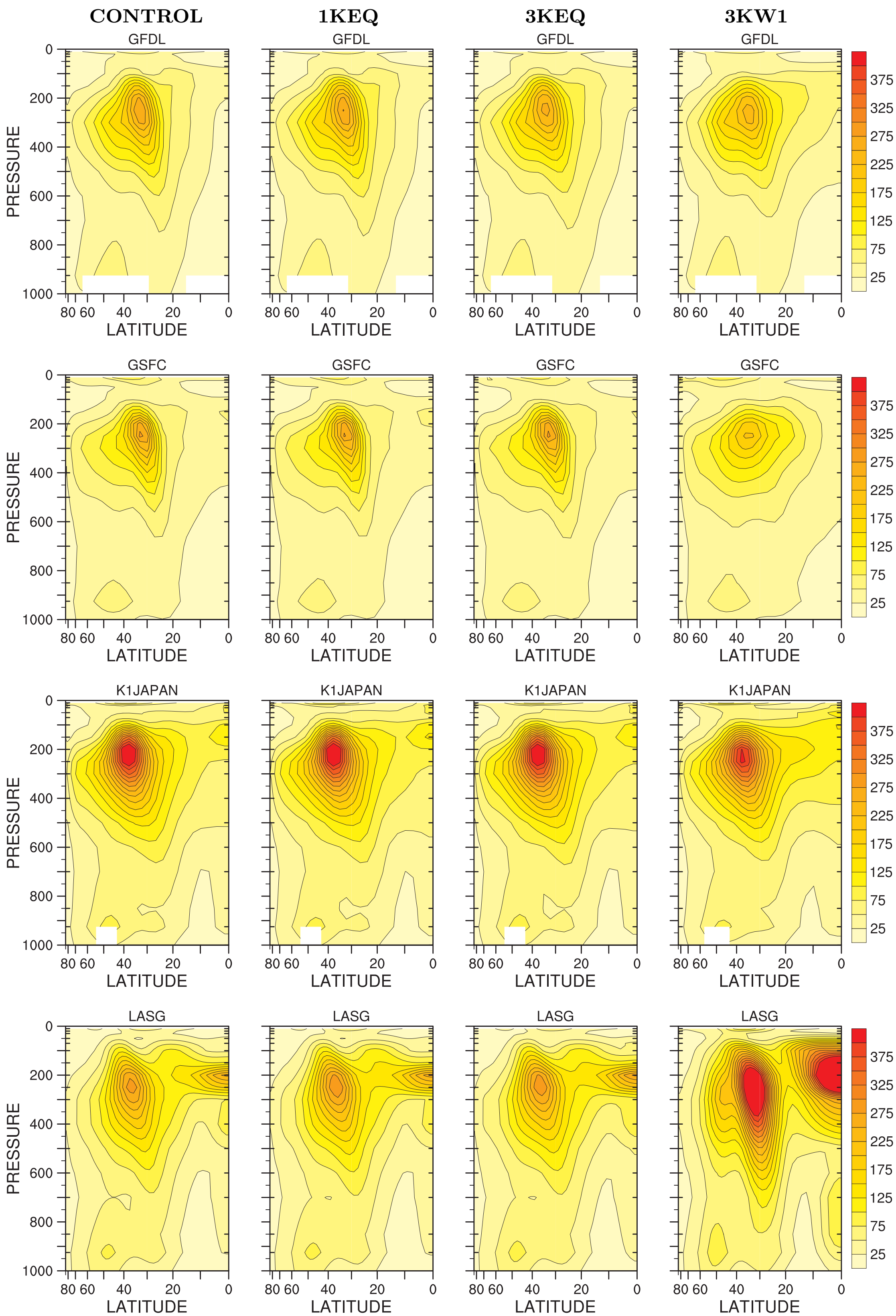

Figure 7.40 (continued): Individual model u variance, transient eddy, te_uu, $\overline{\left[(u'^{*})^{2}\right]}$, m^2 s^{-2}.

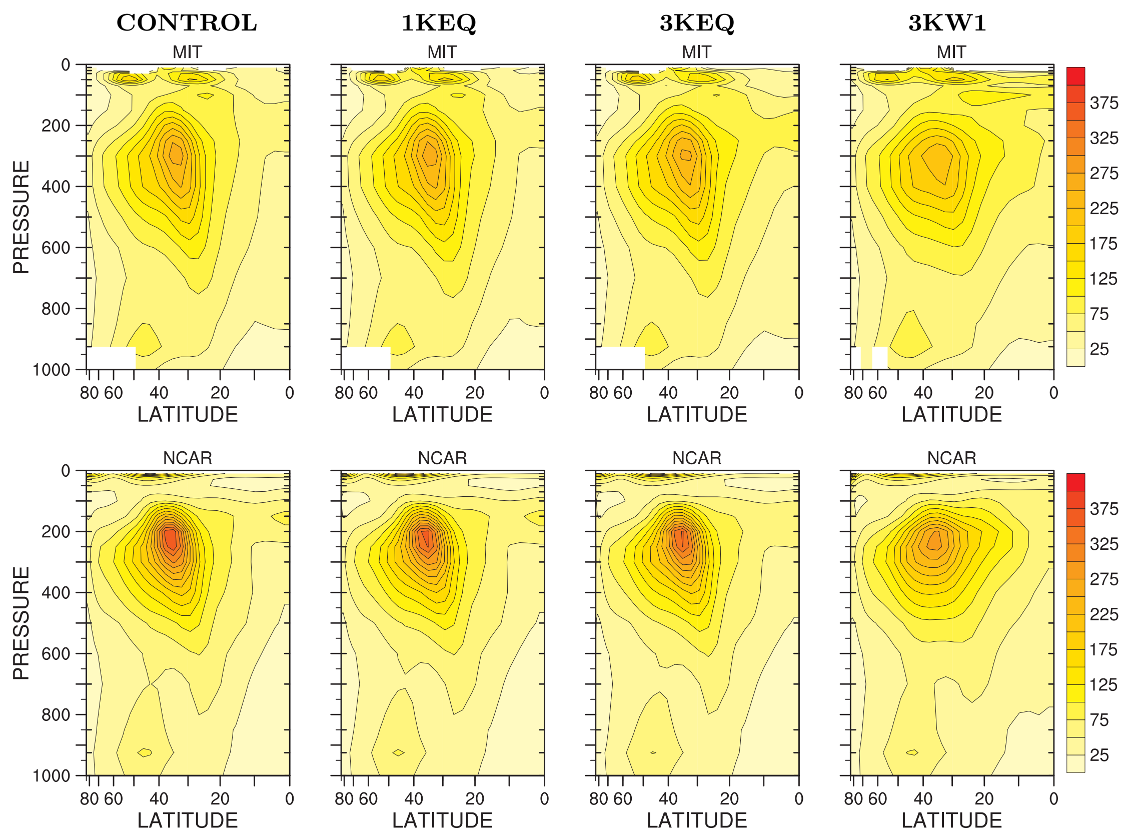

Figure 7.40 (continued): Individual model u variance, transient eddy, te_uu, $\overline{\left[(u'^{*})^{2}\right]}$, m^2 s^{-2}.

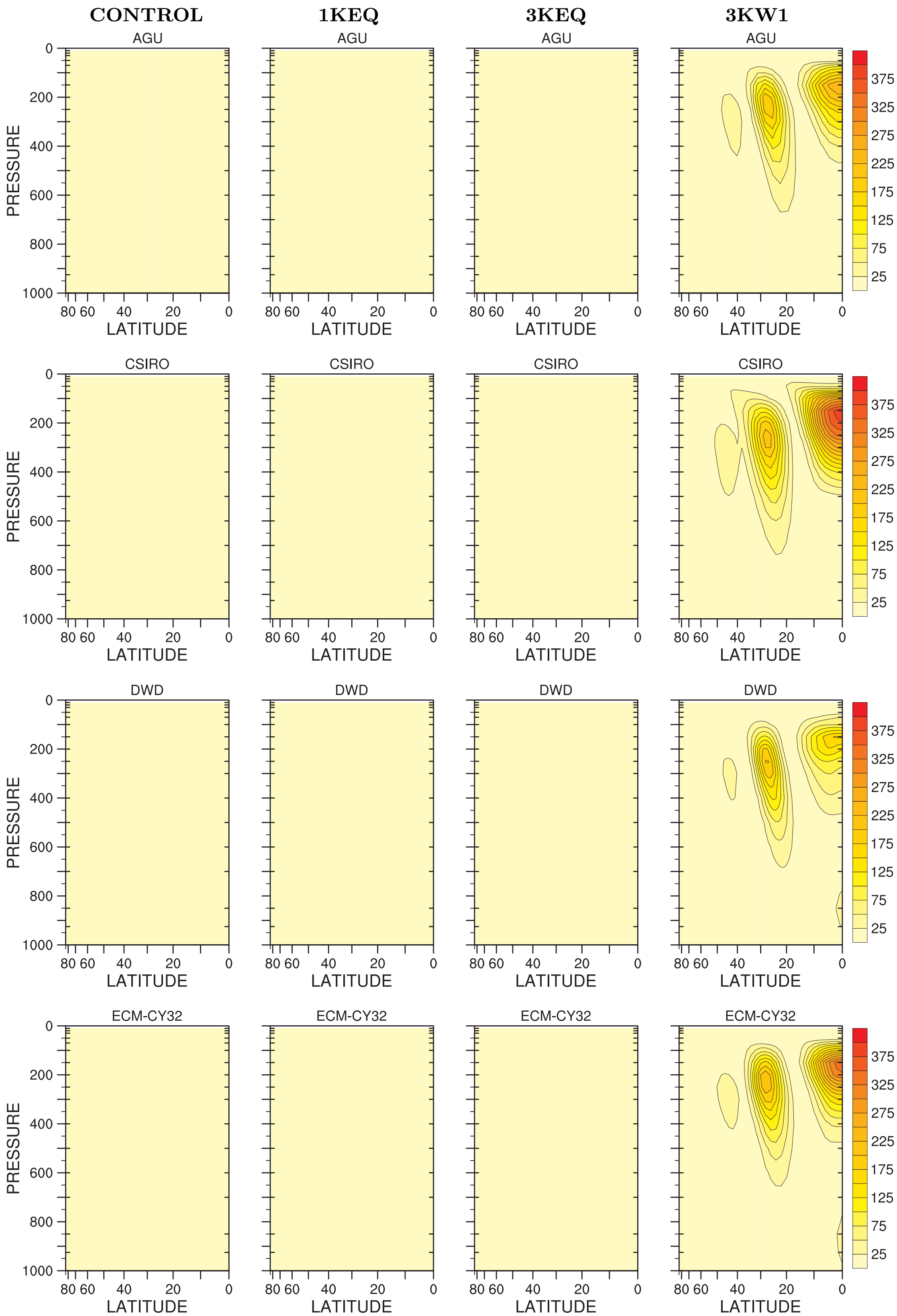

Figure 7.41: Individual model u variance, stationary eddy, se_uu, $[\overline{u}^*\overline{u}^*]$, m^2 s^{-2}.

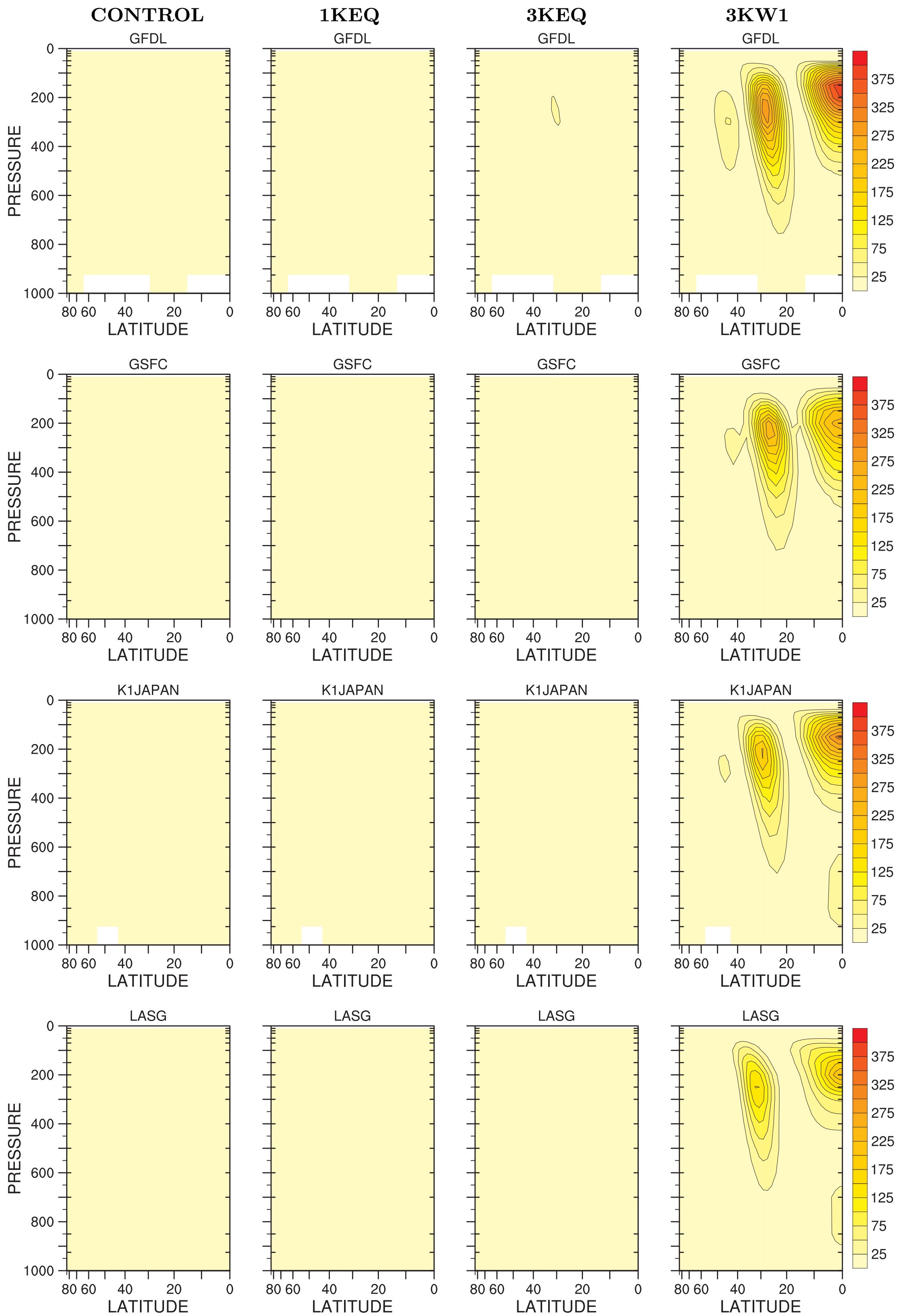

Figure 7.41 (continued): Individual model u variance, stationary eddy, se_uu, $[\overline{u}^*\overline{u}^*]$, m^2 s^{-2}.

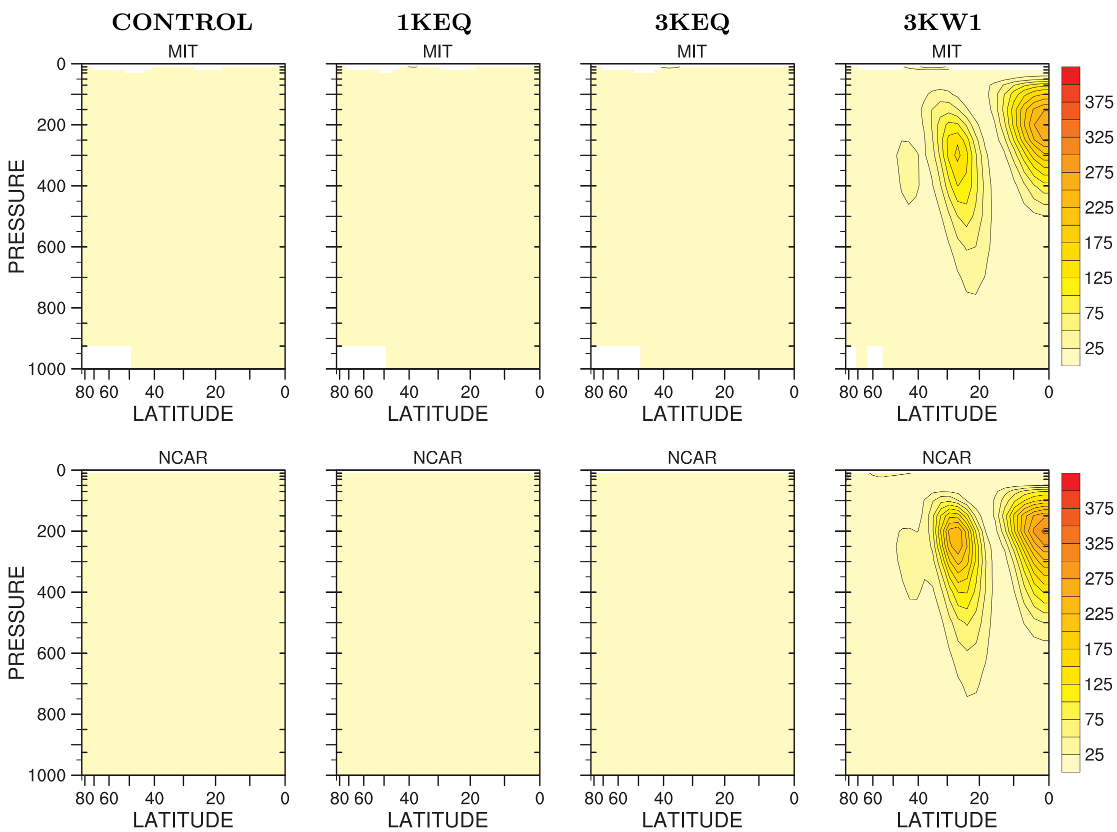

Figure 7.41 (continued): Individual model u variance, stationary eddy, se_uu, $[\overline{u}^*\overline{u}^*]$, m^2 s^{-2}.

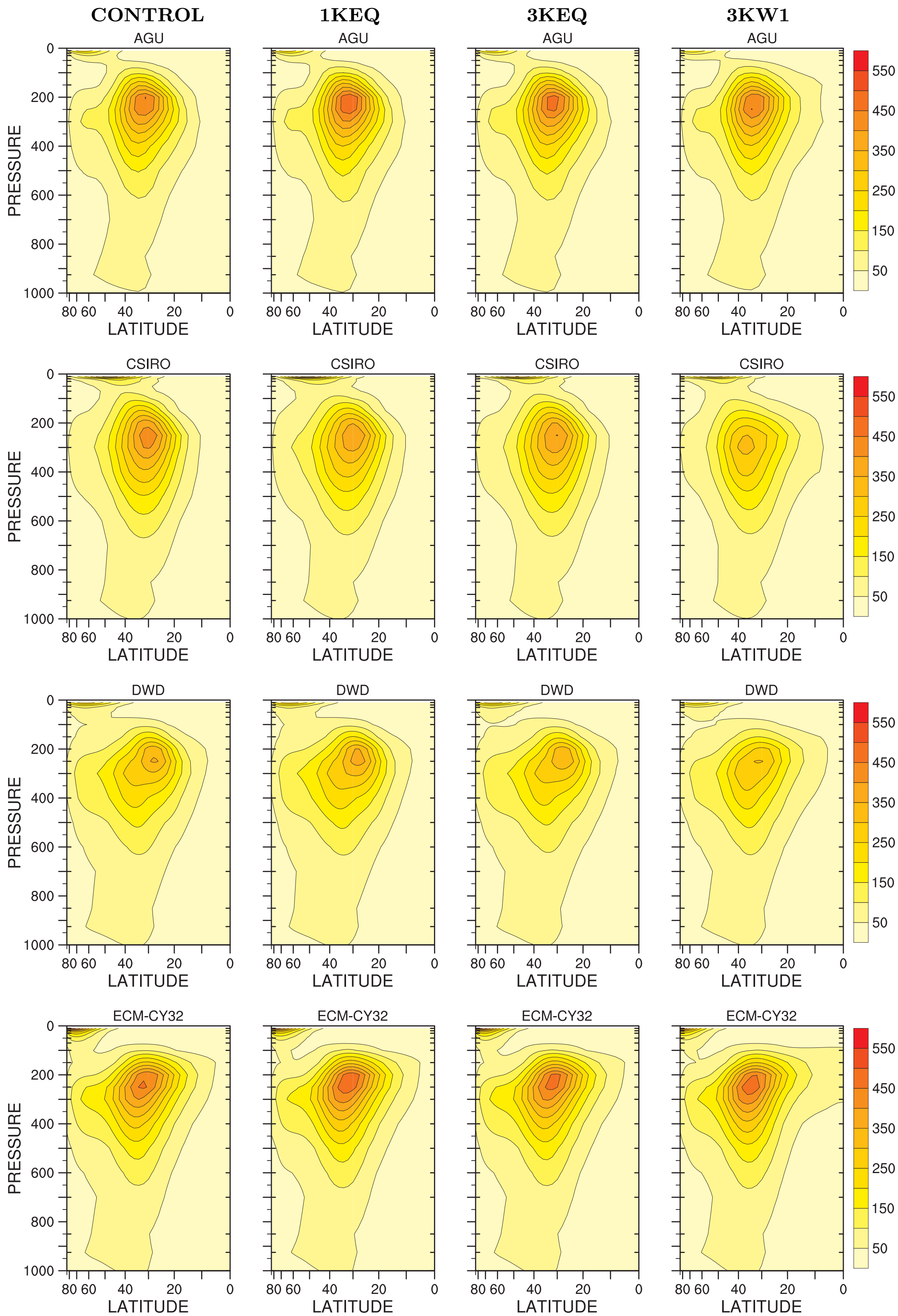

Figure 7.42: Individual model v variance, transient eddy, te_vv, $\overline{\left[(u'^{*})^{2}\right]}$, m^2 s^{-2}.

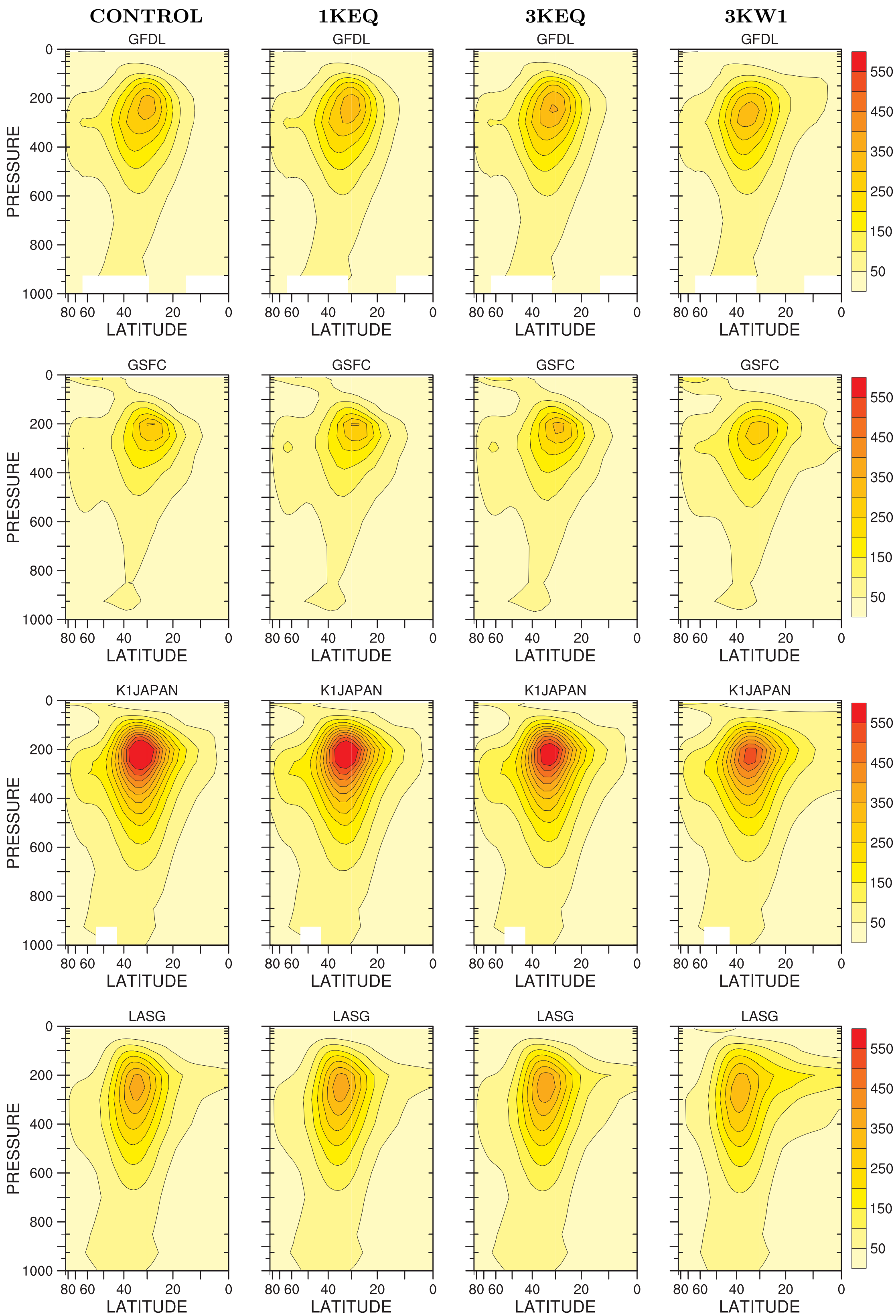

Figure 7.42 (continued): Individual model v variance, transient eddy, te_vv, $\overline{\left[(u'^*)^2\right]}$, m^2 s^{-2}.

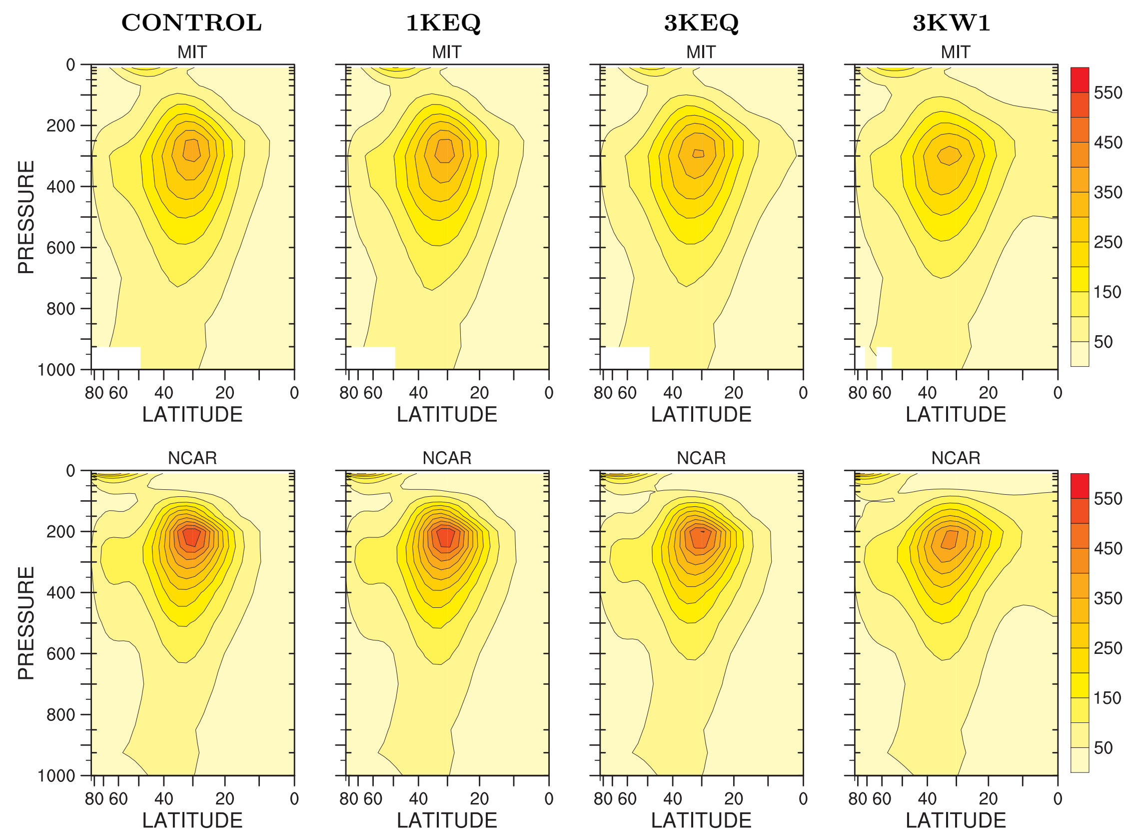

Figure 7.42 (continued): Individual model v variance, transient eddy, te_vv, $\overline{\left[(u'^{*})^{2}\right]}$, m^2 s^{-2}.

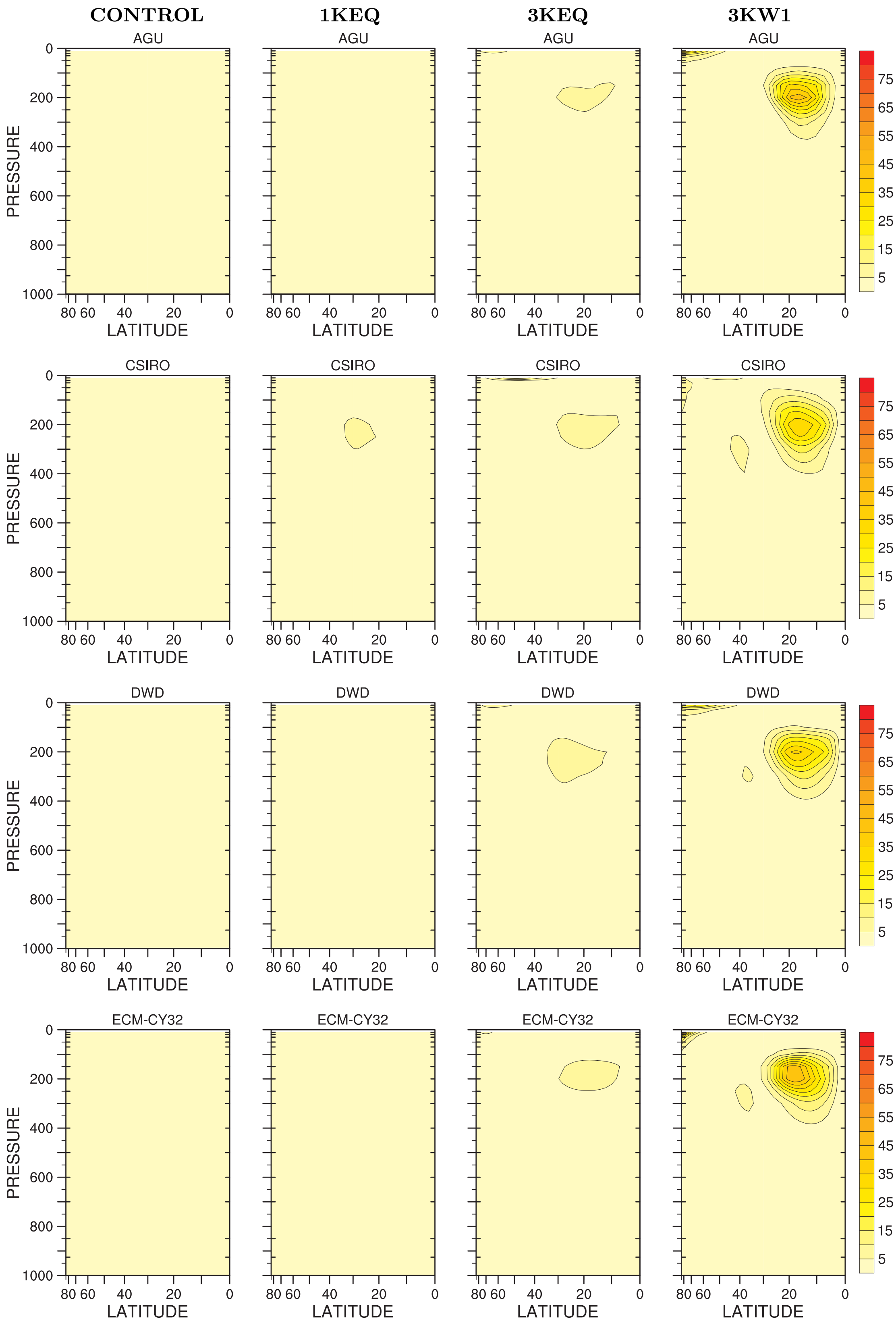

Figure 7.43: Individual model v variance, stationary eddy, se_vv, $[\overline{v}^*\overline{v}^*]$, m^2 s^{-2}.

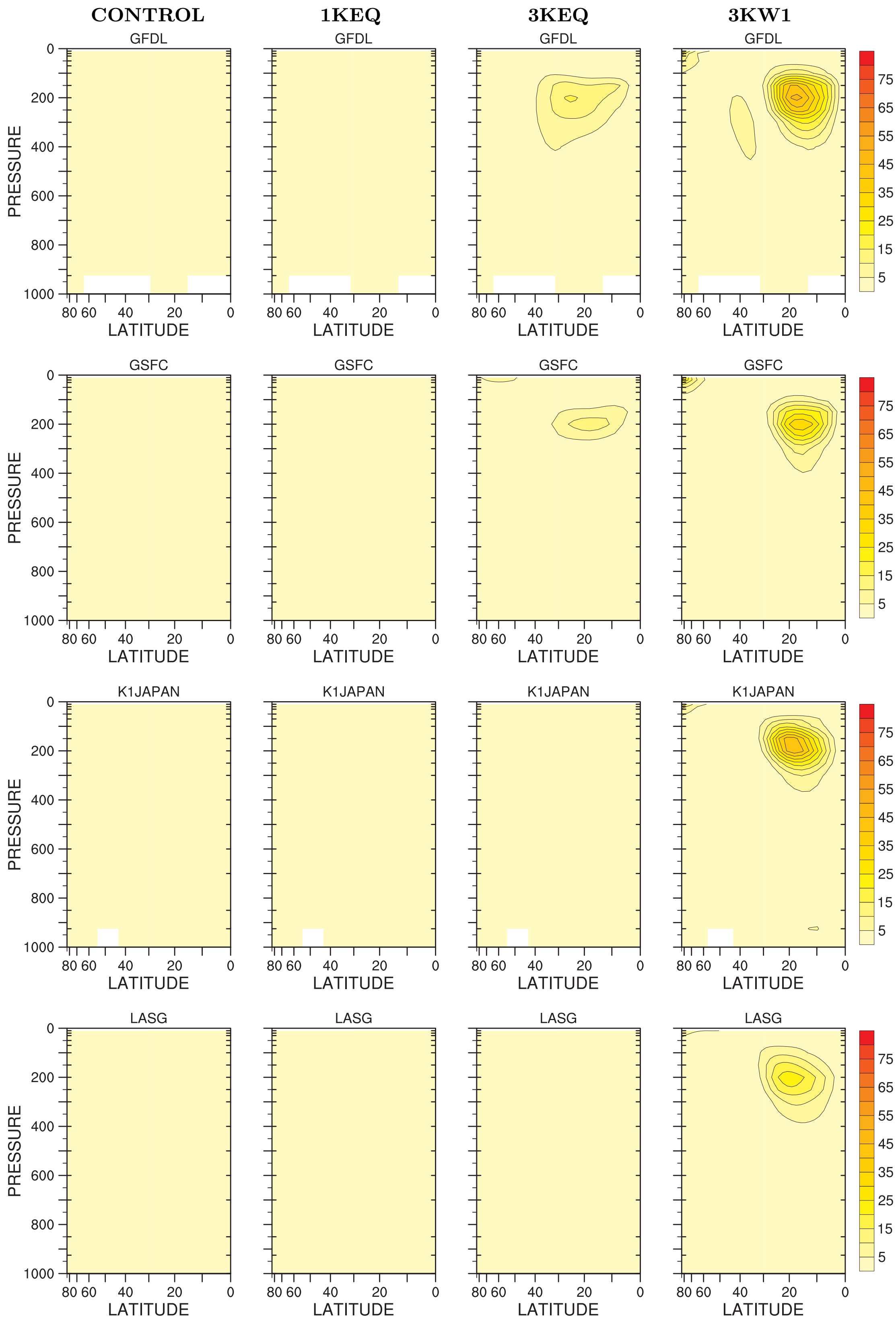

Figure 7.43 (continued): Individual model v variance, stationary eddy, se_vv, $[\overline{v}^*\overline{v}^*]$, m^2 s^{-2}.

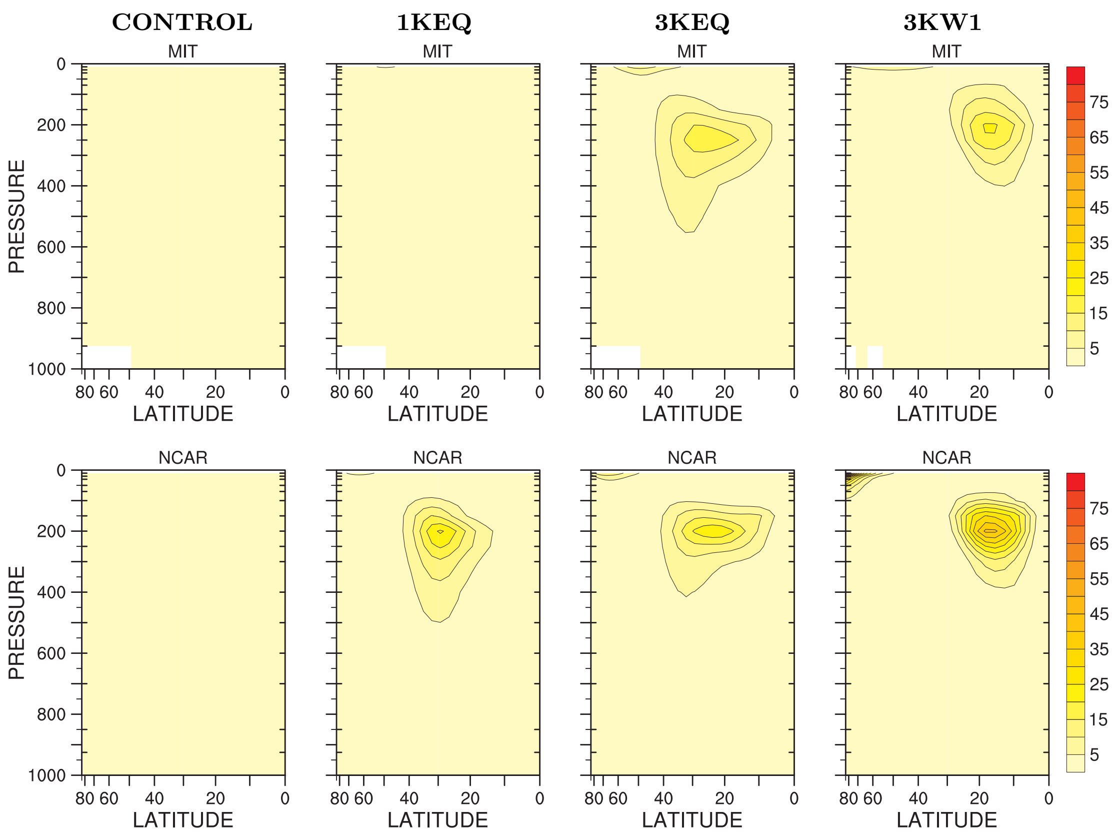

Figure 7.43 (continued): Individual model v variance, stationary eddy, se_vv, $[\overline{v}^*\overline{v}^*]$, m^2 s^{-2}.

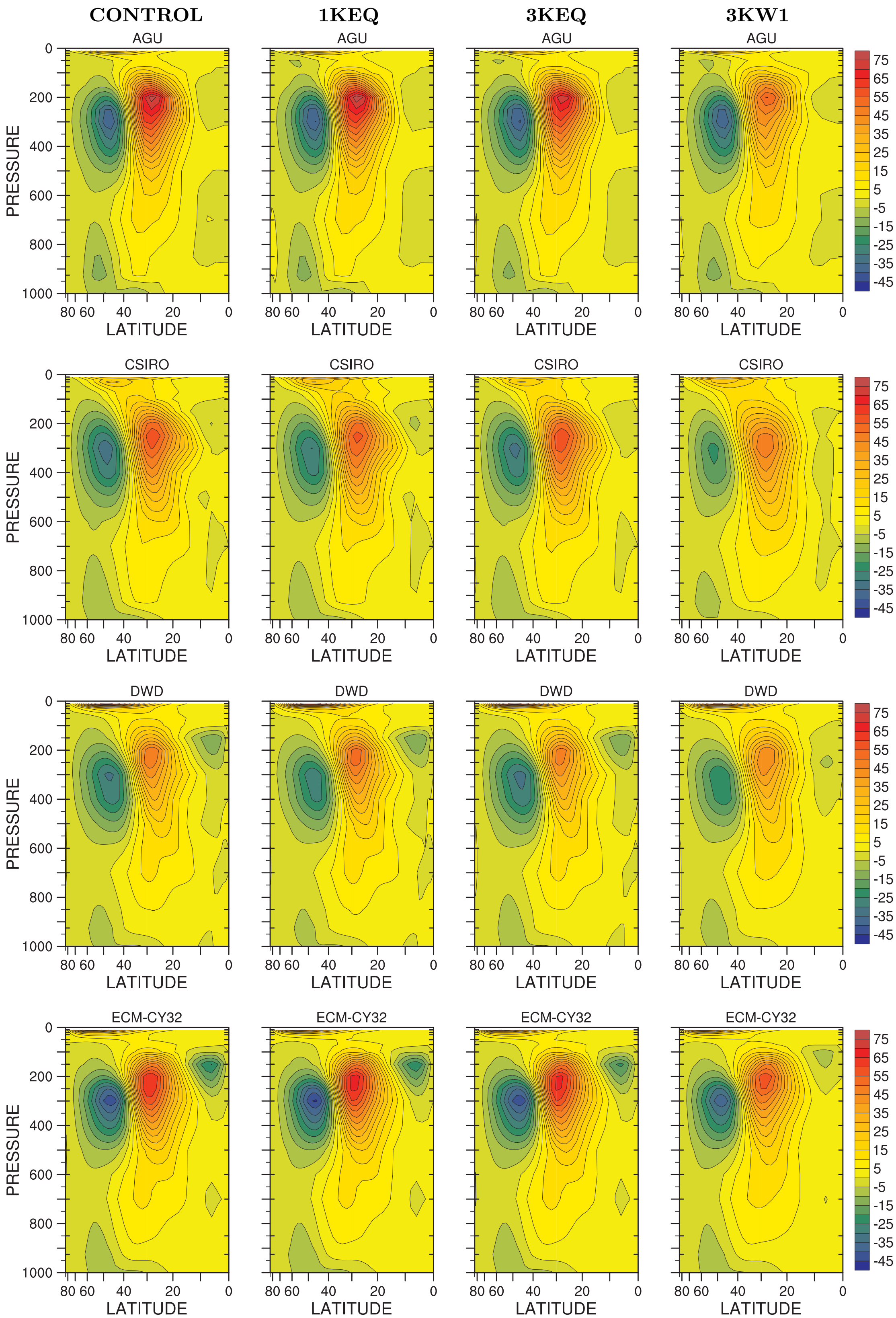

Figure 7.44: Individual model uv co-variance, transient eddy, te_uv, $\overline{[u'^{*}v'^{*}]}$, m^2 s^{-2}.

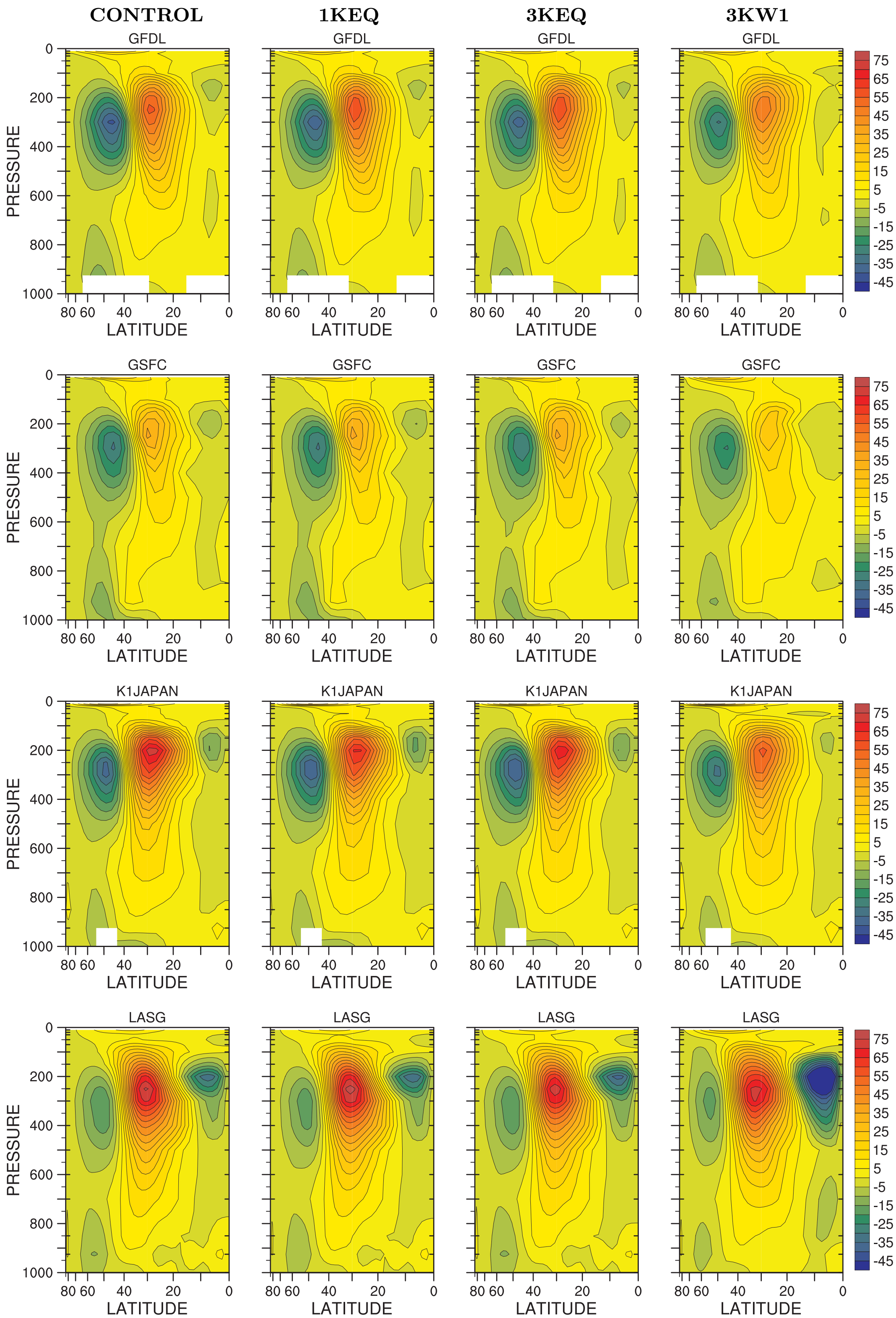

Figure 7.44 (continued): Individual model uv co-variance, transient eddy, te_uv, $\overline{[u'^{*}v'^{*}]}$, m^2 s^{-2}.

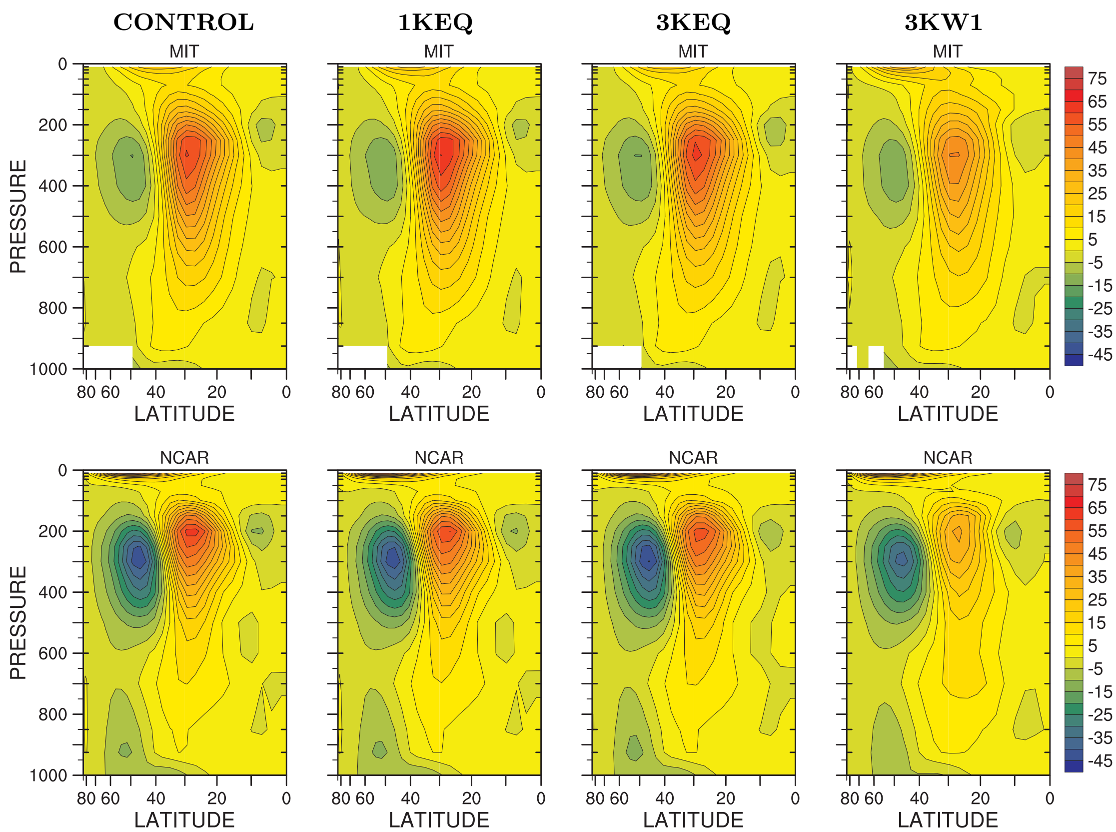

Figure 7.44 (continued): Individual model uv co-variance, transient eddy, te_uv, $\overline{[u'^* v'^*]}$, m^2 s^{-2}.

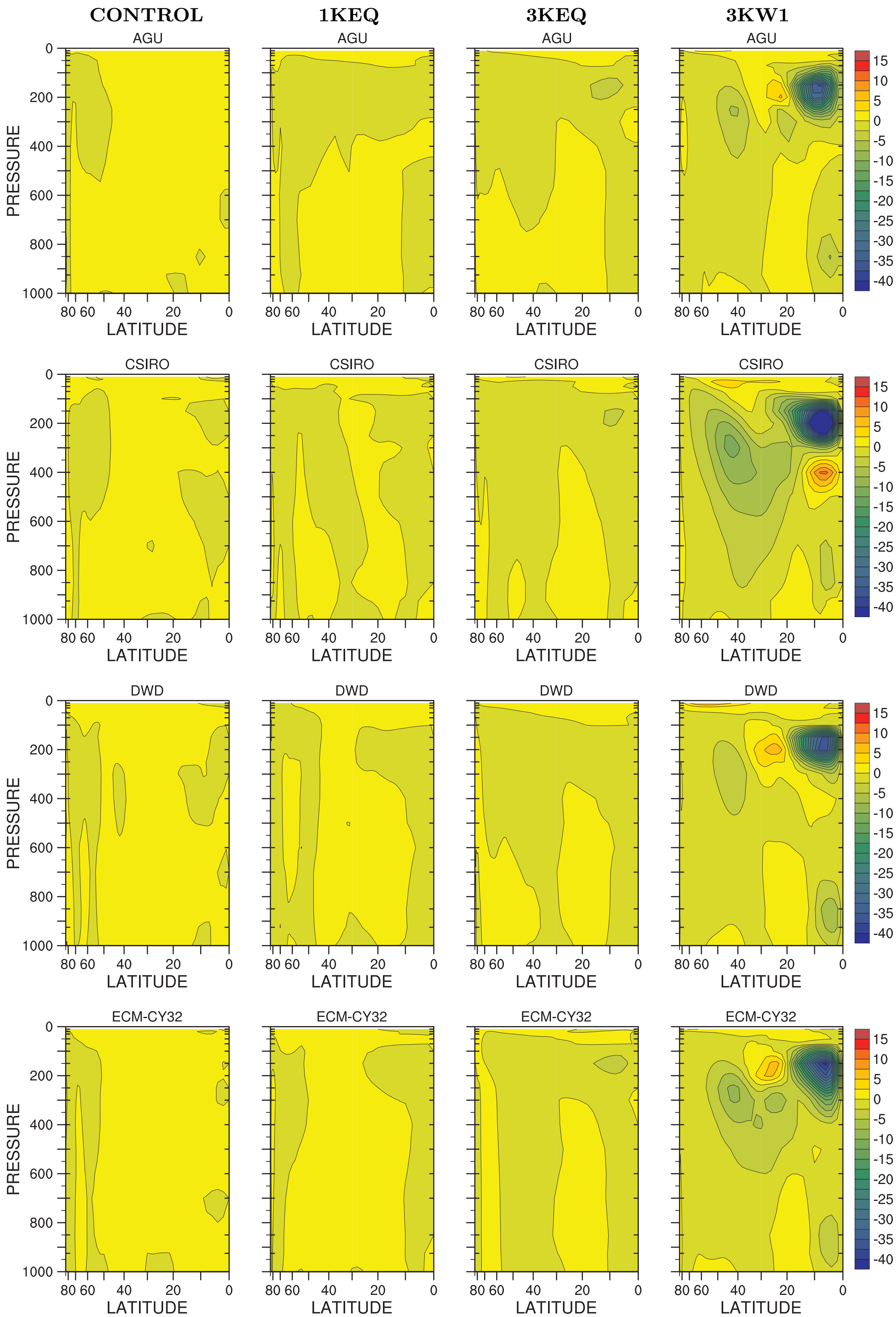

Figure 7.45: Individual model uv co-variance, stationary eddy, se_uv, $[\overline{u}^*\overline{v}^*]$, m^2 s^{-2}.

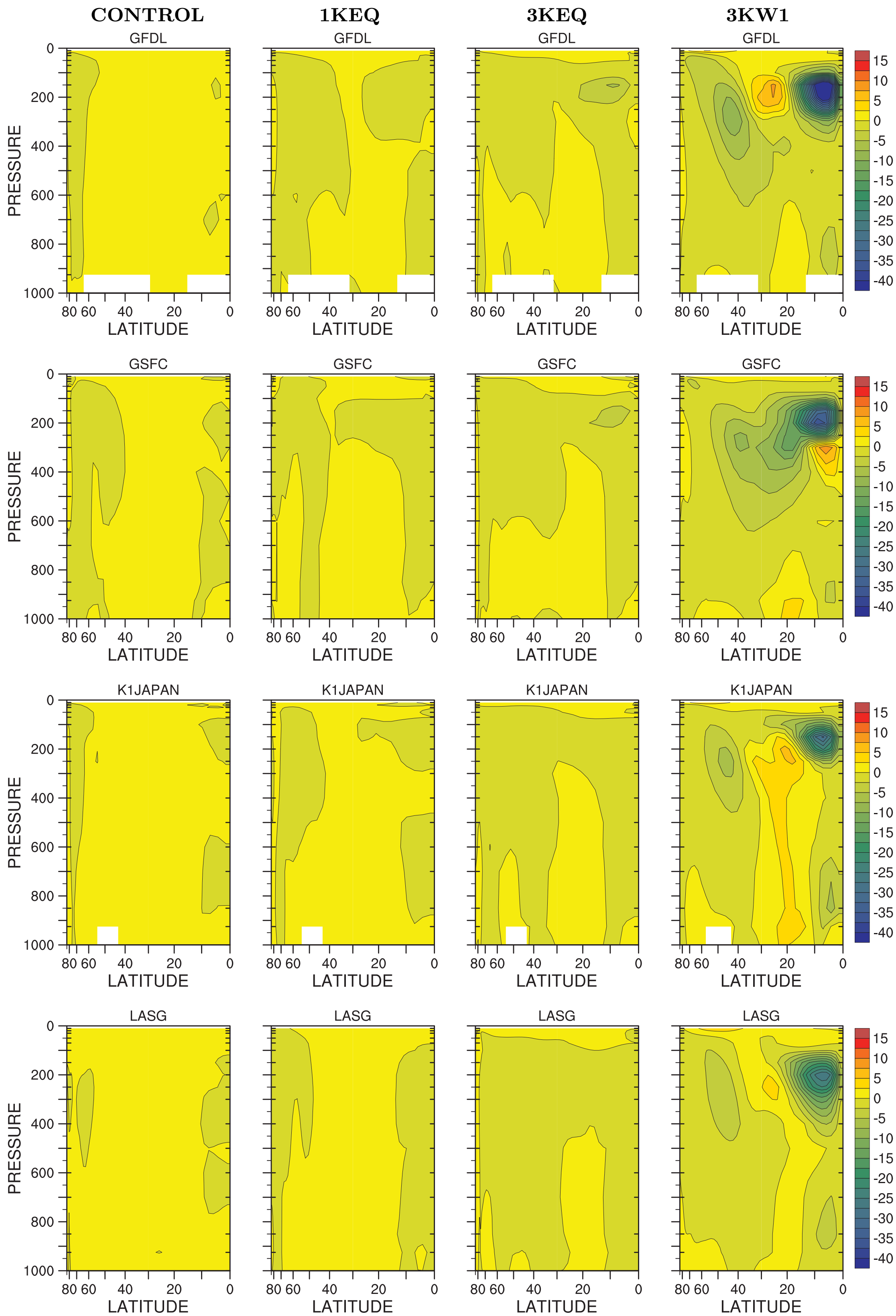

Figure 7.45 (continued): Individual model uv co-variance, stationary eddy, se_uv, $[\overline{u}^*\overline{v}^*]$, $m^2\ s^{-2}$.

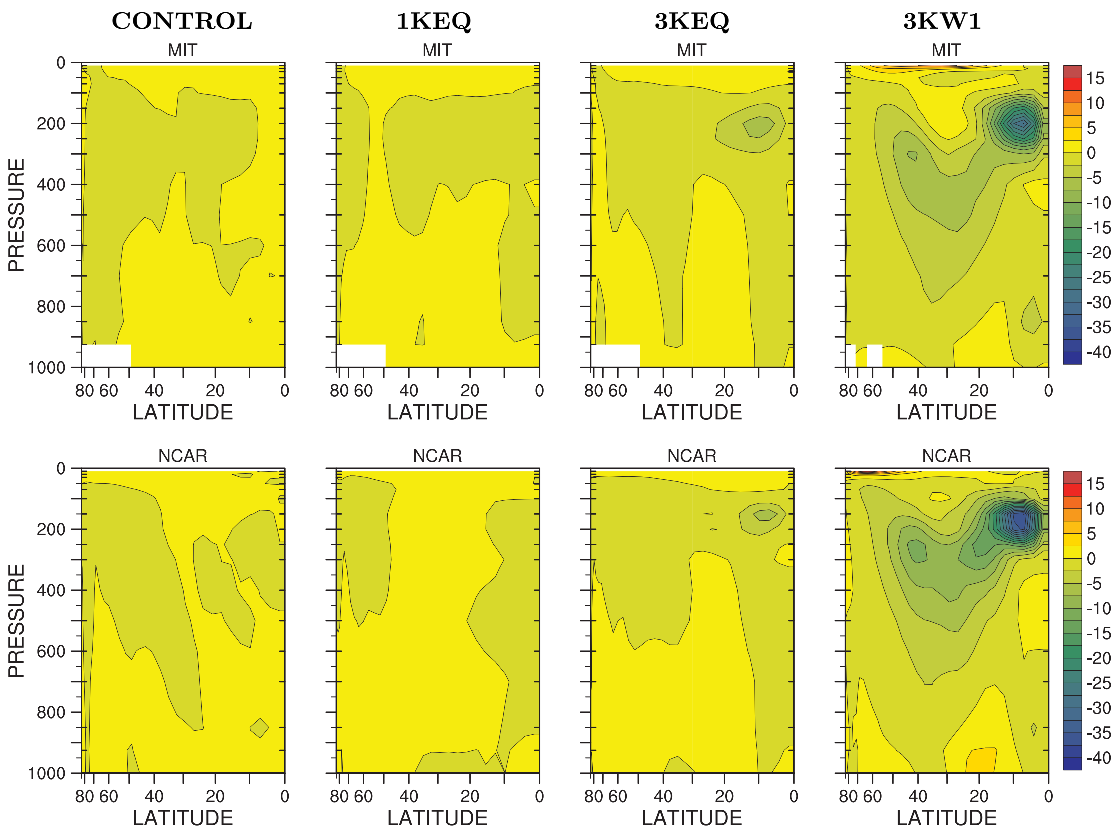

Figure 7.45 (continued): Individual model uv co-variance, stationary eddy, se_uv, $[\overline{u}^*\overline{v}^*]$, $m^2\ s^{-2}$.

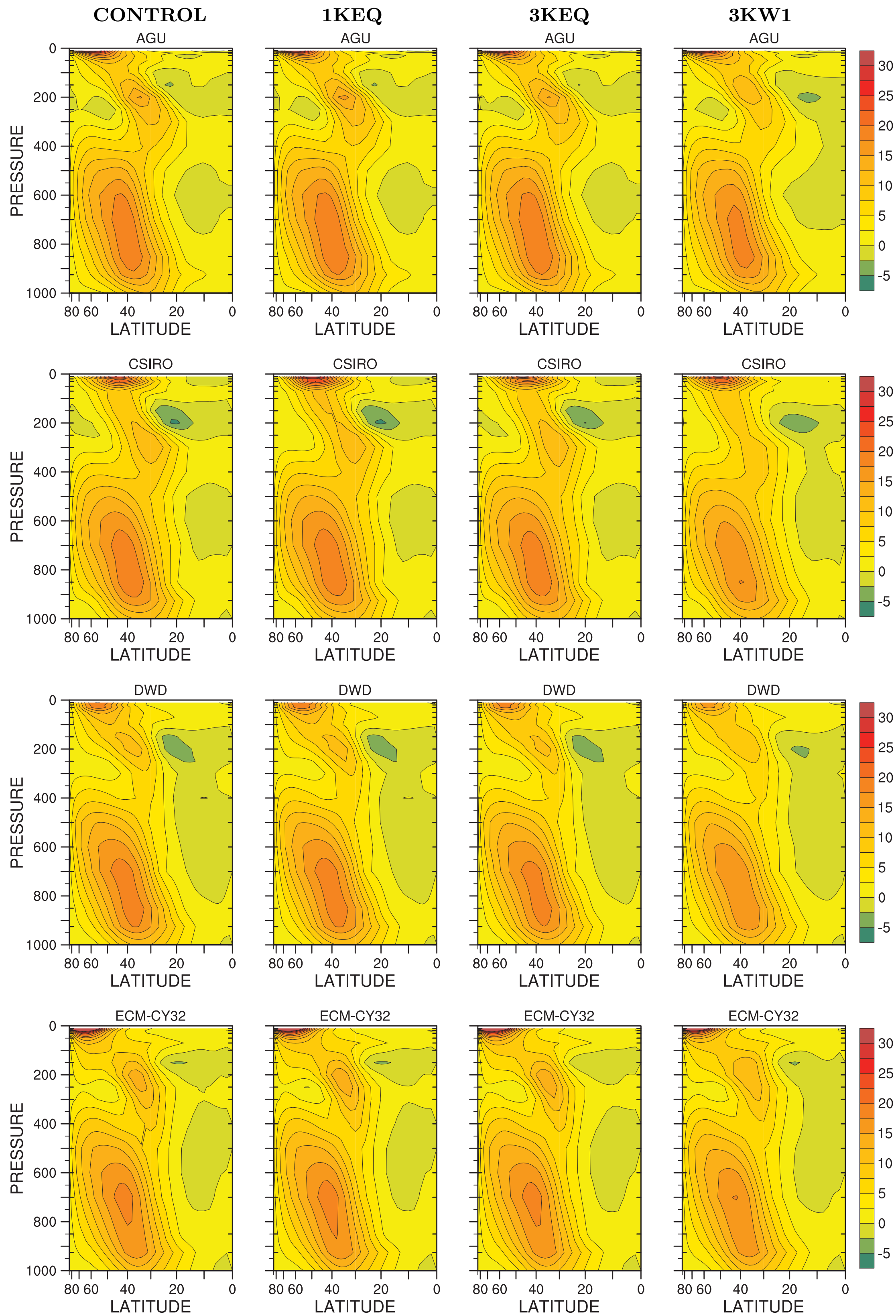

Figure 7.46: Individual model vT co-variance, transient eddy, te_vt, $\overline{[v'^{*}T^{*}]}$, K m s^{-1}.

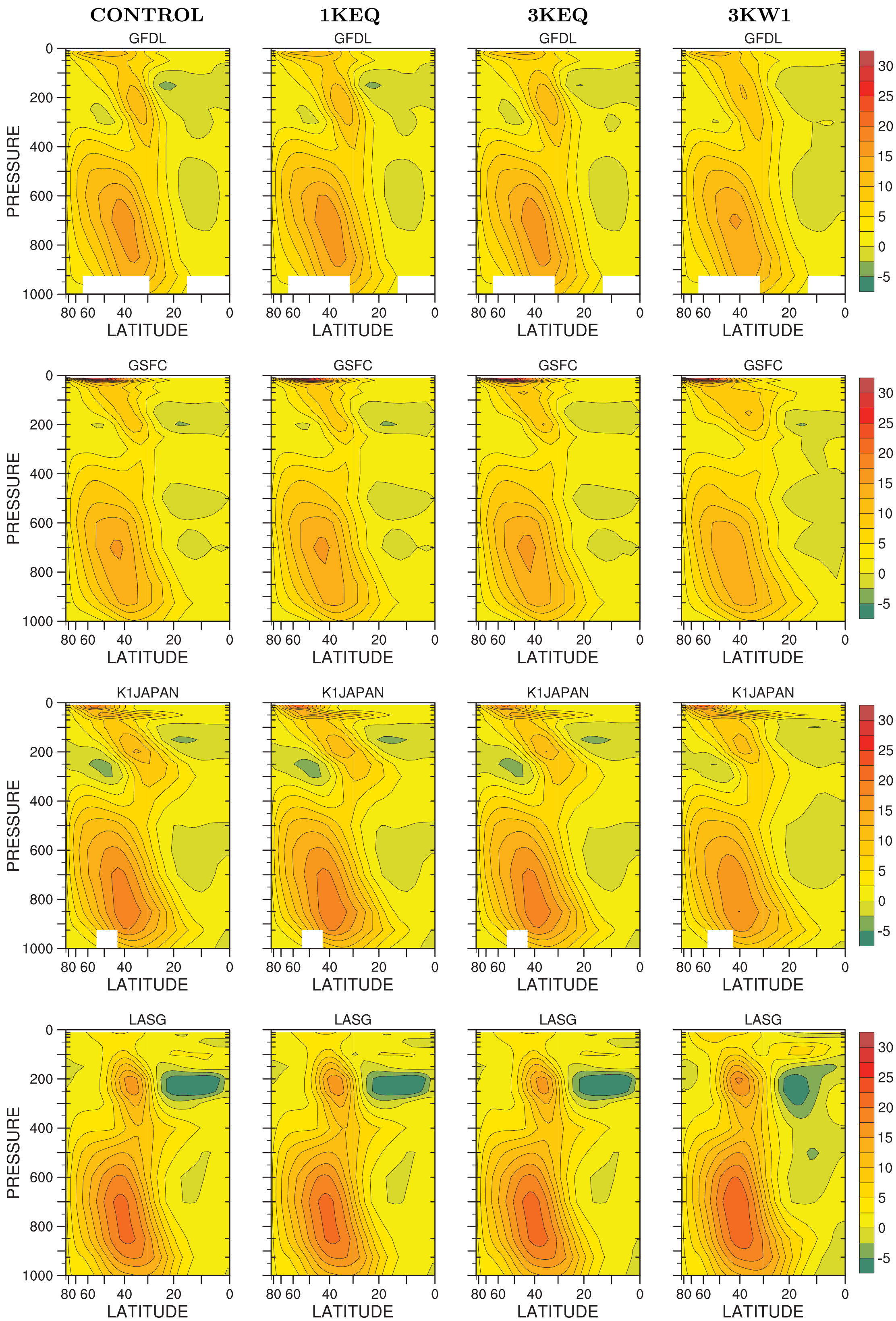

Figure 7.46 (continued): Individual model vT co-variance, transient eddy, te_vt, $\overline{[v'^{*}T^{*}]}$, K m s^{-1}.

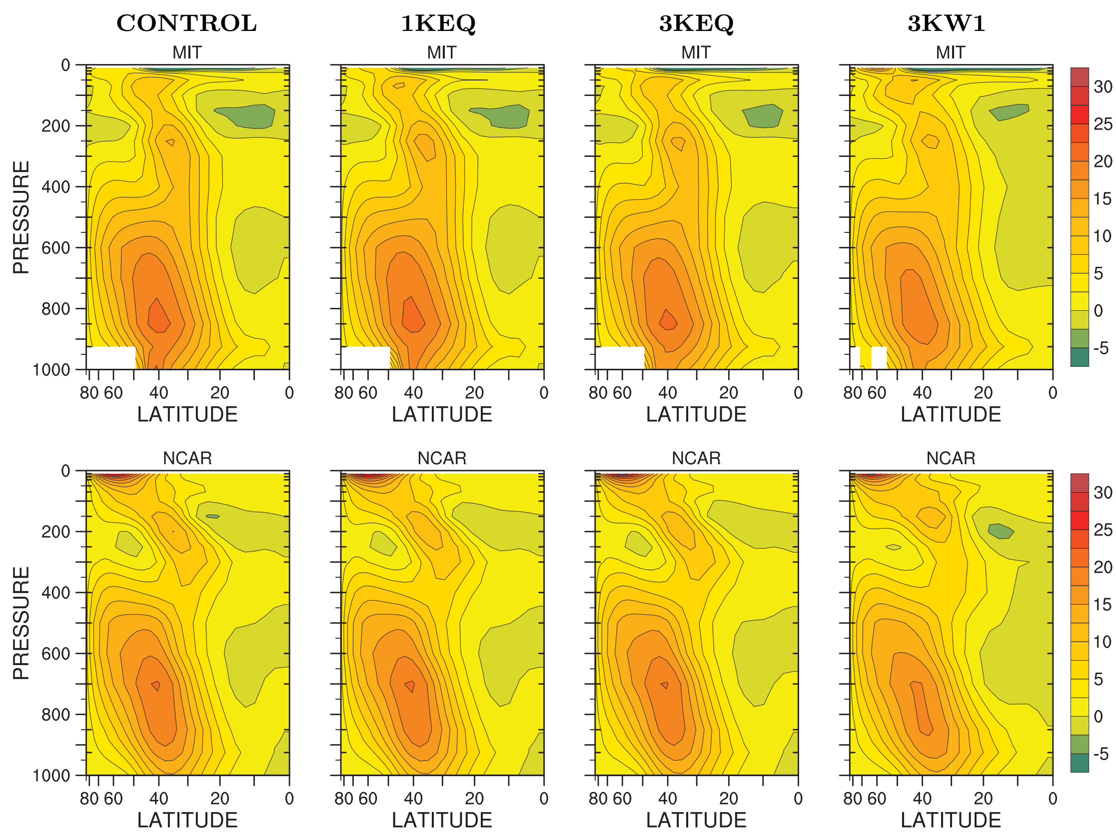

Figure 7.46 (continued): Individual model vT co-variance, transient eddy, te_vt, $\left(\overline{[v'^{*}T'^{*}]}\right)$, K m s^{-1}.

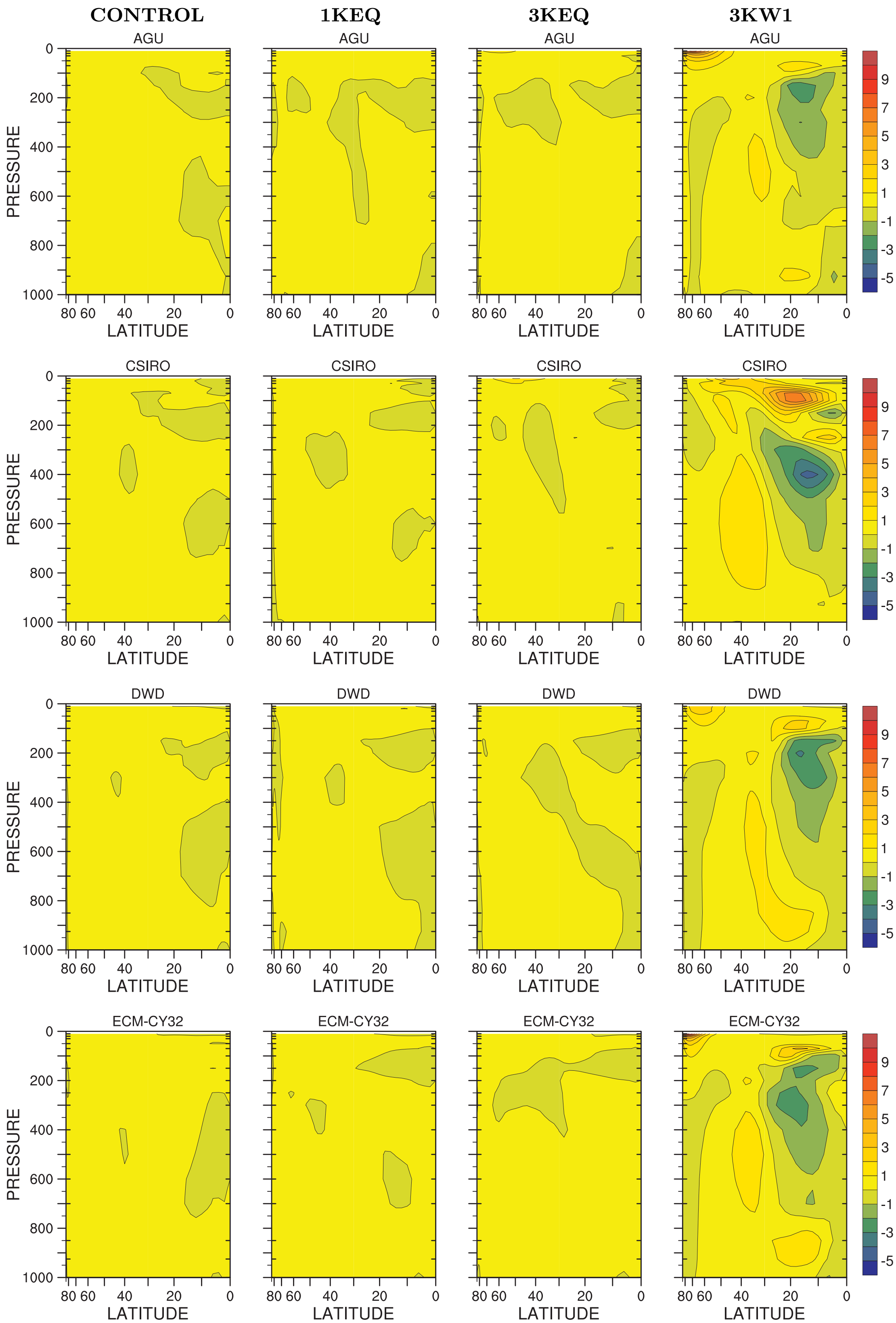

Figure 7.47: Individual model vT co-variance, stationary eddy, se_vt, $\left[\overline{v}^*\overline{T}^*\right]$, K m s^{-1}.

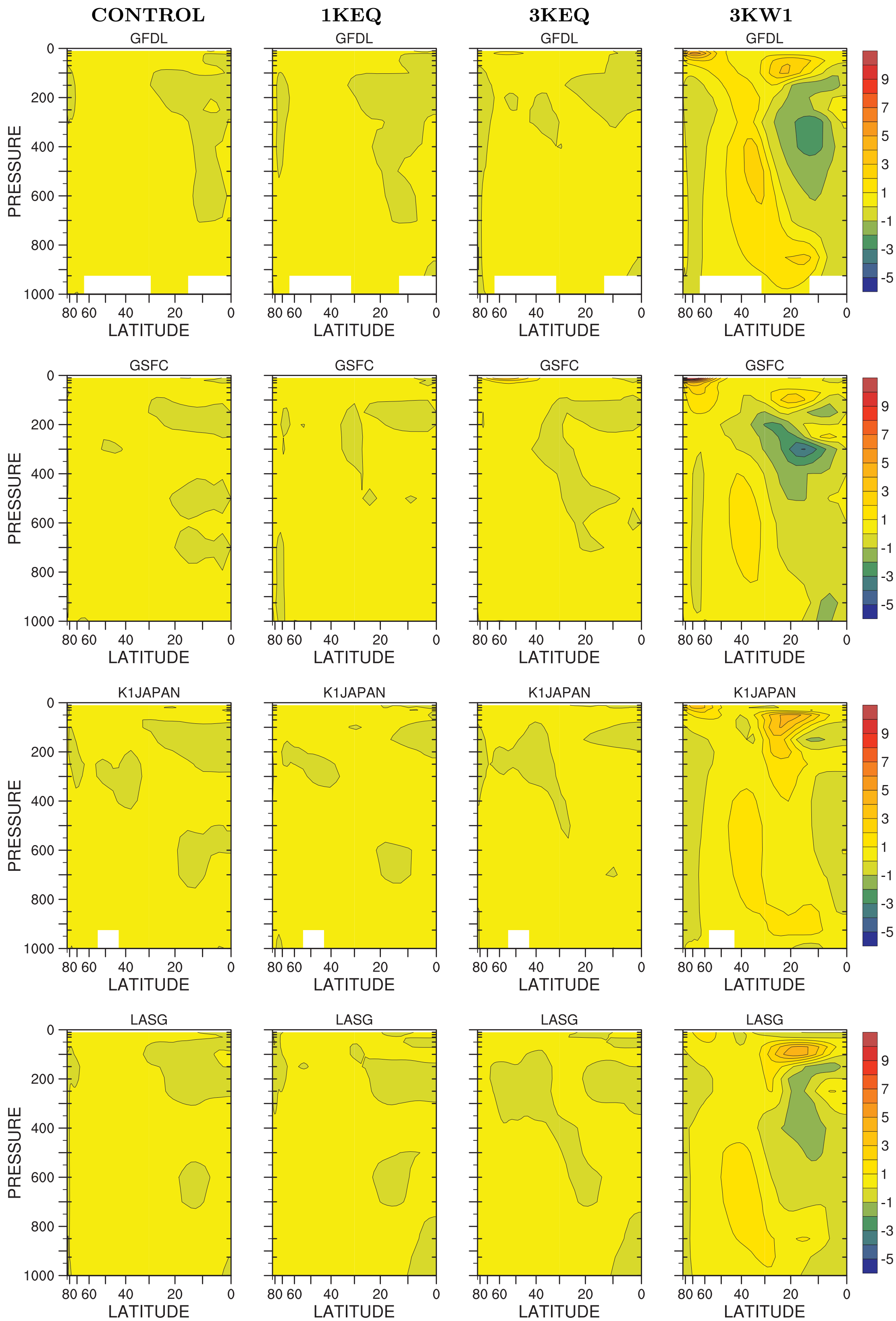

Figure 7.47 (continued): Individual model vT co-variance, stationary eddy, se_vt, $\left[\overline{v}^{\,*}\overline{T}^{\,*}\right]$, K m s^{-1}.

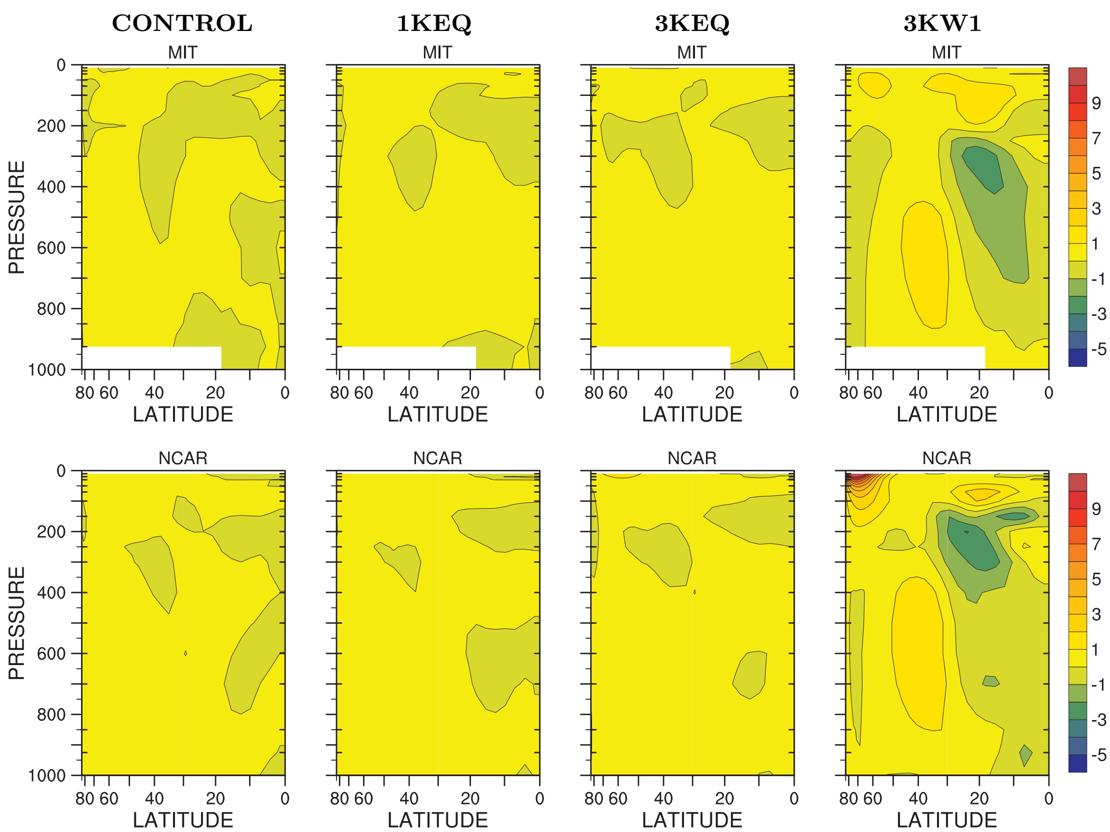

Figure 7.47 (continued): Individual model vT co-variance, stationary eddy, se_vt, $\left[\overline{v}^{*}\overline{T}^{*}\right]$, K m s^{-1}.

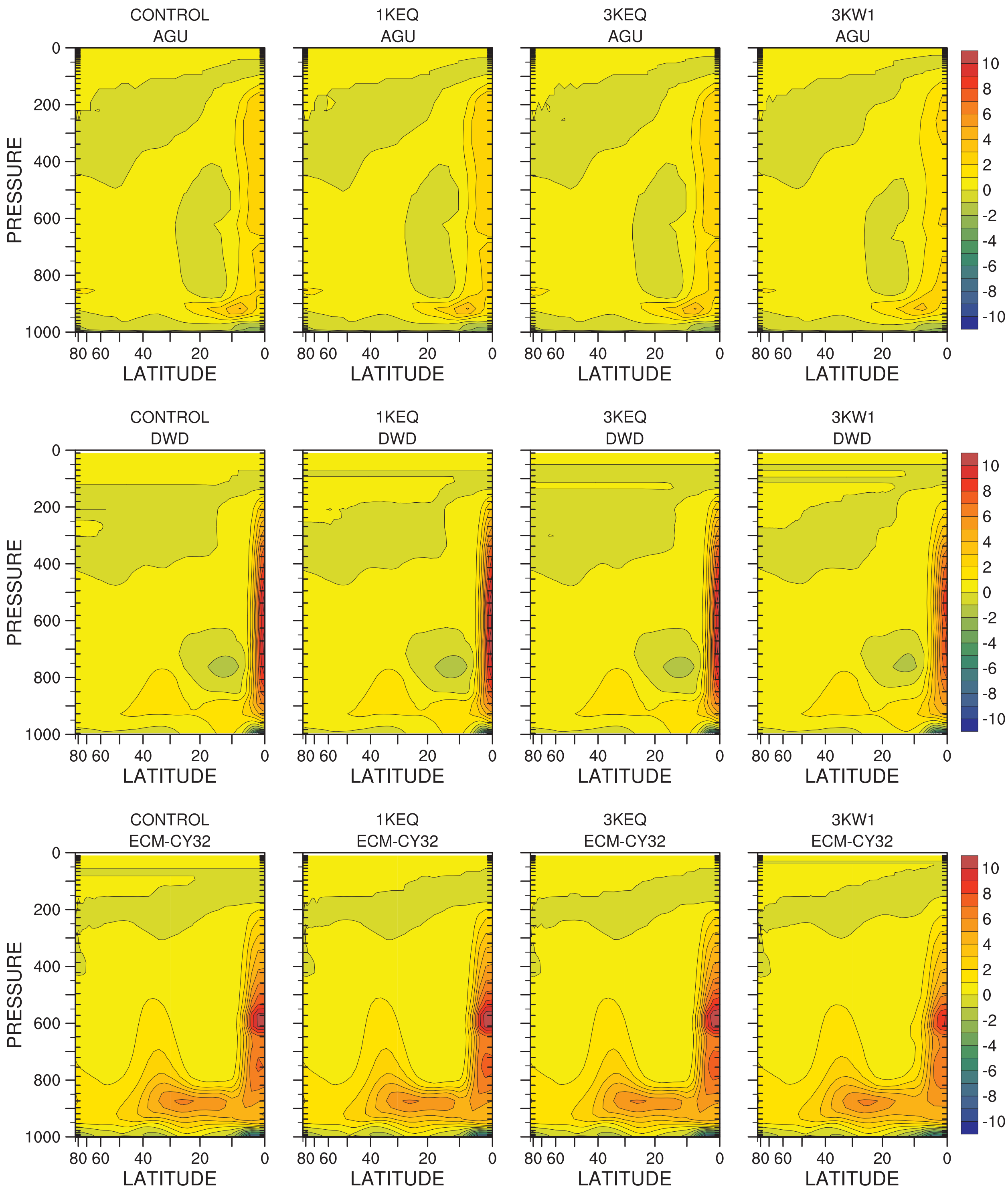

Figure 7.48: Zonal-time average parameterized convection temperature tendency (t_conv) for individual models for CONTROL, 1KEQ, 3KEQ and 3KW1, K day^{-1}.

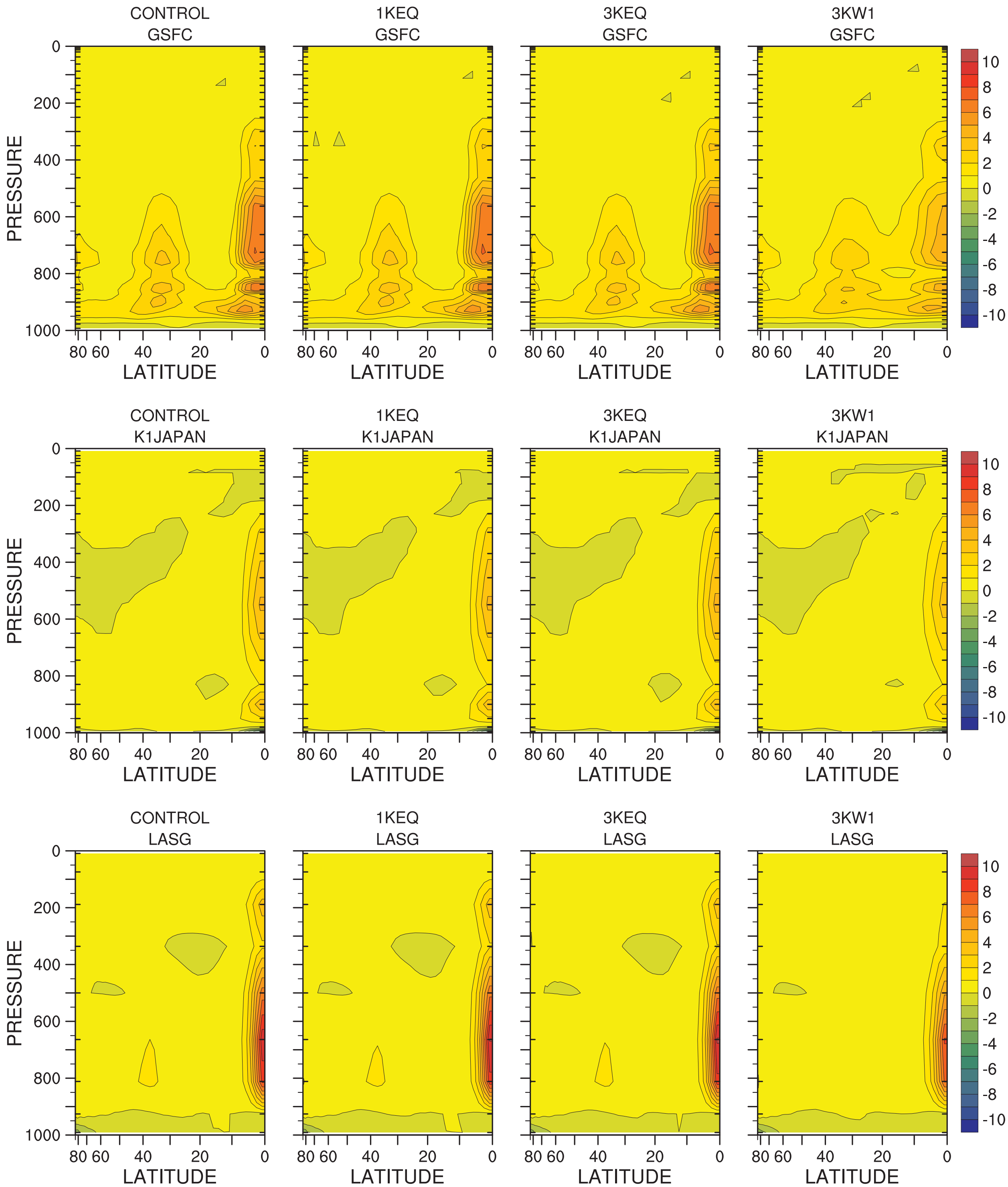

Figure 7.48 (continued): Zonal-time average parameterized convection temperature tendency (t_conv) for individual models for CONTROL, 1KEQ, 3KEQ and 3KW1, K day^{-1}.

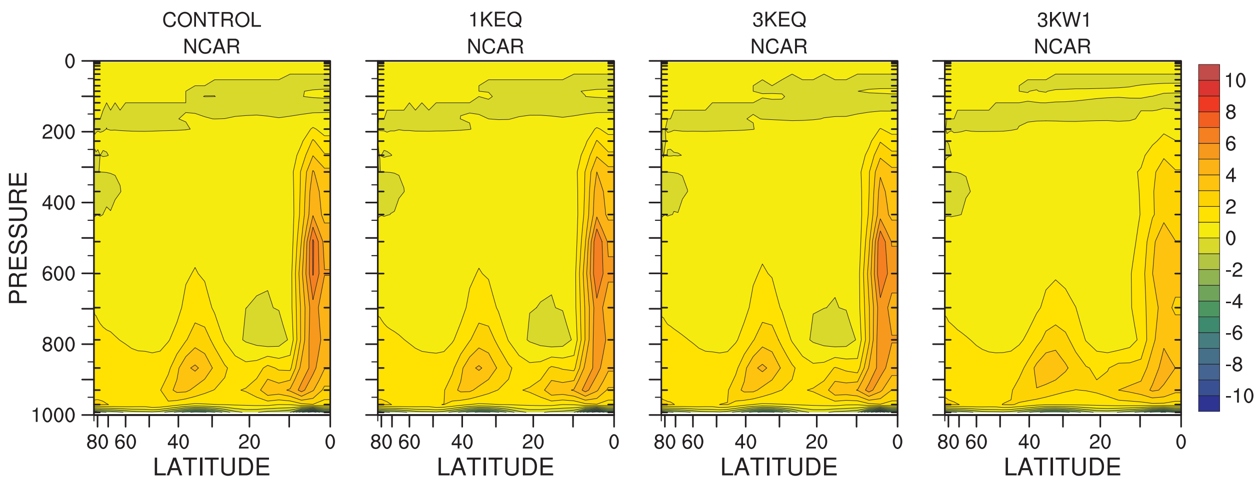

Figure 7.48 (continued): Zonal-time average parameterized convection temperature tendency (t_conv) for individual models for CONTROL, 1KEQ, 3KEQ and 3KW1, K day^{-1}.

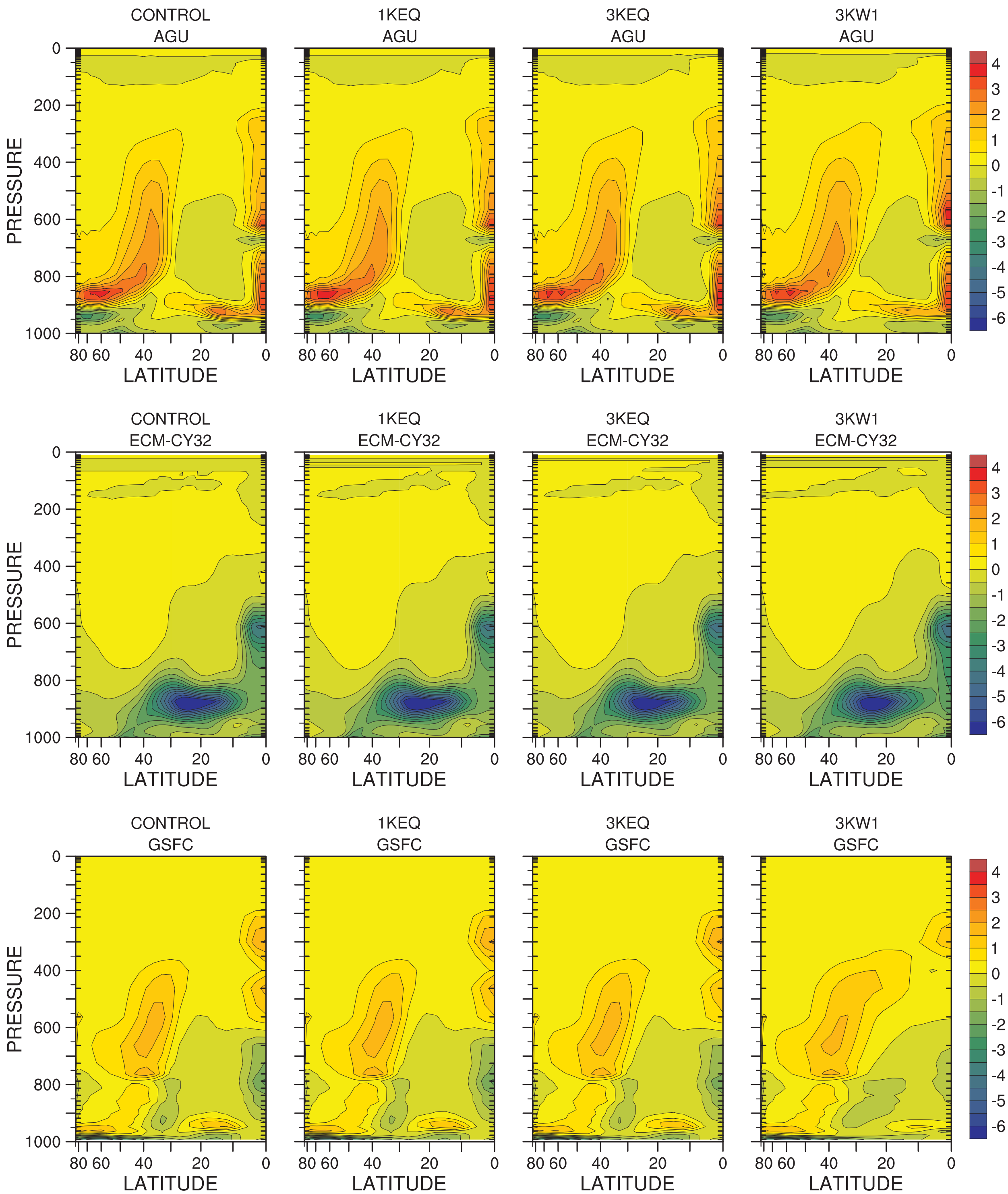

Figure 7.49: Zonal-time average parameterized cloud temperature tendency (t_cld) for individual models for CONTROL, 1KEQ, 3KEQ and 3KW1, K day^{-1}.

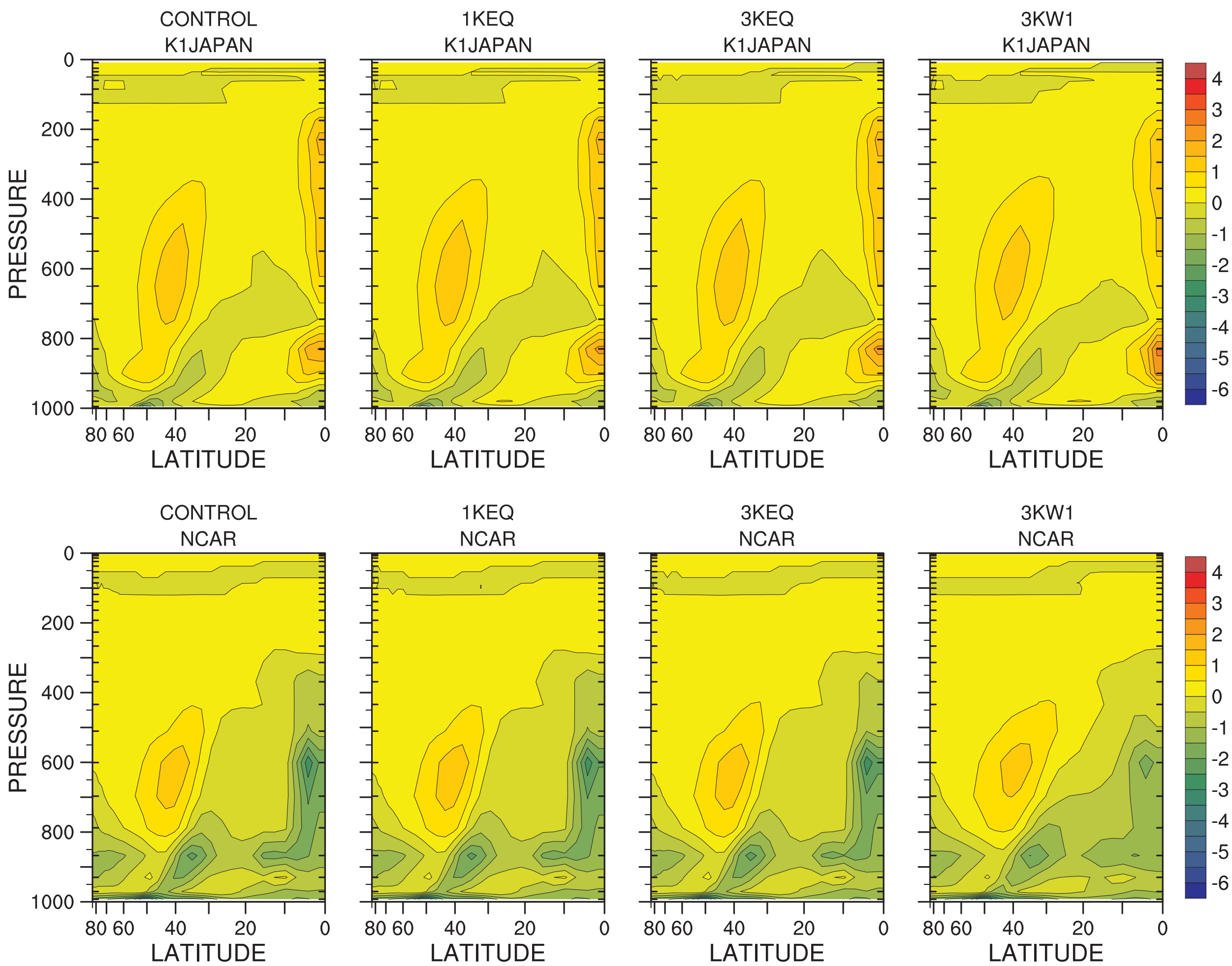

Figure 7.49 (continued): Zonal-time average parameterized cloud temperature tendency (t_cld) for individual models for CONTROL, 1KEQ, 3KEQ and 3KW1, K day^{-1}.

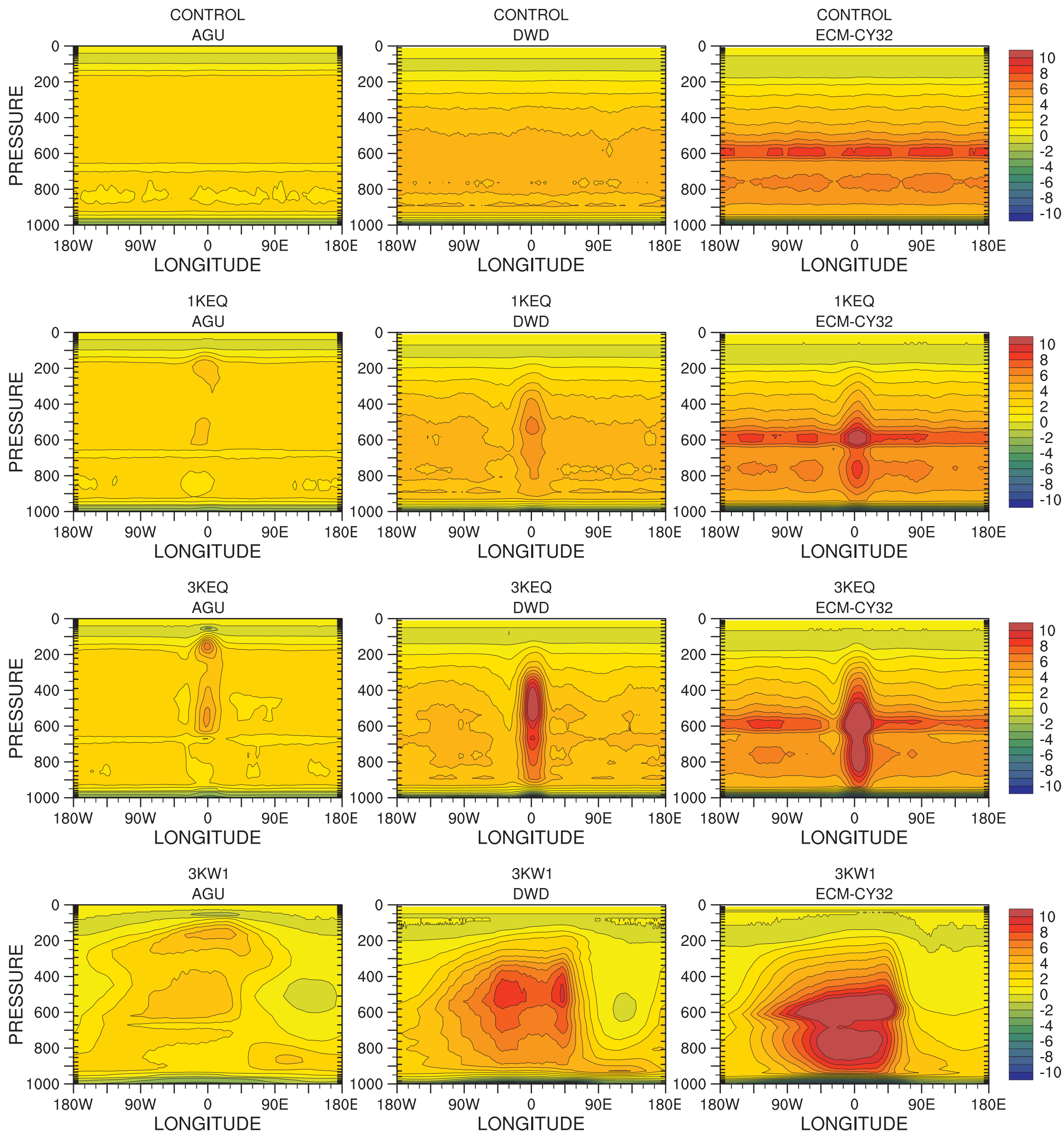

Figure 7.50: Equatorial-time average, $-7 < \varphi < +7$, parameterized convection temperature tendency (t_conv) for individual models for CONTROL, 1KEQ, 3KEQ and 3KW1, K day^{-1}.

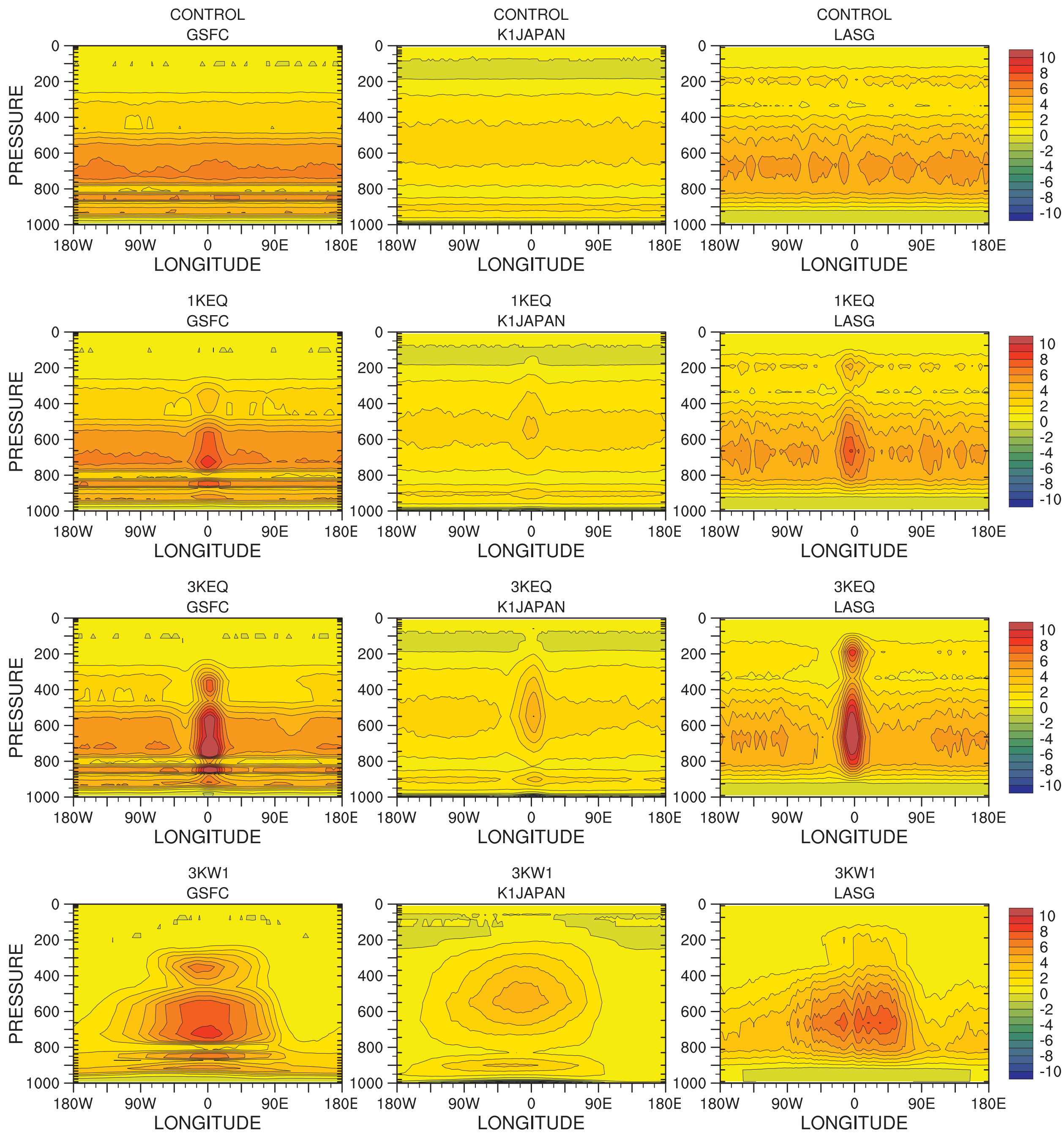

Figure 7.50 (continued): Equatorial-time average, $-7 < \varphi < +7$, parameterized convection temperature tendency (t_conv) for individual models for CONTROL, 1KEQ, 3KEQ and 3KW1, K day^{-1}.

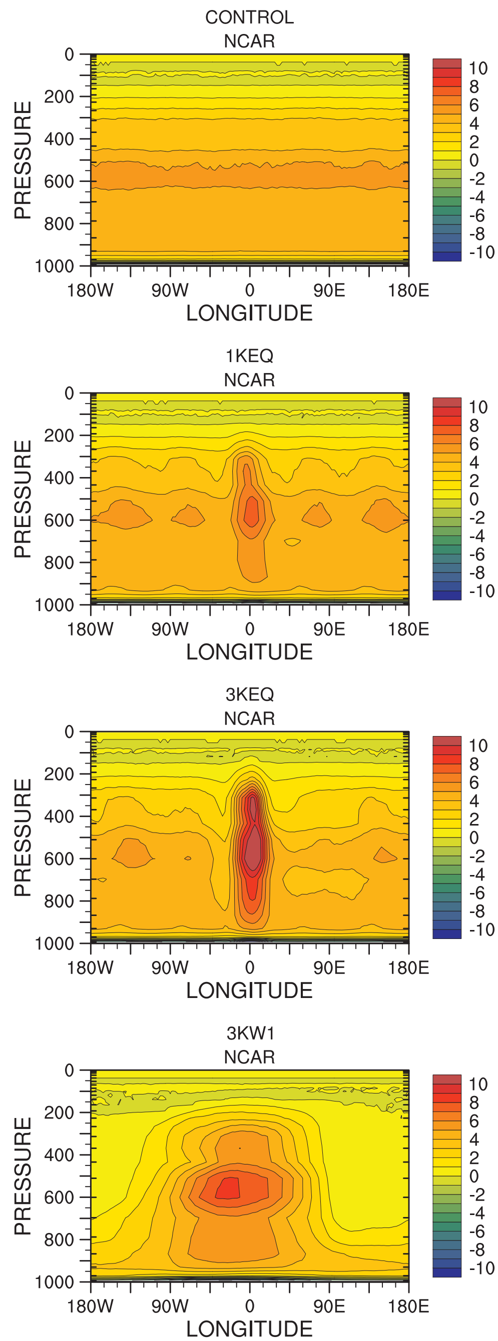

Figure 7.50 (continued): Equatorial-time average, $-7 < \varphi < +7$, parameterized convection temperature tendency (t_conv) for individual models for CONTROL, 1KEQ, 3KEQ and 3KW1, K day^{-1}.

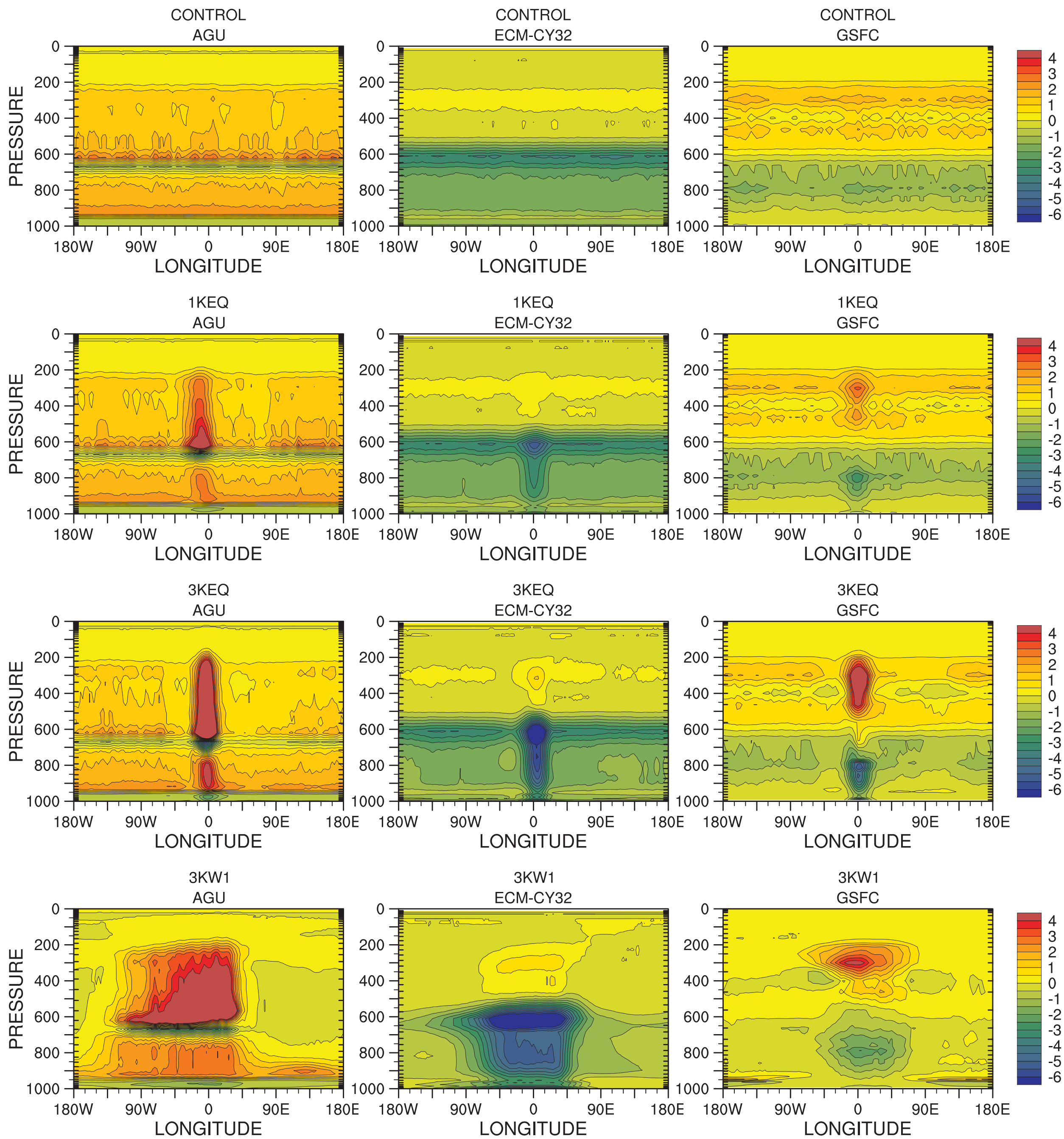

Figure 7.51: Equatorial-time average, $-7 < \varphi < +7$, parameterized cloud temperature tendency (t_cld) for individual models for CONTROL, 1KEQ, 3KEQ and 3KW1, K day^{-1}.

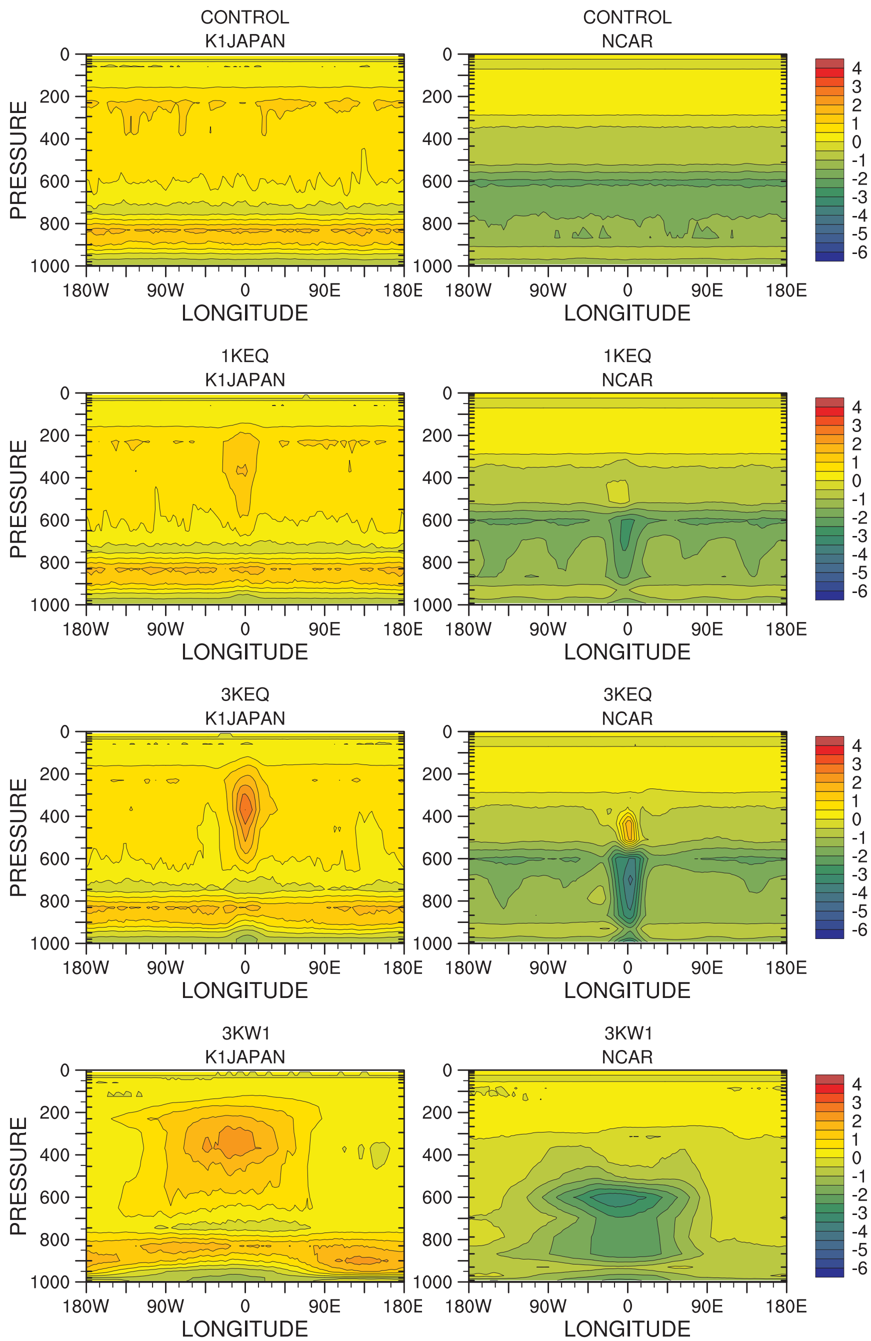

Figure 7.51 (continued): Equatorial-time average, $-7 < \varphi < +7$, parameterized cloud temperature tendency (t_cld) for individual models for CONTROL, 1KEQ, 3KEQ and 3KW1, K day^{-1}.

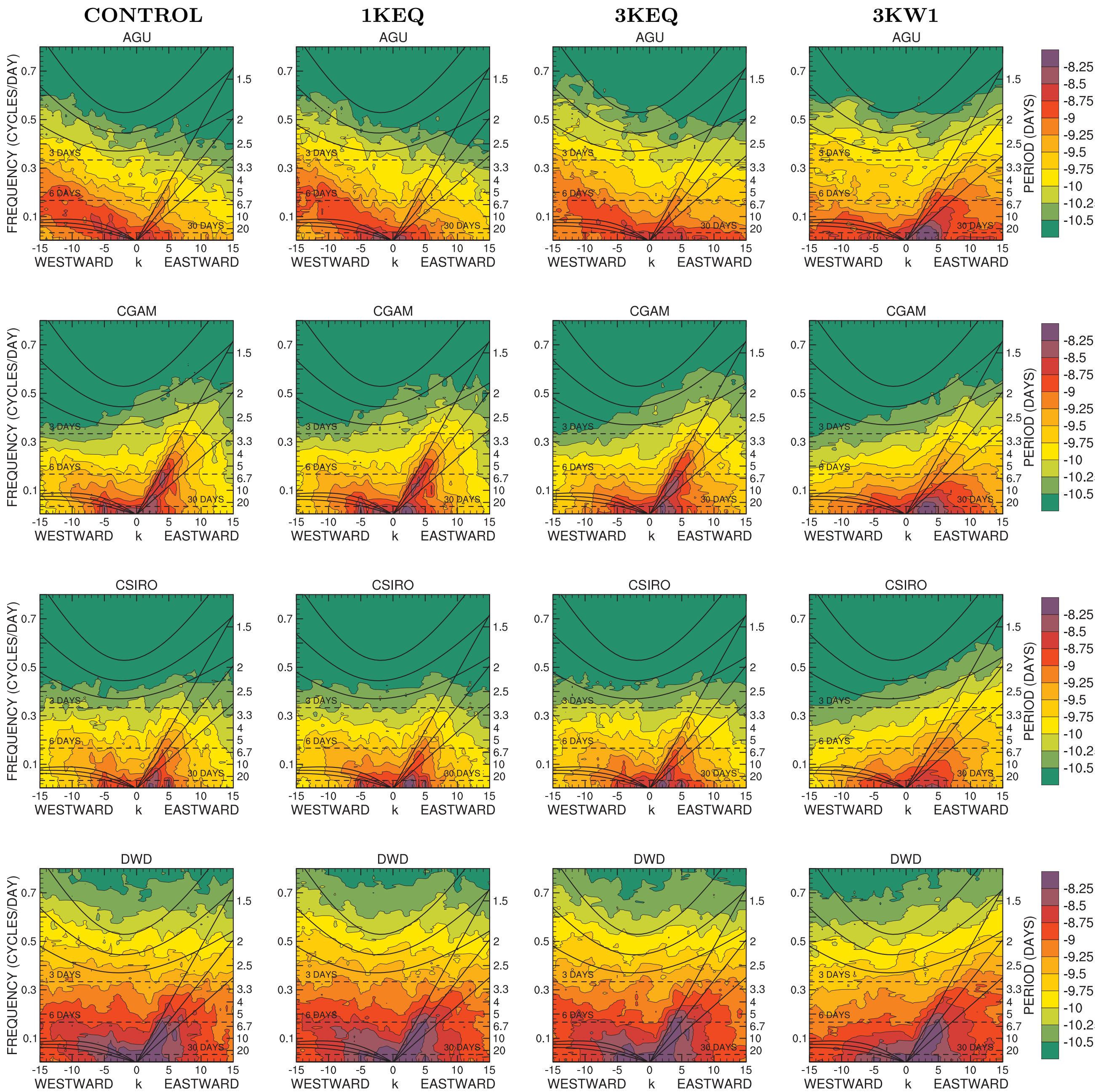

Figure 7.52: Wavenumber-frequency diagrams of log of power of symmetric modes of equatorial precipitation (tppn) for CONTROL, 1KEQ, 3KEQ and 3KW1, 20°S to 20°N.

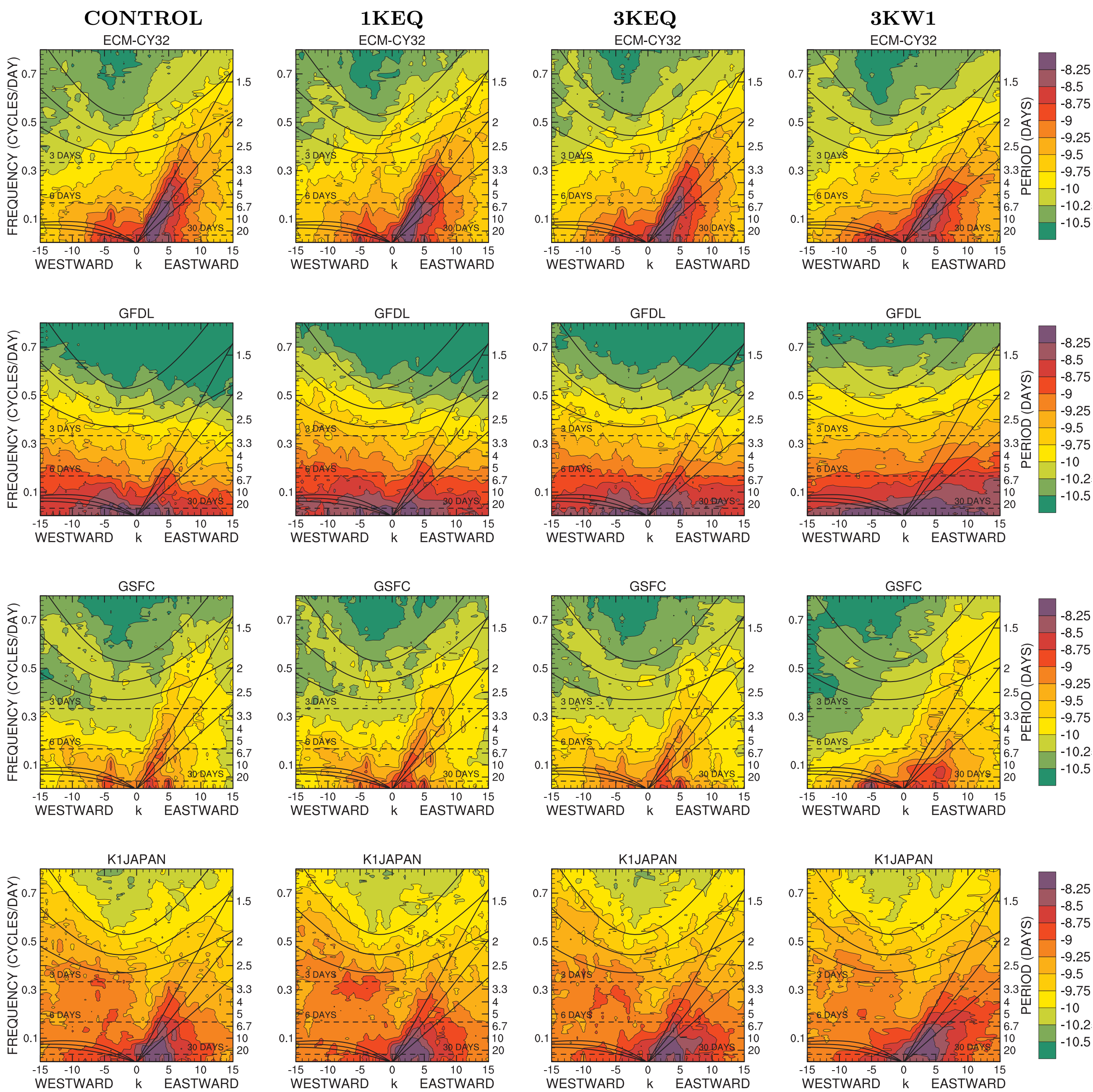

Figure 7.52 (continued): Wavenumber-frequency diagrams of log of power of symmetric modes of equatorial precipitation (tppn) for CONTROL, 1KEQ, 3KEQ and 3KW1, 20°S to 20°N.

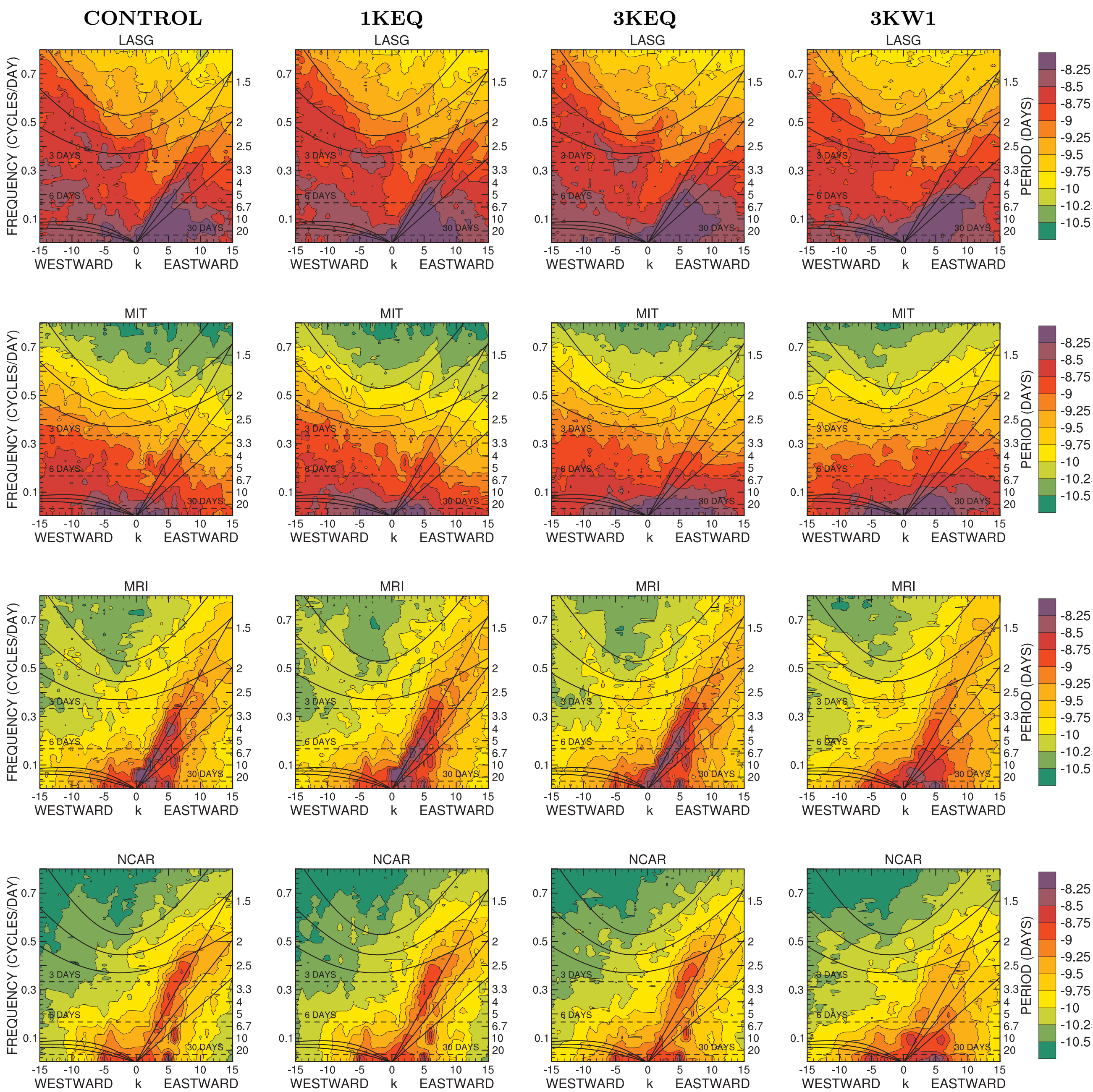

Figure 7.52 (continued) Wavenumber-frequency diagrams of log of power of symmetric modes of equatorial precipitation (tppn) for CONTROL, 1KEQ, 3KEQ and 3KW1, 20°S to 20°N.

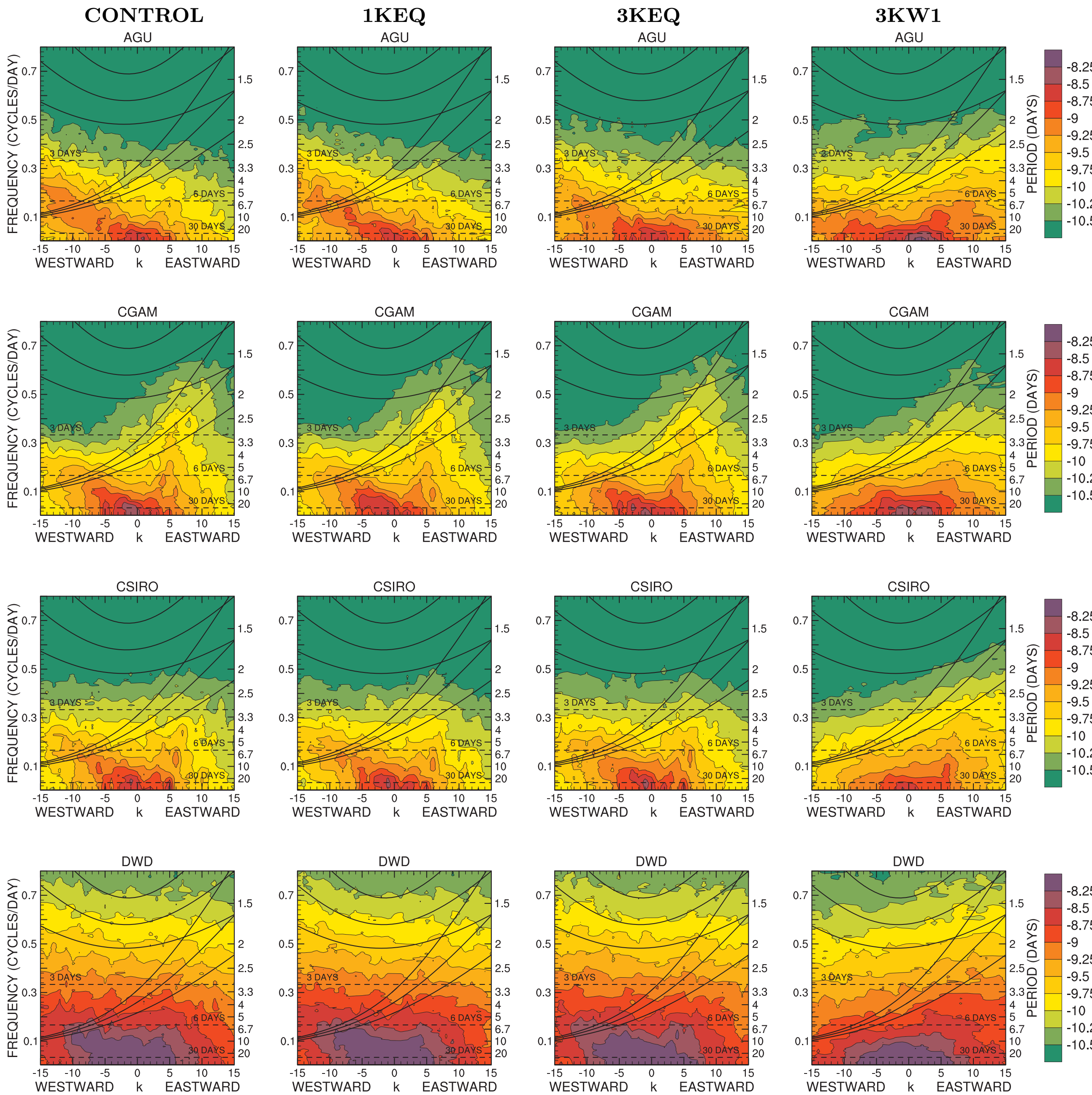

Figure 7.53: Wavenumber-frequency diagrams of log of power of anti-symmetric modes of equatorial precipitation (tppn) for CONTROL, 1KEQ, 3KEQ and 3KW1, 20°S to 20°N.

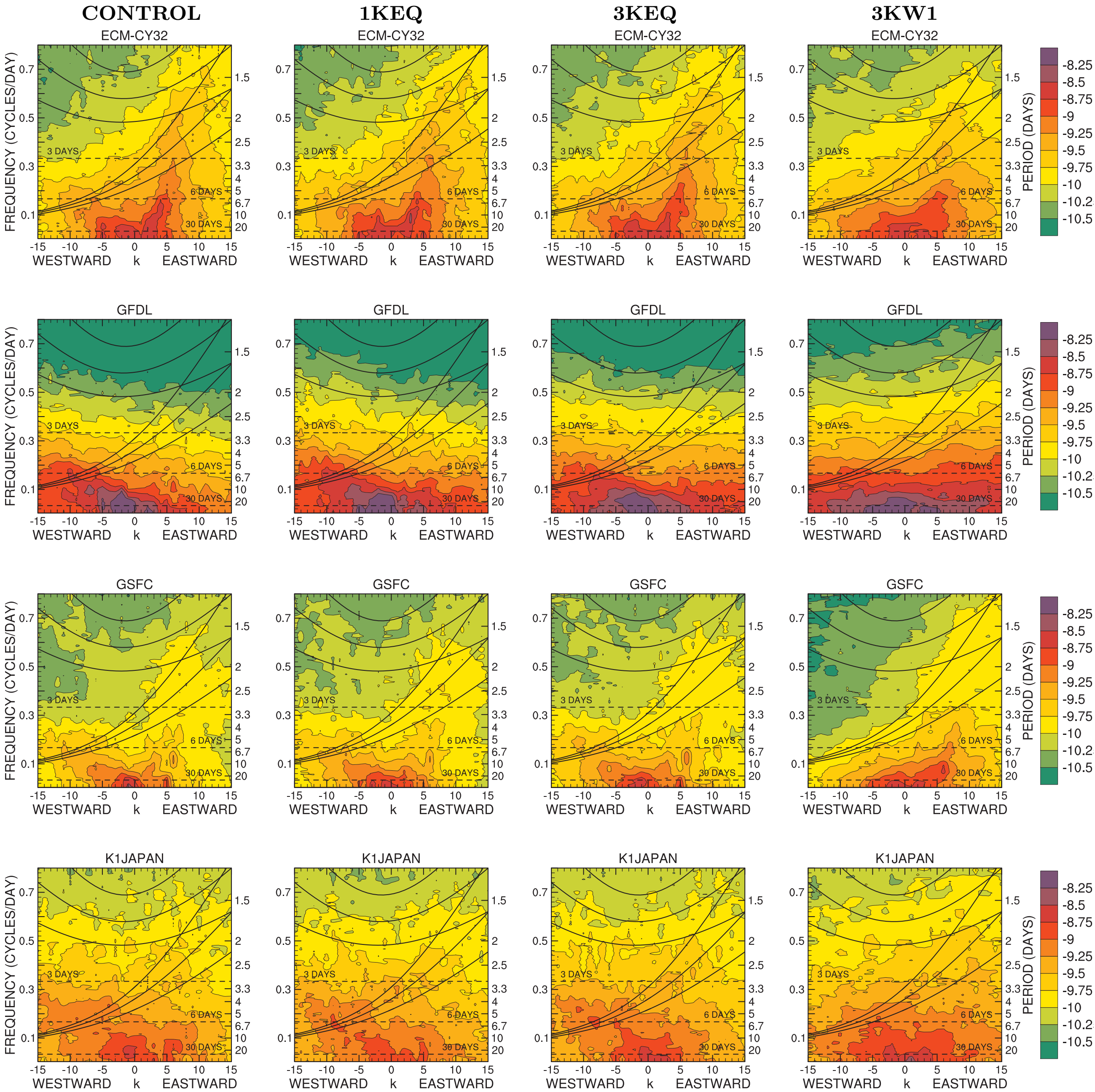

Figure 7.53 (continued): Wavenumber-frequency diagrams of log of power of anti-symmetric modes of equatorial precipitation (tppn) for CONTROL, 1KEQ, 3KEQ and 3KW1, 20°S to 20°N.

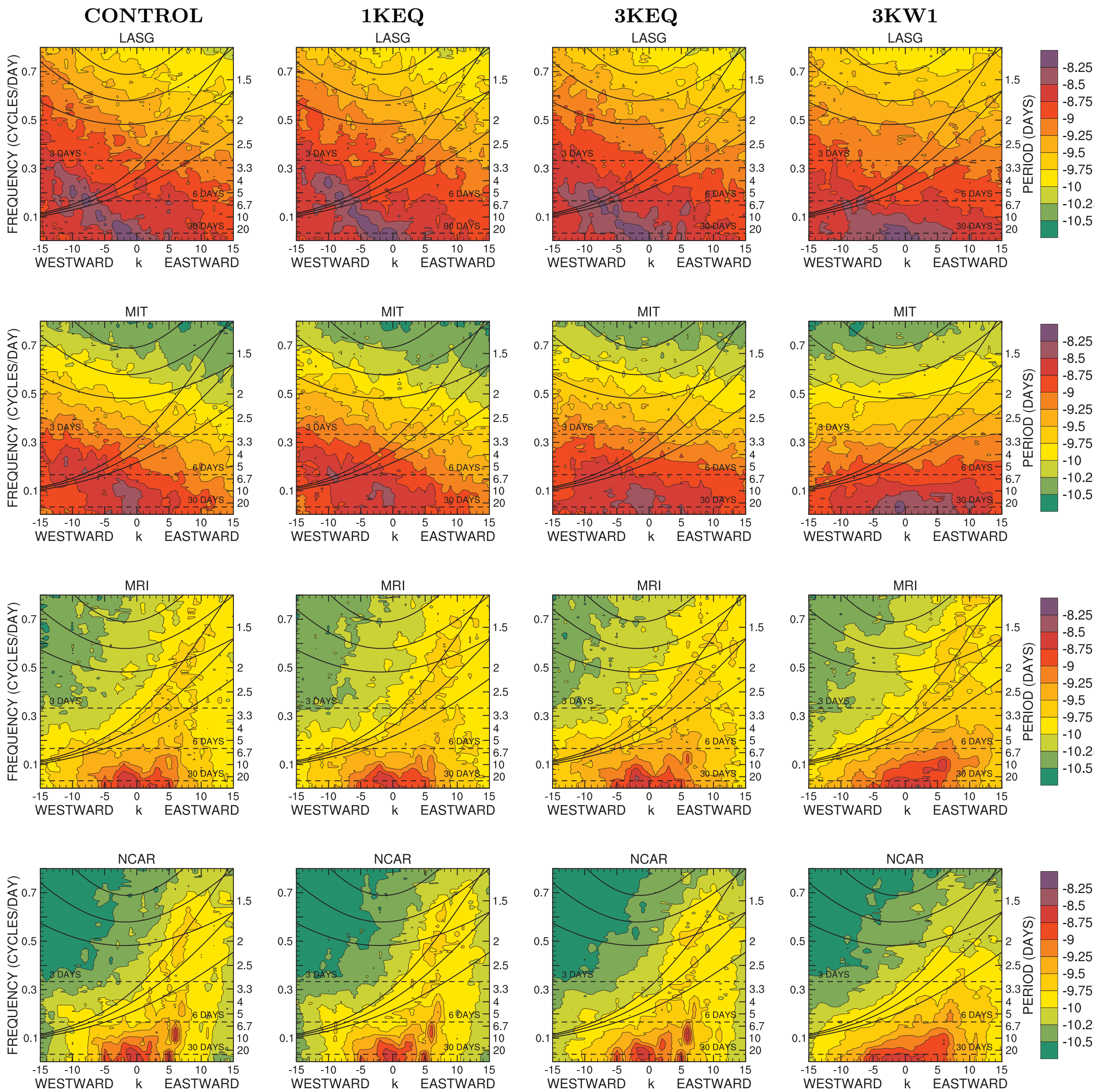

Figure 7.53 (continued): Wavenumber-frequency diagrams of log of power of anti-symmetric modes of equatorial precipitation (tppn) for CONTROL, 1KEQ, 3KEQ and 3KW1, 20°S to 20°N.

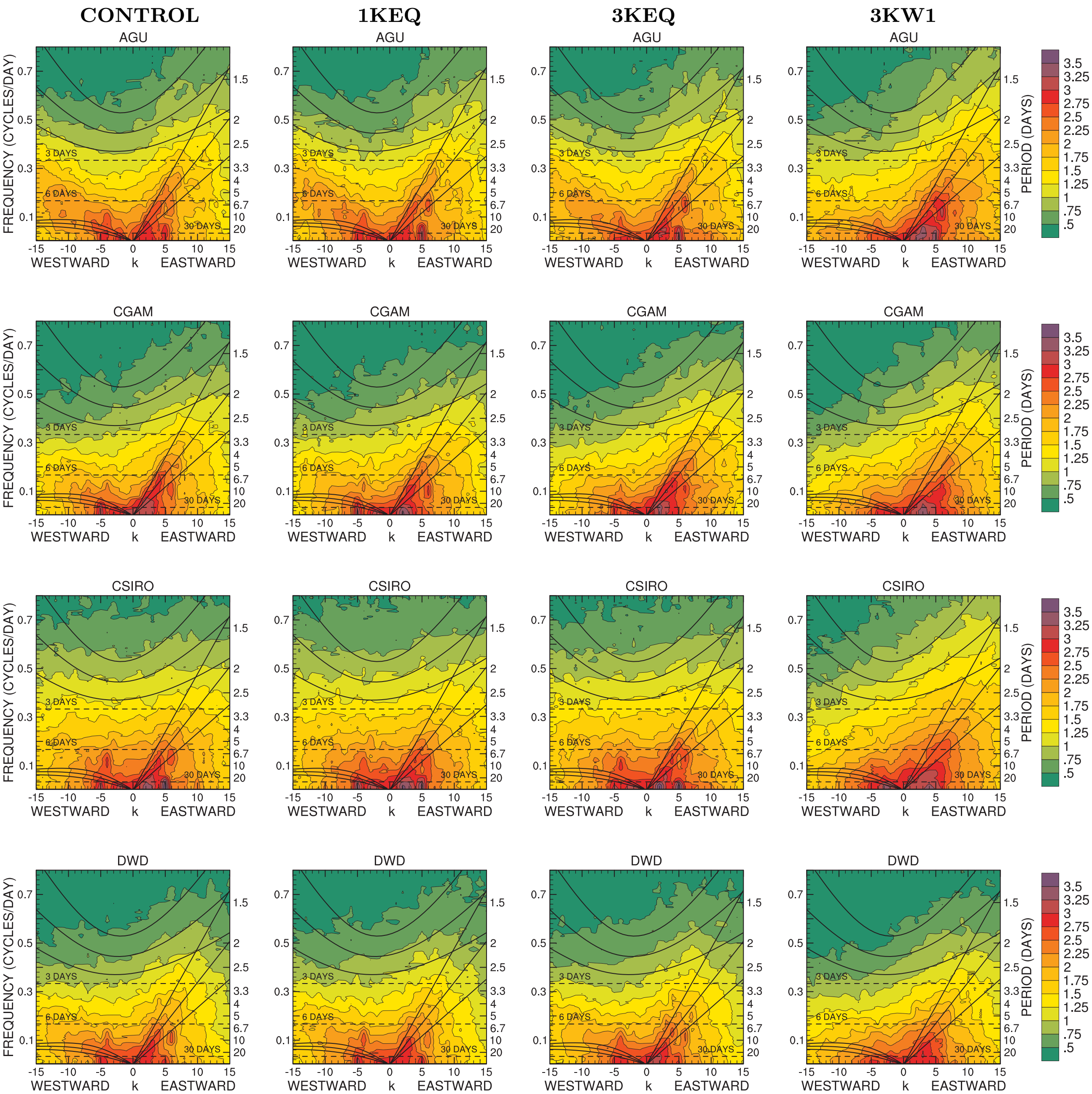

Figure 7.54: Wavenumber-frequency diagrams of log of power of symmetric modes of equatorial OLR (lw_toa) for CONTROL, 1KEQ, 3KEQ and 3KW1, 20°S to 20°N.

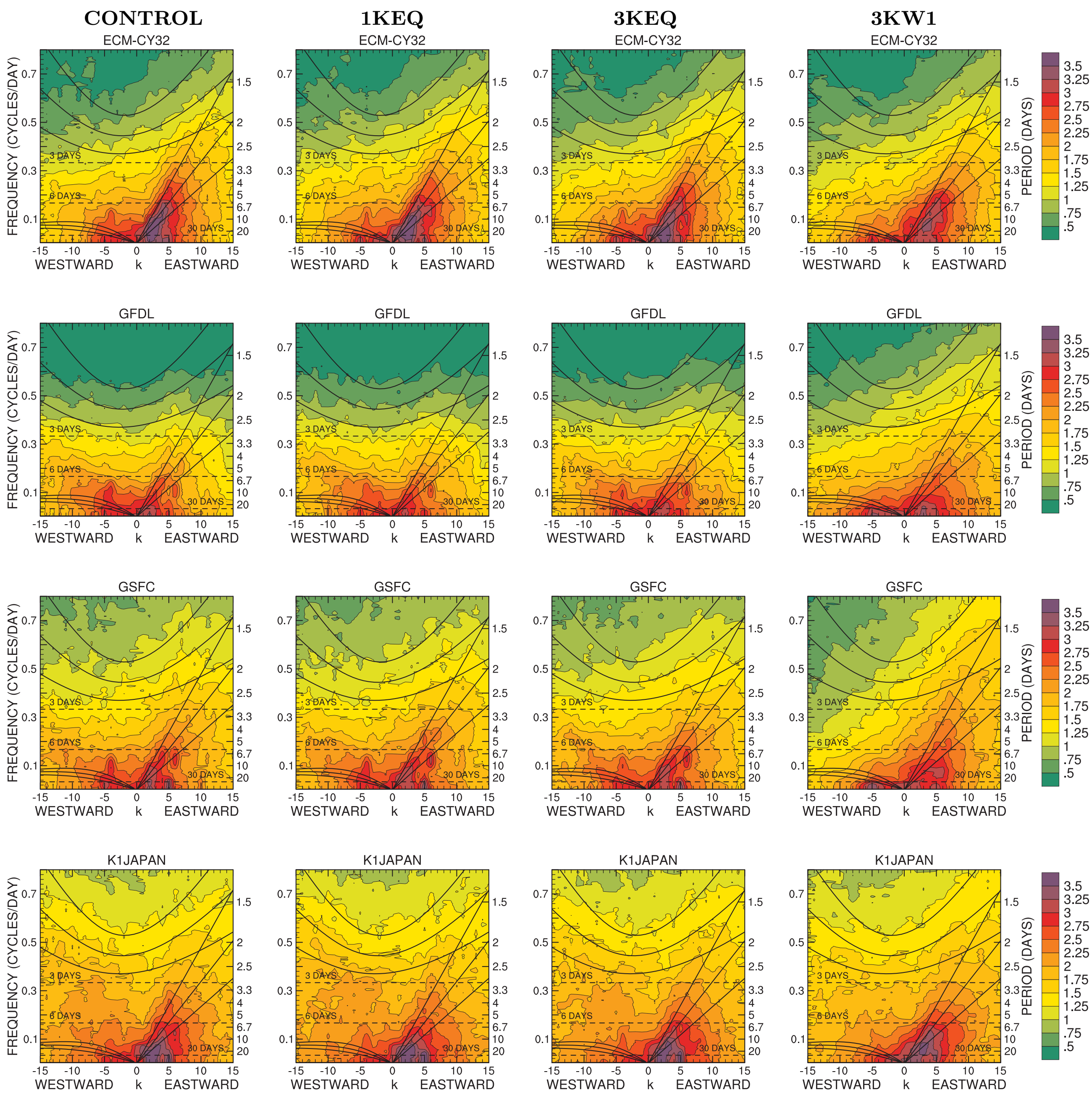

Figure 7.54 (continued): Wavenumber-frequency diagrams of log of power of symmetric modes of equatorial OLR (lw_toa) for CONTROL, 1KEQ, 3KEQ and 3KW1, 20°S to 20°N.

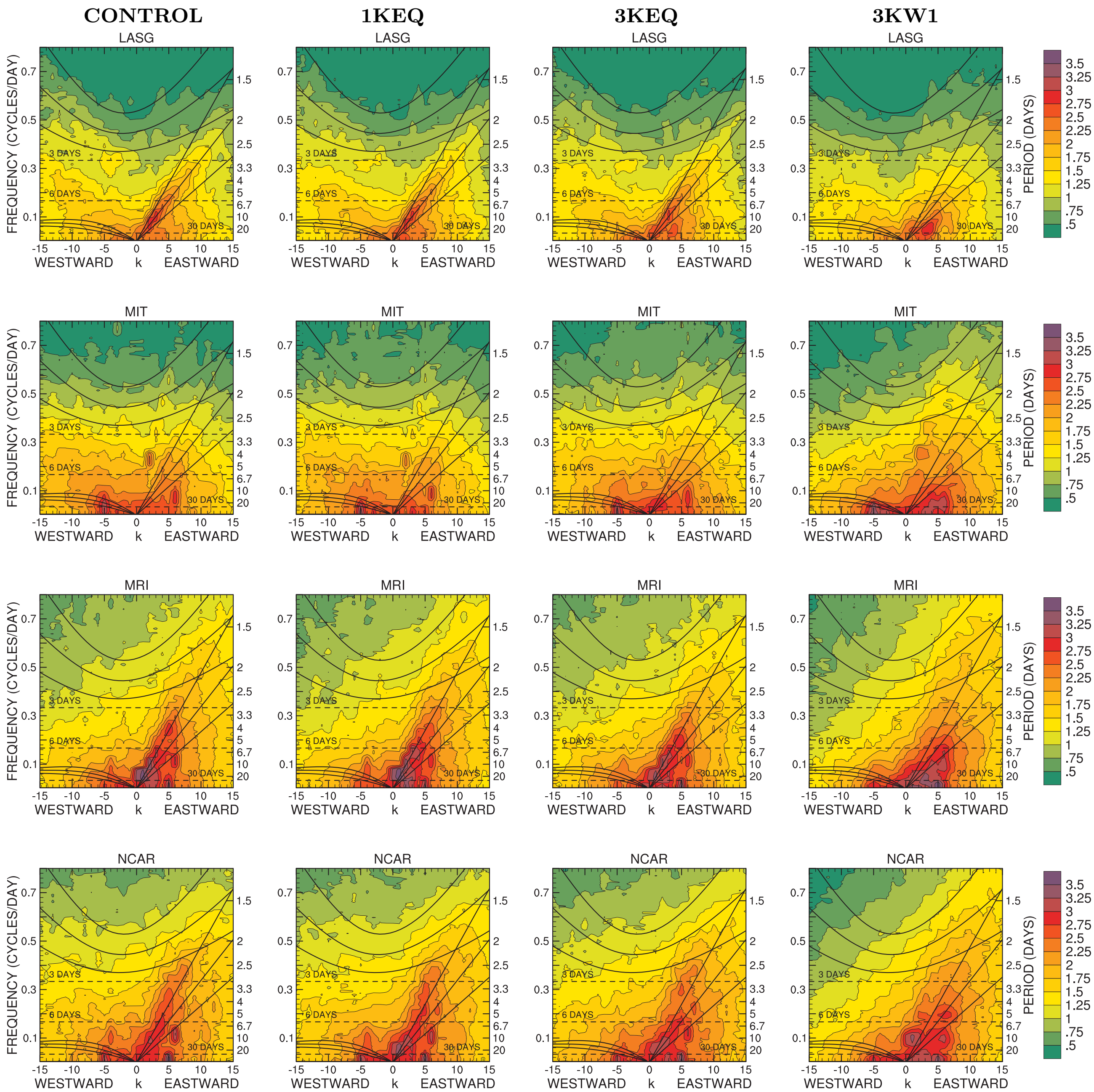

Figure 7.54 (continued): Wavenumber-frequency diagrams of log of power of symmetric modes of equatorial OLR (lw_toa) for CONTROL, 1KEQ, 3KEQ and 3KW1, 20°S to 20°N.

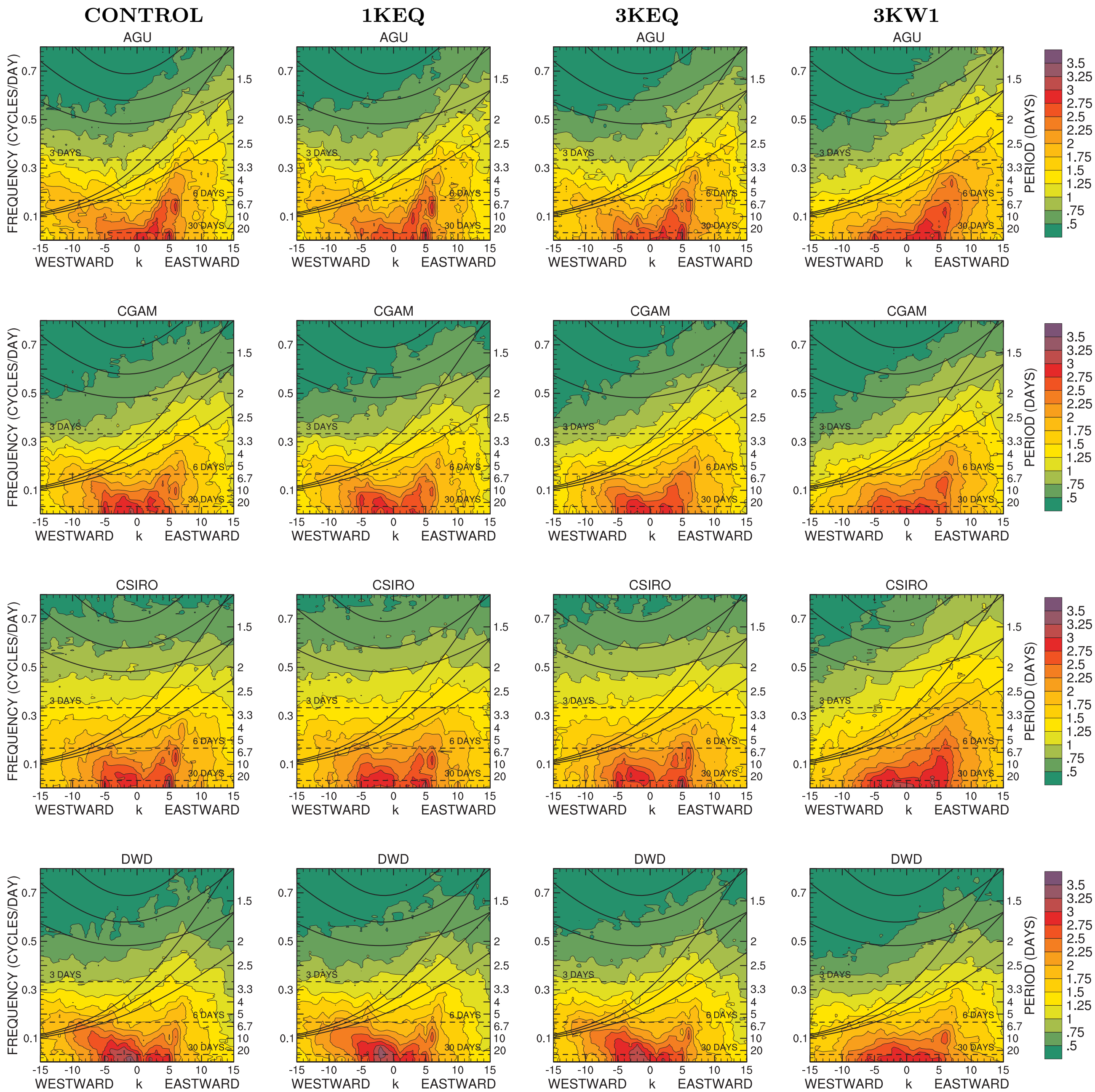

Figure 7.55: Wavenumber-frequency diagrams of log of power of anti-symmetric modes of equatorial OLR (lw_toa) for CONTROL, 1KEQ, 3KEQ and 3KW1, 20°S to 20°N.

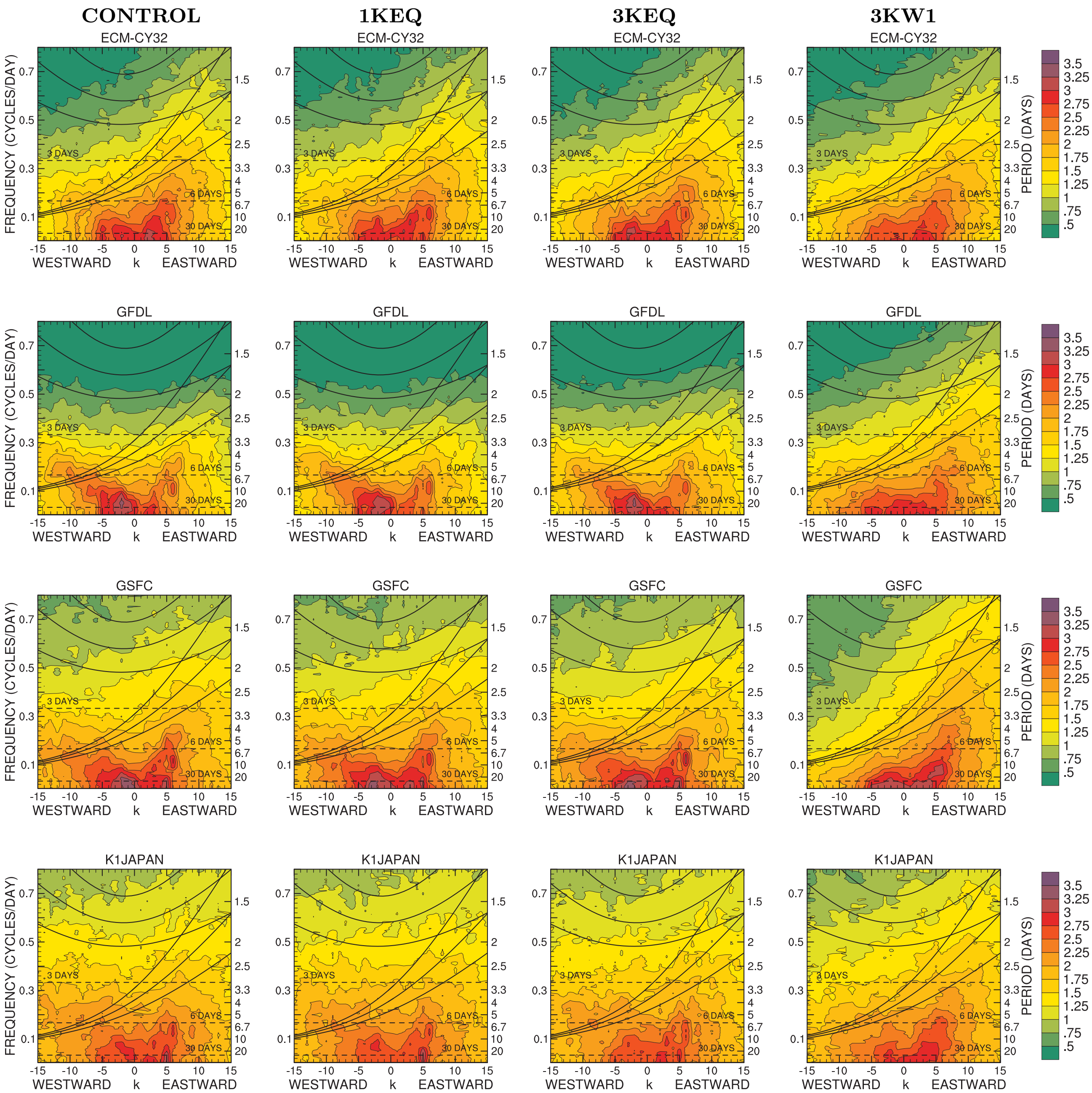

Figure 7.55 (continued): Wavenumber-frequency diagrams of log of power of anti-symmetric modes of equatorial OLR (lw_toa) for CONTROL, 1KEQ, 3KEQ and 3KW1, 20°S to 20°N.

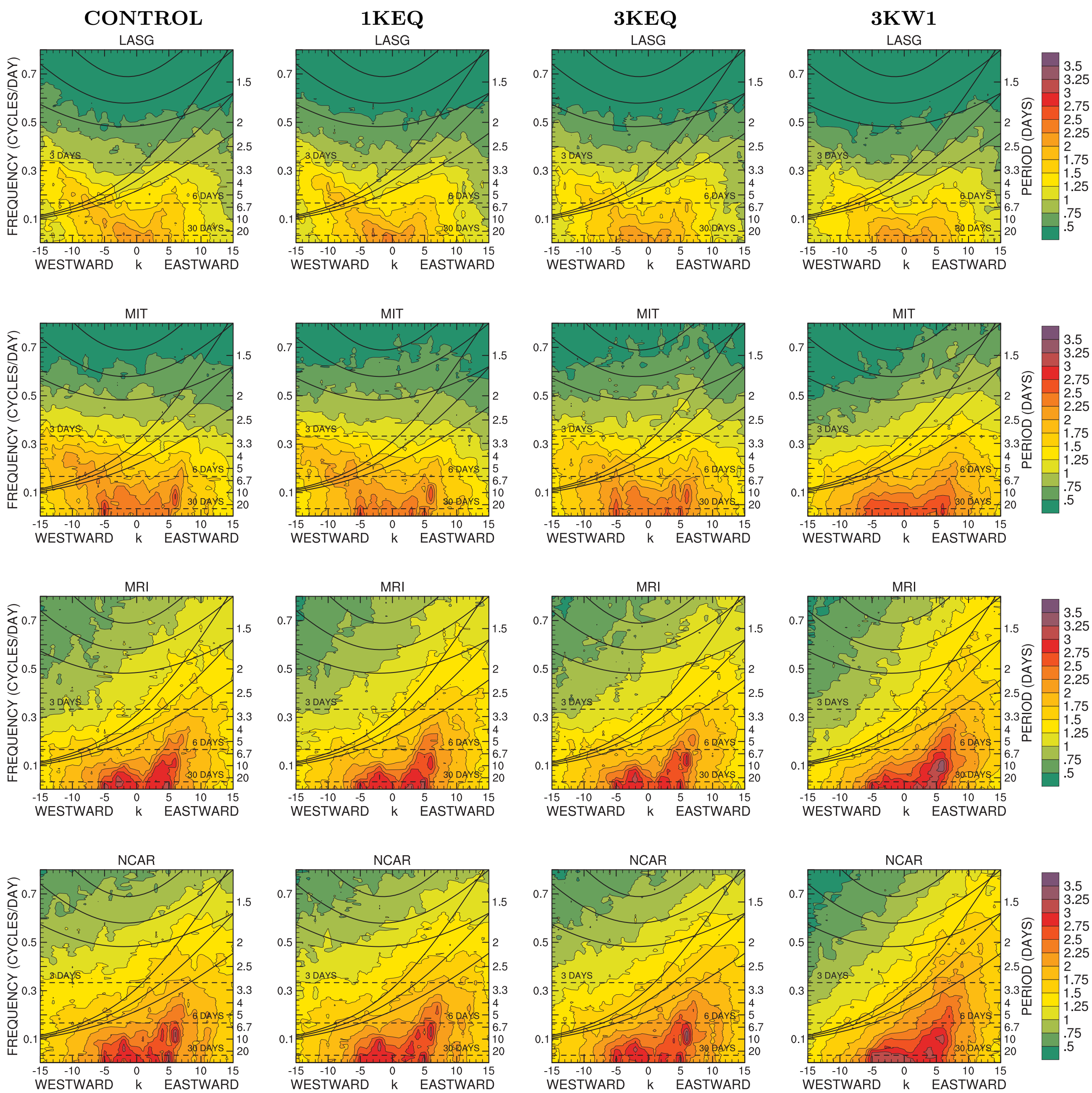

Figure 7.55 (continued): Wavenumber-frequency diagrams of log of power of anti-symmetric modes of equatorial OLR (lw_toa) for CONTROL, 1KEQ, 3KEQ and 3KW1, 20°S to 20°N.

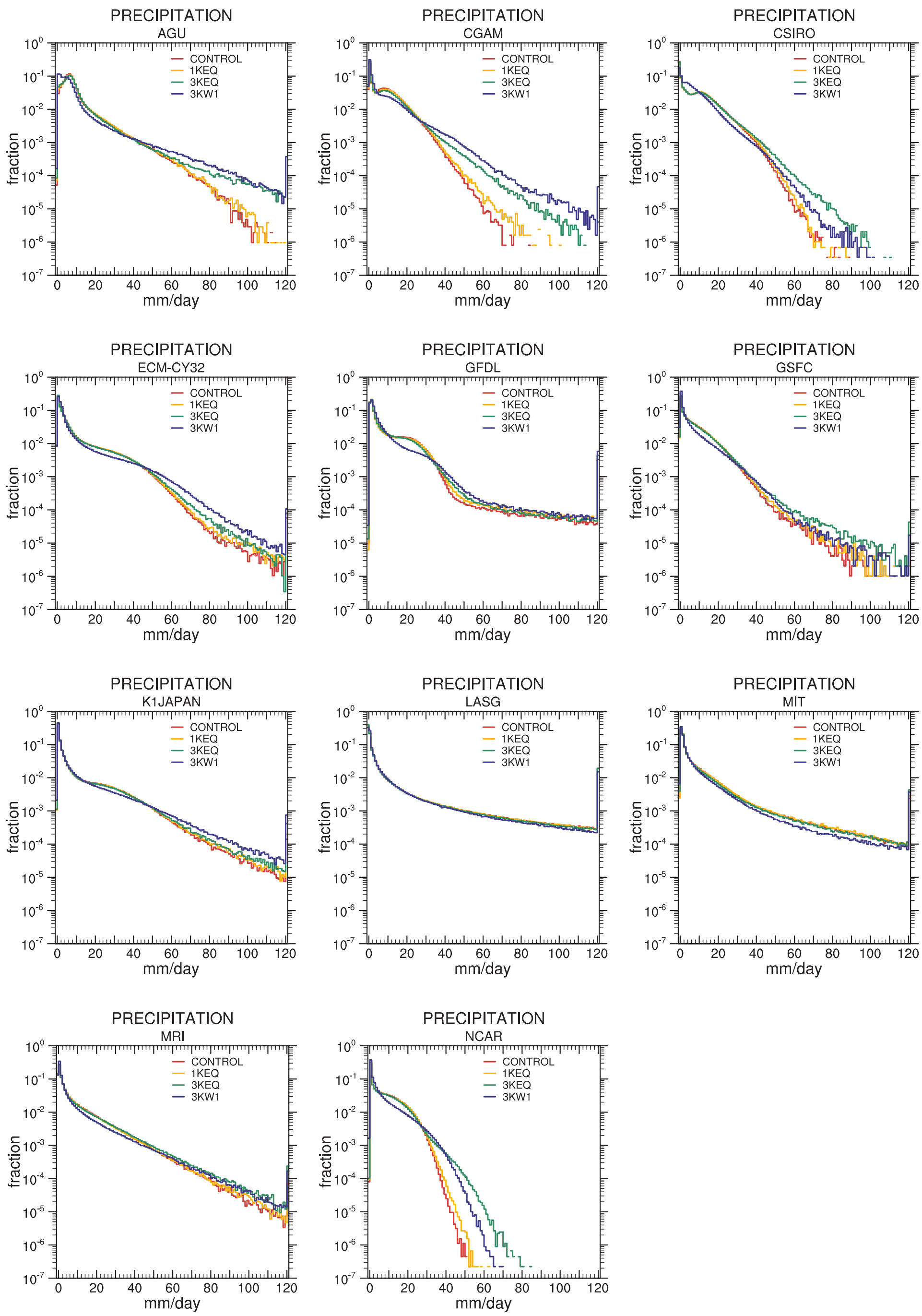

Figure 7.56: Fraction of time precipitation (tppn) from $-20°$ to $+20°$ latitude is in 1 mm day^{-1} bins ranging from 0 to 120 mm day^{-1} for individual models for CONTROL, 1KEQ, 3KEQ and 3KW1 experiments.

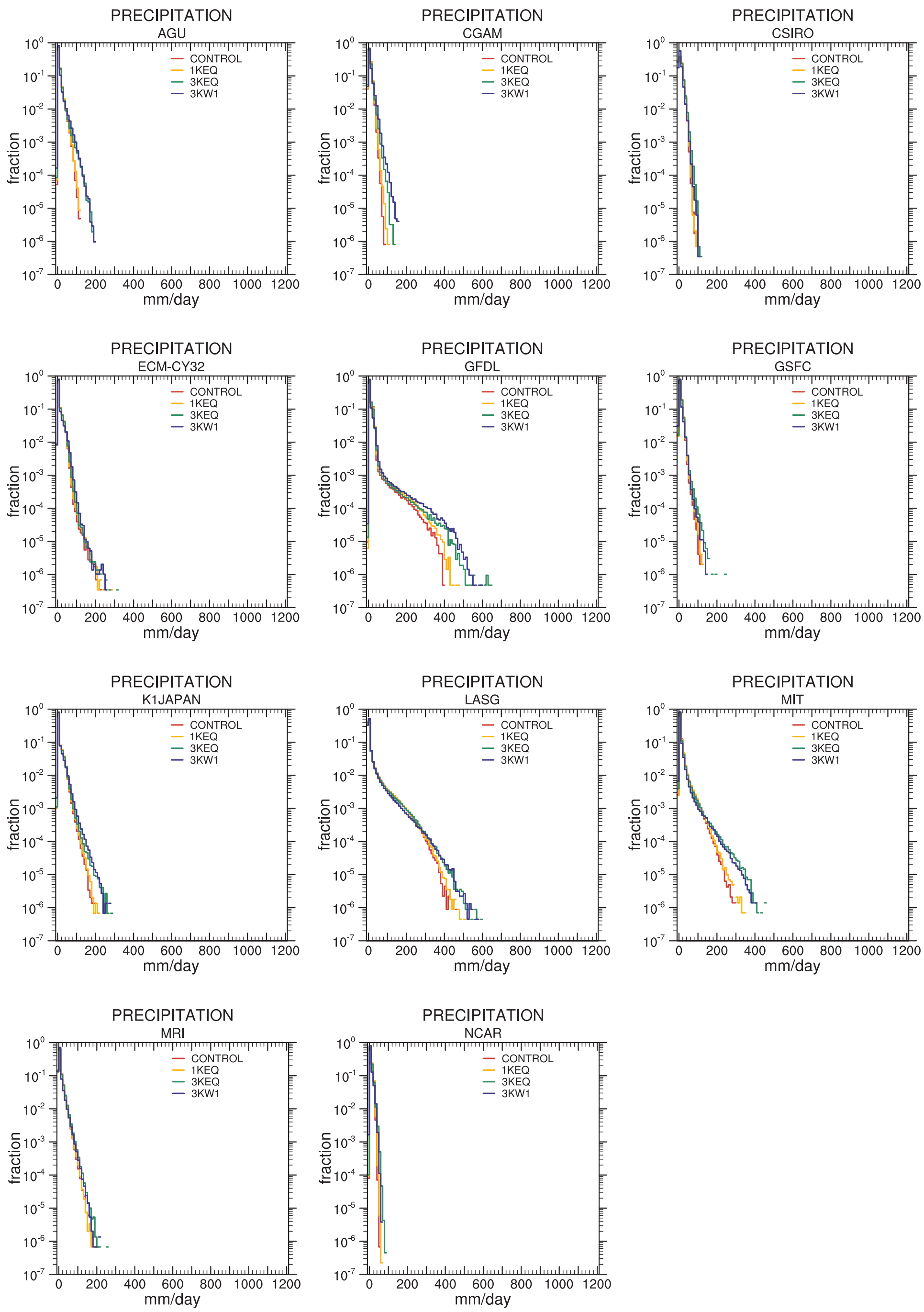

Figure 7.57: Fraction of time precipitation (tppn) from $-20°$ to $+20°$ latitude is in 10 mm day^{-1} bins ranging from 0 to 1200 mm day^{-1} for individual models for CONTROL, 1KEQ, 3KEQ and 3KW1 experiments.

Chapter 8

Comments

Historically, model intercomparison projects were proposed in order to identify systematic model errors, i.e. errors common to the majority of participating models, in the hope that the development community could reduce those errors over time to the benefit of all models. Of course, identification of model specific errors was also an outcome of the intercomparisons. Unlike other model intercomparison projects, the APE climate is unknown and thus aqua-planet model errors cannot be determined. Likewise systematic errors cannot be separated from model specific errors.

This Atlas presents a wide variety of statistics from the 14 participating models for the 8 different aqua-planet experiments. It compares the statistics of the APE simulations but does not contain interpretive analyses of the differences between models. Such analyses are left for journal papers such as those included in the Special Issue of the *Journal of the Meteorological Society of Japan* (2013, Vol. 91A) devoted to the APE.

As with most model intercomparisons the APE shows a large variation in model behaviors even though the problem is a highly constrained, idealized setting. For many statistics, a multi-model mean and standard deviation are included in the Atlas to concisely show the variation between the models. The multi-model mean should not be considered as a reference solution for the aqua-planet. Without variation in the surface forcing, the model APE climates consist primarily of free motions. Many forced phenomena found in earth-like simulations are not included.

Analyses of the APE simulations to date have only scratched the surface. The APE experiment data base holds a wealth of data that is now publicly available. We hope that this Atlas will stimulate future analysis and investigations to understand the cause of the large variation seen in the model behaviors. We also hope that as new models are developed they will repeat the APE simulations.

Bibliography

Adcroft, A. and J.-M. Campin, 2004: Re-scaled height coordinates for accurate representation of free-surface flows in ocean circulation models. *Ocean Modelling*, **7**, 269–284, doi:10.1016/j.ocemod.2003.09.003.

Adcroft, A., J.-M. Campin, C. Hill and J. Marshall, 2004: Implementation of an atmosphere-ocean general circulation model on the expanded spherical cube. *Mon. Wea. Rev.*, **132**, 2845–2863.

Bacmeister, J. T., P. J. Pegion, S. D. Schubert and M. J. Suarez, 2000: Atlas of seasonal means simulated by the NSIPP 1 Atmospheric GCM. NASA Tech. Memo. 17. 194 pp.

Baumgardner, J. R., 1983: A three-dimensional finite element model for mantle convection. Ph.d. thesis, Univ. of California, Los Angeles, 271 pp.

Bechtold, P., J.-P. Chaboureau, A. Beljaars, A. K. Betts, M. Köhler, M. Miller and J.-L. Redelsperger, 2004: The simulation of the diurnal cycle of convective precipitation over land in global models. *Quart. J. Roy. Meteor. Soc.*, **130**, 3119–3137.

Bechtold, P., M. Köhler, T. Jung, F. Doblas-Reyes, M. Leutbecher, M. J. Rodwell, F. Vitart and G. Balsamo, 2008: Advances in simulating atmospheric variability with the ECMWF model: from synoptic to decadal time-scales. *Quart. J. Roy. Meteor. Soc.*, **134**, 1337–1351.

Beljaars, A., P. Bechtold, M. Köhler, J.-J. Morcrette, A. Tompkins, P. Viterbo and N. Wedi, 2004: The numerics of physical parameterization. *Proc. ECMWF Workshop on Recent Developments in numerical methods for atmosphere and ocean modelling*, Reading, UK, European Centre for Medium-Range Weather Forecasts, 113–134.

Beljaars, A. C. M., 1995a: The impact of some aspects of the boundary layer scheme in the ECMWF model, Reading, UK. European Centre for Medium-Range Weather Forecasts, 125–161, Proc. 1995 Seminar on Parametrization of Sub-grid Scale Physical Processes.

Beljaars, A. C. M., 1995b: The parameterization of surface-fluxes in large-scale models under free convection. *Quart. J. Roy. Meteor. Soc.*, **121**, 255–270.

Blackburn, M. and B. J. Hoskins, 2013: Context and aims of the Aqua-Planet Experiment. *J. Meteor. Soc. Japan*, **91A**, doi:10.2151/jmsj.2013-A01.

Blackburn, M., D. L. Williamson, K. Nakajima, W. Ohfuchi, Y. O. Takahashi, Y.-Y. Hayashi, H. Nakamura, M. Ishiwatari, J. L. McGregor, H. Borth, V. Wirth, H. Frank, P. Bechtold, N. P. Wedi, H. Tomita, M. Satoh, M. Zhao, I. M. Held, M. J. Suarez, M.-I. Lee, M. Watanabe, M. Kimoto, Y. Liu, Z. Wang, A. Molod, K. Rajendran, A. Kitoh and R. Stratton, 2013: The Aqua-Planet Experiment (APE): CONTROL SST simulation. *J. Meteor. Soc. Japan*, **91A**, doi:10.2151/jmsj.2013-A02.

Boer, G. J. and B. Denis, 1997: Numerical convergence of the dynamics of a GCM. *Climate Dyn.*, **13**, 359–374.

Boville, B. A., P. J. Rasch, J. J. Hack and J. R. McCaa, 2006: Representation of clouds and precipitation processes in the Community Atmosphere Model Version 3 (CAM3). *J. Climate*, **19**, 2184–2198.

Cash, B. A., P. Kushner and G. Vallis, 2007: Comment on "On the presence of annular variability in an aquaplanet model" by Masahiro Watanabe. *Geophys. Res. Lett.*, **34**, L03 707, doi:10.1029/2006GL027274.

Chou, M.-D., 1990: Parameterizations for the absorption of solar radiation by O_2 and CO_2 with applications to climate studies. *J. Climate*, **3**, 209–217.

Chou, M.-D., 1992: A solar radiation model for use in climate studies. *J. Atmos. Sci.*, **49**, 762–772.

Chou, M.-D. and M. J. Suarez, 1994: An efficient thermal infrared radiation parameterization for use in general circulation models. NASA Tech. Memo 3. 85 pp.

Chou, M.-D. and M. J. Suarez, 1999: A solar radiation parameterization for atmospheric studies. NASA Tech. Memo 15. 40 pp.

Collins, W. D., J. J. Hack, B. A. Boville, P. J. Rasch, D. L. Williamson, J. T. Kiehl, B. Briegleb, J. R. McCaa, C. Bitz, S.-J. Lin, R. B. Rood, M. Zhang and Y. Dai, 2003: *Description of the NCAR Community Atmosphere Model (CAM2)*. National Center for Atmospheric Research, available from: http://www.ccsm.ucar.edu/models/atm-cam/docs/cam2.0.

Collins, W. D., P. J. Rasch, B. A. Boville, J. J. Hack, J. R. McCaa, D. L. Williamson, J. T. Kiehl, B. P. Briegleb, C. M. Bitz, S.-J. Lin, M. Zhang and Y. Dai, 2004: Description of the NCAR Community Atmosphere Model (CAM3.0). Tech. Rep. NCAR/TN-464+STR, National Center for Atmospheric Research.

Collins, W. D., C. M. Bitz, M. L. Blackmon, G. B. Bonan, C. S. Bretherton, J. A. Carton, P. Chang, S. C. Doney, J. J. Hack, T. B. Henderson, J. T. Kiehl, W. G. Large, D. S. McKenna, B. D. Santer and R. D. Smith, 2006a: The Community Climate System Model: CCSM. *J. Climate*, **19**, 2122–2143.

Collins, W. D., P. J. Rasch, B. A. Boville, J. J. Hack, J. R. McCaa, D. L. Williamson, B. P. Briegleb, C. M. Bitz, S.-J. Lin and M. Zhang, 2006b: The formulation and atmospheric simulation of the Community Atmosphere Model Version 3 (CAM3). *J. Climate*, **19**, 2144–2161.

Cullen, M. and T. Davies, 1991: A conservative split explicit integration scheme with fourth order horizontal advection. *Quart. J. Roy. Meteor. Soc.*, **117**, 993–1002, doi: 10.1002/qj.49711750106.

Cullen, M. J. P., 1993: The unified forecast/climate model. *Meteorological Magazine*, **122**, 81–94.

Cusack, S., J. M. Edwards and J. M. Crowther, 1999a: Investigating k-distribution methods for parametrizing gaseous absorption in the Hadley Centre climate model. *J. Geophys. Res.*, **104**, 2051–2057, doi:10.1029/1998JD200063.

Cusack, S., J. M. Edwards and R. Kershaw, 1999b: Estimating the subgrid variance of saturation, and its parametrization for use in a GCM cloud scheme. *Quart. J. Roy. Meteor. Soc.*, **125**, 3057–3076.

Cusack, S., A. Slingo, J. M. Edwards and M. Wild, 1998: The radiative impact of a simple aerosol climatology on the Hadley Centre climate model. *Quart. J. Roy. Meteor. Soc.*, **124**, 2517–2526, doi:10.1002/qj.49712455117.

Davies, T., M. J. P. Cullen, A. J. Malcolm, M. H. Mawson, A. Stainforth, A. A. White and N. Wood, 2005: A new dynamical core for the Met Office's global and regional modelling of the atmosphere. *Quart. J. Roy. Meteor. Soc.*, **131**, 1759–1782, doi:10.1256/qj.04.101.

Delworth, T. L., A. Rosati, R. J. Stouffer, K. W. Dixon, J. Dunne, K. L. Findell, P. Ginoux, A. Gnanadesikan, C. T. Gordon, S. M. Griffies, R. Gudgel, M. J. Harrison, I. M. Held, R. S. Hemler, L. W. Horowitz, S. A. Klein, T. R. Knutson, S.-J. Lin, V. Ramaswamy, M. D. Schwarzkopf, J. J. Sirutis, M. J. Spelman, W. F. Stern, M. Winton, A. T. Wittenberg, B. Wyman, A. J. Broccoli, V. Balaji, J. Russell, R. Zhang, J. A. Beesley, J. Lu, W. F. Cooke, J. W. Durachta, A. R. Langenhorst, H.-C. Lee, F. Zeng, K. A. Dunne, P. C. D. Milly, P. J. Kushner, S. L. Malyshev and E. Shevliakova, 2006: GFDL's CM2 global coupled climate models - Part I: Formulation and simulation characteristics. *J. Climate*, **19**, 643–674.

Dickey, J. O., 1995: Earth rotation. *Global Earth Physics: A Handbook of physical constants*, Ahrens, Ed., AGU, 356–368.

Doms, G., J. Förstner, E. Heise, H.-J. Herzog, M. Raschendorfer, R. Schrodin, T. Reinhardt and G. Vogel, 2005: *A Description of the Nonhydrostatic Regional Model LM. Part II: Physical Parameterization*. Postfach 10 04 65, D-63004 Offenbach, Germany, Deutscher Wetterdienst, DWD.

ECMWF, 2010: IFS documentation. http://www.ecmwf.int/research/ifsdocs/.

Edwards, J. M. and A. Slingo, 1996: Studies with a flexible new radiation code. I: choosing a configuration for a large-scale model. *Quart. J. Roy. Meteor. Soc.*, **122**, 689–719, doi: 10.1002/qj.49712253107.

Emanuel, K. A., 1991: A scheme for representing cumulus convection in large-scale models. *J. Atmos. Sci.*, **48**, 2313–2335.

Emanuel, K. A., 1994: *Atmospheric Convection*. Oxford University Press.

Emanuel, K. A. and M. Živković-Rothman, 1999: Development and evaluation of a convection scheme for use in climate models. *J. Atmos. Sci.*, **56**, 1766–1782.

Emori, S., A. Hasegawa, T. Suzuki and K. Dairaku, 2005: Validation, parameterization dependence and future projection of daily precipitation simulated with a high-resolution atmospheric GCM. *Geophys. Res. Lett*, **32**, doi:10.1029/ 2004GL022306.

Emori, S., T. Nozawa, A. Numaguti and I. Uno, 2001: Importance of cumulus parameterization for precipitation simulation over east asia in June. *J. Meteor. Soc. Japan*, **79**, 939–947.

Fasullo, J. T. and K. E. Trenberth, 2008: The annual cycle of the energy budget. Part II: Meridional structures and poleward transports. *J. Climate*, **21**, 2313–2325.

GAMDT, 2004: The new GFDL global atmosphere and land model AM2/LM2: Evaluation with prescribed SST simulations. *J. Climate*, **17**, 4641–4673.

Gates, W. L., J. S. Boyle, C. C. Covey, C. G. Dease, C. M. Doutriaux, R. S. Drach, M. Fiorino, P. J. Gleckler, J. J. Hnilo, S. M. Marlais, T. J. Phillips, G. L. Potter, B. D. Santer, K. R. Sperber, K. E. Taylor and D. N. Williams, 1999: An overview of the results of the Atmospheric Model Intercomparison Project (AMIP I). *Bull. Amer. Meteor. Soc.*, **80**, 29–55.

Gleckler, P. J., D. A. Randall, G. Boer, R. Colman, M. Dix, V. Galin, M. Helfand, J. Kiehl, A. Kitoh, W. Lau, X.-Y. Liang, V. Lykossov, B. McAvaney, K. Miyakoda, S. Planton and W. Stern, 1995: Cloud-radiative effects on implied oceanic energy transports as simulated by Atmospheric General Circulation Models. *Geophys. Res. Lett.*, **22**, 791–794.

Grant, A. L. M., 2001: Cloud-base fluxes in the cumulus-capped boundary layer. *Quart. J. Roy. Meteor. Soc.*, **127**, 407–421.

Grant, A. L. M. and A. R. Brown, 1999: A similarity hypothesis for shallow-cumulus transports. *Quart. J. Roy. Meteor. Soc.*, **125**, 1913–1936.

Gregory, D., 1995: A consistent treatment of the evaporation of rain and snow for use in large-scale models. *Mon. Wea. Rev.*, **123**, 2716–2732, doi:10.1175/1520-0493(1995)123<2716:ACTOTE>2.0.CO;2.

Gregory, D. and S. Allen, 1991: The effect of convective scale down-drafts upon NWP and climate simulations. *Ninth conference on Numerical Weather Prediction*, American Meteorological Society, Denver, Colorado, 122–123.

Gregory, D., R. Kershaw and P. M. Inness, 1997: Parametrization of momentum transport by convection. II: tests in single-column and general circulation models. *Quart. J. Roy. Meteor. Soc.*, **123**, 1153–1183, doi:10.1002/qj.49712354103.

Gregory, D. and P. R. Rowntree, 1990: A mass flux convection scheme with representation of cloud ensemble characteristics and stability-dependent closure. *Mon. Wea. Rev.*, **118**, 1483–1506, doi:10.1175/1520-0493(1990)118<1483:AMFCSW>2.0.CO;2.

Gregory, D. and P. R. Rowntree, 1996: The sensitivity of climate simulations to the specification of mixed phase clouds. *Climate Dyn.*, **12**, 641–651, doi:10.1007/BF00216271.

Hack, J. J., 1994: Parameterization of moist convection in the National Center for Atmospheric Research community climate model (CCM2). *J. Geophys. Res.*, **99**, 5551–556.

Hack, J. J., J. M. Caron, G. Danabasoglu, K. W. Oleson, C. M. Bitz and J. E. Truesdale, 2006b: CCSM CAM3 climate simulation sensitivity to changes in horizontal resolution. *J. Climate*, **19**, 2267–2289.

Hack, J. J., J. M. Caron, S. G. Yeager, K. W. Oleson, M. M. Holland, J. E. Truesdale and P. J. Rasch, 2006a: Simulation of the global hydrological cycle in the CCSM Community Atmosphere Model Version 3 (CAM3): Mean features. *J. Climate*, **19**, 2199–2221.

Held, I. M. and M. J. Suarez, 1994: A proposal for the intercomparison of the dynamical cores of atmospheric general circulation models. *Bull. Amer. Meteor. Soc.*, **75**, 1825–1830.

Helfand, H. M., M. Fox-Rabinovitz, L. Takacs and A. Molod, 1991: Simulation of the planetary boundary layer and turbulence in the GLA GCM. *Ninth conference on Numerical Weather Prediction*, American Meteorolgical Society, Denver, Colorado, 514–517.

Helfand, H. M. and J. C. Labraga, 1988: Design of a non-singular level 2.5 second-order closure model for the prediction of atmospheric turbulence. *J. Atmos. Sci.*, **45**, 113–132.

Helfand, H. M. and S. D. Schubert, 1995: Climatology of the simulated great plains low-level jet and its contribution to the continental moisture budget of the United States. *J. Climate*, **8**, 784–806.

Holtslag, A. A. M. and B. A. Boville, 1993: Local versus nonlocal boundary-layer diffusion in a global climate model. *J. Climate*, **6**, 1825–1842.

Hurrell, J. W., J. J. Hack, A. Phillips, J. Caron and J. Yin, 2006: The dynamical simulation of the Community Atmosphere Model Version 3 (CAM3). *J. Climate*, **19**, 2162–2183.

Inness, P. M., J. M. Slingo, S. J. Woolnough, R. B. Neale and V. D. Pope, 2001: Organization of tropical convection in a GCM with varying vertical resolution; implications for the simulation of the Madden-Julian Oscillation. *Climate Dyn.*, **17**, 777–793, doi:10.1007/s003820000148.

Iribarne, J. V. and W. L. Godson, 1973: *Atmospheric Thermodynamics*. D. Reidel.

Jakob, C. and S. A. Klein, 2000: A parameterization of the effects of cloud and precipitation overlap for use in general circulation models. *Quart. J. Roy. Meteor. Soc.*, **126**, 2525–2544.

Jakob, R., J. J. Hack and D. L. Williamson, 1993: Solutions to the shallow water test set using the spectral transform method. NCAR Technical Note NCAR/TN-388+STR, National Center for Atmospheric Research, Boulder, Colorado. 82 pp.

K-1 Model Developers, 2004: K-1 coupled model (MIROC) description. *K-1 Technical Report*, H. Hasumi and S. Emori, Eds., Center for Climate System Research, University of Tokyo, 34 pp.

Kiehl, J. T. and P. R. Gent, 2004: The Community Climate System Model, Version 2. *J. Climate*, **17**, 3666–3682.

Kimoto, M., 2005: Simulated change of the East Asian circulation under the global warming. *Geophys. Res. Lett.*, **32**, doi:10.1029/2005GL023383.

Koster, R. D. and M. J. Suarez, 1994: Energy and water balance calculations in the Mosaic LSM. NASA Tech. Memo. 9. 194 pp.

Lacis, A. A. and J. E. Hansen, 1974: A parameterization for the absorption of solar radiation in the Earth's atmosphere. *J. Atmos. Sci.*, **31**, 118–133.

Le Treut, H. and Z. X. Li, 1991: Sensitivity of an atmospheric general circulation model to prescribed SST changes: Feedback effects associated with the simulation of cloud optical properties. *Climate Dyn.*, **5**, 175–187.

Lee, M.-I., M. J. Suarez, I.-S. Kang, I. M. Held and D. Kim, 2008: A moist benchmark calculation for atmospheric general circulation models. *J. Climate*, **21**, 4934–4954.

Liang, X.-Z. and W.-C. Wang, 1996: Atmospheric ozone climatology for use in General Circulation Models. http://www-pcmdi.llnl.gov/projects/amip/AMIP2EXPDSN/OZONE/OZONE2/o3wangdoc.html, Atmospheric Sciences Research Center, State University of New York at Albany.

Lin, S.-J., 2004: A "vertically Lagrangian" finite-volume dynamical core for global models. *Mon. Wea. Rev.*, **132**, 2293–2307.

Lin, S.-J. and R. B. Rood, 1996: Multidimensional flux-form semi-Lagrangian transport schemes. *Mon. Wea. Rev.*, **124**, 2046–2070.

List, R. J., 1951: *Smithsonian Meteorological tables*. 6th ed., Smithsonian Institution Press.

Liu, Y. M., L. Guo, G. X. Wu and Z. Wang, 2010: Sensitivity of ITCZ configuration to cumulus convective parameterizations on an aqua planet. *Climate Dyn.*, **34**, 223–240.

Lock, A. P., A. R. Brown, M. R. Bush, G. M. Martin and R. Smith, 2000: A new boundary layer mixing scheme. Part I: Scheme description and single-column model tests. *Mon. Wea. Rev.*, **128**, 3187–3199.

Louis, J., M. Tiedtke and J. Geleyn, 1982: A short history of the PBL parameterization at ECMWF. *ECMWF Workshop on Planetary Boundary Layer Parameterization*, Reading, UK, 59–80.

Louis, J.-F., 1979: A parameteric model of vertical eddy fluxes in the atmosphere. *Bound.-Layer Meteor.*, **17**, 187–202.

MacVean, M. K., 1983: The effects of horizontal diffusion on baroclinic development in a spectral model. *Quart. J. Roy. Meteor. Soc.*, **109**, 771–783.

Majewski, D., D. Liermann, P. Prohl, B. Ritter, M. Buchhold, T. Hanisch, G. Paul and W. Wergen, 2002: The operational global icosahedral-hexagonal gridpoint model GME: Description and high-resolution tests. *Mon. Wea. Rev.*, **130**, 319–338.

Manabe, S., J. Smagorinsky and R. F. Strickler, 1965: Simulated climatology of a general circulation model with a hydrologic cycle. *Mon. Wea. Rev.*, **93**, 769–799.

Marshall, J., A. Adcroft, J.-M. Campin, C. Hill and A. White, 2004: Atmosphere-ocean modeling exploiting fluid isomorphisms. *Mon. Wea. Rev.*, **132**, 2882–2894.

Martin, G. M., M. A. Ringer, V. D. Pope, A. Jones, C. Dearden and T. J. Hinton, 2006: The physical properties of the atmosphere in the new Hadley Centre Global Environmental Model, (HadGEM1). Part I: Model description and global climatology. *J. Climate*, **19**, 1274–1301, doi:10.1175/JCLI3636.1.

McGregor, J. L., 1996: Semi-Lagrangian advection on conformal-cubic grid. *Mon. Wea. Rev.*, **124**, 1311–1322.

McGregor, J. L., 2003: A new convection scheme using a simple closure. *Current issues in the parameterization of convection*, Bureau of Meteorology, Melbourne, Australia, 33–36.

McGregor, J. L., 2005a: Geostrophic adjustment for reversibly staggered grids. *Mon. Wea. Rev.*, **133**, 1119–1128.

McGregor, J. L., 2005b: C-CAM: Geometric aspects and dynamical formulation. Atmospheric Research Technical Paper 70, CSIRO. 82 pp. (electronic publication).

McGregor, J. L. and M. R. Dix, 2001: The CSIRO conformal-cubic atmospheric GCM. *IUTAM Symposium on Advances in Mathematical Modelling of Atmosphere and Ocean Dynamics*, P. F. Hodnett, Ed., Kluwer, Dordrecht, 197–202.

McGregor, J. L. and M. R. Dix, 2008: An updated description of the conformal-cubic atmospheric model. *High Resolution Simulation of the Atmosphere and Ocean*, K. Hamilton and W. Ohfuchi, Eds., Springer, 51–76.

McGregor, J. L., H. B. Gordon, I. G. Watterson, M. R. Dix and L. D. Rotstayn, 1993: The CSIRO 9-level atmospheric general circulation model. Atmospheric Research Technical Paper 26, CSIRO. 89 pp.

Mellor, G. L. and T. Yamada, 1974: A hierarchy of turbulence closure models for planetary boundary layers. *J. Atmos. Sci.*, **31**, 1791–1806.

Mellor, G. L. and T. Yamada, 1982: Development of a turbulence closure model for geophysical fluid problems. *Rev. Geophys. Space Phys.*, **20**, 851–875.

Miura, H., 2007: An upwind-biased conservative advection scheme for spherical hexagonal-pentagonal grids. *Mon. Wea. Rev.*, **135**, 4038–4044.

Molod, A., 2009: Running GCM physics and dynamics on different grids: Algorithm and tests. *Tellus*, **61**, 381–393.

Moorthi, S. and M. J. Suarez, 1992: Relaxed Arakawa-Schubert: A parameterization of moist convection for general circulation models. *Mon. Wea. Rev.*, **120**, 978–1002.

Morcrette, J.-J., H. W. Barker, J. N. S. Cole, M. J. Iacono and R. Pincus, 2008: Impact of a new radiation package, McRad, in the ECMWF Integrated Forecasting System. *Mon. Wea. Rev.*, **136**, 4773–4798.

Moritz, H., 1992: Geodetic reference system 1980. *Bulletin Geodesique (The Geodesist's Handbook)*, **66(2)**, 187–192.

Nakajima, T., M. Tsukamoto, Y. Tsushima, A. Numaguti and T. Kimura, 2000: Modelling of the radiative process in an atmospheric general circulation model. *Appl. Opt.*, **39**, 4869–4878.

Nakajima, K., Y. Yamada, Y. O. Takahashi, M. Ishiwatari, W. Ohfuchi and Y. Y. Hayashi, 2013: The variety of spontaneously generated tropical precipitation patterns found in APE results. *J. Meteor. Soc. Japan*, **91A**, doi:10.2151/jmsj.2013-A04.

Nastrom, G. D. and K. S. Gage, 1985: A climatology of atmospheric wavenumber spectra of wind and temperature observed by commercial aircraft. *J. Atmos. Sci.*, **42**, 950–960.

Neale, R. B. and B. J. Hoskins, 2000a: A standard test for AGCMs including their physical parameterizations. I: The proposal. *Atmos. Sci. Lett.*, **1**, 101–107, doi:10.1006/asle.2000.0022.

Neale, R. B. and B. J. Hoskins, 2000b: A standard test for AGCMs including their physical parameterizations. II: Results for The Met Office Model. *Atmos. Sci. Lett.*, **1**, 108–114, doi:10.1006/asle.2000.0024.

Nozawa, T., T. Nagashima, H. Shiogama and S. A. Crooks, 2005: Detecting natural influences on surface air temperature change in the early twentieth century. *Geophys. Res. Lett.*, **32**, doi:10.1029/2005GL023540.

Numaguti, A., S. Sugata, M. Takahashi, T. Nakajima and A. Sumi, 1997a: Study on the climate system and mass transport by a climate model. Tech. Rep. CGER's Supercomputer Monograph, Vol. 3, Center for Global Environmental Research, National Institute for Environmental Studies.

Numaguti, A., M. Takahashi, T. Nakajima and A. Sumi, 1997b: Description of CCSR/NIES atmospheric general circulation model. Tech. Rep. CGER's Supercomputer Monograph Report 3, Center for Global Environmental Research, National Institute for Environmental Studies, 1-48 pp.

Ogura, T., S. Emori, M. J. Webb, Y. Tsushima, T. Yokohata, A. Abe-Ouchi and M. Kimoto, 2008: Towards understanding cloud response in atmospheric GCMs: The use of tendency diagnostics. *J. Meteor. Soc. Japan*, **86**, 69–79.

Ohfuchi, W., H. Nakamura, M. K. Yoshioka, T. Enomoto, K. Takaya, X. Peng, S. Yamane, T. Nishimura, Y. Kurihara and K. Ninomiya, 2004: 10-km mesh meso-scale resolving simulations of the global atmosphere on the Earth Simulator: Preliminary outcomes of AFES (AGCM for the Earth Simulator). *J. Earth Simulator*, **1**, 8–34.

Pan, D. M. and D. A. Randall, 1998: A cumulus parameterization with a prognostic closure. *Quart. J. Roy. Meteor. Soc.*, **124**, 949–981.

Phillips, N. A., 1957: A coordinate system having some special advantages for numerical forecasting. *J. Meteor.*, **14**, 184–185.

Phillips, N. A., 1973: Principles of large-scale numerical weather prediction. *Dynamical Meteorology*, P. Morel, Ed., Reidel Publishing Comp., 1–96.

Pope, V. D., M. L. Gallani, P. R. Rowntree and R. A. Stratton, 2000: The impact of new physical parametrizations in the Hadley Centre climate codel: HadAM3. *Climate Dyn.*, **16**, 123–146, doi:10.1007/s003820050009.

Pope, V. D., A. Pamment, D. Jackson and A. Slingo, 2001: The representation of water vapor and its dependence on vertical resolution in the Hadley Centre climate model. *J. Climate*, **14**, 3065–3085, doi:10.1175/1520-0442(2001)014<3065:TROWVA>2.0.CO;2.

Pope, V. D. and R. A. Stratton, 2002: The processes governing horizontal resolution sensitvity in a climate model. *Climate Dyn.*, **19**, 211–236.

Randall, D. and D. M. Pan, 1993: Implementation of the Arakawa-Schubert cumulus parameterization with a prognostic closure. *Meteorological Monograph, The representation of cumulus convection in numerical models*, **46**, 145–150.

Rasch, P. J. and J. E. Kristjansson, 1998: A comparison of the CCM3 model climate using diagnosed and predicted condensate parameterizations. *J. Climate*, **11**, 1587–1614.

Rasch, P. J., M. J. Stevens, L. Ricciardulli, A. Dai, A. Negri, R. Wood, B. A. Boville, B. Eaton and J. J. Hack, 2006: A characterization of tropical transient activity in the CAM3 atmospheric hydrologic cycle. *J. Climate*, **19**, 2222–2242.

Ritchie, H., C. Temperton, A. Simmons, M. Hortal, T. Davies, D. Dent and M. Hamrud, 1995: Implementation of the semi-Lagrangian method in a high resolution version of the ECMWF forecast model. *Mon. Wea. Rev.*, **123**, 489–514.

Ritter, B. and J.-F. Geleyn, 1992: A comprehensive radiation scheme for numerical weather prediction models with potential applications in climate simulations. *Mon. Wea. Rev.*, **120**, 303–325.

Rotstayn, L. D., 1997: A physically based scheme for the treatment of stratiform clouds and precipitation in large-scale models. I: Description and evaluation of the microphysical processes. *Quart. J. Roy. Meteor. Soc.*, **123**, 1227–1282.

Rotstayn, L. D., B. F. Ryan and J. Katzfey, 2000: A scheme for calculation of the liquid fraction in mixed-phase clouds in large-scale models. *Mon. Wea. Rev.*, **128**, 1070–1088.

Satoh, M., 2002: Conservative scheme for the compressible non-hydrostatic models with the horizontally explicit and vertically implicit time integration scheme. *Mon. Wea. Rev.*, **130**, 1227–1245.

Satoh, M., 2003: Conservative scheme for a compressible nonhydrostatic model with moist processes. *Mon. Wea. Rev.*, **131**, 1033–1050.

Satoh, M., T. Matsuno, H. Tomita, H. Miura, T. Nasuno and S. Iga, 2008: Nonhydrostatic Icosahedral Atmospheric Model (NICAM) for global cloud resolving simulations. *J. Comput. Phys.*, **227**, 3486–3514.

Schwarzkopf, M. D. and S. B. Fels, 1991: The simplified exchange method revisited: an accurate, rapid method for computation of infrared cooling rates and fluxes. *J. Geophys. Res.*, **96**, 9075–9096.

Seifert, A., 2003: A revised cloud microphysical parameterization for COSMO-LME. *COSMO Newsletter*, **7**, 25–28.

Senior, C. A. and J. F. B. Mitchell, 1993: Carbon dioxide and climate. the impact of cloud parameterization. *J. Climate*, **6**, 393–418, doi:10.1175/1520-0442(1993)006<0393:CDACTI>2.0.CO;2.

Shi, G. Y., 1981: An accurate calculation and the infrared transmission function of the atmospheric constituents. Ph.D. thesis, Dept. of Sci., Tohoku University of Japan, 191 pp.

Shibata, K. and T. Aoki, 1989: An infrared radiative scheme for the numerical models of weather and climate. *J. Geophys. Res.*, **94**, 14 923–14 943.

Shibata, K., M. H. Yoshimura, Ohizumi, M. Hosaka and M. Sugi, 1999: A simulation of troposphere, stratosphere and mesosphere with an MRI/JMA98 GCM. *Pap. Met. Geophys.*, **50**, 15–53.

Shibata, K. and A. Uchiyama, 1992: Accuracy of the delta-four-stream approximation in inhomogeneous scattering atmosphere. *J. Meteor. Soc. Japan*, **70**, 1097–1109.

Shingu, S., H. Takahara, H. Fuchigami, M. Yamada, Y. Tsuda, W. Ohfuchi, Y. Sasaki, K. Kobayashi, T. Hagiwara, S. Habata, M. Yokokawa, H. Itoh and K. Otsuka, 2002: A 26.58 Tflops global atmospheric simulation with the spectral transform method on the Earth Simulator. *Proc. IEEE/ACM SC2002 Conference*, 52.

Simmons, A. J. and D. M. Burridge, 1981: An energy and angular momentum conserving vertical finite difference scheme and hybrid vertical coordinates. *Mon. Wea. Rev.*, **109**, 758–766.

Simmons, A. J. and R. Strüfing, 1981: An energy and angular-momentum conserving finite-difference scheme, hybrid coordinates and medium-range weather prediction. ECMWF Tech. Report 28, European Centre for Medium Range Weather Forecasts. 68 pp.

Slingo, J. and B. Ritter, 1985: Cloud prediction in the ECMWF model. ECMWF Model. Tech. Report 46, European Centre for Medium Range Weather Forecasts. 56 pp.

Slingo, J. M., 1987: The development and verification of a cloud prediction scheme for the ECMWF model. *Quart. J. Roy. Meteor. Soc.*, **113**, 899–927.

Smith, R. N. B., 1990: A scheme for predicting layer clouds and their water content in a general circulation model. *Quart. J. Roy. Meteor. Soc.*, **116**, 435–460, doi:10.1002/qj.49711649210.

Smith, R. N. B., 1993: Experience and developments with the layer cloud and boundary layer mixing schemes in the UK Meteorological Office Unified Model. *Proceedings of ECMWF/GCSS workshop on parametrization of the cloud-topped boundary layer, 8-11 June 1993*, Reading, UK.

Suarez, M. J. and L. L. Takacs, 1995: Documentation of the Aries/GEOS dynamical core Version 2. NASA Technical Memorandum 104606, 5. 58 pp.

Sud, Y. C. and A. Molod, 1988: The roles of dry convection, cloud-radiation feedback processes and the influence of recent improvements in the parameterization of convection in the GLA GCM. *Mon. Wea. Rev.*, **116**, 2366–2387.

Sugi, M., K. Kuma, K. Tada, K. Tamiya, N. Hasegawa, T. Iwasaki, S. Yamada and T. Kitade, 1990: Description and performance of the JMA operational global spectral model (JMA-GSM88). *Geophysical Magazine*, **43**, 105–130.

Takacs, L. L. and M. J. Suarez, 1996: Dynamical aspects of climate simulations using the GEOS GCM. NASA Technical Memorandum 104606, 10. 56 pp.

Temperton, C., M. Hortal and A. Simmons, 2001: A two-time-level semi-Lagrangian global spectral model. *Quart. J. Roy. Meteor. Soc.*, **127**, 111–127.

Tiedtke, M., 1989: A comprehensive mass flux scheme for cumulus parameterization. *Mon. Wea. Rev.*, **117**, 1779–1800.

Tiedtke, M., 1993: Representation of clouds in large-scale models. *Mon. Wea. Rev.*, **121**, 3040–3061.

Tomita, H. and M. Satoh, 2004: A new dynamical framework of nonhydrostatic global model using the icosahedral grid. *Fluid Dyn. Res.*, **34**, 357–400.

Tomita, H., M. Satoh and K. Goto, 2002: An optimization of the icosahedral grid modified by spring dynamics. *J. Comput. Phys.*, **183**, 307–331.

Tomita, H., M. Tsugawa, M. Satoh and K. Goto, 2001: Shallow water model on a modified icosahedral geodesic grid by using spring dynamics. *J. Comput. Phys.*, **174**, 579–613.

Untch, A. and M. Hortal, 2004: A finite-element scheme for the vertical discretization of the semi-Lagrangian version of the ECMWF forecast model. *Quart. J. Roy. Meteor. Soc.*, **130**, 1505–1530.

Wang, W.-C., X.-Z. Liang, M. P. Dudek, D. Pollard and S. L. Thompson, 1995: Atmospheric ozone as a climate gas. *Atmospheric Research*, **37**, 247–256.

Wang, Z. Z., J. Mao and G. X. Wu, 2008: The wavenumber-frequency characteristics of the tropical waves in an aqua-planet GCM. *AAS*, **24**, 541–554.

Wang, Z. Z., G. X. Wu, T. W. Wu and R. C. Yu, 2004: Simulation of asian monsoon seasonal variations with climate model R42L9/LASG. *Adv. Atmos. Sci.*, **21**, 879–889.

Watanabe, M., 2005: On the presence of annular variability in an aquaplanet model. *Geophys. Res. Lett.*, **32**, L05 701, doi:10.1029/2004GL021869.

Watanabe, M., 2007: Reply to comment by B. A. Cash et al. on "On the presence of annular variability in an aquaplanet model". *Geophys. Res. Lett.*, **34**, L03 708, doi:10.1029/2006GL028669.

Watanabe, M., T. Suzuki, R. Oishi, Y. Komuro, S. Watanabe, S. Emori, T. Takemura, M. Chikira, T. Ogura, M. Sekiguchi, K. Takata, D. Yamazaki, T. Yokohata, T. Nozawa, H. Hasumi, H. Tatebe and M. Kimoto, 2010: Improved climate simulation by MIROC5: Mean state, variability, and climate sensitivity. *J. Climate*, **23**, 6312–6335.

Wheeler, M. C. and G. N. Kiladis, 1999: Convectively coupled equatorial waves: Analysis of clouds and temperature in the wavenumber-frequency domain. *J. Atmos. Sci.*, **56**, 374–399.

Williamson, D. L., M. Blackburn, K. Nakajima, W. Ohfuchi, Y. O. Takahashi, Y.-Y. Hayashi, H. Nakamura, M. Ishiwatari, J. L. McGregor, H. Borth, V. Wirth, H. Frank, P. Bechtold, N. P. Wedi, H. Tomita, M. Satoh, M. Zhao, I. M. Held, M. J. Suarez, M.-I. Lee, M. Watanabe, M. Kimoto, Y. Liu, Z. Wang, A. Molod, K. Rajendran, A. Kitoh and R. Stratton, 2013: The Aqua-Planet Experiment (APE): Response to changed meridional SST profile. *J. Meteor. Soc. Japan*, **91A**, doi:10.2151/jmsj.2013-A03.

Wilson, D. R. and S. P. Ballard, 1999: A microphysically based precipitation scheme for the UK Meteorological Office Unified Model. *Quart. J. Roy. Meteor. Soc.*, **125**, 1607–1636.

Wu, G. X. and Coauthors, 1997: The LASG global ocean-atmosphere-land system model GOALS/LASG and its simulation study. *Appl. Meteor.*, **8**, 15–28.

Zappa, G., V. Lucarini and A. Navarra, 2011: Baroclinic stationary waves in aquaplanet models. *J. Atmos. Sci.*, **68**, 1023–1040.

Zeng, Q. C., 1963: Characteristic parameter and dynamical equation of atmospheric motion. *Acta Meteor. Sinica*, **33**, 472–483, (in Chinese).

Zhang, G. J. and N. A. McFarlane, 1995: Sensitivity of climate simulations to the parameterization of cumulus convection in the Canadian Climate Centre general circulation model. *Atmos. Ocean*, **33**, 407–446.

Zhang, M., W. Lin, C. S. Bretherton, J. J. Hack and P. J. Rasch, 2003: A modified formulation of fractional stratiform condensation rate in the NCAR Community Atmosphere Model (CAM2). *J. Geophys. Res.*, **108**, 4035, doi:10.1029/2002JD002523.

Zhang, X. H., G. Y. Shi, H. Liu and Y. Q. Yu, 2000: IAP global ocean-atmosphere-land system model. *Science Press*, 252 pp.

Zhou, J., Y. C. Sud and K.-M. Lau, 1996: Impact of orographically induced gravity-wave drag in the GLA GCM. *Quart. J. Roy. Meteor. Soc.*, **122**, 903–927, doi:10.1002/qj.49712253206.